



مجلة جامعة بني وليد للعلوم الإنسانية و التطبيقية

26

BANI WALEED UNIVERSITY JOURNAL OF SCIENCES & HUMANITIES



مجلة فصلية محكمة تصدر عن جامعة بني وليد

A QUARTERLY REFEREED JOURNAL ISSUED BY BANI WALEED UNIVERSITY

من محتويات العدد :

- Coastal Landscapes and Geomorphotypes Assessment as Geotourism Sites Northeastern Region, Libya.
- Comparison between Non-linear and ANN Models for Prediction of Corrosion Inhibition Efficiency of Mild Steel .
- Modelling and simulation of Polysiloxane diaphragm pressure sensor with graphene beam.
- Theoretical studies on the efficiencies of some thio compounds as corrosion Inhibitors of mild steel in HCl using PM6.
- Study and simulation of electrical transformer protection using (differential protection).
- Cracks in the walls around the windows and doors openings (CASE STUDY) .
- Radiological assessment of cancer risk and Human Health Risk in Bani Waleed city, Libya.

السنة السادسة العدد السادس والعشرون المجلد الثاني ديسمبر 2022

مجلة جامعة بني وليد للعلوم الإنسانية والتطبيقية - العدد السادس والعشرون - ديسمبر 2022 م

Sixth Year – Twenty-Sixth Issue – Volume II- December 2022

26

26



مجلة جامعة بني وليد للعلوم الإنسانية والتطبيقية

مجلة علمية فصلية محكمة تصدر عن
جامعة بني وليد
بني وليد - ليبيا

السنة السادسة - العدد السادس والعشرون
المجلد الثاني - ديسمبر 2022 م

التوثيق: الدار الوطنية للكتاب بنغازي 2017/ 121

مجلة جامعة بني وليد للعلوم الإنسانية
والتطبيقية
السنة السادسة – العدد السادس والعشرون –
المجلد الثاني – ديسمبر 2022 م

رئيس تحرير المجلة

أ.د. سالم أمحمد سالم التونسي

هيئة تحرير المجلة

د. أسامة غيث فرج

د. الطاهر سعد علي ماضي

د. السنوسي مسعود عبيد الله

د. جعفر الصيد عوض

د. مفتاح أغنية محمد أغنية

د. فاتح عمر زيدان

د. حمزة خليفة ضو

أ. جمال معمر محمد الدبيب

أ. أشرف علي محمد لامة

اللجنة الاستشارية للمجلة

أ.د. أبو العيد الطاهر عبد الله الفقهي

أ.د. أحمد ظافر محسن

أ.د. أنور حسين عبد الرحمن

أ.د. بلقسام السنوسي أبو حمرة

أ.د. رضا علي عبد الرحمن

أ.د. فخر الدين عبد السلام عبد المطلب

أ.د. مرتجن مصطفى أبو كريشة

قواعد النشر بمجلة جامعة بني وليد للعلوم الإنسانية والتطبيقية

مجلة جامعة بني وليد للعلوم الإنسانية والتطبيقية
مجلة علمية فصلية محكمة تهتم بنشر البحوث والدراسات
العلمية الأصيلة والمبتكرة في العلوم الإنسانية والتطبيقية .
وإذ ترحب المجلة بالإنتاج المعرفي والعلمي للباحثين في
المجالات المشار إليها تحيطكم علماً بقواعد النشر بها وهي
كالتالي :

1- تقبل البحوث باللغتين العربية والإنجليزية على أن تعالج
القضايا والموضوعات بأسلوب علمي موثق يعتمد الإجرائية
المعتمدة في الأبحاث العلمية، وذلك بعرض موضوع الدراسة
وأهدافها ومنهجها وتقنياتها وصولاً إلى نتائجها وتوصياتها
ومقترحاتها.

2- يكون التوثيق بذكر المصادر والمراجع بأسلوب أكاديمي
يتضمن:

أ- الكتب : اسم المؤلف، عنوان الكتاب، مكان وتاريخ النشر،
اسم الناشر، رقم الصفحة .

ب- الدوريات : اسم الباحث، عنوان البحث، اسم المجلة، العدد
وتاريخه، رقم الصفحة .

3- معيار النشر هو المستوى العلمي والموضوعية والأمانة
العلمية ودرجة التوثيق وخلو البحث من الأخطاء التحريرية
واللغوية وأخطاء الطباعة.

4- أن يكون النص مطبوعاً على برنامج (Microsoft Word)
ويكون حجم الخط (14) ونوعه (Simplified Arabic)، على
حجم ورق A4 .

5- أن لا يزيد حجم الدراسة أو البحث على (25) صفحة كحد
أقصى وان يرفق بخلاصة للبحث أو المقالة لا تتجاوز(60)كلمة
تنشر معه عند نشره .

6- ترحب المجلة بتغطية المؤتمرات والندوات عبر تقارير لا تتعدى (10) صفحات (A4) كحد أقصى، يذكر فيها مكان الندوة أو المؤتمر وزمانها وأبرز المشاركين، مع رصد أبرز ما جاء في الأوراق والتعليقات والتوصيات .

7- ترحب المجلة بنشر مراجعات الكتب بحدود (10) صفحات (A4) كحد أقصى على أن لا يكون قد مضى على صدور الكتاب أكثر من عامين. على أن تتضمن المراجعة عنوان الكتاب وأسم المؤلف ومكان النشر وتاريخه وعدد الصفحات، وتتألف المراجعة من عرض وتحليل ونقد، و أن تتضمن المراجعة خلاصة مركزة لمحتويات الكتاب، مع الاهتمام بمناقشة أطروحات المؤلف ومصداقية مصادره وصحة استنتاجاته .

8- يرفق مع كل دراسة أو بحث تعريف بالسيرة الأكاديمية والدرجة العلمية والعمل الحالي للباحث .

9- لا تدفع المجلة مكافآت مالية عما تقبله للنشر فيها .

10- لا تكون المواد المرسلة للنشر في المجلة قد نشرت أو أرسلت للنشر في مجلات أخرى.

11- تخضع المواد الواردة للتقييم، وتختار هيئة تحرير المجلة (سرياً) من تراه مؤهلاً لذلك، ولاتعاد المواد التي لم تنشر إلى أصحابها.

12 - يتم إعلام الباحث بقرار التحكيم خلال شهرين من تاريخ الإشعار باستلام النص، وللمجلة الحق في الطلب من الباحث أن يحذف أي جزء أو يعيد الصياغة، بما يتوافق وقواعدها.

13- تحتفظ المجلة بحقها في نشر المادة وفق خطة التحرير، وتؤول حقوق الطبع عند إخطار الباحث بقبول بحثه للنشر للمجلة دون غيرها.

14- مسؤولية مراجعة و تصحيح و تدقيق لغة البحث تقع علي الباحث، على أن يقدم ما يفيد بمراجعة البحث لغوياً، ويكون ذلك قبل تقديمه للمجلة .

15- ترسل البحوث والدراسات والمقالات باسم مدير التحرير.

بخصوص البحوث والدراسات والمقالات التي تسلم إلى مقر
المجلة، فإن البحث يسلم على قرص مدمج (CD) مرفقا بعدد 2
نسخة ورقية .

للمزيد من المعلومات والاستفسار يمكنكم المراجعة عبر :

البريد الإلكتروني
jurbwu@bwu.edu.ly

صفحة المجلة على فيسبوك
(مجلة جامعة بني وليد للعلوم الإنسانية و التطبيقية)

مقر المجلة
إدارة المكتبات والمطبوعات والنشر بالجامعة – المبنى الإداري
لجامعة بني وليد
بني وليد – ليبيا

محتويات العدد

الصفحة	اسم الباحث	عنوان البحث
10	Ibrahim M. Abou El Leil Ahmed Mohammed Farag Adam	Coastal Landscapes and Geomorphotypes Assessment as Geotourism Sites Northeastern Region, Libya
29	Ibrahim M. Abou El Leil Saad Adam Ashraf M. Zobi	A COMPARATIVE STUDY BETWEEN PIPESIM SIMULATION MODEL AND SOFTWARE APPROACH FOR ESP DESIGN
45	Ibrahim M. Abou El Leil Fatema Omar	GEOHERMAL ENERGY EXTRACTION FROM ABANDONED OIL WELLS AS SUSTAINABLE SOURCES OF RENEWABLE ENERGY
70	Wanes, Benlama	Patient-Centred Pain Management of Fibromyalgia Patient following a Holistic Approach and Mantra (Keep Calm and Forget the Pain)
81	Suaad Ghait Abdarrhman Abuhamra	STUDY OF TEMPERATURE AND TIME EFFECT ON STORED GRAIN WHEAT
90	Abdulrahman Abdulsalam Bin Zayd	Effect of Water Salinity on Concrete Strength
95	Omar Kalifa Hammuda Aluhwal	CO2 INJECTION IN A CARBONATE RESERVOIR FOR EOR PROCESS
101	Ashraf M.L.Milad Nori.S.A.Ateig Juhaynah .S.Alshukri Nooralden.A.Abubakr	Comparison of opening deep beam shapes under concentrated load
108	SALIM .O. MIFTAH	A review of the Microbiological Influenced on Corrosion rates in Oil seawater systems and three-phase transport pipelines

محتويات العدد

الصفحة	اسم الباحث	عنوان البحث
119	Bashir M. Aburawi	Investigation of the effects of Wax Additives On the asphalt binder
128	RAMZI JALGHAM	Comparison between Non-linear and ANN Models for Prediction of Corrosion Inhibition Efficiency of Mild Steel
137	Amar Omran Alshmam	Effect of salinity on seed germination and seedling growth of bread wheat
144	Badradin Elforjani, Samieh Abusaad, Dr Fung, Dr A Ball	Thermal Energy Harvesting based Novel Wireless Sensor Node with Wired Measurement for Condition Monitoring of Gearbox
152	Faoziya S. Musbah	A Cubic B-Spline Collocation Method for Solving Anomalous Sub-diffusion Equation
158	Mohamed Elmahdi Ali	Modeling and simulation of Polysiloxane diaphragm pressure sensor whit graphene beam
167	Atigah A. Karnaf	Identification of Measles Rash spots by Image Contrast Enhancement
172	Abdelhamed I. Ganaw	Engagement of marble powder in self compacting concrete
177	Waleed Ahmoda Allam Musbah Al Allam	Theoretical studies on the efficiencies of some thio compounds as corrosion inhibitors of mild steel in HCl using PM6
184	M. O tman. M.Elbasir.	Thermal stability and mechanic al properties of alkaline activated mortars synthesized from POFA after exposure to elevated temperatures

محتويات العدد

الصفحة	اسم الباحث	عنوان البحث
191	Mohamed Baqar, Hamza Meelad, Hana Sheikh, Ayman Allsaed, Mohammed Mohammed, Bader Aweda	Applications of EOR Azzaytuna Analysis as a New Tool for Screening of Enhanced Oil Recovery Methods
198	Allam Musbah, Waleed Ahmoda, Khaled Mohamed Oraibi, Mohamed Alfitouri Masoud, Mohammed Ahmed Ahbil	An overview: Environmental influence of wastewater
207	Rashid El-feres	Statistical Distribution State Estimation Algorithm to Determine Electric Network State Variables
223	Ali Abead Dh , Abdulate.A.M.Elghanai	The phenomenon of corona and its effect on the transient wave in the transmission line
233	Mahfoud Aghanaya	Radiological assessment of cancer risk and Human Health Risk in Bani Waleed city, Libya
243	Abdalfettah Aljedk	Study and simulation of electrical transformer protection using (differential protection)
255	Salem Milad Abdel Hamid Omar Ahmed Mohamed Walid Emhammed Ghaithc Meshaal Suliman Almuktard	Planning preventive maintenance of textile machines in the woolen industries complex in Bani Walid
260	Naji Amhimmid Salih	Cracks in the walls around the windows and doors openings(CASE STUDY)

Coastal Landscapes and Geomorphotypes Assessment as Geotourism Sites Northeastern Region, Libya

Ibrahim M. Abou El Leil^a, *Ahmed Mohammed^b & Farag Adam^b

^aPetroleum Engineering Department, Faculty of Engineering, Tobruk University, Libya

^bGeology Department, Faculty of Science, Tobruk University, Libya

Abstract: Geotourism represents a special form of tourism that focuses on geology and landscape forms. Therefore, we can say that geotourism is connected to sustainable development of some area. Geotourism started being popular in some tourists' circles, e.g. to the tourists who search for new adventures and are interested in geological features. Geotourism promotes tourism to 'geo-sites' and conservation of geodiversity and understanding of earth sciences through appreciation and learning. The aim of geotourism is to make visitors aware of, and to gain some understanding of geological features that surround them. It has links with adventure tourism, cultural tourism and ecotourism, but is not synonymous with any of these forms of tourism. It is about creating a geotourism product that protects geoheritage, helps build communities and promotes geological heritage, and works with a wide range of different people. Geotourism has an increasingly important contribution to the economy by creating jobs for local residents: tour companies, drivers, guides and accommodation providers. Geodiversity might be useful as a way of recording diverse features within a given area, but it should not be treated as a value-judgement on the significance of individual sites. This paper presents the outcomes of a geomorphological investigation carried out along the coast of the north-east Libya Latitudes 31°16'24" and 32°56'28" North, and Longitudes 20°18'53" and 25°09'08" provides a detailed classification of the coastline based on the identification and definition of specific coastal geomorphotypes. The paper aims to evaluate the different geomorphological landscapes as attractive elements of natural geosites. The results of field surveys, supported by photo interpretation, have led to the classification of a coastal geomorphological features which outlines the processes and related deposits and landforms. This study concluded that the geomorphotypes under consideration are representing geosites destination and can be used as geotourism to achieve sustainable development.

Keywords: geomorphotypes; coastal landscapes; geotourism; geosites; Libya.

Introduction

Geomorphology is a relatively young science, although its roots are very ancient. Thus, (Chorley et al., 1964) pointed out that the first recorded observations and interpretations concerning relief and topography emerged in ancient Greece, including pioneering ideas on fluvial incision and the hydrological cycle (Bauer, 2004). Nevertheless, the consolidation of geomorphology among the environmental sciences occurred during the 18th and particularly the 19th centuries, with the practical and theoretical work of Hutton (1726-1797; Theory of the Earth), Lyell (1797-1875; Principles of Geology), and G. K. Gilbert (1843-1918; Report on the geology of the Henri mountains, and Lake Bonneville). Hutton is considered by some geomorphologists to be the founder of modern geomorphology (Bauer, 2004). During Hutton's time, nature was an open book ready to be discovered and interpreted, and the success of geomorphologists lay in their precise observation of landforms and deposits. Most probably they were independent scientists. Geographers and geologists related landforms to various structural aspects of the Earth's surface or to ancient cold climatic stages, and built the basis for explaining the temporal and spatial aspects of the relief. The classification and description of landforms were the basis for an increasingly consistent science.

Geomorphology and Landscape

Since the 18th century geomorphologists have tried to explain landforms using various theoretical frameworks. Religion has always tried to control the development of science, and to adapt scientific advancement to the most conservative biblical ideas of the Earth's development, based on the most

restrictive reading of the Bible. This explains the initial success of catastrophism in justifying rapid landscape development over short periods of time. Fortunately, the uniformitarianism of Lyell represented a rationalization of landscape development (Bauer, 2004), based on the uniformity of laws and processes. The most significant idea of Lyell was that "the present is the key of the past" (Gutierrez, 2005). This means that the explanation for landforms development rests on geomorphic processes occurring at present; in other words, that old landforms can be studied in the light of present processes. This consistent idea led to the relatively early development of climatic geomorphology, a concept first introduced by (De Martonne, 1913) in the publication *Le climate, facteur du relief*. Surprisingly, the geographical cycle (or erosion cycle) (Davis, 1899) gave secondary roles to the spatial and temporal variability of climate, such that relief evolved through stages of youth, maturity and old age, providing a simplistic and deterministic view of landscape evolution, the end of product of which would be a peneplain (Leopold et al., 1964). For Davis, the identification of certain landscape characteristics was sufficient to provide information on past and future landscape development. Perhaps this was the reason for the popularity of Davis' geographical cycle and ideas, which dominated geographical investigations until the mid-20th. Some authors have stressed, perhaps overly, that Davis' ideas were responsible for decades of backwardness in the science of geomorphology relative to the environmental sciences (Tricart, 1965),(Tricart, 1978), particularly because of the marginalization of climate-driven geomorphic processes (Passarge, 1931). A change in paradigm occurred with (Strahler, 1952) and Leopold(Leopold et al., 1964), who gave a marked impetus to geomorphology by emphasizing the role of field and laboratory research, physics and mathematics in quantitative geomorphology, which was pioneered by the studies of (Horton, 1945)on the morphometry of rivers and basins. From theoretical, extremely complex and valuable approaches, some authors established simplistic solutions, classifying countries, schools and scientists as geomorphologic ally positives, historicist or non-positivist (Capel, 1983).

Objective of Study

The main aim of this study is to evaluate the different geomorphological landscapes as attractive elements of natural geosites throughout identification and classification the various geomorphological features as well as the spatial distribution of coastal landforms.

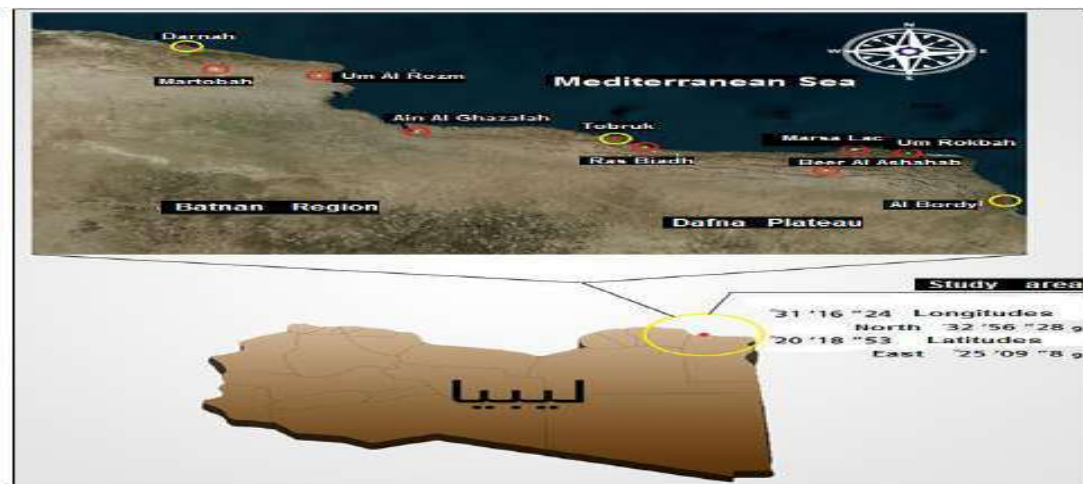
Materials and Methods

1. Location of Study

According to the previous geological studies, generally Libya can be classified into four major regions as following:

1. Northwestern region
2. Northcentral region
3. Southwestern region
4. Northeastern region

This study has been conducted on the geomorphological features of coast line in the northeastern



region for identification, classification and spatial distribution of coastal landforms, including six areas. These areas Wadi Al Khabta at Ras Al Tean, Wadi Abou Al Gomel (Tobruk), Wadi Al Sahl (Tobruk), Wadi Al Raheb (Kambout), Wadi Rezq (Al Borden) and Wadi Al Sawani (Al Borden).

The coordinate of this region is represented between Latitudes $31^{\circ}16'24''$ and $32^{\circ}56'28''$ North, and Longitudes $20^{\circ}18'53''$ and $25^{\circ}09'8''$ (Figure 1). The lithology of the different rock formation in the studied areas are mainly represented by calcareous types e.g. limestone, fossiliferous limestone, dolomitic limestone, in addition to other rock types such as sandstone, shale, marl and alluvial deposits.

Fig. 1: Geologic map of the studied areas

The coastline of the studied areas is dominated by vertical cliffs, indented bays, cliffy coves and inlets developed on limestone formations. This work offers a detailed classification of the coastal landscape through the classification of coastal geomorphotypes, which are defined by specific topographical, lithostructural and geomorphological features. It presents a landforms and deposits derived from marine, karst, fluvial and gravitational processes.

2. Methodology

The methodology of the study is relying on the collecting samples of rock formations, field observation description. Whereas, selected naturally attractive geosites have been chosen to undergo this study and to be evaluated upon their naturally parameters that can be representing as tourism destination.

Results and Discussion

1. Lithology and Stratigraphy

In general, the characterization lithology of the studied area is encountered in a few rock types that represented by calcareous fossiliferous rocks, shale, sandy shale and conglomerate (Banerjee, 1980; Megerisi, 1980).

The stratigraphic succession shows some variation from location to another in thickness and extent due the variation of depositional environments and depositional factors.

The thick sedimentary section exposed especially noticed along the cliffs overlooking the Mediterranean Sea are classified into three main stratigraphic formations belonging to Early Tertiary e. g. Al Jaghbub Formation, Al Faidiyah Formation and Al Khowaymat Formation. Besides, Quaternary deposits were recognized near the foot slopes of the cliffs and inward covering older units. The following units were recognized in the field as given below:

Quaternary

Alluvium deposits

Beach and coastal sand dune

Sabkha sediments

Eolian deposits

Tertiary

Lower-Middle Miocene: Al Jaghbub Formation

Upper Oligocene-Lower Miocene: Al Faidiyah Formation Upper Eocene-Lower Oligocene:

Al Khowaymat Formation: The section exposed at Wadi Rezq described as following: (Industrial Research Centre, 1977).

Al Faidiyah Formation: limestone, faint brown to dark yellow, sandy and marly. Lithologically the formation is made of alternating limestone, marly limestone and clay beds. The beds are nearly horizontal, thin to thin-bedded and highly fossiliferous (Figure 2). It is including the following assemblage of macrofauna: *Cardium gallicum*, *Strombus* sp. Worm tubes, *Brissoposis frassi* and *Tlina lacunose*

Al Khowaymat Formation: dolomitic limestone, yellowish white, hard compact, fossiliferous including ; *Globgerina* spp., *Globorotalia* spp. and *Nummulites*.

Al Jaghbub Formation: marly limestone, dark yellow and moderately hard (Figure 3). It is including the following assemblage of macrofauna: *Ostreaverleti*, *Ostreadigitalina*, *Cardium merinaceum* and *Pecten cristato*.



Fig. 2: The main fossil species in the studied area

A-B-C: (Bivalve –*Pecten*); E-F-G-H: Echinoderms –*Clypeaster*; D: (Bivalve –*Ostrea*)

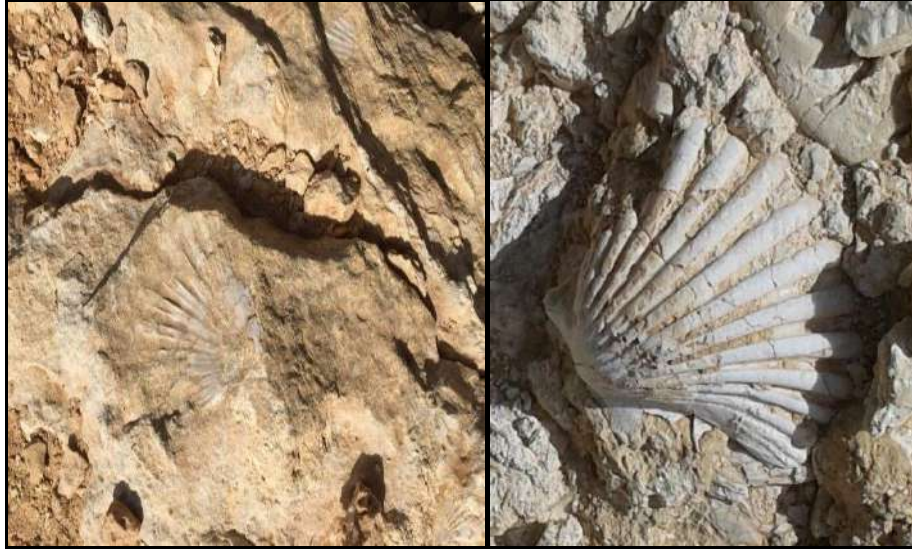


Fig.3: Fossiliferous limestone with *Pecten* species

2. Structural and geological setting

The tectonic setting of the studied areas is characterized by highly tectonic structures that representing by faulting and folding throughout the different valleys (Locally named Wadies), in addition to the cracks fishers and mass wasting. The Industrial Research Centre, 1977 investigated these areas and described these structures as general.

3. The geomorphotypes of coast region

Generally the Mediterranean region suffered from severe tectonic movements led to the formation of different topographic features that represented by different landscapes and structural forms (Said and Schembri, 2010).

The rocky coastline of the studied area can be classified into eleven coastal geomorphotypes, which are characterized by peculiar topographical, lithostructural and geomorphological features as following:

(1) Plunging cliff: vertical or sub-vertical cliff descending into a considerable depth far below low-tide level without any development of shore platform or ramp. Figure 4 depicts the different types of cliffs in the investigated locations.

A



B



C



D



E





Fig. 4: Coastal geomorphotypes: plunging cliff; (A) Al Khabta, (B) Abou Al Gomel, (C) Al Sahl, (D) Al Raheb, (E) Al Sawani, (F) Rezq.

(2) Sloping coast: low-lying rocky coast with slope dips ranging between 20° and 45° (Figure 5).

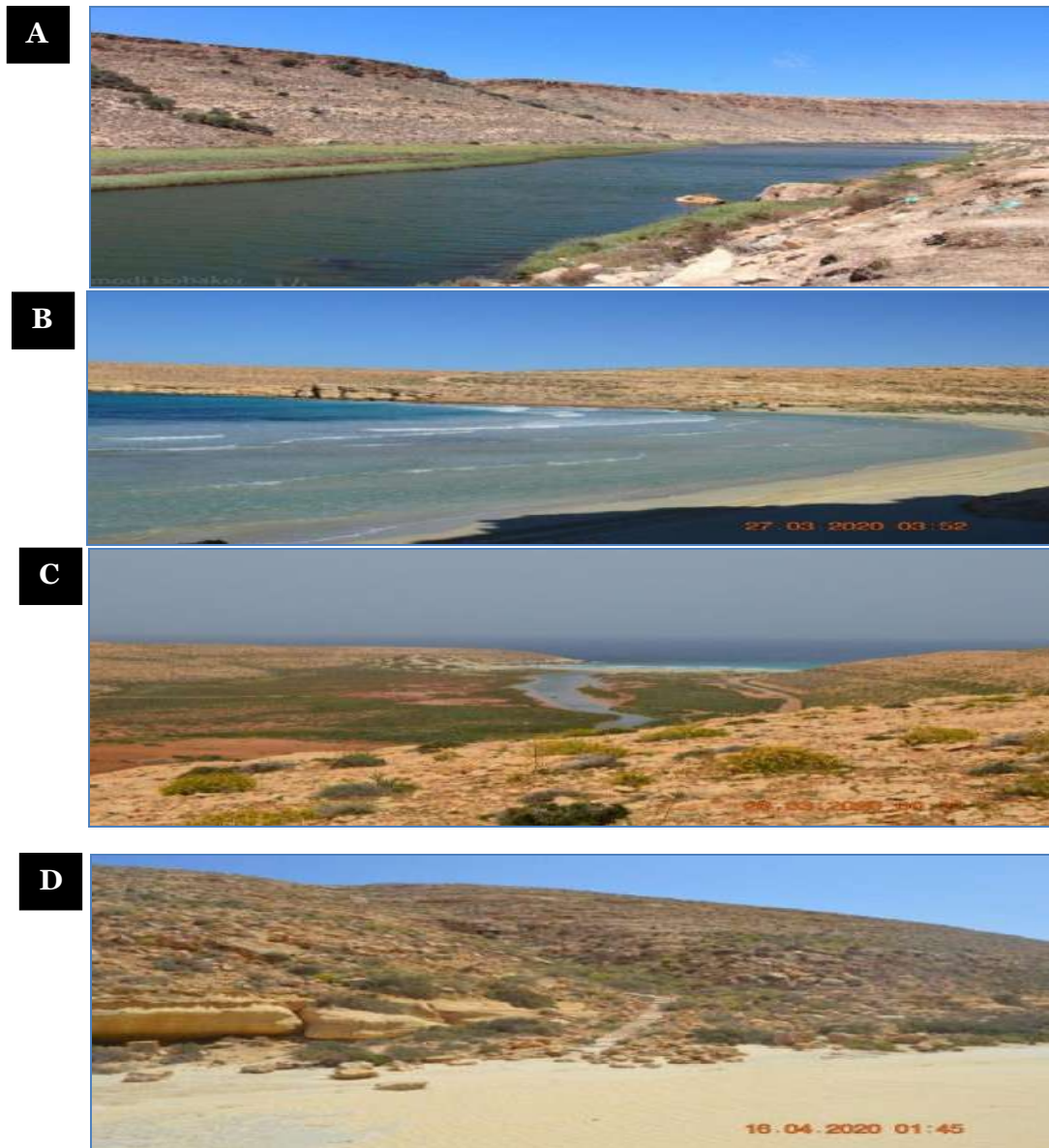
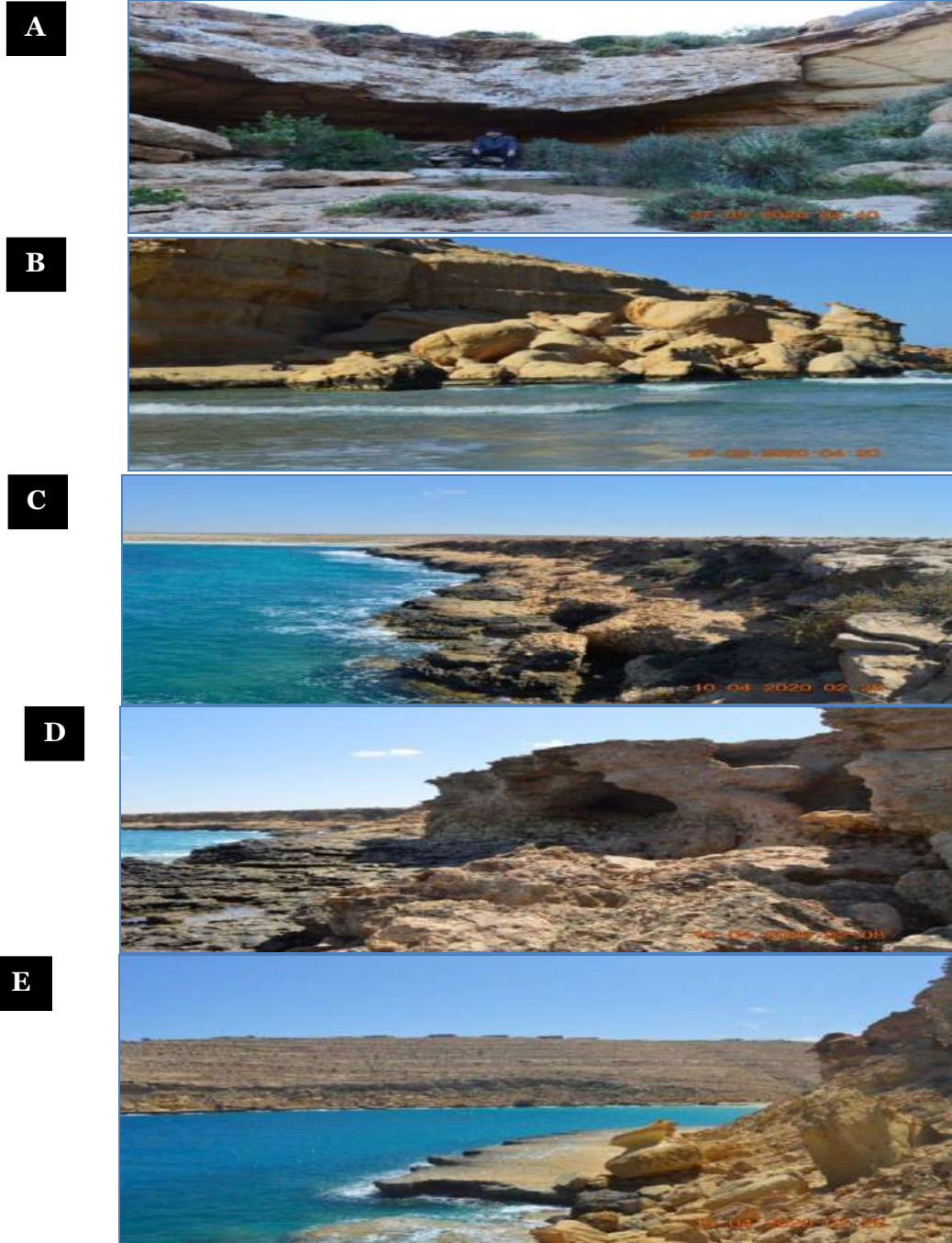


Fig. 5: Coastal geomorphotypes: Sloping coast; (A) Al Khabta, (B) Abou Al Gomel, (C) Al Sahl, (D) Rezq

(3) Shore platform: from horizontal to sub-horizontal rock surface (0° – 5°) produced along a shore by the action of marine processes (wave erosion, biogeochemical dissolution and other weathering processes) and the retreat of a cliff in the intertidal zone (Figure 6). Shore platforms can be observed at the intertidal level or 5–10 m above sea level. The latter developed on bedding planes, following their slope, they are never submerged but are affected by wave action and marine spray. Usually, a deeply carved abrasional notch occurs at mean sea level.



F



Fig. 6: Coastal geomorphotypes: Shore platform; (A) Abou Al Gomel, (B) AL Khabta, (C) Al Sahl, (D) Al Raheb, (E) Rezq, (F) Al Sawani.

(4) Screens: this scenery is characterized by extensive slope-failure deposits, which are located between coastline and karst plateaus. Landslide accumulations cover the clayey terrains and consist of chaotic and heterogeneous blocks moved mainly by extremely slow-moving landslides such as rock spreads and block slides (Figure7).

A



B



C





Fig. 7: Coastal geomorphotypes: Screens; (A) Abou Al Gomel, (B) Al Sahl, (C) Rezq, (D) Al Sawani

(5) Cliffs: vertical or sub-vertical steep slope descending to the sea with a concave shaped ramp (Figure 8).



Fig. 8: Coastal geomorphotypes: Cliffs; A) Abou Al Gomel, (B) Al Sahl

(6) Pocket beach: sand, gravel or pebble deposits in the inner portions of bays and inlets (Figure 9).





Fig. 9: Coastal geomorphotypes: Pocket beach; (A) Al Khabta, (B) Abou Al Gome1, (C) Rezq, (D) Al Sawani

(7) **Built-up coast:** intensely urbanized coast. The landscape is significantly modified by human activities (Figure 10).



Fig. 10: Coastal geomorphotypes: Built-up coast; (A) Al Sawani, Al Bordy port, (B) Al Bordy restore While plunging cliffs and sloping coasts are observed in the most investigated locations formed mainly of limestone formations. Shore platforms and cliffs have been shaped on the relatively soft limestone formation in the examined locations. Screens are observed in all location except Al Sahl, where landslides are dominant all over the studied sites. Pocket beaches are commonly found along the main bays particularly in Al Sahl, Abou Al Gomel, Rezq and Al Sawani.

(8) Solidified and loose sand dunes: this rock known as calcherinite, that belonging to Ajdabya formation occurs along coast in some of the investigated locations as shown in Figure 11.



Fig. 11: (A) Solidified sand dunes; (B) loose sand dunes

(9) Ripple marks: appear to be regular in some places and in regular in another as shown in Figure 12.

(10) Weathering pits: These pits outcrops at rocks exposures on the slopes formed by calcareous rocks all over the area and usually associated joints and cracks, and also what is called taffonis pits that arises due to the solution solubility (Figure 13)





Fig. 12: (A) Ripple marks with regular shape (B) irregular shape

(11) Honey comb: These are holes and small pits are adjacent together, and characterized that small sizes comparing with taffonis pits and formed due to chemical processes (Figure13).

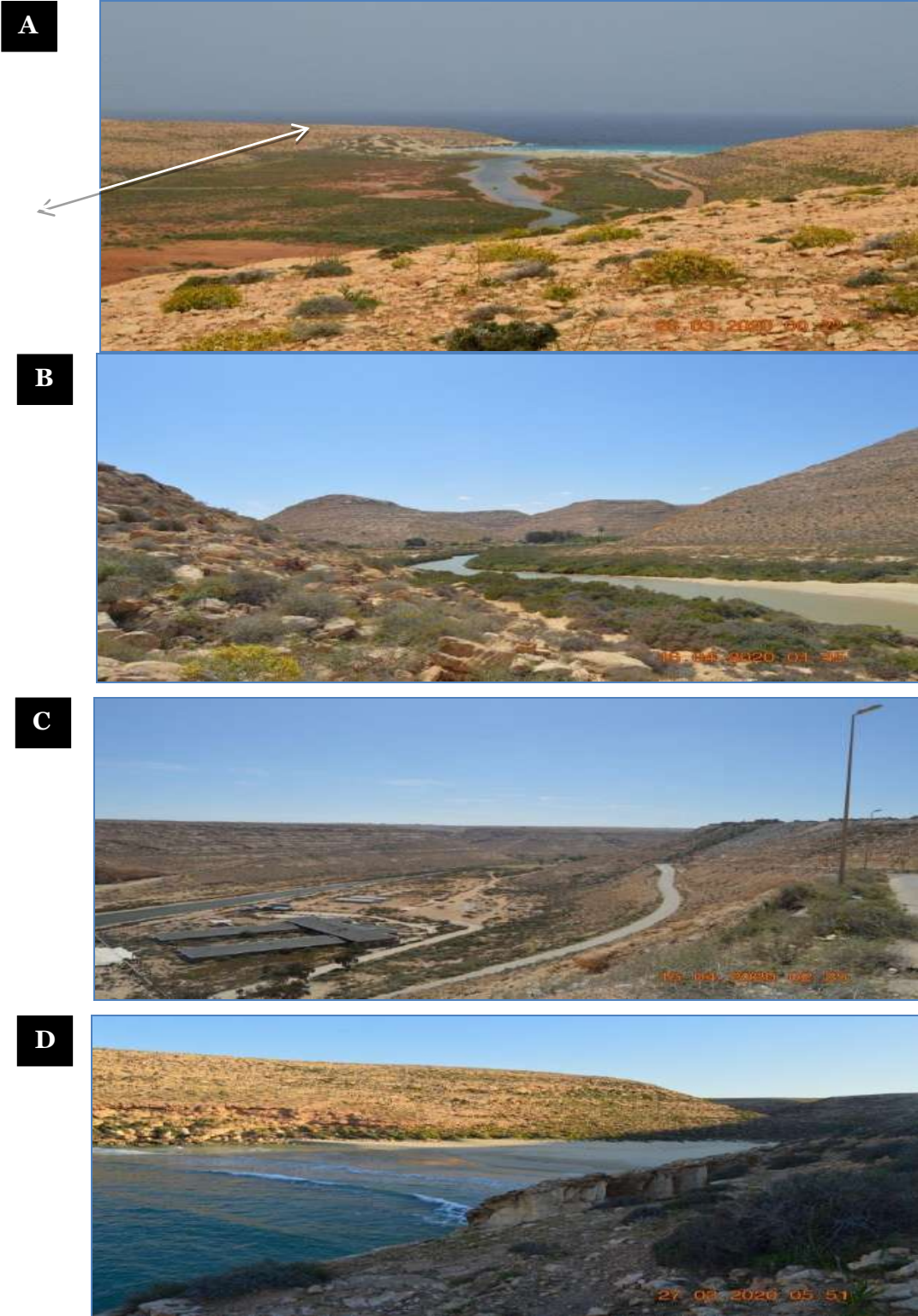


Fig. 13: Honey comb

The geomorphological Features

1. Structural elements and landforms

The geomorphological landscape the studied locations strongly influenced by the structural setting of the area. The SW-NE-oriented horst-graben system, which has developed in several wadies, controls the location of the lowlands (grabens) and headlands (horsts). The main discontinuity is the great faults system, which crosses the locations mainly from NE to SW. The great faults system starts on the northern coast, at Wadi Al Sahl, Al Khabta, Rezq and Al Sawani, where the throw is up to 100 m (Figure 14 (A-G)). The fault plane outcrops for more than 2 km along the coastline with a maximum throw of more than 200 m in most cases.



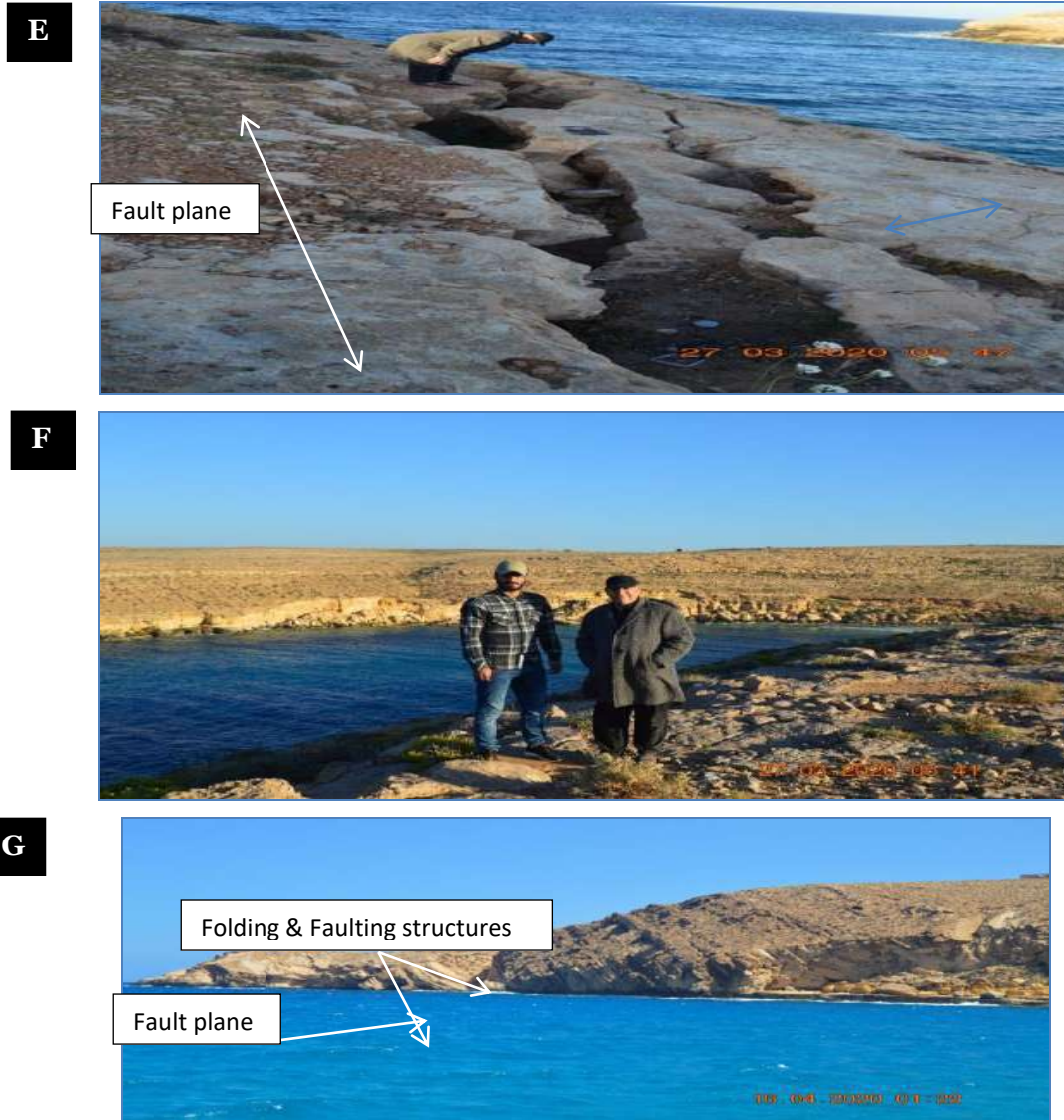


Fig. 14: Tectonic landforms: (a) Great fault plane at Wadi Al Sahl extended from east to west direction; (b) Great fault plane at Wadi Rezq running from NE-SW; (c) Al Sawani fault plane at Al Borden coast line area; (D, E,F) Abou Al Gomel; (G) Folding and faulting Rezq coast line.

Pocket beaches are dominant and mainly occur in Al Khabta, Rezq and Al Sawani and are occupied by sandy deposits. Also, Marine gorges mainly occur in the most studied locations, commonly associated with steep discontinuities enlarged by marine processes (Figure 15 (A)). The coastal scenery is characterized by many stacks, arches and sea caves (Figure 15 (B, C, & D)).

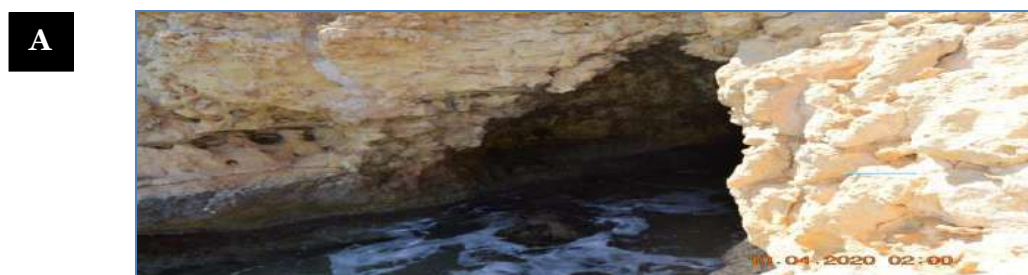
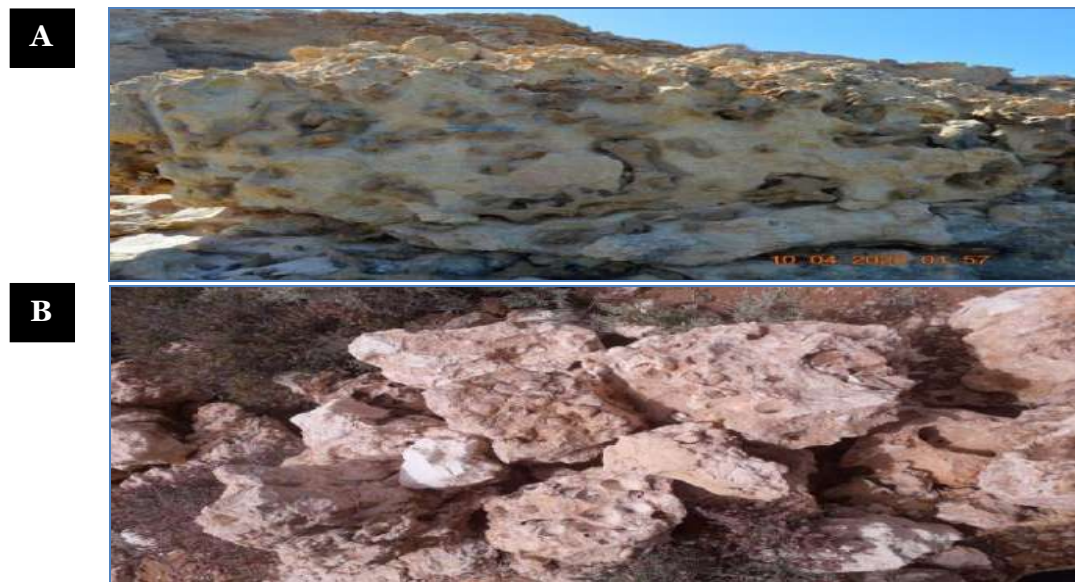




Fig. 15: Coastal features: (A) marine gorge; (B) marine stack; (C) marine cave and pillars; (D) marine cave at Al Raheb coralline Limestones at Wadi Al Raheb

Figure 16 (A -D) show the occurrence of encrusted marine shells and bioforms on the boulders and rock beds proves their marine origin.



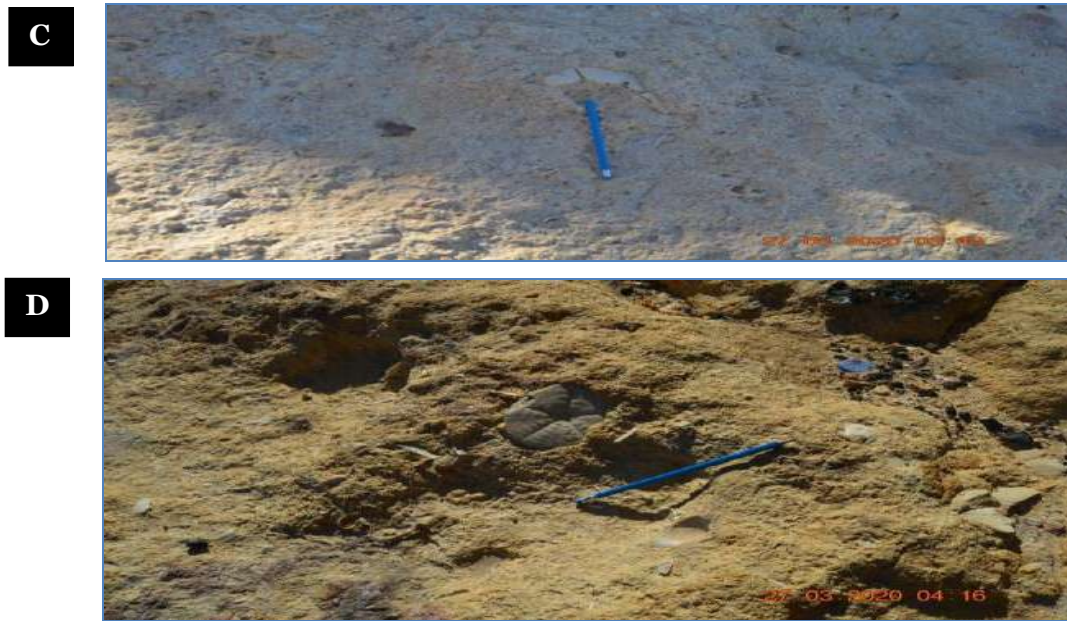


Fig. 16: (A & B) Location of the boulder deposits; (C & D) coast line rock beds at Abou Al Gomel

2. Karst landforms

Karst features are well developed on the limestone formations. Sinkholes have been defined according to their diameter. All the surveyed sinkholes are characterized by a flat shape and their genesis is usually caused by the collapse of cave roofs (Figure 17 (A)). However, large coastal caves are rare and poorly developed (Figure 17 (B)); therefore not all circular bays may be attributed to a collapsed sinkhole origin.



Fig.17: Karst features: (A) collapsed sinkhole; (B) sinkhole originated by collapsed at Wadi Rezq

3. Gravity-induced landforms and deposits

Landslides are widespread in all over the studied locations. The geological setting favours the development of extensive block slides and rock spreads (Figure 18 (A & B)). Rock spreads affect

limestone plateaus favoured by vertical discontinuities, whose persistence may exceed 200 m in length. The lateral extension of rock masses often evolves into block slides and may be accompanied by rockfalls and rock topples. Block sliding can be favoured by moistening of the clay slopes, which are also affected by earth flows and earth slides.



Fig. 18: Rock spreads and blocks slides: (A) Cliff failure; (B) Growing plant in boulder rock.

Conclusions

From the previous study the following conclusions can be drawn:

1. This paper provides the identification, classification and spatial distribution of the coastal landforms of the north-eastern region of Libya. Particular attention has been devoted to the representation of coastal features, which are strongly influenced by the tectonic setting and the lithological characteristics of outcropping rocks.
2. The rocky coastline of the studied area can be classified into eleven coastal geomorphotypes, which are characterized by peculiar topographical, lithostructural and geomorphological features as following: Plunging cliff, Sloping coast, Shore platform, Scree, Cliffs, Pocket beach, Built-up coast, Solidified and loose sand dunes, Ripple marks, Weathering pits and Honey comb
3. The geomorphological landscape the studied locations strongly influenced by the structural setting of the area. The SW-NE-oriented horst-graben system, which has developed in several wadies, controls the location of the lowlands (grabens) and headlands (horsts). The main discontinuity is the great faults system, which crosses the locations mainly from NE to SW. The great faults system starts on the northern coast, at Wadi Al Sahl, Al Khabta, Rezq and Al Sawani, where the throw is up to 100 m
4. Pocket beaches are dominant and mainly occur in Al Khabta, Rezq and Al Sawani and are occupied by sandy deposits. Also, Marine gorges mainly occur in the most studied locations,

5. Karst features are well developed on the limestone formations. Sinkholes have been defined according to their diameter. All the surveyed sinkholes are characterized by a flat shape and their genesis is usually caused by the collapse of cave roofs
6. Landslides are widespread in all over the studied locations due to the gravity action and can be described as mass wasting.
7. The results of field surveys, supported by photo interpretation, have led to the classification of a coastal geomorphological features which outlines the processes and related deposits and landforms.
8. The geomorphotypes under consideration are representing geosites destination and can be used as geotourism to achieve sustainable development.

References

- Banerjee, S. (1980). Stratigraphic lexicon of Libya. Department of geological researches & mining. Bulletin, (13).
- Bauer, B.O. (2004). Geomorphology. In: A.S. Goudie (ed.). Encyclopedia of Geomorphology, Routledge, London, pp. 428-435.
- Chorley, R. J., Dunn, A. J., & Beckinsale, R. P. (1964). history of the study of landforms, or, The development of geomorphology. Vol. 1, Geomorphology before Davis.
- Capel, H. (1983). Positivismo y antipositivismo en la ciencia geográfica el ejemplo de la geomorfología. Geo Critica. Cundernos Criticos de geografica Humana 43, 55 pp., Univ. Barcelona.
- Davis, W. M. (1899). The geographical cycle. The Geographical Journal, 14(5), 481-504.
- De Martonne, E. (1913). Le climat facteur du relief. Scientia, 7(13).
- Gutierrez, M. (2005). Climatic Geomorphology. Elsevier, Amsterdam, 760 pp.
- Gilbert, G.K., (1877). Report on the geology of the Henry mountains. U.S. Geographical and Geological Survey of the Rocky Mountain Region, Washington, DC
- Hutton, James. (1788). "Theory of the Earth." Transactions of the Royal Society of Edinburgh 1: 209–305.
- Horton, R. E. (1945). Erosional development of streams and their drainage basins; hydrophysical approach to quantitative morphology. Geological society of America bulletin, 56(3), 275-370.
- Industrial Research Centre, (1977), Geological Map of Libya, Explanatory Book lat, (AL – Bardia sheet, 1:250.000).
- Industrial Research Centre, (1977). Tripoli, Department of Geological Researches and Mining, Bulletin, vol. 12, 86 p.
- Lyell, Charles. (1830–1833). Principles of Geology, Being an Attempt to Explain the Former Changes of the Earth's Surface by Reference to Causes Now in Operation. London: John Murray.
- Leopold, L. B., Wolman, M. G., & Miller, J. P. (1964). Fluvial processes in geomorphology. Freeman and Co., San Francisco, 522 pp.
- Megerisi, M. F. (1980). The Upper Cretaceous-Tertiary formations of northern Libya: a synthesis.
- Passarge, S. (1931). Geomorfología, Editorial Labor, Barcelona, pp. 189.
- Strahler, A. N. (1952). Dynamic basis of geomorphology. Geological society of america bulletin, 63(9), 923-938.
- Said G, Schembri J (2010) Malta. In: Bird ECF (ed) Encyclopedia of the World's coastal landforms. Springer, pp 751–759.
- Tricart, J. (1965). Principes et méthodes de la Geomorphologie Masson et Cie. Editeurs, Paris.
- Tricart, J. (1978). Géomorphologie applicable. Masson, Paris, 204 pp.

A COMPARATIVE STUDY BETWEEN PIPESIM SIMULATION MODEL AND SOFTWARE APPROACH FOR ESP DESIGN

*Ibrahim M. Abou El Leil^a, Saad Adam^b & Ashraf M. Zobi^b

^aPetroleum Engineering Department, Faculty of Engineering, Tobruk University

^bMechanic Engineering Department, Faculty of Engineering, Tobruk University

Abstract: This study considers the design of an electric submersible pumping (ESP) system, an analysis of the production system that is used to determine the potential of any well and a discussion of a case study of an oil well in Sarir oilfield for ESP design throughout the various parameters. Artificial well lifting will become increasingly important in the coming years. A large portion of the world's fields are entering their late life production; Sarir field is a mature field, with increasing water production and decreasing reservoir pressure. The operator company has used electrical submersible pumps (ESPs) to assist struggling wells in order to increase production and extend the life of the field. The main objective of this study is determining how to design the most ideal ESP systems that can extend the life of the systems, given that the installation cost of ESP is very high. So, the majority of this work was done by hand calculations and run in production software approach and Pipesim simulation model, which involved manipulating both modeling the subjected wells and a series of simple detailed calculations to find the most efficient and optimum ESP equipment. The procedure path is titled: designing the ESP pump, motor, cable, and determining surface voltage. According to the study's findings, the design of ESP varies depending on various parameters from well to well. However, the obtained results exhibit of manual calculation and software approach are close to results of Pipesim simulation model. Based on this research, it is possible to conclude that the REDA D800N pump is the best submersible pump for Well C-349H-65, with a pump efficiency of approximately 62 %; from the designing this well can return to produce at desired flow rate 580 STB/Day.

Keywords: Sarir oilfield, ESP design, software, Pipesim, model, production rate .

Introduction

Oil is the most important source of energy on the planet. Crude oil can be extracted either naturally or artificially. Because the natural energy in their reservoirs is insufficient, the vast majority of the world's oil wells require some kind of artificial lifting mechanism to bring their liquid to the surface. Electrical Submerged Pumps are a type of artificial lift that has been used for decades (ESP) [1]. Because of the presence of mature reservoirs and high deep wells, as well as the availability of produced gas, the artificial lift methods that are widely used in Libya are SRP, gas lift, and ESP, which is the cornerstone of this work [2]. In terms of early history, ESP was invented and developed in the late 1910s by a Russian named Armais Arutunoff. Arutunoff conducted his initial experiments in the Baku oilfields near the Caspian Sea and later founded the Russian Electrical Dynamo of Arutunoff (REDA). The first submersible pumping unit was installed in an oil well in 1928 [3, 4], and the concept has proven itself throughout the oil-producing world since then. It is currently regarded as an efficient and cost-effective method of lifting large volumes of fluids from great depths under a variety of well conditions. Since their inception, ESP units have excelled at lifting much higher liquid rates than most other types of artificial lift and have found their best application in high-rate onshore and offshore applications. High gas production, rapidly changing liquid production rates, viscous crudes, and other conditions that were once extremely detrimental to ESP operations are now easily handled by modern units. Submersible pumping installations are thought to produce approximately 10% of the world's oil supply today [5].

Problem Statement

Petroleum production rates sometimes declining with time in several wells, this attributed to different factors; one of them is the choice of the suitable ESP for well characteristics, fluid behavior and reservoir properties. This study shows the design of an ESP artificial lift system and production optimization of a well in Sarir field. Concerning this well, reservoir issues such as pressure depletion and high water cut can result in sand formation and subsequent sand production. By having and understanding a little bit of well history, it is necessary for production engineer to design the most ideal ESP systems that can overcome the production problem and can extend life of the systems as installation cost of ESP are very expensive.

Objectives of Study

The purpose of this research is to estimate the appropriate design of submersible electric pump (ESP) components for oil well. This design will be completed by both running it through production software and hand calculations to determine the most efficient and optimal ESP components. We will compare the efficiency and number of stages of different types of pumps in the same operation condition by using different types of components such as the pump. Based on the results, we can determine the appropriate ESP components such as pump, motor, and cable from running different types of components from different manufacturers.

Scope and Limitations of Study

The scope of this study is limited to the use of a manual method and Pipesim software to optimize production by designing an ESP for artificial lift. There are other softwares that can be used to design an ESP system, but Pipesim is used for this project due to its availability. The research is being carried out in the Sarir fields, and an appropriate ESP will be implemented to increase the well's production potential.

Importance of Study

The significance of this study in the petroleum industry is that it demonstrates the importance of designing ESP for wells as well as the use of artificial lift in maximizing oil production.

Location of Study

1. Overview of Sarir Field

The Sarir or, more specifically, the Sarir "C" field is the largest oil field in Libya, located on the western edge of the Calanscio sand sea in the southern portion of the Sirte basin. It is found on the southern edge of the Upper Cretaceous-Tertiary Sirte basin, which contains all of Libya's major oil fields and is the most prolific oil-producing basin in North Africa. The Sarir "C" field, part of a complex of three fields, is 56 kilometers long and 40 kilometers wide, covering approximately 378 kilometers². To its north is the Sarir "L" accumulation, which covers roughly the same area as the Sarir North pool. The ultimate recovery from the "C" field is estimated to be 3.8 billion barrels of oil, and the ultimate recovery from the "L" field is estimated to be 1.2 billion barrels of oil, ranking them as the 51st and 201st largest fields in the Carmalt and St. compilation John's 1986 (Lewis and Sanford).

Figure 1 a map showing the location of Sarir oilfield.

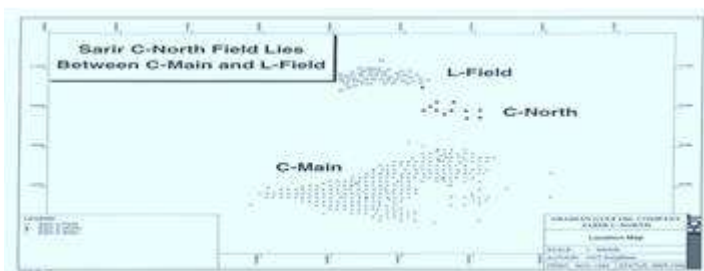


Fig. 1: Sarir C-North is lying between C-Main and L-Field [6]

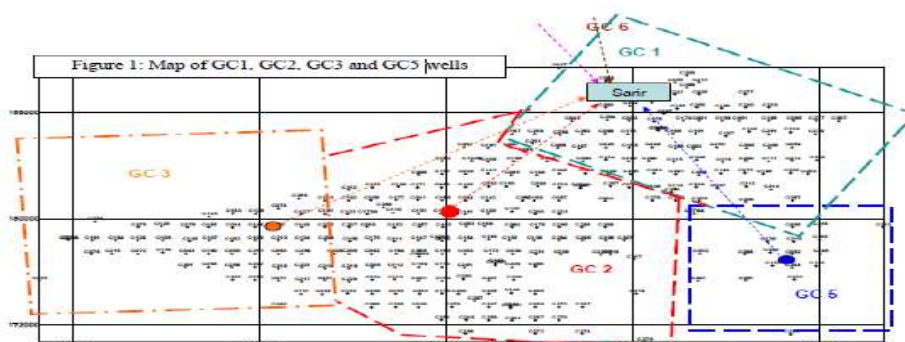


Fig. 2: Map showing the location of Map of GC-1, GC-2, GC-3 and GC-5 [7]

As a result of this depletion, some form of artificial lift was required in 1980 in order to lift oil from the producing interval to the surface and onto stations. The first candidate well for an ESP installation was C002-65, which was depleted to 3200 psi in 1983, and was followed by two wells, C-117-65 and C-073-65, in 1984.

Approximately 400 wells are currently producing by ESP, and this method has proven to be very successful. Sarir entire output is derived from electrical submersible pumped wells. Many tools can be run in the hole to monitor pump efficiency, temperature, motor vibration, current leakage, and other parameters.



Fig. 3: Map showing the location of GC-4 and GC-6 [7]

The field production infrastructure consists of a large network of gathering pipes that connect each wellhead to the gathering center (GC) that receives the crude oil. Each group of wellheads is linked to a

gathering point determined by the distribution of wells over a specific area. Each gathering center (GC1, GC2, GC3, GC4, GC5, and GC6) is linked to the GC main via a trunk line (Figures 2 & 3).

Methodology

This study's main methodology is concerned with the design of an ESP system using basic hand calculations and Pipesim simulation software. This chapter provides brief information about the fields used in this study.

1. Electrical Pump Design

An ESP installation, like other artificial lift methods, is complicated and varies greatly depending on well conditions and the type of fluids to be pumped. Good quality data covering these conditions is required to ensure proper installation design. The procedure for sizing submersible pumps and designing an entire ESP system is given below:

1.1. Data Requirements

The proper design of an ESP installation necessitates knowledge of a wide range of data. The most important of these is consistent data on the well's productivity, which allows the desired fluid rate from the well to be calculated [5]. Necessary input data can be grouped as given here.

1. Well physical data
2. Well performance data
3. Fluid properties
4. Surface power supply parameters
5. Unusual operating conditions

2. PIPESIM

PIPESIM is a petroleum engineer and facilities design, operation, and optimization software modeling tool. PIPESIM is a tool for production engineers that cover a wide range of applications in the oil and gas industry. The software allows for the creation of well models that take into account all variables, such as well configuration, fluid characteristics (PVT), multiphase VLP correlations, and various IPR models.

2.1. Basic Theory of PIPESIM

Fluid properties as a function of pressure and temperature must be predicted in order to accurately predict pressure and temperature changes from the reservoir, along the wellbore, and through the flow line tubular. The Black Oil PVT model is used in the vast majority of applications. The Black Oil model in PIPESIM can be used for a variety of purposes. In black oil fluid modeling, correlation models are used to simulate the key PVT fluid properties of the oil/gas/water system.

These empirical correlations, in contrast to the more rigorous multi-component compositional model methods, treat the oil/gas system as a simple two-component system. In relation to stock tank conditions, the hydrocarbon is simply treated as a liquid component (if present) and a gas component. For most applications, a minimum of production data, oil gravity, gas gravity, solution gas/oil ratio, and, if water is present in the system, the water cut are all that is required [8, 9].

A COMPARATIVE STUDY BETWEEN PIPESIM SIMULATION MODEL AND SOFTWARE APPROACH FOR ESP DESIGN

PIPESIM is used throughout this work for all calculations regarding setting up of a reliable model and building on it a productive ESP lift system [10].

2.2. Building a Model

When modeling a new well in PIPESIM, the first step is to choose a method and fill out a system summary, as shown in Figure 4.



Fig. 4: Layout of Pipesim system summary

Start with entering general data, followed by tubular data, deviation survey, down hole equipment, heat transfer, completions, and surface equipment data. Following the entry of the basic data for the well model. Second, the artificial lift method can be chosen based on the design requirements. Then, at the bottom hole, a well model is built and a Nodal Analysis is performed (At this stage, it is assumed that there is no pump in the well) [10].

2.3. Pump Selection/Design In selecting and designing the ESP, with the aim to determine the following:

- The number of stages required
- The pump HP required.
- Generate a Pump Performance Plot showing the potential operating flow rate range for desired frequency.

Figure 5 depicts the requirements of input data for ESP design.

3.1 Programing Using Visual Basic Language

Visual Basic (VB) is a high level and one of the most commonly used programming languages developed by Microsoft used for developing computer programs. It is evolved from the earlier DOS version called BASIC. BASIC means Beginners' All-purpose Symbolic Instruction Code. The code looks a lot like English Language. Over time the community of programmers developed third party components. VB is a third-generation event-driven programming language and integrated development environment (IDE) for its Component Object Model (COM) programming model first released in 1991. VB was derived from BASIC, a user-friendly programming language designed for beginners, and it is a programming environment in which a programmer uses a Graphical User Interface (GUI) to choose

and modify preselected sections of code written in the BASIC programming language. Like other languages, VB is not case sensitive.

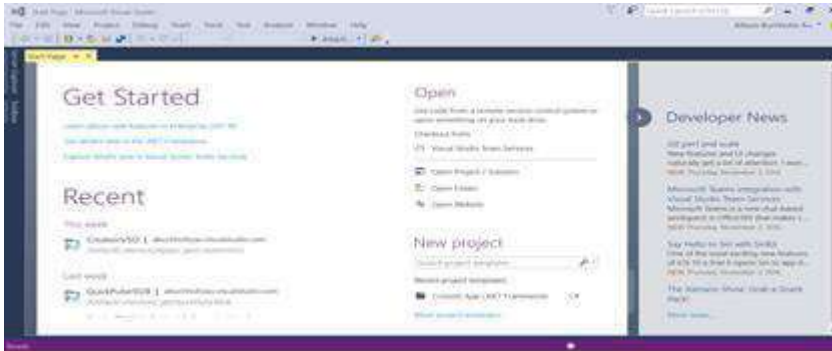


Fig. 5: Input data needs for ESP design

3.1.1. Visual Studio 2017 Enterprise

Visual Basic 2017 is the latest version of Visual Basic launched by Microsoft in 2017. Visual Basic 2017 is bundled together with other Microsoft Programming languages C#, C++, F#, JavaScript, Python and other development tools in an integrated development environment called Visual Studio Enterprise 2017 Release Candidate. Microsoft has added many new features in Visual Studio 2017 particularly those features for building mobile applications and gaming as well as web and cloud-based applications.

3.1.2. Visual Studio Enterprise 2017 Start Page

The Visual Studio Enterprise 2017 Start Page as shown in Figure 6.

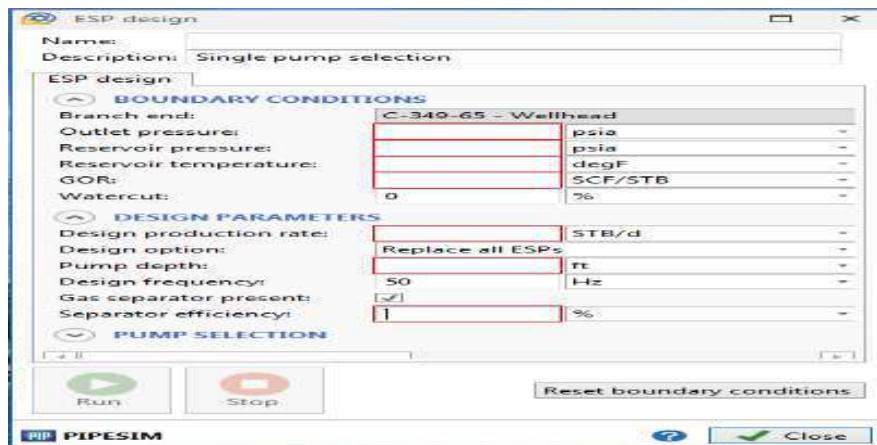


Fig. 6: Visual Studio Community 2017 Start Page

Now click on New Project under Start to launch the New Project window, as shown in Figure 7.

A COMPARATIVE STUDY BETWEEN PIPESIM SIMULATION MODEL AND SOFTWARE APPROACH FOR ESP DESIGN

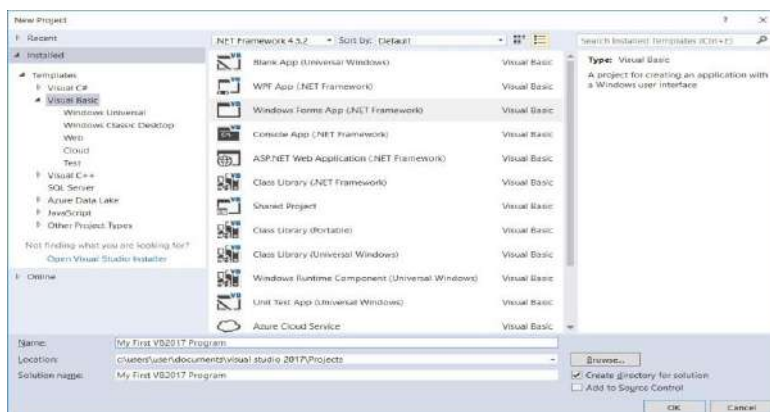


Fig. 7: New Project Window

Results and Discussion

If the data is reliable, the design of an ESP system is usually not too difficult. Before beginning the design procedure, it must be determined that sufficient well data is available.

1. ESP Design for Productive Well of Sarir field

1.1. Input Data and Information

General Information

Location C-NOTRTH GC-6
 Field & Lease Sarir-65
 Well Name C-349H-65
 API Well Reg. # 37.7

Well and electric submersible pumping system data are presented in the Table 1.

Table 1: Required data of Well C-349H-65 for reservoir, fluid and desired conditions and mechanical data

Reservoir Data		Fluid Data		Desired Conditions	
Static Reservoir pressure SBHP	2520 psi	Current Production rate	180 BFPD	Desired Production rate	580 BFPD
Bubble Point Pressure	520.3 psig	Water Cut	0 %	Frequency	50 Hz
Productivity Index	0.5 STB/D/psi	Oil Gravity	37.7 API	Wellhead Pressure	350 psig
Gas Oil Ratio	112 SCF/STB	Specific Gravity of Water	1.14	Pump Setting Depth	6577 ft
Bottom hole temperature	230°F	Specific Gravity of Gas	0.85		
Perforation Intervals MD	9183-10817 ft	Specific Gravity of Oil	0.8363		
Perforation Depth	9175ft	Wellhead Pressure	350 psig		
oil volume formation factor (B _o)	1.140 bbl./STB				
water volume formation factor (B _w)	1.040bbl/STB				
Datum Depth	8756 ft				
Mechanical Data (Casing Data)					
OD Size (inch)	ID Size (inch)	Weight lbm/ft	Roughness	Length, ft	
13.375	12.515	61	0.00065	3185	
9.625	8.835	40	0.00065	8042	
3.5	2.992	9.3	0.00065	6473.6	

2. ESP Design by Hand Calculations

However, these calculations include the following:

1. Calculating Producing Pressure and Pump Intake Pressure
2. Gas, Oil, and Water Calculations
3. TDH calculations
4. Calculate minimum pump depth
5. The Selection of ESP Pump
6. The Selection of ESP Motor
7. The Cable Selection
8. The transformer selection

The results of hand calculations are presented in Table 2.

3. Building a Base Model for Well C-349H-65

The physical model is the first step in modeling any well. Building the physical model, as depicted in Figure 8, entails introducing all of the well items from the source to the sink. The reservoir, completion, tubing, and well head are the only items modeled in this case.

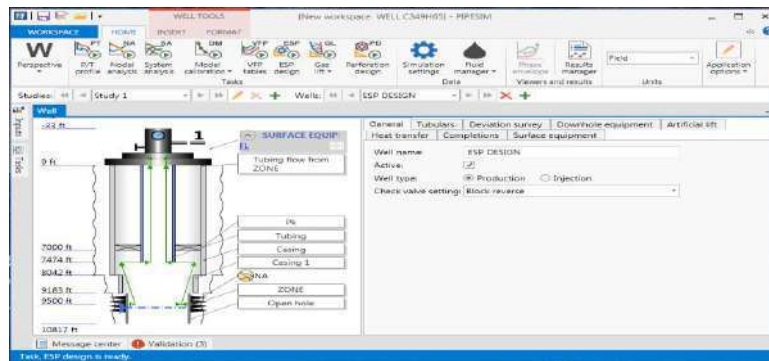


Fig. 8: Physical Model for C-349H-65

Pipesim generates a production profile for the hypothetical well based on the input parameters. Because the well is weak producing oil, it must be considered uneconomical. (Figure 9)

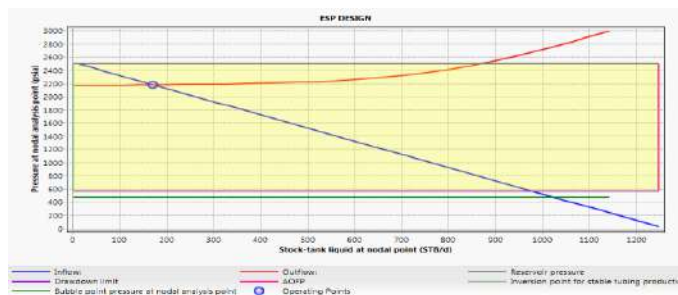


Fig. 9: Well C-349H-65 with no artificial lift (weak intersection between IPR and VLP “situation today”)

A full workover is required to implement gas lift or ESP in the well. ESPs are built into the tubing, and the well lacks side pockets that would allow wireline installation of gas lift valves. PIPESIM simulations, on the other hand, use the current well completion. The model includes the inner and outer diameters of casings, tubings, and liners. The inner diameter of restrictions such as the

A COMPARATIVE STUDY BETWEEN PIPESIM SIMULATION MODEL AND SOFTWARE APPROACH FOR ESP DESIGN

downhole safety valve is also taken into account. The inside roughness of the tubing and casing is 0.00065 inch.

3.1.1. Modeling the Well C-349H-65 with ESP

Selections of equipment start with pump section, a list of pumps matching the design criteria is used for choosing the most suitable pump and number of stages is calculated for a given frequency. Pump list includes the maximum and minimum recommended rates of the pumps. While selecting the pump unit it was desired to find the closest rate at peak efficiency to the theoretical rate. An equipment data base is available in the programs' features. Once the design of the production system completed appropriate equipment can be chosen from that data base. The pump design data were entered into the Pipesim database using the ESP design conditions, and the Select Pump button was clicked, which filtered the pump database for all the pumps that met the design criteria (Figures 10 & 11). The model uses these coefficients to calculate pump curves (Figure 12), allowing one to simulate for any condition.

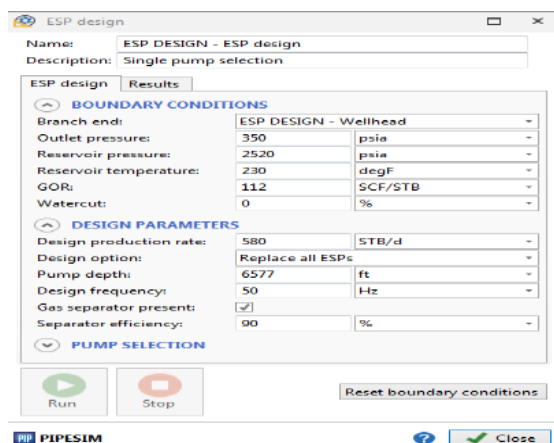


Fig. 10: ESP Design input layout

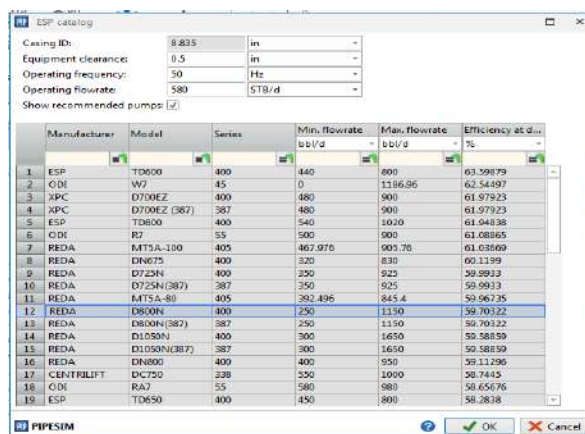


Fig. 11: ESP input pump selection layout

3.1.2. ESP Design Using Pipesim Model

Following are ESP design parameters obtained using Pipesim simulation.



Fig. 12: Well C-349H-65 ESP design parameters obtained using software simulation

4. ESP Design Using Software approach

Characteristic features and properties of ESP design can be determined by using software program as mentioned previously, and the results are illustrated in Figures 13 through 15.

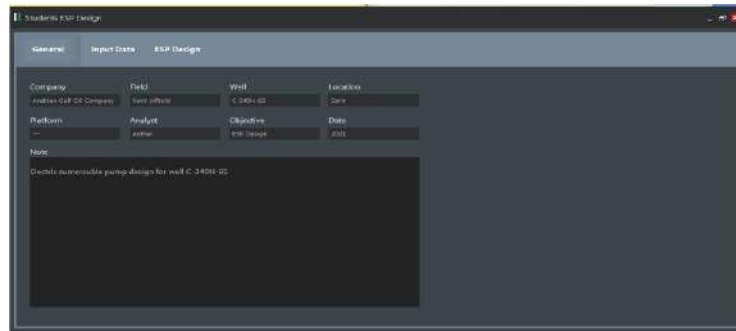


Fig. 13: The first step of software program for calculations

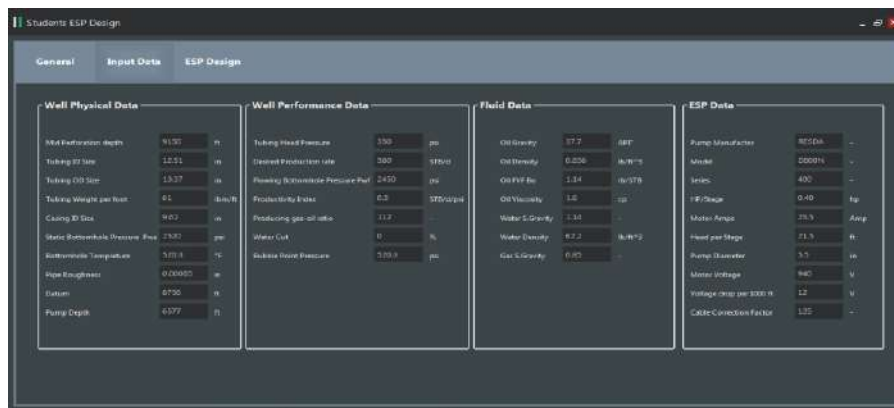


Fig. 14: The second step of software program for calculations

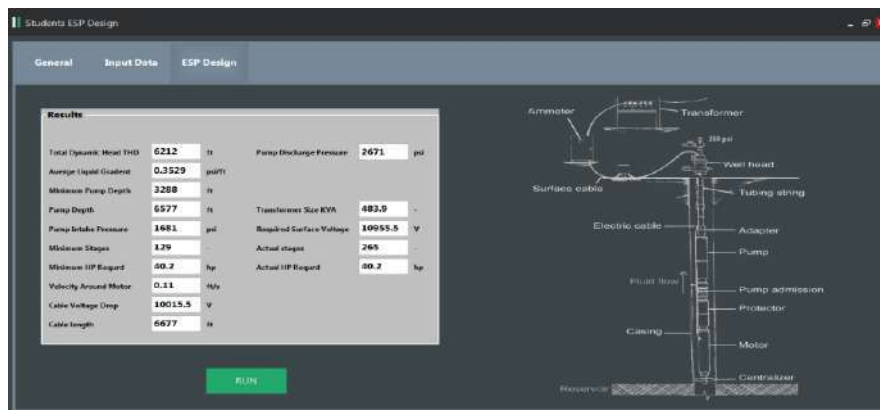


Fig. 15: The third step of software program for calculation

At throughput of production rate, from chart in Figure 16 we can get the pumping head per stage, horse power an ESP efficiency (Table 2).

A COMPARATIVE STUDY BETWEEN PIPESIM SIMULATION MODEL AND SOFTWARE APPROACH FOR ESP DESIGN

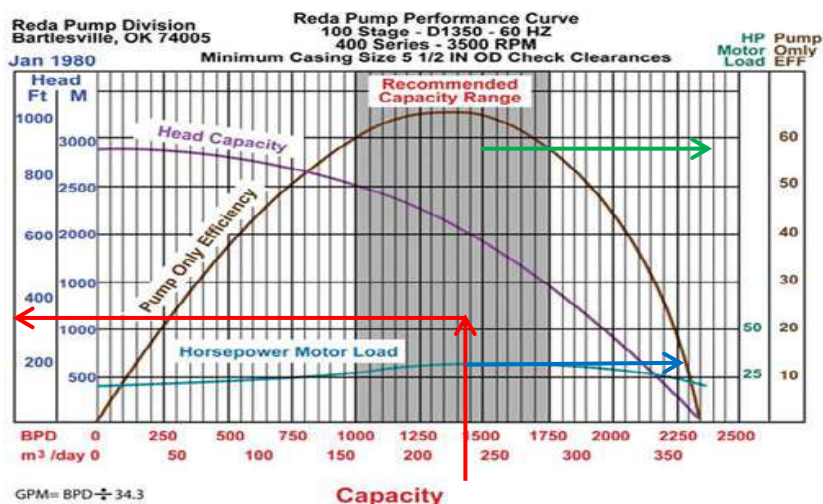


Fig. 16: Estimation parameters of ESP design

Table 2: ESP design results for well C-349-H-65

Parameters	Hand calculations	Pipesim model	Software approach
Pump Type	D800N	D800N	D800N
Series	400	400	400
No. Stages	269	262	265
Efficiency %	62	61.02	63.0
Horse Power	52	35.60	40.2
PIP (psi)	420	619	568
TDH (ft)	6450	5936	6212
Design Frequency, Hz	50	50	50

The ESP system horse power is the pump horse power plus the gas separator horse power. Since gas separator is installed, the system horse power is the pump's which the sum of horse power of each stage. This submersible pump needs 269 numbers of stages. The power required is about 52 hp.

We notice a high number of required stages (269 stages) in the proposed design, so we need to put down two pumps (Tandem Pumps) of the same design, i.e. D800N, to cover the number of required stages, a high operating point, and to maintain the pump's longest run life.

Because the series of down-hole motors are available different in power rating, therefore the chosen motor should be with next available power rating higher horsepower than the calculated horse power which was considered in selecting the motor. The motor horse power required a form hand calculation is 57 HP and as a result the chosen motor power rating is 62.5 (Table 3).

Table 3: The proposed motor parameters, selected cable characteristics and desired surface power data for well C-349-65

Motor Parameters		Cable Characteristics		Desired Surface power	
Manufacturer	REDA	Manufacturer	REDA	Surface Voltage ,Volts	1090
Series	562	Type	Redahot	Transformer, KVA	68
Type	S	Size	2 Cu	Frequency, Hz	50
Name Plate Power, HP	62.5	Shape	Round		
Name Plate Voltage, Volts	1000	Conductor Type	Solid		
Name Plate Current, Amps	36	Maximum Conductor Temperature, °F	300		
Design Frequency, Hz	50	Voltage Drop	90		
Length	7.1 ft	Frequency, Hz	50		
Weight	534 lbm				
Fluid Velocity, ft/sec	0.2				
Well Fluid Temperature, °F	230				

Figure 17 depicts a comparison between some ESP design parameters for the investigated oil well. It is obviously from this comparison between hand calculations, Pipesim model and software approach that there is no much difference between them, except the pressure intake pump (PIP). Accordingly, the software approach can be applied for ESP to achieve the requirements of production rates.

5. Production Performance (Well C-349H-65)

The wells produce significantly more than in the ESP case and in the base case (no artificial lift). The total liquid rate of the well is well within the pump's operating range, between the minimum and best efficiency line. This means that there is still plenty of room for more fluid. Figure 18 depicts the production point, which is the point at which the VLP and IPR curves intersect.

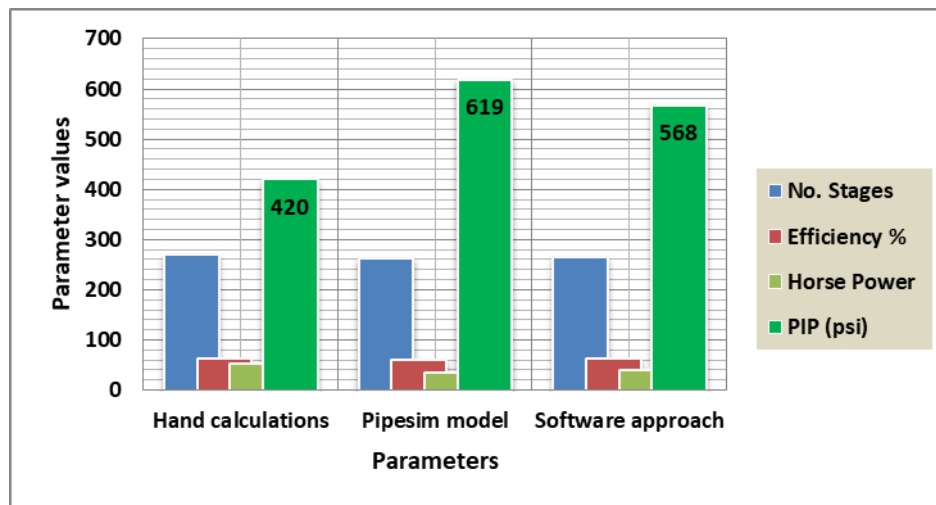


Fig. 17: A comparative bar chart for ESP design

A COMPARATIVE STUDY BETWEEN PIPESIM SIMULATION MODEL AND SOFTWARE APPROACH FOR ESP DESIGN

The intersection of IPR and VLP in Figure represents the operating point of 580 STB/day achieved by ESP installation.

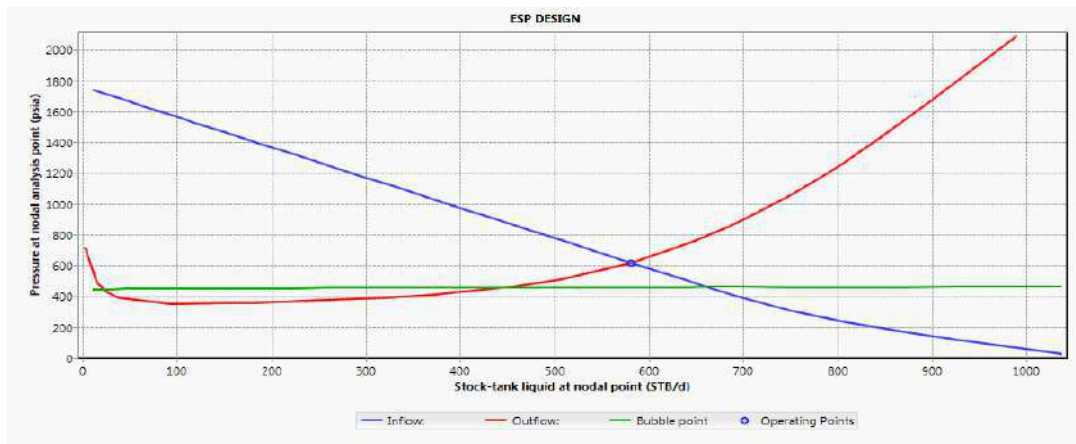


Fig. 18: Effect of ESP design on inflow and outflow curves (intersection of IPR and VLP)

Figure 18 shows that, designing ESP have improved VLP curve and it also made improvement in the well performance and it made liquid production rate to increase to 580 STB/day. Furthermore, designing an ESP can also be applied when the well cannot flow and the reservoir pressure is low. Regarding well C-349H, before in Figure 9, it was shown that when the reservoir pressure decreased, there was Weak (not desired) flow inside the well, but as it is shown Figure 18 after setting an ESP inside the well, the designed ESP provided enough pressure for the well to start to flow.

Figure 19 shows three different operating frequencies for the designed ESP in order to see how the well production performance will respond to those frequencies.

It is shown in Figure 19, when the operating frequency for the designed ESP increased from 30 to 40 to 50 and to 60 Hertz, the well performance has also increased, and it will facilitate the achievement of the production rate. On the other hand, when the operating frequency was reduced to 40 Hertz, a lesser performance was observed in well C-349H-65.

From all the figures shown above, it is observed that the intersection of inflow and outflow satisfy the condition when oil is produced. The intersection of each intake curve with the IPR plotted above is to show a comparison of flow rates provided or not provided by ESP methods.

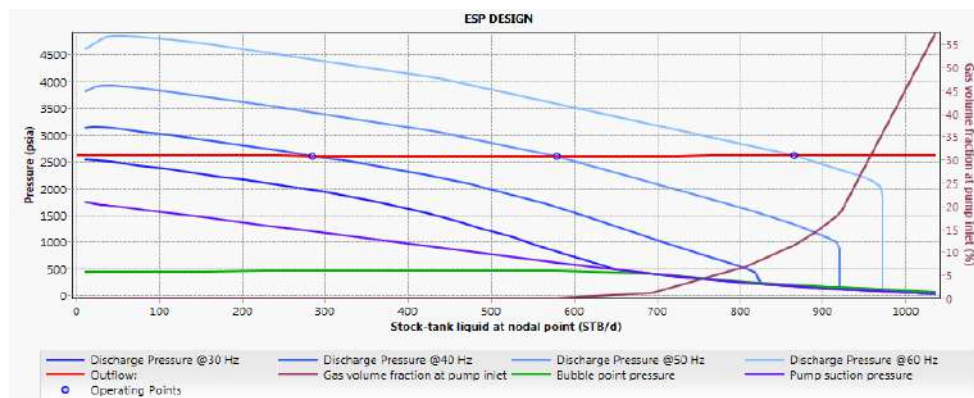


Fig. 19: Effect of changing ESP operating frequency Performance Plot

Figure 20 present the effect of ESP on oil production performance for well C 349H-65. There is a sharp increase in the liquid production as the ESP installed with efficiency of 62 %. Thereafter the liquid production starts to stabilize and reaches a maximum rate of approximately 580 BFPD. Currently the well is stabilized at production rate of 680 BFPD with 0 % water-cut and 110 GOR (SCF/STB).

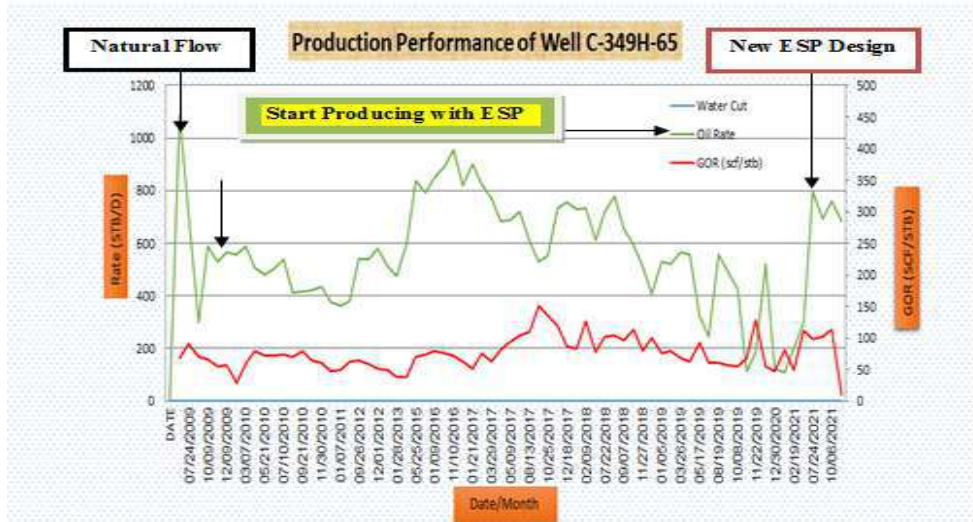


Fig. 20: Production performance of Well C-349H-65

Figure 21 illustrates the production history of well with cumulative oil production in April 2021 was estimated at 1.174 MM bbls and without water produced through the life yet, as when the first ESP applications were started. It doesn't notice any rise of the water cut was. The new ESP design was installed after the well stop to produce (No flow) on June 2021. The design has been developed to overcome the production engineering challenges which have been encountered following the commencement production from the stage oil field .Using ESP Method as kind of artificial lift will contribute in increasing the cumulative of oil to achieve the production to economical rate as show in Figure 21.

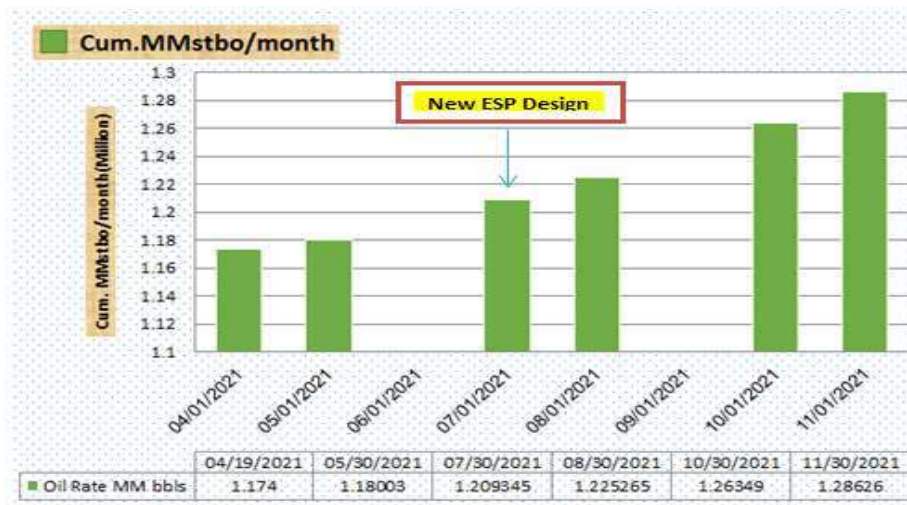


Fig. 21: Cumulative oil production of Well C-349H-65

A COMPARATIVE STUDY BETWEEN PIPESIM SIMULATION MODEL AND SOFTWARE APPROACH FOR ESP DESIGN

However, the incremental in oil production has been even as of the date 30/11/2021 that has been 106.230 Mbbls , and so on the price of Crude oil as average price recently 60 Dollars (\$) (106.230 *60=6373800 (6.37 MM \$) that is economically beneficial and the cumulative of oil production increased which is 1.28626 MMbbls. The pump continues to produce until today.

To summarize, Table 4 provides detailed information for each base case scenario:

Table 4: Economic base case condition

Scenario	Minimum Economic Production Rate Produced	Maximum Economic Production Rate Produced
Without ESP	110 (oil production)	289 (oil production)
With ESP	280 stb/d at 2520 psia at 40 Hz with 0 %WC	860 stb/d at 2520 psia at 60 Hz with 0 %WC

Looking at the review of each base case scenario, it can be concluded that has giving higher volume of oil production, ESP is considered as more economical. However, ESP is an effective method to lift large volume of oil.

Conclusion

To produce to its full potential and have a successful run life, an ESP well must have optimal production conditions, which means that ESP down-hole and surface equipment must be properly designated and operated. After developing detailed simple calculations, the best design was implemented using Pipesim model and software approach.

The production issue was analyzed and designed an electrical submersible pump (ESP) system that addresses the well data and issues. Furthermore, ESP is the best artificial lift method for wells with high water cut and pressure depletion. Installing ESP allows for more oil to be recovered in less time, improving field economics. Because there are numerous ESP system designs on the market today, we must design the most optimum and ideal ESP systems as stated in the study objective from the start. ESP is, once again, a dynamic displacement, multistage centrifugal turbine pump connected by a short shaft to a downhole electrical motor powered by a cable that extends to the surface. As in the production engineer discipline, it is necessary to design the best ESP system possible in order to extend the life of ESP components, which are a costly investment for the company. Based on this research, it is possible to conclude that the REDA D800N pump is the best submersible pump for Well C-349H-65, with a pump efficiency of approximately 62 %; from the designing this well can return to produce at desired flow rate 580 STB/Day.

Recommendations

The findings of this study are pertinent to the objectives. If we broaden the scope of this work to include more parameters, we will be able to study a lot more theories while also gaining more knowledge in the artificial lift discipline. Here, I'd like to make a few recommendations to future work for this research:

- Because variable speed drive (VSD) technology was not used during the design procedure for ESP applications, the study could be improved by including that option in ESP systems.

- Future research on this topic may include progressive cavity pumps, as that artificial lift method is available to use in those fields.
- Conduct a cost-benefit analysis for each ESP component. We can then select the most efficient and economical option.
- ESP design and installation in extreme conditions, such as a gassy well.

References

- [1] Matthew, A., "Artificial Lift Systems" Artificial Lift Methods and Surface Operations PGE 482 Lecture Note, 2013.
- [2] Clegg, J. D., Bucaram, S. M. and Hein, N. M., Jr.: "Recommendations and Comparisons for Selecting Artificial-Lift Methods." JPT, December 1993, 1128–67.
- [3] Brown, K.E., "The Technology of Artificial Lift Methods", Vol. 2b, Penn Well Publishing Company, Tulsa, Oklahoma, 1980.
- [4] Brown, K.E., "The Technology of Artificial Lift Methods", Vol. 4, Penn Well Publishing Company, Tulsa, Oklahoma, 1984.
- [5] Gabor Takacs, "Electrical submersible pump manual: design, operations, and maintenance", published by Elsevier Inc., 2018.
- [6] Arabian Gulf Oil Company: Sarir Field Data base and History File.
- [7] AGOCO, Sarir 3D Seismic Interpretation Areas 1 and 3 Final Report (Preliminary Draft) - Reply to Geo Quest Comments from Sarir Reservoir Engineering Group, 1998.
- [8] Guo B and et al, " Petroleum Production Engineering, A Computer-Assisted Approach Publisher: Elsevier Science & Technology Books, 2007.
- [9] Schlumberger, (2017). Pipesim.
<https://www.software.slb.com/products/pipesim>.
- [10] Schlumberger, (2017). PIPESIM user Manual.

GEOTHERMAL ENERGY EXTRACTION FROM ABANDONED OIL WELLS AS SUSTAINABLE SOURCES OF RENEWABLE ENERGY

Ibrahim M. Abou El Leil^a & Fatema Omar^b

^aPetroleum Engineering Department, Faculty of Engineering, Tobruk University

^bRenewable Energy Department, Tobruk Academy for Higher Study

Abstract:

Geothermal energy is a natural heat inside the Earth accumulated in rocks and fluids filling rock pores and crevices. As a renewable source of energy and heat, it is an alternative to conventional raw materials. Geothermal energy is an important emerging renewable technology that has the potential to provide power from a virtually unlimited reserve worldwide. Geothermal energy is an increasingly attractive source for renewable energy that can be used for power generation, heating/cooling, and a multitude of other direct-use applications. Each application will require a distinctive fluid temperature, with power generating operations requiring the highest fluid temperatures. Globally, the installed geothermal energy capacity has burgeoned from 1,300 MWe in 1975 to more than 10,715 MWe in 2015. The rise in geothermal energy is due to a higher global energy demand, rising energy prices, new innovative technologies, and the growing need to reduce the anthropogenic impact on the environment. Geothermal energy is important since it is accessible from anywhere in the world, provides a steady source of thermal power, is easily scaled up, and can be switched on/off to follow demand. The main disadvantage of extracting geothermal energy from deep resources is the high capital cost needed to drill the well(s), in order to access the higher temperature resources. The drilling phase is the most significant financial burden on any geothermal investment. It takes on average up to 70% of total investment costs, often making a potential investment economically unprofitable. Retrofitting abandoned petroleum wells for the purpose of geothermal extraction is a novel idea due to the fact that petroleum wells are generally deep enough to access high temperature strata. This paper has been carried out on twelve abandoned wells at Nafora oil field to look forward for reutilizing them by using subsurface data related to thermal characteristics of the produced water. The results of this data revealed that it could be used this produced water as a heat source due to their large quantity and higher enthalpy with an

average value 243.58°C that can be used in different applications particularly electricity generation by using flash steam power plant to sustainable development.

Keywords: Geothermal, renewable energy, abandoned, oil wells, sustainable, resources.

Introduction

Geothermal energy is one of the most talked about sources of renewable energy in today's world. With the correct technology, it has the potential to be regarded as the best source of effective, clean and not to mention renewable energy. "Geothermal" energy is basically the energy of the earth, stored in it in the form of thermal energy. This thermal energy is generated due to the geothermal gradient. So, in order to reduce the costs of building a geothermal energy generation plant, the use of abandoned wells in this regard, in order to exploit the geothermal gradient of the earth, has been a widely considered idea. After the production of petroleum from a reservoir through a well reaches its limit, i.e. no more production is possible through the same well, it is decided that the well should be plugged or abandoned. This process is done with the minimum costs required and under any government regulations [1]. An abandoned well is of no use to the company which owns the already exploited oilfield where the said well is present. So, if we can somehow use the fact that very deep wells are present at high temperature conditions to our need, then the otherwise useless abandoned wells can be used to our advantage. For the generation of energy, the abandoned wells are to be "rebooted" before any kind of energy generation can be done. After the "rebooted" work is over, a circulating fluid (water) is pumped down to produce saturated steam, which rises up the well, and is used to run a turbine placed above the ground [2].

There are three types of petroleum wells potentially capable of supplying geothermal energy for electric power generation: (a) a producing oil or gas well with a water cut, (b) an oil or gas well abandoned because of a high water cut, and (c) a geopressured brine well with dissolved gas. This paper considers the basic technical and economic aspects of power generations from the second type of wells and presents case of estimating the available power capacity of a typical well (or a group of wells) in each of the above categories.

The power capacity of wells in the first category is determined primarily by the production rate and temperature of the produced water, ambient temperature, and conversion efficiency of the geothermal power plant. The factors that control the wellhead temperature of the produced fluid are: formation temperature, well depth, well diameter and production rate.

The power capacity of an abandoned oil well depends on: (a) production rate and temperature of the produced water, (b) ambient temperature, (c) conversion efficiency of the geothermal power plant, (d) water salinity, (e) gas content in the produced fluid and (f) the characteristics of the equipment used to generate power from the produced water. The production rates of water from such a well depend on the hydraulic properties of the formation, gas content (dissolved as well as free) in the formation water, formation temperature and pressure, and well design. It is shown that the well's productivity could be substantially improved by working it over; both pumping and self-flowing the well are considered [3].

Objectives of Study

The main objectives of this study are:

1. Potentiality of retrofitting abandoned oil wells for the purpose of geothermal extraction.
2. Looks forward to reutilizing these abandoned wells by using subsurface data related to thermal characteristics of rock sequence.
3. The needs of power generation sources.

Location of Study

This study was performed on twelve abandoned oil wells that denoted by GX1 to GX12 at Nafora oilfield (Figure 1).

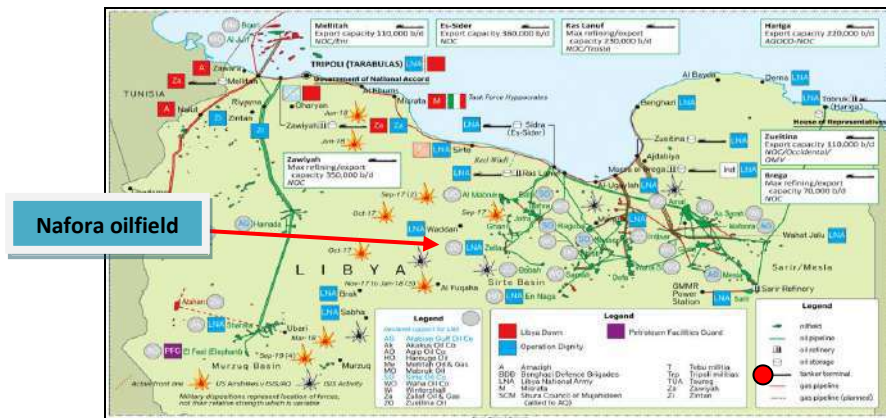


Fig. 1: A map shows Nafora oilfield [4]

Literature Review

The bulk of the research that has been carried out on capturing geothermal energy from abandoned petroleum wells has focused on open loop designs. The open loop designs for existing petroleum wells seek to repurpose the oil/gas reservoir as a groundwater geothermal reservoir. Many countries have supported research and work into retrofitting an abandoned petroleum resource with an open loop geothermal design, including: AI, China [6], Croatia [7], Hungary [8], New Zealand [9], Poland [10], and the United States [11].

The overwhelming majority of the research that has been done concerning closed loop designs retrofitted to abandoned wells has been with u-tube and double pipe heat exchangers. There is only one available paper concerning the modeling of a u-tube heat exchanger in an abandoned well, and it focuses on the need to model the convective heat flow in the porous medium surrounding the borehole [12]. There are only a few published papers concerned with the retrofitting of double pipe heat exchangers to existing petroleum wells, namely: Kujawa et al. [13], Davis & Michaelides [14].

Types and Applications of Geothermal Resources

There are many different classifications of exploitable geothermal resources with different possible applications. The general method for extracting energy from a geothermal system is to pump a fluid which has been heated by hot rock to the surface and then to utilize the heat energy within that fluid. These can vary widely in chemical composition of hydrothermal fluid, amount of fluid present, geothermal gradient of the region, and many other factors. No two sites are exactly alike, but many share similar characteristics which are useful for classifying them. Among the most important of these are water dominated fields, steam dominated fields, and hot dry rock systems. Economic viability is a very important part of determining whether or not a geothermal resource is worth developing, and is generally measured by the comparative cost of production of a unit of energy against other sources.

1. Water Dominated Fields

Water dominated fields are defined by pressure within the fluid reservoir coming mostly from liquid water. These fields can exist at both high and low temperatures, though higher

temperature fields require high pressure to maintain the liquid phase of the water [15]. There are two primary types of water dominated fields; hot water fields and wet steam fields [15]. The distinction between these two is that hot water fields have water in a liquid phase as a result of low temperature while wet steam fields have water in a liquid phase as a result of high pressure. Typically, the reservoirs of hot water fields will contain liquid water at all depths due to low temperature and geothermal gradient. Hot water fields are generally only considered economically viable if they are near the surface, have low salt content, and have high flow rates [15].

2. Geothermal Power from Co-Produced Oil Field Waters

Water produced along with the oil or gas from petroleum well is separated and injected back. If this water has adequate temperature, it is possible to extract the geothermal energy in the produced water and generate electric power before injecting the water. No drilling cost would presumably be involved in such a power generation project from co-produced water from active oil or gas wells compared to a conventional geothermal project, where the drilling cost typically amounts to 30% to 40% of the total capital cost of a project. As such, the capital cost for a geothermal project from co-produced water can be significantly lower per kilowatt generation capacity than for a conventional geothermal project. The potential power capacity of an oil or gas well, or a group of wells, producing with a water-cut would be determined primarily by the following variables:

1. Water production rate from the well or a group of wells;
2. Temperature of the produced water at the collection point or the outlet of the storage tank;

3. Water salinity;
4. Ambient temperature at the site via the temperature of the water; and
5. Conversion efficiency of the power plant to be used.

3. Production of Geothermal Water from Abandoned Oil Well

The power capacity of an abandoned water well depend on: (a) production rate and temperature of the produced water, (b) ambient temperature, (c) conversion efficiency of the geothermal power plant, (d) water salinity, (e) gas content in the produced fluid, and (f) the characteristics of the equipment used to generate power from the produced water. The production rate of water from such a well depends on the hydraulic properties, temperature and pressure of the formation, gas content (dissolved as well as free) in formation water, and well design.

4. Steam Dominated Fields

Steam dominated fields are high temperature high pressure underground reservoirs of steam and other gases. Steam dominated fields are generally much higher in temperature than wet steam fields. Because of the pressure necessary to maintain this body of steam, an impermeable cap rock covering the reservoir is necessary to prevent rapid depressurization and loss of the fluid within the reservoir [15, 16].

5. Hot Dry Rock

Hot dry rock systems are regions of rock without a usable amount of fluid within them for geothermal energy capture by typical methods. Frequently, the lack of a fluid reservoir is a result of the rock being impermeable. These systems present the largest source of

potentially accessible geothermal energy as they are not limited to fault zones and can be found almost anywhere at sufficient depth. The cost of drilling geothermal wells increases exponentially with depth, however, meaning that these systems will not always be economically viable for energy production [17].

6. High Temperature Applications

High temperature geothermal resources are typically used for the generation of electricity. This is accomplished through the use of heat and pressure differences between the reservoir and the surface to produce mechanical energy which is then used to turn turbines and generate electricity. Steam-based electricity generation is the most effective geothermal electricity generation method as steam dominated fields tend to contain the most energy per unit volume of fluid [15].

7. Low Temperature Applications

A geothermal resource is considered low temperature if its temperature is less than 150°C [17]. Low temperature geothermal resources are typically used for direct heating in both industrial and non-industrial applications. This energy is used in industrial settings for increasing the efficiency of refining ore, dehydration of foods, drying of timber, and many other applications [17]. The use of geothermal heat pumps can warm houses in the winter, cool them in the summer, and provide hot water year round [17].

Classification of Geothermal Resources

Geothermal resources can be sorted into low, intermediate and high enthalpy sources according to the average reservoir temperature (Table 1). The classes of resources depicted

in Table 1 are divided subjectively according to different authors. The authors cited do not reach a consensus on the appropriate temperature ranges to describe each class of geothermal resource. In the case of a closed loop geothermal system the corrected bottomhole temperature of the borehole is a good estimate of the reservoir temperature, as the geothermal reservoir is the surrounding rock mass in this case.

Table 1: Classification of geothermal resources by temperature

Resource	Muffler & Cataldi, 1978 [18]	Hochstein, 1990 [19]	Benderitter & Cormy, 1990 [20]	Haenel, 1988, Dickson, 1990 [21]
Low enthalpy	<90°C	<125°C	<100°C	≤150°C
Intermediate enthalpy	90–150°C	125–225°C	100–200°C	---
High enthalpy	>150°C	>225°C	>200°C	>150°C

Temperature and enthalpy alone cannot define properly the state of geothermal fluids.

Despite that fact, geothermal resources are classified as high–enthalpy fields (temperature is >150°C), medium– enthalpy fields (temperature is 90°C to 150 °C) and low–enthalpy fields (temperature is < 90°C) according to their reservoir fluid temperatures (Figure 2) [18, 22, 23].

Geothermal Energy Power Plants

Geothermal power plants use *hydrothermal* resources (both water and heat) that come from either dry steam or hot water. These hydrothermal resources are accessed by drilling wells into the earth and then pumping steam or hot water to the surface. The hot water or steam powers a turbine–generator that generates electricity. The three types of geothermal power

plants are *dry steam*, *flash steam*, and *binary cycle* [24]. Choice of design is determined by the geothermal resource and load demands of the application. Using geothermal energy reduces global dependence on fossil fuels and provides continuous baseload electricity. Geothermal power plants have the potential to regulate electricity production throughout the day from 100 percent operational capacity to only 10 percent depending on the load demands which reduces production of unused energy [25]. In 2013, the global geothermal capacity was estimated at 11,700 MW [26].

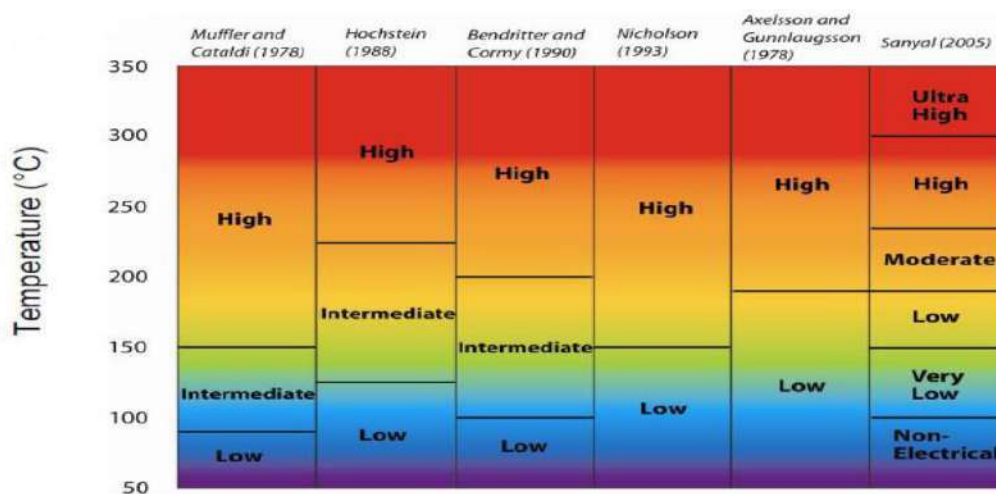
Types of Technology

Several types of geothermal power plants exist.

1. Dry steam power plants

The geothermal fluid is high–pressure superheated dry steam at between 180°C and more than 350°C that drives the turbine of a Rankine cycle power plant. The resulting cooled water is injected back into the geothermal reservoir.

Dry steam plants use hydrothermal fluids that are primarily steam. The steam goes directly



to a turbine, which drives a generator that produces electricity (Figure 4).

Fig. 2: Classification of geothermal resources Temperature/Enthalpy

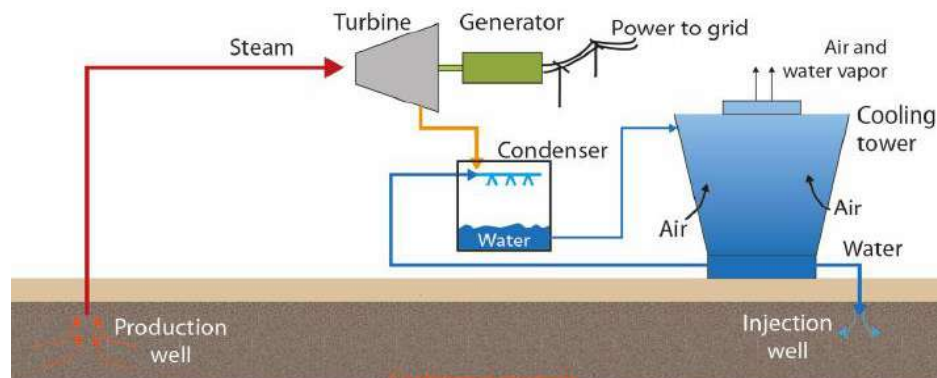
2. Flash steam power plants

The geothermal fluid is high-pressure wet steam (a mix of water and steam) at a temperature above 180°C. The dry saturated steam, separated from the wet steam in one or two flash tanks, drives the turbine of a Rankine cycle power plant.

Flash steam power plants tap into reservoirs of water with temperatures higher than 180°C. As it flows, the fluid pressure decreases and some of the hot water boils or "flashes" into steam. The steam is then separated at the surface and is used to power a turbine/generator unit (Figure 5).

3. Hydrothermal power plants

The geothermal fluid is high-pressure water at 125°C to 180°C. To efficiently convert in



electricity the heat recovered from water at such temperatures, a binary cycle power plant is required [27].

Fig. 3: Dry steam power plant

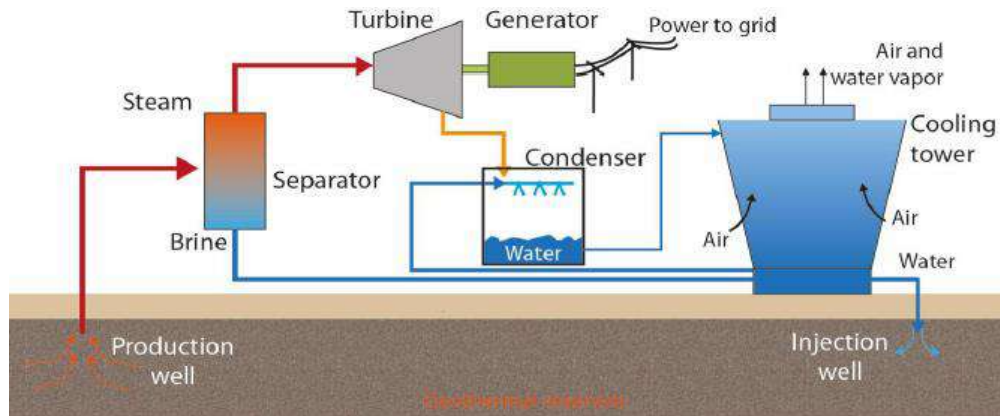


Fig. 4: Flash steam power plant

4. Binary cycle power plants

Operate on water at lower temperatures of about 105–180°C. These plants use the heat from the geothermal water to boil a working fluid, usually an organic compound with a low boiling point (Figure 6).

Geothermal Gradient

Table 2 was made based on the analyses of foreign experience. The table shows the value of the generated power depending on the depth of a well and the amount of the geothermal gradient.

Table 2: Geothermal gradient impact on the output power [29–33]

Authors	Power output, kW	Well depth, m	Geothermal gradient, °C/km
Kujawa et al. [33]	140	3950	25
Bu et al. [34]	59.4	4000	38
Cheng et al. [35]	239	6000	50

Noorollahi et al. [36]	133	3861	29.6
	364	4423	31.2
Wight and Bennett [37]	217	6000	50

From the Table 2 it is clear that the higher value of the geothermal gradient, the more power can be generated, while the value of the depth doesn't influence so much.

Using Abandoned Oil Wells for Geothermal Energy Production

Petroleum wells are abandoned when the oil/gas reservoir becomes unfeasible for petroleum extraction, or when a dry hole is drilled. Dry holes refer to drilled wells that contain an economically unfeasible amount and/or type of petroleum deposit.

Retrofitting abandoned petroleum wells for the purpose of geothermal extraction is a novel idea due to the fact that petroleum wells are generally deep enough to access high temperature strata. The depth of exploratory and developmental wells for crude oil, natural gas, and subsequent dry holes drilled in the US from 1949 to 2008 range from 945 to 2560 meters feet in depth [38]. The US has drilled over 2.5 million petroleum wells since the 1950's and has the highest rate of oil and gas drilling in the world [39], therefore the US provides a satisfactory illustration of the characteristics of petroleum wells worldwide.

Both open loop and closed loop geothermal systems can be retrofitted to existing petroleum wells. An open loop system will make use of the petroleum reservoir, as long as there are at least two wells drilled into the same resource. The groundwater can be stored in the abandoned reservoir in order to gain heat from the surrounding rock, before being extracted

from existing petroleum well. Closed loop geothermal systems adapted to a single well are generally designed to use either a u-tube heat exchanger or a double pipe heat exchanger.

Conditions Necessary for Using Wells in Oil Fields

For geothermal purposes the oil field should have:

1. Suitable wells for extraction of geothermal heat
2. Stable temperature and constant production rate
3. Suitable conditions for reinjection of reservoir waters
4. Potential users of the heat energy nearby

To determine the above-mentioned geological conditions (stable temperature and production) it is necessary to determine:

1. Structural and stratigraphic conditions of the reservoir and the field (usually well-known at this stage of production)
2. Exploitation conditions (types of fluids, water conditions, run of production, fluctuation of pressures)
3. Geothermal parameters (temperature gradient, reservoir pressure, possibility of production)
4. Hydrological conditions (examination and description of infiltration zone and outcrop area of reservoir horizons, direction of fluid migration, fluid chemistry).

Results and Discussion

1. Case Study

This study was performed on twelve abandoned oil wells at Nafora oilfield as shown in Table 3. These wells exhibit a variation for their depths, fluid production, pressure, temperature and temperature gradient as well as salinity content.

According to Lindal [28] for the different applications of geothermal fluids as a function of their temperature, modified after ORC denotes the Organic Rankine Cycle, the studied wells can be used for a wide range of applications because of high temperature sources that ranges from 170°C (Well GX9) and 246°C (Well GX10) with an average value 214.58°C (Table 3). These applications involve conventional electricity generation, electricity generation by ORC or Kallina Cycle, heat generation and heat pumps.

2. Geothermal Resources Classification

According to the reported authors [18–21] the geothermal resources can be classified by temperature into different enthalpy as presented in Table 4.

Table 3: Abandoned oil wells at Nafora oilfield

No.	Abandoned oil wells	Depth (ft)	Pressure (psia)	Fluid production, Q (bb/d)	Fluid temperature (°C)	Temperature gradient (°C/100 m)	Salinity (ppm)
1	GX1	9700	2571	1300	210	3.89	215514
2	GX2	8990	3053	1500	218	3.75	406012
3	GX3	8980	3521	1192	245	3.65	306514
4	GX4	9328	3949	1000	200	3.84	202132
5	GX5	10250	4690	2619	216	3.91	412415
6	GX6	9753	4431	1147	232	3.78	331542
7	GX7	9320	3390	5010	200	3.70	221150
8	GX8	7120	4380	23774	180	3.66	55800
9	GX9	8760	3390	8000	170	3.71	60260
10	GX10	10285	4200	1500	246	3.98	177840
11	GX11	9900	3095	859	238	3.84	222130
12	GX12	9276	4012	5000	220	3.76	120000
\bar{x}	-----	9305.17	3723.5	4408.15	214.58	3.79	227609

$N_2 = 1.70$ mol. % $CO_2 = 20.8$ % , GOR = 500 scf/STB, Viscosity = 1.08 cp

Table 4: Classification of geothermal resources by temperature of investigated wells

No.	Abandoned oil wells	Fluid temperature (°C)	Muffler & Cataldi, 1978	Hochstein, 1990	Benderitter & Cormy, 1990	Haenel, 1988, Dickson, 1990
1	GX1	210	High enthalpy	Low enthalpy	High enthalpy	High enthalpy
2	GX2	218	High enthalpy	Low enthalpy	High enthalpy	High enthalpy
3	GX3	245	High enthalpy	High enthalpy	High enthalpy	High enthalpy
4	GX4	200	High enthalpy	Low enthalpy	Intermediate enthalpy	High enthalpy
5	GX5	216	High enthalpy	Low enthalpy	High enthalpy	High enthalpy
6	GX6	232	High enthalpy	Intermediate enthalpy	High enthalpy	High enthalpy
7	GX7	200	High enthalpy	Low enthalpy	Intermediate enthalpy	High enthalpy
8	GX8	180	High enthalpy	Low enthalpy	Intermediate enthalpy	High enthalpy
9	GX9	170	High	Low enthalpy	Intermediate	High

			enthalpy		enthalpy	enthalpy
10	GX10	246	High enthalpy	High enthalpy	High enthalpy	High enthalpy
11	GX11	238	High enthalpy	High enthalpy	High enthalpy	High enthalpy
12	GX12	220	High enthalpy	Low enthalpy	High enthalpy	High enthalpy

3. Flash Steam Power Plants

Tap into reservoirs of water with temperatures higher than 180°C. As it flows, the fluid pressure decreases and some of the hot water boils or "flashes" into steam. The steam is then separated at the surface and is used to power a turbine/generator unit. Hence the average temperature value of the produced water is 214.58°C the flash steam power plants can be used for electricity generation besides the other different applications.

On the other hand, the output power based on geothermal gradient of studied wells and according to the authors [33–37] can be determined as reported in Table 5.

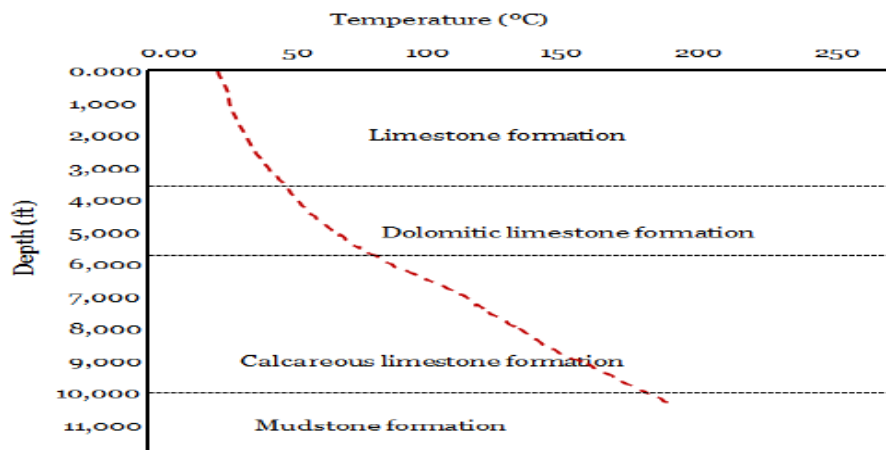
Table 5: Output power based on geothermal gradient of studied wells

No.	Abandoned oil wells	Depth (ft)	Temperature gradient (°C/100 m)	Authors				
				Kujawa et al.	Bu et al.	Cheng et al.	Noorollahi et al.	
				Power output, kW				
1	GX1	9700	3.89	140	59.4	---	364	364

GEOTHERMAL ENERGY EXTRACTION FROM ABANDONED OIL WELLS AS SUSTAINABLE SOURCES OF RENEWABLE ENERGY

2	GX2	8990	3.75	140	---	---	364	364
3	GX3	8980	3.65	140	---	---	364	364
4	GX4	9328	3.84	140	59.4	---	364	364
5	GX5	10250	3.91	140	59.4	---	364	364
6	GX6	9753	3.78	140	59.4	---	364	364
7	GX7	9320	3.70	140	---	---	364	364
8	GX8	7120	3.66	140	---	---	364	364
9	GX9	8760	3.71	140	---	---	364	364
10	GX10	10285	3.98	140	59.4	---	364	364
11	GX11	9900	3.84	140	59.4	---	364	364
12	GX12	9276	3.76	140	59.4	---	364	364

However, the geothermal gradient of the investigated oil wells throughout the different rock



formations is illustrated in Figure 13.

Fig. 5: shows the geothermal gradient in rock formations

Figure 14 shows the temperature versus depth correlation for some wells. It is obviously that is a linear relationship between the two variables.

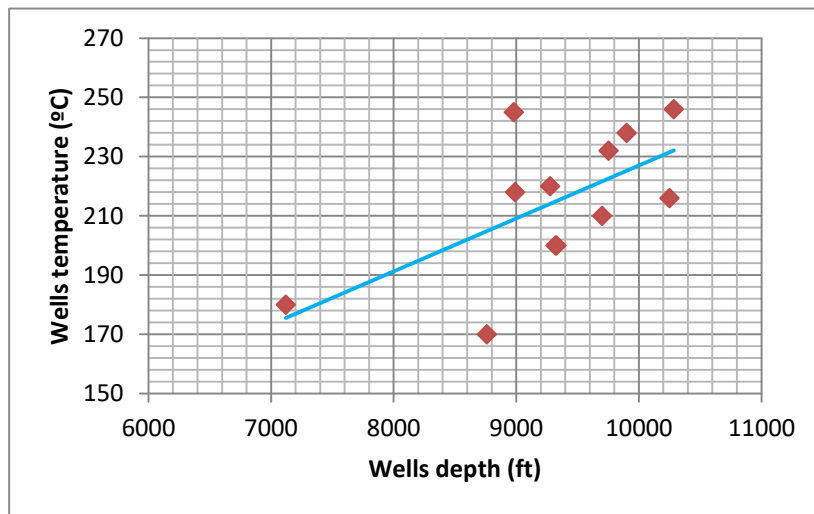


Fig. 6: Temperature versus depth of investigated abandoned wells

Conclusion

In the light of the previous study the following conclusions could be drawn:

1. Geothermal energy is a powerful natural resource with the potential to shape the future of human society.
2. It is relatively clean and environmentally friendly when compared to present energy sources such as fossil fuels.

3. Geothermal resources can be used in a wide variety of applications from melting snow on sidewalks to generating electricity.
4. Geothermal heat pumps are a high-efficiency means of heating and cooling buildings.
5. Geothermal energy still requires a lot of efforts in research, to optimize technology, to use new materials and to reduce the investment risk.
6. Geothermal energy may provide an important contribution to energy efficiency in many processes (most of our energy consumption is for heating)
7. Geothermal energy is very suitable for co-production, co-generation, hybrid systems. We need to test and prove it.
8. The obtained data from the investigated produced water from oil wells indicated high temperature source of a wide range (170–246°C) with an average value 214.58°C.
9. According to this temperature, it could be applied in a wide range of uses particularly the electricity generation using flash steam power plants.
10. Classification of geothermal resources by temperature of investigated wells can be classified into low, intermediate and high enthalpy based on different authors.

References

- [1] Gluyas, J.G.; Auld, A.; Adams, C.; Hirst, C.M.; Hogg, S.; Craig, J. (2018) Geothermal potential of the global oil industry. In Renewable Geothermal Energy Explorations; Ismail, B.I., Ed.; InTechOpen: London, UK.
- [2] Provoost, M.; Albeda, L.; Godschalk, B.; van der Wer_, B.; Schoof, F. (2019) Geothermal energy use, country update for The Netherlands. In Proceedings of the European Geothermal Congress, The Hague, The Netherlands, 11–14 June 2019; Available online:

<http://europeangeothermalcongress.eu/wpcontent/uploads/2019/07/CUR-19-Netherlands.pdf> (accessed on 25 June 2020).

[3] Watson, S.M.; Falcone, G.; Westaway, R. (2020) Repurposing hydrocarbon wells for geothermal use in the UK: A preliminary resource assessment. In Proceedings of the World Geothermal Congress, Reykjavik, Iceland; Available online:

<https://pangea.stanford.edu/ERE/db/WGC/papers/WGC/2020/16024.pdf>

(accessed on 25 June 2020).

[4] Arab Petroleum Investments Corporation, APICORP (2018) Apricorp Energy Research, Vol. 03 No. 14 | November 2018.

[5] Lund, J. W., Freeston, D. H., & Boyd, T. L. (2005). World-Wide Direct Uses of Geothermal Energy 2005. Proceedings World Geothermal Congress 2005. Antalya, Turkey: Geo-Heat Center, Oregon Institute of Technology.

[6] Wei, Y., Wang, F., & Ren, B. (2009). Drainage and production by using geothermal in Huabei oil region. Renqiu: Huabei Oilfield Production Technology Research Institute.

[7] Kurevija, T., & Vulin, D. (2011). High Enthalpy Geothermal Potential of the Deep Gas Fields in Central Drava Basin, Croatia. Water Resour Manage, 25:3041–3052.

[8] Kujbus, A. (2007). New Approach in the Hungarian Geothermal Exploration. Transactions – Geothermal Resources Council, 605–607.

[9] Reyes, A. (2007). Abandoned oil and gas wells –a reconnaissance study of an unconventional geothermal resource. Avalon: GNS Science Report.

[10] Barbacki, A. P. (2000). The Use Of Abandoned Oil And Gas Wells In Poland For Recovering Geothermal Heat. Proceedings World Geothermal Congress 2000. Kyushu – Tohoku, Japan: Polish Academy of Science, Mineral and Energy Economy Research Institute.

[11] Limpasurat, A. (2010). Artificial Geothermal Energy Potential of Steam-flooded Heavy Oil Reservoirs. Texas A&M University.

[12] Ghoreishi-Madiseh, S. A., Hassani, F. P., & Al-Khawaja, M. J. (2012, May 13–17). A novel technique for extraction of geothermal energy from abandoned oil wells. Retrieved January 2013, from World Renewable Energy Forum:

https://ases.conferenceservices.net/programme.asp?conferenceID=2859&action=prog_titles

[13] Kujawa, T., Nowak, W., & Stachel, A. A. (2005). Analysis of the Exploitation of Existing Deep Production Wells for Acquiring Geothermal Energy. Journal of Engineering Physics and Thermophysics, Vol. 78, No. 1, pg 127–135.

- [14] Davis, A. P., & Michaelides, E. E. (2009). Geothermal power production from abandoned oil wells. *Energy* 34, pp. 866–872.
- [15] Barbier, Enrico (2002) Geothermal energy technology and current status: An overview.” *Renewable and Sustainable Energy Reviews*: 3–65. Print.
- [16] Rybach, Ladislaus (2007) Geothermal Sustainability Assessment Framework.” *GHC Bulletin* : 1–7. Print.
- [17] Mock, John E., Jefferson W. Tester, and P. Michael Wright. (1997) “GEOHERMAL ENERGY FROM THE EARTH: Its Potential Impact as an Environmentally Sustainable Resource.” *Annual Review of Energy and the Environment*: 305–356. Print.
- [18] Muffler, P., & Cataldi, R. (1978). Methods for regional assessment of geothermal resources. *Geothermics*.
- [19] Hochstein, M. (1990). Classification and assessment of geothermal resources. Rome, Italy: In: Dickson MH and Fanelli M (eds) *Small Geothermal Resources*. UNITAR/UNDP Centre for Small Energy Resources.
- [20] Benderitter, Y., & Cormy, G. (1990). Possible approach to geothermal research and relative cost estimate. Rome, Italy: In: Dickson MH and Fanelli M (eds) *Small Geothermal Resources*. UNITAR/UNDP Centre for Small Energy Resources.
- [21] Haenel, R. R. (1988). *Handbook of Terrestrial Heat-Flow Density Determination*. Dordrecht, Netherlands: Kluwer Academic.
- [22] Sanyal, S.K. (2010). On minimizing the levelized cost of electric power from Enhanced Geothermal Systems. In: *Proceedings World Geothermal Congress 2010*, Bali, Indonesia, 25–30 April 2010. Available at: www.geothermal-energy.org/pdf/IGAstandard/WGC/2010/3154.pdf.
- [23] Rybach, L. (2010). Legal and regulatory environment favourable for geothermal development investors. In: *Proceedings World Geothermal Congress 2010*, Bali, Indonesia, 25–30 April 2010. Available at: www.geothermal-energy.org/pdf/IGAstandard/WGC/2010/0303.pdf.
- [24] “Geothermal Energy and the Environment (2016) Energy Explained. US Energy Information Administration, 7 Dec. 2015. Web. 14 Dec. 2016. http://www.eia.gov/Energyexplained/?page=geothermal_environment
- [25] “How Geothermal Energy Works.” UCSUSA. Union of Concerned Scientists, 22 Dec. 2014. Web. 4 Oct. 2016. http://www.ucsusa.org/clean_energy/our-energy-choices/renewable-energy/how-geothermal-energy-works.html#.V-sdm_krK00

- [26] Eliasson, E. T., Thorhallsson, S., & Steingrímsson, B. (2011). Geothermal Power Plants. Santa Tecla, El Salvador: UNU-GTP and LaGeo.
- [27] Duffield, W. A., & Sass, J. H. (2004). Geothermal Energy– Clean Power from the Earth's Heat. Denver, Colorado, United States: U.S. Geological Survey. Retrieved from <http://pubs.usgs.gov/circ/2004/c1249/>
- [28] Lund, J.W., (2006) 'Chena Hot Springs', Geo-Heat Center Quarterly Bulletin, Vol. 27, No. 3 (September), Klamath Falls, OR, USA, pp. 2–4.
- [29] Kujawa, T. W. Nowak, and A. A. Stachel (2006) Utilization of existing deep geological wells for acquisitions of geothermal energy // Energy. Vol. 31, №5. – P. 650 – 664.
- [30] Bu, X. Ma, W. and Gong Y. (2014) Electricity generation from abandoned oil and gas wells // Energy Sources. Vol. 36, №9. – P. 999 – 1006.
- [31] Cheng, W. T. Li, Y. Nian, and K. Xie (2014) Evaluation of working fluids for geothermal power generation from abandoned oil wells // Applied Energy. Vol. 118. – P. 238 –245.
- [32] Noorollahi, Y. M. Pourarshad, S. Jalilinasrabady (2015) Numerical simulation of power production from abandoned oil wells in Ahwaz oil field in southern Iran // Geothermics. Vol. 55. – P. 16 – 23. URL: <http://www.sciencedirect.com/science/article/pii/S0375650515000127> (accessed: 13.01.2018).
- [33] Wight and N. M. Bennett N. S. (2015) Geothermal energy from abandoned oil and gas wells using water in combination with a closed wellbore // Applied Thermal Engineering. Vol. 89. – P. 908 – 915. URL: <http://www.sciencedirect.com/science/article/pii/S1359431115005840> (accessed: 13.01.2018).
- [34] Kujawa T., Nowak, W. and Stachel A. A. (2008) Utilization of existing deep geological wells for acquisitions of geothermal energy // Energy. Vol. 37, №8. – P. 5840 – 600.
- [35] W. Cheng, T. Li, Y. Nian, and K. Xie Evaluation of working fluids for geothermal power generation from abandoned oil wells // Applied Energy. – 2014. – Vol. 118. – P. 238 – 245.
- [36] Y. Noorollahi, M. Pourarshad, S. Jalilinasrabady Numerical simulation of power production from abandoned oil wells in Ahwaz oil field in southern Iran // Geothermics. – 2015. – Vol. 55. – P. 16 – 23. URL: <http://www.sciencedirect.com/science/article/pii/S0375650515000127> (accessed: 13.01.2018).

[37] N. M. Wight and N. S. Bennett Geothermal energy from abandoned oil and gas wells using water in combination with a closed wellbore // Applied Thermal Engineering. – 2015. – Vol. 89. – P. 908 – 915

URL:<http://www.sciencedirect.com/science/article/pii/S1359431115005840>

(Accessed: 13.01.2018)

[38] EIA. (2012, October). Petroleum and Other Liquids. Retrieved January 2013, from US Energy Information Administration:

http://www.eia.gov/dnav/pet/pet_crd_welldep_s1_a.htm

[39] Baker Hughes. (2012). Baker Hughes Investor Relations. Retrieved January 2013, from http://investor.shareholder.com/bhi/rig_counts/rc_index.cfm?showpage=int

Patient-Centred Pain Management of Fibromyalgia Patient following a Holistic Approach and Mantra (Keep Calm and Forget the Pain)

Wanes, Benlama*

Physiotherapy Department , Faculty Of Medical Technology/ Bani Waleed University, Libya

Abstract: Fibromyalgia is a musculoskeletal disease, which can result in chronic pain and it's an arthritis-related condition which impairs joints and soft tissues. The most common symptom is pain, which is severe and sharp sometimes and dull ache the other time in the form of constant and relentless aches all over the body. This study is based on a 45 years old male university professor who is diagnosed and suffering from fibromyalgia for the last 2.5 years (Appendix). Symptoms of fibromyalgia started gradually and in later stages, he use to feel chronic muscle pain, especially in the neck and back area. Other symptoms were muscle spasms, and moderate to severe fatigue, and he used to feel low energy during his routine work. Due to fibromyalgia, his daily life, interaction with family and job is badly affected and this paper will discuss a bio-psychosocial approach for holistic management of his symptoms and improve his quality of life by employing a mantra i.e. Keep calm and forget the pain.

Keywords: (Bio-Psychosocial, Chronic Pain, Fibromyalgia, Holistic Management, And Physiotherapy.)

Introduction

Pain is a disagreeable sensation that everybody recognizes and feels in life (Cervero 2012)[1]. It's an unpleasant sensory and emotional experience associated with actual or potential tissue damage or described in terms of such damage (IASP 2012)[2]. Nay and Featherstonehaugh (2012)[3] stated that pain is emotional, cognitive and physical and further classified it as somatic, visceral, neuropathic, centrally generated or peripherally generated and has a protective effect. According to Griensven, Strong and Unruh (2014)[4], many factors are considered in the perception of pain in an individual, such as age, gender, level of disability, and social and culture. Considering these statements about pain, it can be understood that pain is a complex phenomenon and its management need good knowledge and skills and implication of bio-psychosocial approach to read outpatient views and eradicate misinterpretations.

Fibromyalgia is one of the diseases, which can result in chronic pain and it's an arthritis-related condition which impairs joints and soft tissues. The most common symptom is pain, which is severe and sharp sometimes and dull aches the other time in the form of constant and relentless aches all over the body (Chandler 2011)[5]. Other symptoms are dizziness, fatigue, morning stiffness, mood fluctuations, numbness or tingling in hands or feet, irritable bowel syndrome, temporomandibular joint disorder, and sleep disturbance which severely affects the quality of life and escalate stress level in fibromyalgia patients (Wallace and Wallace 2003)[6].

The etiology of fibromyalgia syndrome (FMS) is unknown, but research suggests that improper sleep, changes in muscles metabolism due to decreased blood flow and thus low oxygen flow to the muscles can

be a reason, peripheral or central sensitization, hormonal and genetic influences and abnormalities in the autonomic nervous system could be the possible reasons (Ostalecki and Tamler 2009)[7].

There is no diagnostic test for fibromyalgia; however American College of Rheumatology proposed a classification criterion in 1990 based on widespread pain and tender points (ACR 2013)[8]. A revised version of this diagnostic criterion was published in 2010 which confirms the presence of FMS in a patient if he has 11 out of a total of 18 tender points and 2010 ACR criteria were found to be an effective diagnostic tool in most of the patients with FM (Hauser and Wolfe 2012) [9]. However, another study by Stahl (2009)[10] suggests that tender points are not an adequate tool to diagnose fibromyalgia.

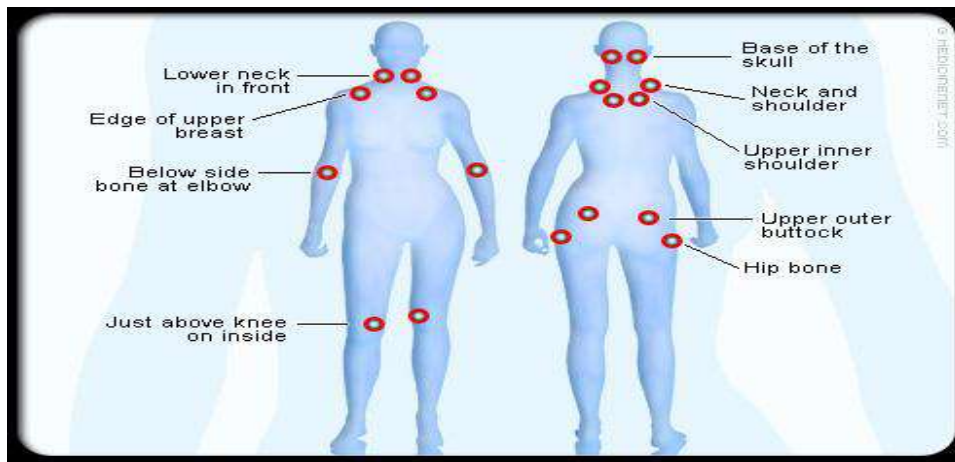


Fig. 1: FM pain area

Pain Mechanism:

Persistent or intense nociception in FM patients can lead to transcriptional and translational changes in the spinal cord and brain resulting in central sensitization and pain (Staud and Rodriguez 2006)[12]. Woolf (2011)[13] explained that central sensitization is a state of CNS which is related to the evolution and preservation of chronic pain. Once central sensitization has been established, only minimal nociceptive input is required for the maintenance of the chronic pain state. Other factors, including pain-related negative affect, have been shown to significantly contribute to clinical fibromyalgia pain.

According to Staud (2006)[12], the mechanism behind this central sensitization in FM patients is due to the hyper-excitability of dorsal horn neurons (DHS) whose primary function is to transmit nociceptive stimulus to the brain. As a result, low-intensity input generates a high level of nociceptive stimulus to the brain and pain perception.

Prolonged stimulus from A-δ and C fibers depolarize DHS which leads to the removal of magnesium ions from NMDA-gated ion channels followed by an influx of extracellular calcium ions and the production of nitric oxide resulting in the diffusion of DHS. According to Latremoliere and Woolf (2009)[14], nitric oxides facilitate the increased release of excitatory amino acids and substance P and make dorsal horn neurons hyper-excitabile. Due to this reason, any physical activity done by FM patient gets amplified in the spinal cord and results in heightened pain perception. Evidence also suggests that stress, depression, poor sleep

and interpersonal and environmental factors also contribute to and result in central sensitization in FM patients (Hansson 2014)[15].

In research by Gosselin et al. (2010)[16], they suggested that glial cells dorsal horn enhance hypersensitivity in chronic pain. In central sensitization, many factors like nitric oxide and substance-P result in the activation of glial cells. Once activated, these cells facilitate the release of inflammatory cytokines, substance-P, nitric oxide, L-1RA, IL-6 and IL-8, prostaglandins, excitatory amino acids, and ATP, which in response, further increase the discharge of excitatory amino acids and substance P from the A- δ and C afferents that synapse in the dorsal horn and also enhance the hyper-excitability of the dorsal horn neurons. It is affirmed by Gosselin et al. (2010)[16] that Pro-inflammatory levels of cytokines IL-1RA, IL-6 and IL-8 are increased in FM patients supporting the role of glial cells in central sensitization in FM patients. Furthermore, many types of muscle abnormalities like ragged red and moth-eaten fibres have been seen in FM patients which appear due to repeated micro-trauma and contribute to continuous muscle tension and pain and also lead to ischemia that results in central sensitization of pain (Staud 2011)[17].

According to Griensven, Strong and Unruh (2014)[4], continuous nociceptive stimulus from nociceptive specific neurons put an inhibitory impact on wide dynamic range neurons (receives stimulus from nociceptive specific neurons and A β fibres) and alters the way A β fibres transmit the information which results in low excitability by nociceptive stimulation. These all changes lead to low threshold stimulus, unable to pass through DHS and finally not being felt. Furthermore, prolonged stimulation from A δ and C fibres depolarizes DHS and forces magnesium ions to leave N-methyl-D-aspartate (NMDA), leading to calcium influx. Calcium influx results in nitric oxide production which thus leads to irregular liberation of substance P. This increased amount of substance P not only results in more and more calcium intrusion but also keeps dorsal horn neurons (DHN) hyperactive. Due to continuous calcium intrusion and hyperactive DHN, low-intensity stimulation is presumed as high intensity and the body feels too much pain even when the stimulus is not painful. When this state is preserved for a long time, it changes into central sensitization. Glutamate and substance P also play role in preserving central sensitization by lowering down threshold of AMPA and NMDA receptors which leads to hyper-intrusion of calcium ions which keep gates open and keep DHN hyper-active.

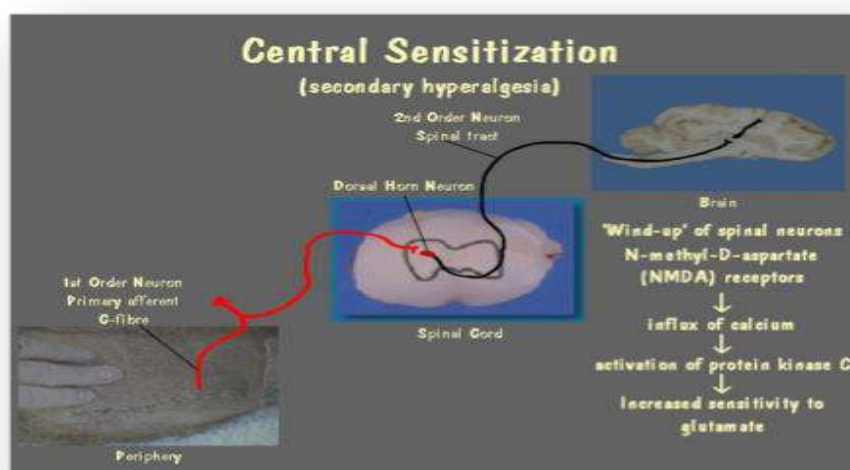


Fig.2 : Central sensitization

Meeus and Nijs (2007)[18] confirm the presence of temporal summation or wind-up in FM patients. Wind-up is a central spinal mechanism in which repetitive noxious stimulation results in a slow temporal summation that is experienced in humans as increased pain. During this process, NMDA receptors are activated, which results in calcium intrusion which activates nitric oxide release. Nitric oxide in response escalates the release of sensory neuropeptides especially substance-P from presynaptic neurons, therefore contributing to the development of hyperalgesia and maintenance of central sensitization. They also confirmed that there is no evidence for peripheral sensitization as the cause of hyperalgesia as there is no real tissue damage in FM patients.

The presence of central sensitization and wind-up phenomena in FM patients is confirmed by various researchers like Griensven, Strong and Unruh (2014)[4], Woolf (2011)[19], Yunus (2007)[20], Staud, Robinson and Price (2007)[21]. Furthermore, a most recent systematic review by Cagnie et al. (2014)[22] also confirms decreased functional connectivity in the descending pain-modulating system and increased activity in the pain matrix related to central sensitization in FM patients. Additionally, distress, depression, disturbed sleep and social and environmental factors could be converted into pain and central sensitization through forced hyperactivity of the sympathetic component of the stress response system (Lavin 2012)[23].

Management of Mr. B's Case

Managing pain, improving sleeping, reducing fatigue, increasing muscular strength, and giving patients confidence to deal with all psychological and social issues are the prime aims for my fibromyalgia-affected patient. Addressing these issues is critical to avoid further depression and permanent disability. The management plan will be pharmacological and non-pharmacological. Furthermore, a mantra i.e. "Keep calm and forget the pain" will be wielded in the management plan.

Pharmacological Management:

FM patients are advised with pain-killers, opioids, muscle relaxants, sleep medicines and anti-depressants depending upon disease severity and present condition of the patient (NHS Choices 2014; Shipley 2014) [24,25]

Pain Killers:

Paracetamol is a commonly advised and used pain-killer in FM patients and found to be effective (Shipley 2014)[25]. NSAIDs are also advised for FM patients but current evidence suggests that NSAIDs are not useful in the long-term management of fibromyalgia as it's not an inflammatory disease (Slim, Villademoros and Calandre 2013)[26].

Opioids:

The most commonly prescribed opioid to FM patients is tramadol, however, long-term use of opioids is discouraged as it leads to physical dependence and can produce a chronic pain state (NIH 2014)[27]. Recent studies like Merchant et al. (2013)[28], Tripathi, Shah and Sharma (2012)[29], and Slim, Villademoros and Calandre (2013)[26] recommend that paracetamol with tramadol combination was found to be effective in FM patients.

Anti-depressants and sleep medicines:

Pregabalin is a well-tolerated drug that remarkably improves sleep for FM patients (Arnold et al. 2014) [30]. Patients who used Pregabalin reported less body pain as well (Roth et al. 2012)[31]. As mentioned above, stress and depression contribute to and result in central sensitization in FM patients so it should be addressed. Antidepressant treatment for fibromyalgia was effective in patients with and without major depression, but the functional response was greater in depressed patients (Marsa et al. 2011)[32].

Non- Pharmacological Management:

Fibromyalgia is a pathology, which can't be dealt with by medicines only. It needs a holistic approach by a multi-disciplinary team (Griffith and Zarrouf 2008)[33]. Below is the list of research-suggested non-pharmacologic options which can be utilized in FM patients.

Physiotherapy, exercises and daily life activities:

Exercise interventions have excellent effects on fatigue and sleep dysfunction in FM patients (Russell et al. 2014)[34]. Exercise reduces depressive symptoms in FM patients. Patients doing proper exercise training achieve the largest antidepressant effects (Herring et al. 2012)[35]. Physiotherapy, aerobic and strength training to improve physical fitness and function, reduce fibromyalgia symptoms, and improve quality of life in FM patients (Busch et al. 2011)[36]. Furthermore, my patient can be encouraged to take part in his favorite sports activities as he will not be bored, and will forget his pain and depression for some time which will help in decreasing muscle stiffness and pain. Water-based exercises with intensity and duration on patient preferences also have good effects on pain, sleep and fatigue (Hauser et al. 2010)[37].

Cognitive behavioral therapy (CBT):

CBT has shown excellent results in managing psycho-social, emotional and behavioral issues in FM patients (Slim, Villademoros and Calandre 2013)[26]. Although CBT doesn't have direct effects on pain,

fatigue and sleep disturbances, it improves depressed mood and helps FM patients to cope with the pain. CBT in individuals with FM improves insomnia which, in turn, lowers the intensity of pain (Edinger et al. 2013)[38].

CBT in FM patients includes educating and discussing with the patient about pain, pain mechanism, fibromyalgia itself, sleep, diet, exercises and necessary changes that the patient should bring into his lifestyle. He should be explained the process for which he is the victim i.e. central sensitization. This will help him to recognize that it's his perception that is causing more fatigue, pain and sleeplessness and will help him to cope with it. (Lee et al. 2014)[39]. CBT is talking with the patient about his problems, fears, psychosocial issues and giving confidence and knowledge to the patient and making him ready to fight with the thing which is more in his thoughts and exists to a very little extent in reality.

CBT can also be attributed to talking therapy which helps people identify and develop skills to change negative thoughts and behaviours and make them enough confident and strong to cope with pain; sleep disorder, stress and psycho-social issues. (Koffel, Koffel and Gehrman 2014)[40].

Mind-body therapy / Mindfulness-Based Stress Reduction (MBSR):

MBSR is an 8-week group program teaching mindfulness meditation and mindful yoga exercises and is developed by Jon Kabat-Zinn. (Cash et al. 2014)[41]. MBSR is found to be an effective treatment for a variety of psychological problems and is especially effective for reducing anxiety, depression, and stress. It improves the ability to cope with the symptoms of fibromyalgia, as well as improving quality of life and decreasing pain severity (Thiagarajah et al. 2014)[42].

Balneotherapy / Spa therapy:

Balneotherapy or SPA therapy is defined as the treatment of disease by bathing, usually at a SPA resort, using hot or cold water rich in minerals, and including also drinking, inhalation, massage through moving water, mud-baths, relaxation, or stimulation. (Gutenbrunner et al. 2010)[43]. In a systematic review by Terhorst and Schneider (2012)[44], it was concluded that balneotherapy provides beneficial effects in patients with fibromyalgia by increasing blood flow which dissolves and eliminates toxins from the body, bringing improved nourishment to stiff fibromyalgic muscles. It also encourages FM patients who can't do full weight-bearing exercises on land; can exercise vigorously and comfortably in water (Ablin, Häuser and Buskila 2013)[45].

Massage Therapy:

According to Sanchez et al. (2011)[46], massage and myofascial release techniques improve pain and quality of life in patients with fibromyalgia. It increases the number of sleep hours and decreases substance-P levels which have a significant role in contributing to the development of hyperalgesia and maintenance of central sensitization (Field et al. 2002) [47]. A recent systematic review by Li et al. (2014) [48] confirms that massage therapy with a duration of ≥ 5 weeks has immediate beneficial effects on improving pain, anxiety, and depression in FM patients. High-quality evidence for the effectiveness of manual therapy in FM patients is concluded by Clar et al. (2014)[49].

Furthermore, deep oscillation vibration massage (Kraft, Kanter and Janik 2013)[50] and Shiatsu massage (Yuan, Berssaneti and Marques 2013) [51], Tai-Chi (Raman , Mudedla and Wang 2014)[52] are safe and well tolerated in FM patients and improve pain intensity, pressure pain threshold, sleep quality, and quality of life.

Ayurveda Treatment

Ayurveda therapy is non-inferior to conventional treatment in patients with severe FM and has significant improvements in the Fibromyalgia impact questionnaire (FIQ) (Kessler et al. 2013)[53].

Craniosacral Therapy (CST):

It's a gentle way of working with the body using light therapeutic touch, aiming to release restrictions around the spinal cord and brain and subsequently restore body function (Jakel and Hauenschild 2012) [54]. CST improves the quality of life of patients with fibromyalgia, reducing their perception of pain and fatigue and improving their night rest and mood, with an increase in physical function.

Role And Importance Of Mantra And Its Implication In The Current Case:

A mantra can be a word, a phrase or a verbal instrument to produce something in one's mind. When you hear something again and again or repeat a rumour, again and again, it can become a reality in your mind (Newman 2014)[55]. It's purely dependent on a mantra user whether to take benefit or damage from it as it's like a fire, which has both destructive and helpful qualities

As the evidence mentioned above suggests that pain in FM patients is centrally sensitized. Its presence is far less than being pictured in FM patients. CBT, educating the patient about FM and pain mechanisms along-with goal setting and following a mantra i.e. "Keep calm and forget the pain" will help the patient to understand the reality. As Newman (2014)[55] suggested, repeating a mantra, understanding it and implementing it can help to wipe out the fake picture of pain in mind, my patient has to understand it. I will have face-to-face sittings with him; will listen to his fears, problems, and psycho-social issues, and then make a short-term and long-term plan. However, following the mantra i.e. "Keep calm and forget the pain" exactly supports the pain mechanism behind his pathology. He should remain calm, try to forget the pain and busy himself with constructive activities.

Holistic Management:

Dealing with FM patient is not a responsibility of a GP or a therapist alone and need a systematic biopsychosocial approach and team effort of the interdisciplinary team comprising a medical consultant, occupational therapist, physiotherapist and psychologist (Dubin 2014) [56]. The patient is already in much stressful condition and needs confidentiality, respect and polite behavior This will encourage him to share his fear and personal problems and social issues with the service provider. Without winning patient confidence, every therapy will fail so patient empowerment and patient-centered care are critical to be employed in FM patients. Furthermore, a discussion session should be done with the patient's employer to reduce the number of hours they work and cooperate with them to adapt to their current job. Employers can be asked to make necessary changes in their office furniture to make patients comfortable and services of the occupational therapist should be acquired to design a more comfortable workstation.

How to measure progress in FM patients?

The Fibromyalgia Impact Questionnaire (FIQ) is an assessment and evaluation instrument developed to measure FM patient status, progress and outcomes. It let service providers assess the clinical effectiveness of interventions being given. It is a self-administered instrument that takes approximately 5 minutes to complete and is a valid and reliable scale (Bennett 2005)[57]

Fibromyalgia Assessment Status (FAS) index is a valid three-item instrument (pain, fatigue and sleep disturbances) that performs at least as well as the FIQ in FM patients, and is simpler to administer and score (Iannuccelli et al. 2011)[58]. Furthermore, Fatigue VAS can be utilized as an assessment tool to measure improvements in fatigue in FM patients (Crawford et al. 2011) [59].

Conclusion:

This study has increased the researcher's clinical reasoning, knowledge and skills and will be more confident in the management of his patient as a physiotherapist. Generally, the treatment plan for fibromyalgia could be combined with a lot of options otherwise the most important point is psychosocial factors and Evidence cited above clearly suggests that the management of FM needs a holistic approach, team effort, patient centered care. These steps along with patient empowerment and educating him clearly and thoroughly about the pathology and convincing him to implement the mantra i.e. "Keep calm and forget the pain" will help to decrease pain, and disability and improve quality of life.

Appendix/Case Study

Mr. B is 45 years old, male university professor, diagnosed with and suffering from fibromyalgia for the last 2.5 years. Being a university professor, he had many sleepless nights and long working days during his career. Symptoms of fibromyalgia started gradually and in later stages, he use to feel chronic muscle pain, especially in the neck and back areas. Other symptoms were muscle spasms, and moderate to severe fatigue, and he used to feel low energy during his routine work. His sleep is also disturbed and he feels stiffness during his gym work and normal walking and in conditions in which he used to be in the same position for longer times i.e. standing during giving lectures and sitting for self-study before lectures etc. His pain becomes worse in the winter season and due to increased pain, fatigue, morning stiffness and stress, he took many leaves from university in the last 2 years.

He uses anti-depressants and tramadol for pain relief. He is under immense stress due to his body pains which have disturbed his daily routine i.e. job, gym workout, hang-out with family, shopping etc. Sleep disturbance notices from the head of the department due to many off days and less interaction with family members and staying away from leisure activities are increasing his stress factor day by day.

Keeping this case study in mind, a pain management strategy will be devised for Mr X in this study, focusing on mantra: (Keep calm and forget the pain).

References

1. CERVERO, Fernando (2012). Understanding Pain: Exploring the Perception of Pain. 1st ed., USA, MIT Press.
2. IASP (2012). IASP TAXONOMY. [online]. Last accessed 15 DECEMBER 2014 at: <http://www.iasp-pain.org/Taxonomy?navItemNumber=576>

3. NAY, R. and FETHERSTONHAUGH, D. (2012). What is pain? A phenomenological approach to understanding. *International Journal of Older People Nursing* , 7 (3), 233-239.
4. GRIENSVEN, Hubert van, STRONG, Jenny and UNRUH, Anita (2014). *Pain: A Textbook for Health Professionals*. 2nd ed., China, Elsevier Health Sciences.
5. CHANDLER, Pati (2011). *Fibromyalgia Basics: A Beginner's Guide*. 1st ed., Oklahoma, Tate Publishing.
6. WALLACE, Daniel J. and WALLACE, J.B. (2003). *Fibromyalgia : An Essential Guide for Patients and Their Families: An Essential Guide for Patients and Their Families*. New York, Oxford University Press.
7. OSTALECKI, Sharon and TAMLER, Martin S. (2009). *100 Questions & Answers About Fibromyalgia*. 1st ed., Sudbury, Jones & Bartlett Learning.
8. ACR (2013). *Fibromyalgia*. [online]. Last accessed 14th December 2014 at: http://www.rheumatology.org/Practice/Clinical/Patients/Diseases_And_Conditions/Fibromyalgia/
9. HAUSER, W. and WOLFE, F. (2012). Diagnosis and diagnostic tests for fibromyalgia (syndrome). *Reumatismo*, 64 (4), 194-205
10. STAHL, Stephen M. (2009). Fibromyalgia—pathways and neurotransmitters. *Human Psychopharmacology: Clinical and Experimental*, 24 (S1), 11-17.
11. QUEIROZ, Luiz Paulo (2013). Worldwide Epidemiology of Fibromyalgia. *Current Pain and Headache Reports*, 17 (8),.
12. STAUD , Roland and RODRIGUEZ, Miguel E (2006). Mechanisms of disease: pain in fibromyalgia syndrome. *Nature Reviews Rheumatology*, 2 (2), 90-98.
13. WOOLF, Clifford J (2011). Central sensitization: Implications for the diagnosis and treatment of pain. *Pain*, 153 (2),.
14. LATREMOLIERE, Alban and WOOLF, Clifford J. (2009). Central Sensitization: A Generator of Pain Hypersensitivity by Central Neural Plasticity. *The Journal of Pain*, 10 (9), 895-226.
15. HANSSON, Per (2014). Translational aspects of central sensitization induced by primary afferent activity: What it is and what it is not. *PAIN*, 155 (10), 1932-1934.
16. GOSELIN, Romain-Daniel, et al. (2010). Glial Cells and Chronic Pain. *The Neuroscientist*, 16 (5), 519-531.
17. STAUD, Roland (2011). Peripheral Pain Mechanisms in Chronic Widespread Pain. *Best Practice & Research Clinical Rheumatology*, 25 (2), 155-164.
18. MEEUS, Mira and NIJS, Jo (2007). Central sensitization: a biopsychosocial explanation for chronic widespread pain in patients with fibromyalgia and chronic fatigue syndrome. *Clinical Rheumatology*, 26 (4), 465-473.
19. WOOLF, Clifford J. (2011). Central sensitization: Implications for the diagnosis and treatment of pain. *PAIN*, 152 (3), 2-15.
20. YUNUS, Muhammad B. (2007). Fibromyalgia and overlapping disorders: the unifying concept of central sensitivity syndromes. *Seminars in Arthritis and Rheumatism*, 36 (6), 339-356.
21. STAUD, Roland , ROBINSON, Michael E. and PRICE, Donald D. (2007). Temporal Summation of Second Pain and Its Maintenance Are Useful for Characterizing Widespread Central Sensitization of Fibromyalgia Patients. *The Journal of Pain*, 8 (11), 893-901.
22. CAGNIE, Barbara , et al. (2014). Central sensitization in fibromyalgia? A systematic review on structural and functional brain MRI. *Seminars in Arthritis and Rheumatism*, 44 (1), 68-75.
23. LAVIN, Manuel Martinez (2012). *Fibromyalgia: When Distress Becomes (Un)sympathetic Pain*. *Pain Research and Treatment*, 2012, 1-6.
24. NHS CHOICES (2014). *Fibromyalgia - Treatment - NHS Choices*. [online]. Last accessed 14 December 2014 at: <http://www.nhs.uk/Conditions/Fibromyalgia/Pages/Treatment.aspx>
25. SHIPLEY, Michael (2014). Chronic widespread pain and fibromyalgia syndrome. *Medicine*, 42 (5), 271-274.

26. SLIM, Mahmoud , VILLADEMOROS, Fernando Rico- and CALANDRE, Elena P. (2013). Current concepts in the treatment of fibromyalgia. *JOURNAL OF SYMPTOMS AND SIGNS*, 2 (4),.
27. NIH (2014). Role of opioids in the treatment of chronic pain. [online]. Last accessed 14th December 2014 at: <https://prevention.nih.gov/programs-events/pathways-to-prevention/workshops/opioids-chronic-pain>
28. MERCHANTE, Ignacio Morón, et al. (2013). Tramadol/Paracetamol Fixed-Dose Combination for Chronic Pain Management in Family Practice: A Clinical Review. *ISRN Family Medicine*, 2013,.
29. TRIPATHI, Sachidanand , SHAH, Rima and SHARMA, D C (2012). Analgesic activity of fixed dose combinations of paracetamol with diclofenac sodium and paracetamol with tramadol on different pain models in healthy volunteers - A randomized double blind crossover study. *Journal of Anaesthesiology Clinical Pharmacology* , 28 (4), 465-469.
30. ARNOLD, L., et al. (2014). Pregabalin is effective irrespective of antidepressant class in fibromyalgia patients currently receiving antidepressant medication for comorbid depression. *The Journal of Pain*, 15 (4),.
31. ROTH, Thomas , et al. (2012). Effect of pregabalin on sleep in patients with fibromyalgia and sleep maintenance disturbance: A randomized, placebo-controlled, 2-way crossover polysomnography study. *Arthritis Care & Research*, 64 (4), 597-606.
32. MARSÁ, Marina Díaz-, et al. (2011). Psychological Factors Affecting Response to Antidepressant Drugs in Fibromyalgia. *Psychosomatics*, 52 (3), 237-244.
33. GRIFFITH, James P. and ZARROUF, Fahd A. (2008). A Systematic Review of Chronic Fatigue Syndrome: Don't Assume It's Depression. *The Primary Care Companion - Journal of Clinical Psychiatry*, 10 (2), 120-128.
34. RUSSELL, D, et al. (2014). The effectiveness of exercise in the management of fatigue and sleep dysfunction in fibromyalgia syndrome: A systematic review. *Rheumatology* , 53 (1),.
35. HERRING, Matthew P., et al. (2012). Effect of Exercise Training on Depressive Symptoms Among Patients With a Chronic Illness. A Systematic Review and Meta-analysis of Randomized Controlled Trials. *Archives of Internal Medicine*, 172 (2), 101-111.
36. BUSCH, Angela J., et al. (2011). Exercise Therapy for Fibromyalgia. *Current Pain and Headache Reports*, 15 (5), 358-367.
37. HAUSER, Winfried , et al. (2010). Research article Efficacy of different types of aerobic exercise in fibromyalgia syndrome: a systematic review and meta-analysis of randomised controlled trials. *Arthritis Research & Therapy*, 12 (79)
38. EDINGER, J., et al. (2013). Can CBT for insomnia also improve pain sensitivity in fibromyalgia patients?: results from a randomized clinical trial. *Sleep Medicine*, 14 (1),.
39. LEE, J. , et al. (2014). Chronic widespread pain, including fibromyalgia: a pathway for care developed by the British Pain Society. *British Journal of Anaesthesia*, 112 (1),.
40. KOFFEL, Erin A. , KOFFEL, Jonathan B. and GEHRMANN, Philip R. (2014). A meta-analysis of group cognitive behavioral therapy for insomnia. *Sleep Medicine Reviews*,.
41. CASH, Elizabeth , et al. (2014). Mindfulness Meditation Alleviates Fibromyalgia Symptoms in Women: Results of a Randomized Clinical Trial. *Annals of Behavioral Medicine*,.
42. THIAGARAJAH, Angeline S, et al. (2014). The relationship between fibromyalgia, stress and depression. *International Journal of Clinical Rheumatology*, 9 (4), 371-384.
43. GUTENBRUNNER, Christoph , et al. (2010). A proposal for a worldwide definition of health resort medicine, balneology, medical hydrology and climatology. *International Journal of Biometeorology*, 54 (5), 495-507.
44. TERHORST , L and SCHNEIDER, M (2012). Complementary and alternative medicine in the treatment of pain in fibromyalgia: a systematic review of randomized controlled trials. *BMC Complementary and Alternative Medicine*, 12 (1),.
45. ABLIN, Jacob N. , HÄUSER, Winfried and BUSKILA, Dan (2013). Spa Treatment (Balneotherapy) for Fibromyalgia—A Qualitative-Narrative Review and a Historical Perspective. *Evidence-Based Complementary and Alternative Medicine*, 2013,.

46. SANCHEZ, Adelaida María Castro-, et al. (2011). Benefits of Massage-Myofascial Release Therapy on Pain, Anxiety, Quality of Sleep, Depression, and Quality of Life in Patients with Fibromyalgia. *Evidence-Based Complementary and Alternative Medicine*, 2011,.
47. FIELD, Tiffany, et al. (2002). Fibromyalgia Pain and Substance P Decrease and Sleep Improves After Massage Therapy. *Journal of Clinical Rheumatology*, 8 (2), 72-76.
48. LI, Yan-hui, et al. (2014). Massage Therapy for Fibromyalgia: A Systematic Review and Meta-Analysis of Randomized Controlled Trials. *Plos One*, 9 (2),.
49. CLAR, Christine , et al. (2014). Clinical effectiveness of manual therapy for the management of musculoskeletal and non-musculoskeletal conditions: systematic review and update of UK evidence report. *Chiropractic & Manual Therapies*, 22 (14),.
50. KRAFT, Karin , KANTER, Susanne and JANIK, Hubert (2013). Safety and Effectiveness of Vibration Massage by Deep Oscillations: A Prospective Observational Study. *Evidence-Based Complementary and Alternative Medicine*, 2013,.
51. YUAN, Susan L.K., BERSSANETI, Ana A. and MARQUES, Amelia P. (2013). Effects of Shiatsu in the Management of Fibromyalgia Symptoms: A Controlled Pilot Study. *Journal of Manipulative and Physiological Therapeutics*, 36 (7), 436–443.
52. RAMAN , Gowri , MUDEDLA , Sreenivasu and WANG, Chenchen (2014). How Effective Is Tai Chi Mind-Body Therapy for Fibromyalgia: A Systematic Review and Meta-Analysis. *The Journal of Alternative and Complementary Medicine*, 20 (5),.
53. KESSLER, Christian S., et al. (2013). Additive Complex Ayurvedic Treatment in Patients with Fibromyalgia Syndrome Compared to Conventional Standard Care Alone: A Nonrandomized Controlled Clinical Pilot Study (KAFA Trial). *Evidence Based Complementary Alternative Medicine*, 2013,.
54. JAKEL, Anne and HAUENSCHILD, Philip von (2012). A systematic review to evaluate the clinical benefits of craniosacral therapy. *Complementary therapies in medicine* , 20 (6), 456–465.
55. NEWMAN, Pam (2014). *The Magic Of Mantra*. 1st ed., USA, Raphael Walrond.
56. DUBIN, Ruth (2014). Keep it simple: Easing the care burden of fibromyalgia. *Canadian Family Physician*, 60 (7), 599-601.
57. BENNETT, R. (2005). The Fibromyalgia Impact Questionnaire (FIQ): a review of its development, current version, operating characteristics and uses. *Clinical and Experimental Rheumatology*, 5 (39), 154-62.
58. IANNUCELLI, C. , et al. (2011). Psychometric properties of the Fibromyalgia Assessment Status (FAS) index: a national web-based study of fibromyalgia. *Clinical and Experimental Rheumatology* , 6 (69), 49-54.
59. ,CRAWFORD, B., et al. (2011). Assessing fibromyalgia-related fatigue: content validity and psychometric performance of the Fatigue Visual Analog Scale in adult patients with fibromyalgia. *Clinical and Experimental Rheumatology* , 29 (6), 34-43.

STUDY OF TEMPERATURE AND TIME EFFECT ON STORED GRAIN WHEAT

Suaad Ghait Abdarrahan Abuhamra

Biology Department, Faculty of Education, Bani Wleed University, Bani Waleed City, Libya

ABSTRACT: Grain wheat had been being stored at different storage temperatures for five months in order to investigate the effectiveness of temperature and duration on this food in Bani Waleed city. The bad storage condition is not significantly proper for a reserve human food. The high rate of insects infestation and weight loss is the main problem during storage period. The grain wheat had been being stored for 5 months (from 20th of April up to 20th of September) at 20 °C (a room with air conditioner), 37 °C (inside a room at ambient conditions) and 55 °C (outside under sun rays with a simple cover which is represent the local traditional store). A kilogram had been taken from each sample and all samples were weighted every (15, 30, 45, 60,75, 90, 105, 120,135 and 150) days in order to calculate number of insects/kg and the weight loss. The data had been analyzed by IBM SPSS software version 25 statistics and expressed as mean± standard deviation using Two-way ANOVA. The obtained results at the end of storage period demonstrated that weight loss and insects' population were at the highest values of 34% and 348 insect/kg into storage of 37 °C. In addition, the weight loss and insects' population were 23% and 183 insect/kg into storage of 55 °C. However, the weight loss and insects' population were 0.40% and 25 insect/kg into storage of 20 °C. Furthermore, the Duncan's multiple range test analysis exposed that is a significant difference between whole samples at different temperatures and time (P-value < 0.05). In conclusion, the lower temperature storage is the appropriate method in order to limit insect invasion and post harvested food loss. Moreover, the domestic traditional store is not a convenient way for postharvest grain wheat.

Keywords: Grain wheat, different temperature storage, insect population, weight loss

INTRODUCTION

Many foods are very sensitive to storage conditions. Stored product insects may cause a significant damage and loss to food in stores (De Groote, *et al.*, 2013) as well as during processing, manufacture or transportation (Begum, *et al.*, 2007) (Mullen, *et al.*, 2012) as a result of improper facilities (Oerke, 1994). Therefore, the inconvenient condition of storage food is a very serious problem. The major determinants of storage risk are temperature, and time of storage. Consequently, the high environmental temperatures can create satisfactory circumstances that might accelerate insect development within the food mass (Vassilakos and Athanassiou, 2013) which results to increase food losses. For instance, moisture content is an important factor that influences rice quality such as developing fungi which lead to increase the rate of rice deterioration. The harvested maize remained in improper stores for about twelve months without industrial insecticide treatment. This improper storing condition results to contaminate the maize by insect pest infestation (Alonso-Amelot and Avila-Núñez, 2011). Stored produce of agricultural can be attacked by many species of beetle pests such as moths and mites which causing quantitative and qualitative losses (Mansour, *et al.*, 2012). Furthermore, the shelf life of a food product depends upon the environmental conditions. For example, the initial quality of food such as taste, color, texture, nutrition content which includes

carbohydrates, fat, minerals, vitamins, potassium, sugar, proteins etc., can be lost as a result of storing at ambient temperature and humidity (Baeza, *et al.*, 2007). In addition, a study shown that the rate of losing vitamin B (thiamine) in pasta is high at ambient condition fluctuated from 25 to 45 °C in the storage (Baeza, *et al.* 2007; Kamman, *et al.*, 1981). These nutrition content which have positive impact to the human health may be affected by inconvenient temperature. However, deterioration of stored food leads to decrease the nutrition value due to infestation of insects and microorganisms which results to be unhealthy food. Therefore, the bad storage conditions cause damage and lose to food quality and quantity. On the other hand, the proper storage facilities are very important to keep food in safe and it is the main challenge today and, in the future, which reflects a good quality food supply (Kaale and Eikevik, 2014). The most important physical factor in food storage is the temperature. This determinant drastically provides appropriate conditions that some of species such as insects which can attack the reserved foods in the storages. Therefore, the population of these pests can be increased inside the food materials which cause to grow the mold. It is generally accepted that climatic conditions that lead to physical changes in quality and quantity of commodity through the movement of moisture and rising of temperature level. Therefore, the whole food might be thoroughly deteriorated. Grain wheat has been selected for experiment run to investigate the changes in quality that occurred during storage for about 5 months at average temperature of 22.5 °C. The results shown that population of rice weevil (*Sitophilus oryzae*) which infested the grains increased and the growth of storage fungi increased (Fourar-Belaifa, *et al.*, 2010). The grain maize stored for 6 months in the ambient conditions at about 21°C. The results shown that the grain maize weevil (*Sitophilus zeamais*) has been infested with large numbers weevils from the second month and the numbers increased gradually up to 95 weevils over the next months. In addition, the investigation showed that the grain damage reached about 80% which depict that the most of food has been deteriorated. Similarly, the weight of grain loss increased up to 33% during this period (De Groote, *et al.*, 2013). Similarly, grain maize remained for 6 months at 22.5 °C. The maize has been attacked by larger grain borer (*Prostephanus truncates*) and the its population increased sharply till about 31 weevils and 225 of maize grain weevils (*Sitophilus zeamais*) after 4 months (De Groote, *et al.*, 2013). The maize grain damage has been estimated and the study shown that about 80% of damaged grain. Furthermore, the estimation shown that weight loss was about 26% (De Groote, *et al.*, 2013). Likewise, grain maize sample were infested in the storage with larger grain borer (*Prostephanus truncates*) and maize grain weevils (*Sitophilus zeamais*) at ambient storage condition of 26 °C. The number of weevils increased dramatically up to 60 weevils during six months. In addition, the damaged grains were about 12% (De Groote, *et al.*, 2013). Therefore, the objective of this work study is to investigate the effectiveness of temperature and duration on the stored food.

1 Materials and Methods

1.1 Source of Grain Wheat

Domestic fresh grain wheat samples without any apparent physical or organisms damage were selected from a Bani Waleed valley for this experiment run. The grain wheat samples were harvested at the end of April, 2021. The grain wheat samples were harvested at the last stage of growth which were brown and hard. After harvest, the all grain wheat samples were kept in plastic sacks and completely prepared to be stored at different locations whereas temperature is the very important factor which affects the produce.

2.2 Storage conditions

There were three storage conditions that used for the experiment. The first storage was a room contains an air conditioner which was set at 20 °C. The second storage was a room at ambient temperature of 37 °C. The third storage was outside under sun rays at average temperature of 55 °C with a simple traditional cover such as medium thick linen. Each sample contains 20 kilograms of grain wheat. The duration of store started from 20th of April 2021 till 20th of September 2021. In other word, the period of storage was 5 months, this period has been chosen to simulate the domestic traditional average storage time in this city.

2.3 Insects Estimation

The power of the insects to gnaw may be affected by the size and shape of the mouthparts, and the position of the mandibles relative to the axis of the body. For instance, larvae of red flour beetle (*Tribolium castaneum*) have penetrated cellophane and polyethylene bags when sealed in without food. Furthermore, such penetration might not result simply from a search for food. Larvae of many stored-product insects pupate preferentially amongst edible or inedible debris, and chewing at a film creates debris. Consequently, the food and products which are sealed by polyethylene bags or cellophane could be prone to insect pest infestation during storage or at the processing stage and the products are easily infested and after a period of time the numbers of insects increase due to their reproduction and the whole materials or food completely becomes physically damaged (Newton, 1988). A kilogram of grain wheat had been being taken randomly from each sample per 15 days in order to calculate the number of insects that infested the samples prolonged storage period of 5 months.

2.4 Measurement Weight Loss

The food weight loss may refer to the vanishing of food which can be calculated as a percentage of weight loss. The calculation of weight loss in the sample can be carried out by the differential between initial and final weight of grain wheat divided by the initial weight. The following equation can be used to estimate the percentage of grain wheat loss (Fregonesi, *et al.*, 2014) and (Alonso-Amelot and Avila-Núñez, 2011). All samples were weighted per 15 days in order to calculate the weight loss of samples prolonged storage period of 5 months.

$$\text{Weight loss\%} = \left(\frac{\text{initial weight} - \text{final weight}}{\text{initial weight}} \right) \times 100 \quad (1)$$

2.5 Statistical Analysis

The IBM SPSS software version 25 statistics was used for analyzing obtained samples data. Variance analysis (Two-way ANOVA) and Duncan's multiple range method were utilized to compare any significant differences between grain samples. Values were expressed as means ± standard deviations. Differences were considered significant at P-value < 0.05. All the analyses were carried out in triplicates.

3 Results and discussion

The effectiveness of duration and storage temperature on postharvest of grain wheat samples was drastically revealed after the statistical analysis work.

3.1 Weight loss

From the ANOVA runs, it can be noticeable that the effectiveness of the different independent variables on the grain wheat weight was very clear. Therefore, the percentage of weight loss at

temperature of 20 °C can be negligible. On the other hand, the findings illustrated a remarkable weight loss differences at 37 °C compared to the other storage conditions. Figure 1 shows that grain weight loss percent significantly increased during storage, so the highest value was about 34% at 37 °C and 23% at 55 °C. Consequently, ANOVA runs revealed that is a significant difference between whole storage conditions as a result of influences of times and temperature as show in Table 1 (P-value < 0.05). Additionally, Table 2 shows the mean and significant differences between effectiveness parameters. Figure 2-4 depict percentage of weight loss of different samples with different storage temperatures.

Table 1: Dependent variable: Weight loss, %

Parameter	df	Mean Square	F	P-Value
Temperature	2	742.591	1528.315	0.00
Time	9	433.028	891.208	0.00
Temperature * Time	18	121.693	250.454	0.00
Error	60	0.486		
Total	90			

Table 2: Weight loss, %: Mean \pm standard deviation and significant differences

Duncan's multiple range test		
Parameter		Mean of Weight loss %
Temperature, °C	20	0.04 \pm 0.127c
	37	9.95 \pm 0.127a
	55	5.74 \pm 0.127b
Time, day	15	0.00000 g
	30	0.00000 g
	45	0.000233 \pm 0.232g
	60	0.3671 \pm 0.232g
	75	1.377 \pm 0.232f
	90	3.022 \pm 0.232e
	105	4.933 \pm 0.232d
	120	8.277 \pm 0.232c
	135	14.988 \pm 0.232b
	150	19.478 \pm 0.232a

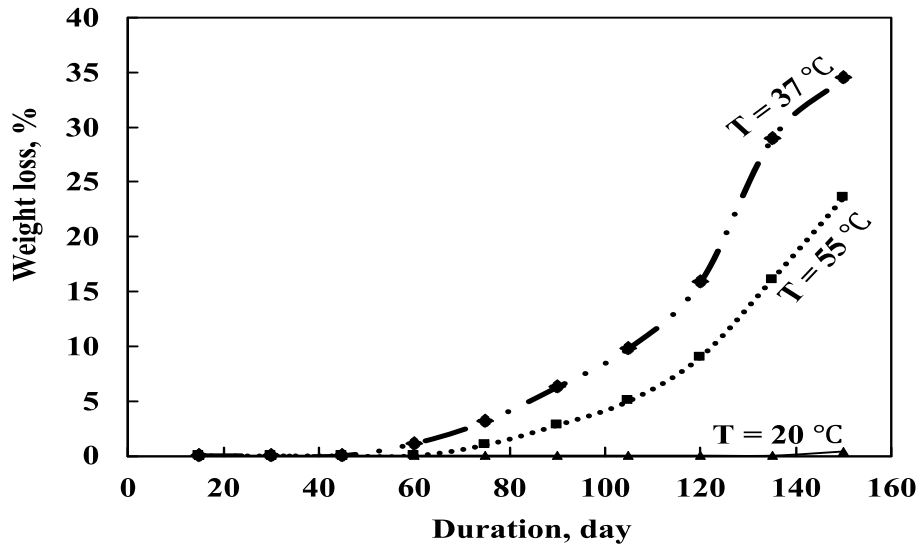


Fig. 1: Weight loss % at different temperatures

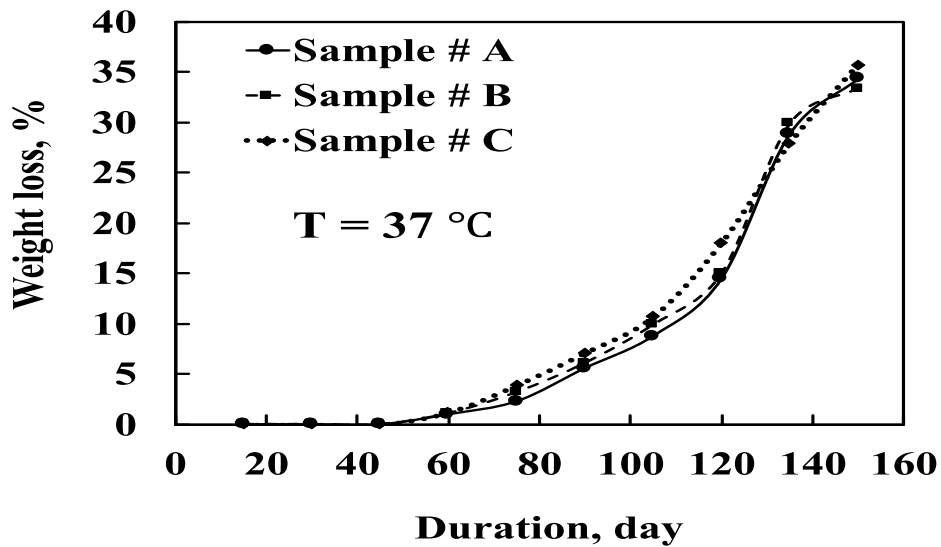


Fig. 2: Weight loss % at 37 °C

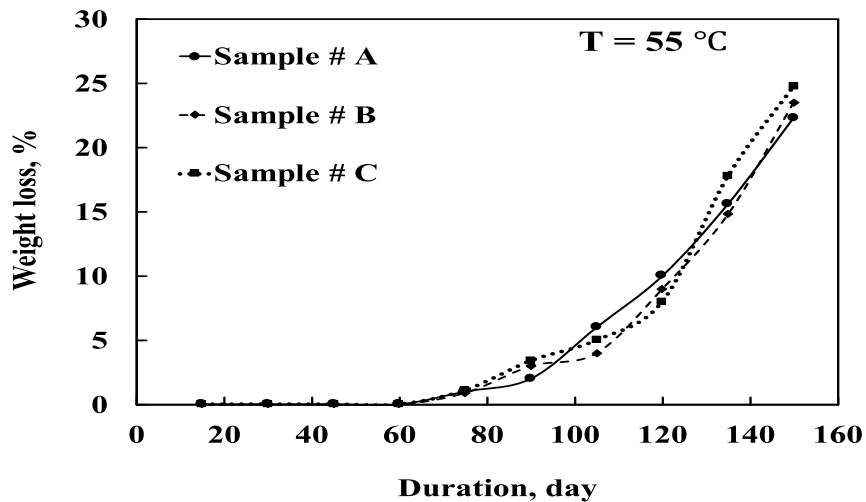


Fig. 3: Weight loss % at 55 °C

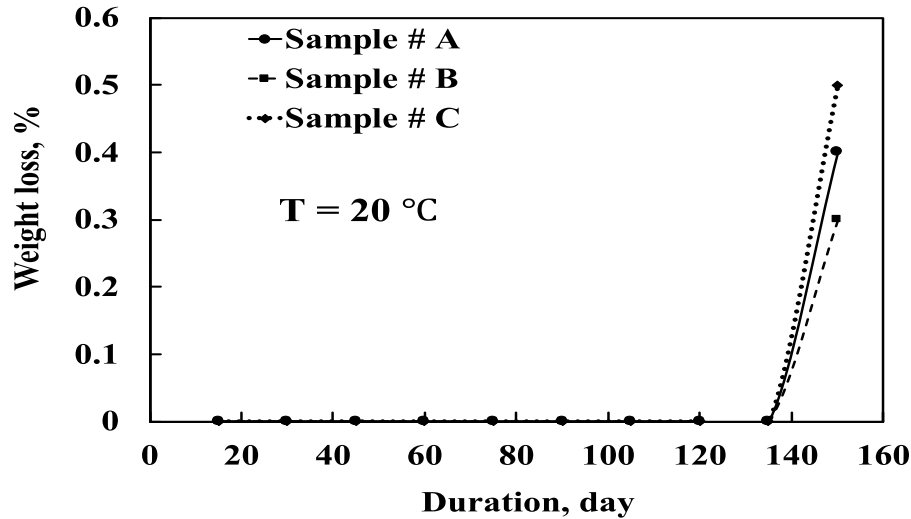


Fig. 4: Weight loss % at 20 °C

3.2 Insects population

Similarly, the ANOVA run demonstrated that number of insects per kilogram of grains wheat was drastically affected by temperature and time. Figure 5 displays the higher insects' population in the whole storage conditions. The population of insects at room with air conditioner was not significantly affected by temperature. However, the population sharply increased at the end of storage period up to 348 and 183 insects/kg at temperature of 37 °C and 55 °C respectively. Consequently, the Duncan multiple mode illustrated that number of insects was a significantly vary by time and temperature in all storage (P -value < 0.05) as shown in Table 3. This study is in agreement with previous study that conducted by Fourar-Belaifa, *et al.*, (2010) who have shown the population of rice weevil increased inside the storage at temperature of 22.5 °C. In addition, Figure 6-8 depict percentage of insects' population per kilogram of grain wheat of different samples with different storage temperatures. Moreover, Table 4 depicts the mean value and significant differences between effectiveness parameters.

Table 3: Dependent variable: Number of insects/kg

Parameter	df	Mean Square	F	P-Value
Temperature	2	185,619.478	5,076.194	0.00
Time	9	58,926.425	1,611.479	0.00
Temperature * Time	18	15,848.688	433.419	0.00
Error	60	36.567		
Total	90			

Table 4: Number of insects/kg: Mean \pm standard deviation and significant differences

Duncan's multiple range test		
Parameter		Mean of number of insects
Temperature, °C	20	11.43 \pm 1.10 ^c
	37	168.73 \pm 1.10 ^a
	55	87.96 \pm 1.10 ^b
Time, day	15	0.44 \pm 2.02 ^g
	30	2.55 \pm 2.02 ^{g,f}
	45	7.89 \pm 2.02 ^f
	60	27.77 \pm 2.02 ^e
	75	47.44 \pm 2.02 ^d
	90	100.11 \pm 2.02 ^c
	105	156.88 \pm 2.02 ^b
	120	182.33 \pm 2.02 ^a
	135	183.11 \pm 2.02 ^a
150	185.22 \pm 2.02 ^a	

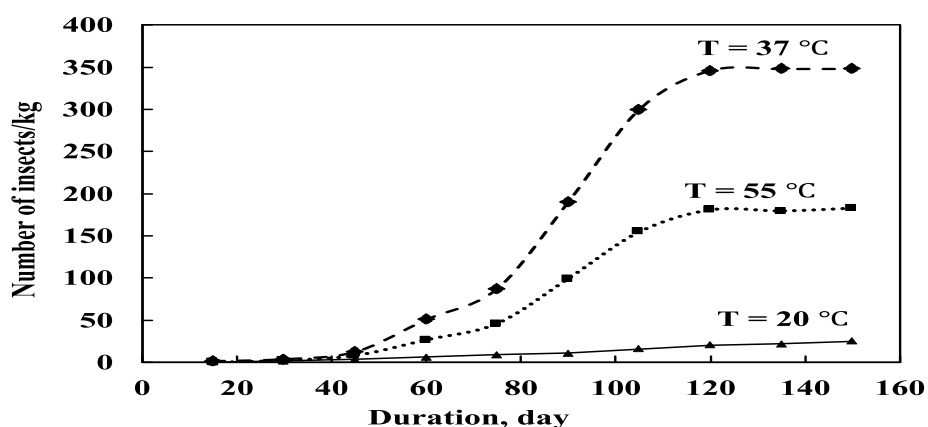


Fig. 5: Number of insects of different storages

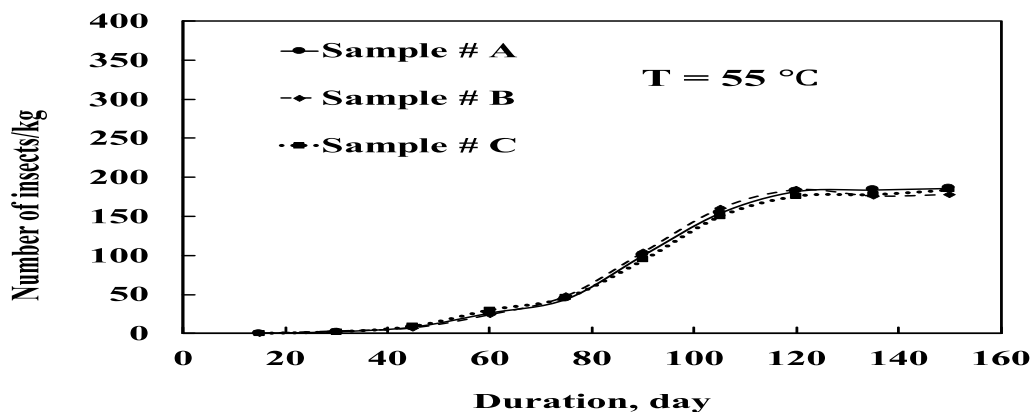


Fig. 6: Number of insects a 55 °C

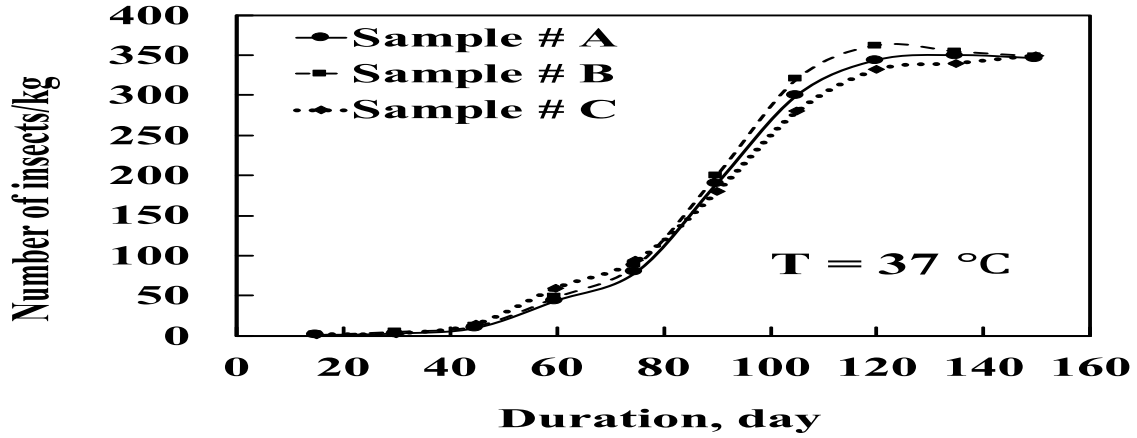


Fig. 7: Number of insects at 37 °C

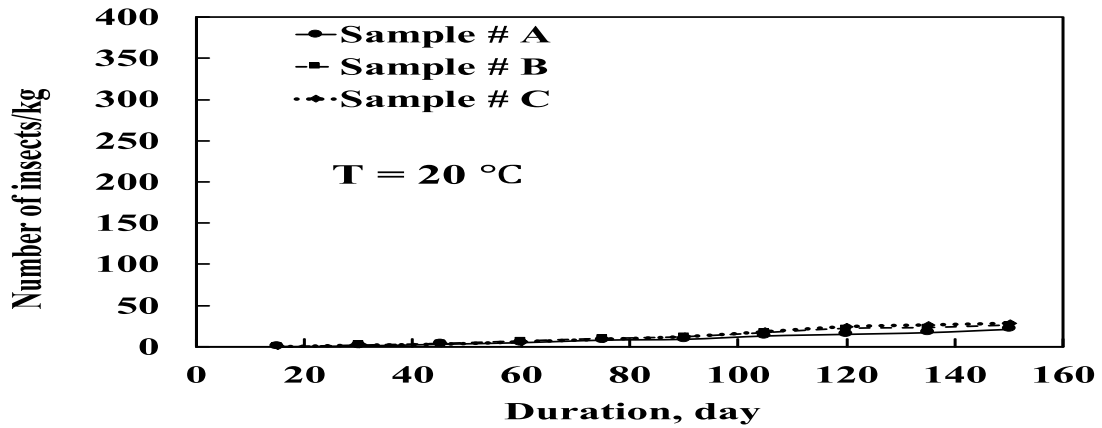


Fig. 8: Number of insects at 20 °C

4 Conclusion

This study displayed overall Bani Waleed food such as grain wheat which can be influenced by traditional storage condition as seen in the around local markets where the grain wheat susceptible to high temperature and sun rays while the cover is not proper. Consequently, the temperature and time can sharply effect the food into storage. The weight loss and insect population increase at high temperatures. However, low temperature storage is the best condition to keep the food in better situation.

References

1. Alonso-Amelot, M. E., and Avila-Núñez, J. L. (2011). Comparison of seven methods for stored cereal losses to insects for their application in rural conditions. *Journal of Stored Products Research*, 47(2), 82-87.
2. Baeza, R., Mielnicki, D., Zamora, M. C., and Chirife, J. (2007). Effect of environmental daily temperature fluctuations over one-year storage on the prediction of non-enzymatic browning in reduced-moisture foods stored at "ambient" temperature. *Food control*, 18(12), 1532-1537.
3. Begum, K., Reddy, P. V., Leelaja, B. C., Rajashekar, Y., and Rajendran, S. (2007). Studies on insect infestation in chocolates. *Journal of Stored Products Research*, 43(2), 118-122.

4. De Groote, H., Kimenju, S. C., Likhayo, P., Kanampiu, F., Tefera, T., and Hellin, J. (2013). Effectiveness of hermetic systems in controlling maize storage pests in Kenya. *Journal of stored products research*, 53, 27-36.
5. Fourar-Belaifa, R., Fleurat-Lessard, F., and Bouznad, Z. (2010). A systemic approach of qualitative changes in the stored wheat ecosystem: prediction of deterioration risks in unsafe storage conditions in relation to relative humidity, infestation by *Sitophilus oryzae* (L.), and variety influence. *Julius-Kühn-Archiv*, (425), 111.
6. Fregonesi, R. P., Portes, R. D. G., Aguiar, A. D. M., Figueira, L. C., Gonçalves, C. B., Arthur, V., and Trindade, M. A. (2014). Irradiated vacuum-packed lamb meat stored under refrigeration: Microbiology, physicochemical stability and sensory acceptance. *Meat Science*, 97(2), 151-155.
7. Kaale, L. D., and Eikevik, T. M. (2014). The development of ice crystals in food products during the superchilling process and following storage, a review. *Trends in Food Science and Technology*, 39(2), 91-103.
8. Kamman, J. F., Labuza, T. P., and Warthesen, J. J. (1981). Kinetics of thiamin and riboflavin loss in pasta as a function of constant and variable storage conditions. *Journal of food science*, 46(5), 1457-1461.
9. Mansour, E. E., Mi, F., Zhang, G., Jiugao, X., Wang, Y., and Kargbo, A. (2012). Effect of allylthiocyanate on *Sitophilus oryzae*, *Tribolium confusum* and *Plodia interpunctella*: Toxicity and effect on insect mitochondria. *Crop protection*, 33, 40-51.
10. Mullen, M. A., Vardeman, J. M., and Bagwell, J. (2012). 12 Insect-Resistant Packaging. *Stored product protection*, 135.
11. Newton, J. (1988). "Insects and packaging - a review." *International biodeterioration* 24(3): 175-187.
12. Oerke, E. C. (1994). Estimated crop losses due to pathogens, animal pests and weeds. *Crop Production and Crop Protection*. Elsevier Science Publishing, New York, NY, 535-597.
13. Vassilakos, T. N., and Athanassiou, C. G. (2013). Effect of temperature and relative humidity on the efficacy of spinetoram for the control of three stored product beetle species. *Journal of Stored Products Research*, 55, 73-77.

Effect of Water Salinity on Concrete Strength

Abdulrahman Abdulsalam Bin Zayd
Civil Engineering, Higher Institute of Engineering Technology/Zliten, Libya

Abstract: this paper to aim study the effect of mixing concrete with salinity of well water, sea water and fresh water on concrete strength. Forty-five (45) concrete cubes were used for testing. The mixing ratio for all mixtures was 1:1.68:3.33 and the ratio of water to cement was 0.6. The concrete cubes were first immersed in well water (water sample was taken from three different wells), and testing during a period of 7,28 and 60 days, respectively. The dissolved salts concentration for the first well was 2388 mg/L, and the average compressive resistance of concrete recorded was 19.4 N/mm², 26 N/mm² and 30.1 N/mm², respectively. For the second well, the dissolved salts concentration was 3114 mg/L, and the average compressive resistance was 23.9 N/mm², 35.5 N/mm² and 36.45 N/mm², respectively. And, the dissolved salts concentration was 3161 mg/L and the average compressive resistance was 15.95 N/mm², 28.4 N/mm² and 33.05 N/mm² for the third well. The concrete compressive resistance to sea water during the test period was 17.55 N/mm², 27.15 N/mm² and 28.1 N/mm², respectively. For the reference sample, fresh water, the concrete compressive resistance during the same test period was 22.45 N/mm², 32.9 N/mm² and 36.73 N/mm². The results obtained for well water and sea water indicated an increase in concrete strength as the age of the concrete increased.

Keywords: (well water, sea water, fresh water, concrete cubes, concrete resistance)

1- Introduction

Sea water represents about 97% of the total water on earth and only 3% of usable water [4]. Also, some regions of the world will suffer from a shortage of drinking water, according to the United Nations and the World Meteorological Organization [5]. Libyan coast cities suffer from the scarcity of natural water resources because they are located in arid and semi-arid regions [1]. Among these cities is the city of Zliten, which has a highly increase in population where they depend on underground water (well water) to satisfy their water needs. Due to the increase in population and the growth in agricultural, industrial and construction activities, the consumption rate has increased dramatically which led to shortage in well water and rise of dissolved salts [2]. The underground water suffers from pollution due to the interference of sea water [3]. With the lack of fresh water, it is necessary to look for alternative sources of water for use in concrete. Sea water has the characteristic of salinity, whose quantity per kilogram is about (3-5 %) [6] due to the amount of chlorides present in the water, which tends to cause moisture to persist and flourish on concrete [7]. Also, the researchers in field of concrete construction did not seriously study the possibility of using sea water, which can reduce the use of fresh water and help to encounter lack of fresh water in regions to accelerate the development of infrastructure through the use of building materials.

2- MATERIALS AND METHODS

The materials were used to prepare required samples namely; water, cement, coarse aggregate, and fine aggregate. All used material were collected from Zliten area.

2-1 Water

Water is an essential component of concrete. Water occupies 6-8% of the composition of fresh concrete [8]. Combining water with a cementations material forms a cement paste by the process of hydration. The used water in this study are:

2-1-1 Well Water

Water was collected and prepared for three wells with high salinity, based on a previous study I participated in. Table (1) shows the salinity of well water.

Table 1: The amount of salt in water wells [2].

No. Of well	Name of well	TDS mg/L
W ₁	Gwellat	2388
W ₂	Ka'am	3114
W ₃	Al Shaheed Hamza	6131

2-1-2 Sea water

Earth’s surface is covered by water around 71% in that mostly by oceans. The remaining is land consisting of continents, lakes, islands and rivers [4]. The average, sea water in the world's oceans has a salinity of about 3.5% (35 g/L) [9]. Most seawater is fairly uniform in chemical composition, and the primary chemical constituents of sea water are the ions of chloride, sodium, magnesium, calcium and potassium.

2-1-3 Fresh Water

Fresh water was used as a reference sample, and it was prepared from Al Mawred desalination plant.

2-1-4 Water curing

The water used throughout the curing of concrete in this study for all cubes is river water.

2-2 Cement

Cement generally represent 12-14% of concrete weight[8]. The cement was obtained from a local factory (Al-borj for cement – Zliten).

2-3 Coarse aggregate

The aggregate was supplied from Zliten area. Several tests were done on. Figure (1) shows the grading curve of coarse aggregate to ensure that it has good grading according to specifications, ASTM C136 [10]. Also the

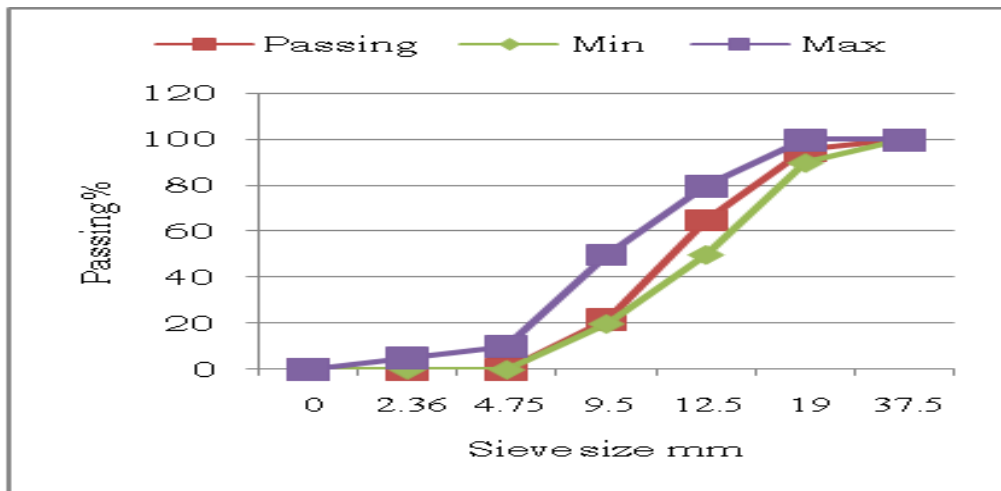


Fig. 1: Grading curve of aggregate(5/10)mm

physical properties of aggregate such as aggregate specific gravity test, water absorption, and Los Angeles abrasion test, were performed at Al-Asmarya University, faculty of engineering laboratory, and shown in table (2), according to ASTM C127, C131 [11], [12].

Table 2: Properties of aggregate observed in laboratory test.

No	Description	Test Result	Range Specification	ASTM
1	specific gravity test	2.667	2.5 – 2.75	C127[11]
2	water absorption %	2.15	Max = 2.5%	C127[11]
3	Los Angeles Abrasion test %	26.9	Max = 40%	C131[12]

2-4 Fine aggregate

Fine aggregate was tested for its physical properties such as specific gravity and water absorption in accordance with ASTM C128[13], as shown in table (3). Figures (2) shows the grading curve of fine aggregate to ensure that it has good grading according to specifications ASTM C136 [10].

Table 3: Physical properties of fine aggregate.

No	Description	Test Result	Range Specification	ASTM
1	specific gravity test	2.63	2.5 – 2.75	C128[13]
2	water absorption %	0.94	Max = 2.5%	C128[13]

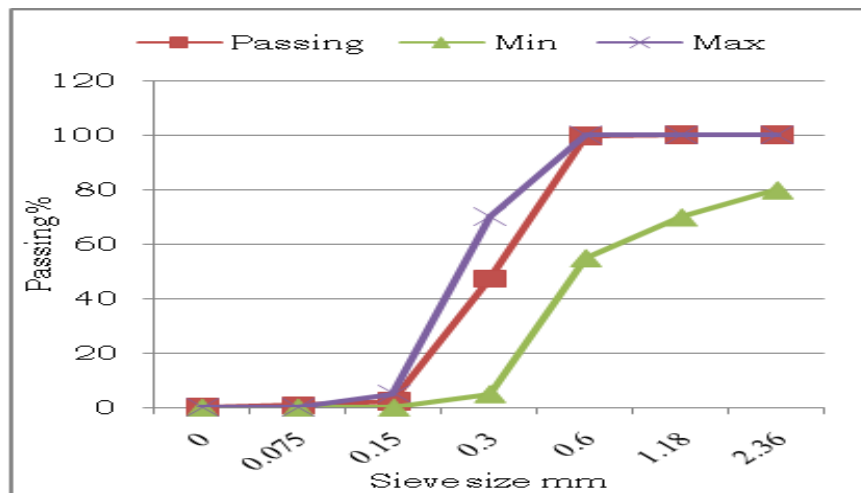


Fig. 2: Grading curve of fine aggregate

3- Mix design

The process of mixing and preparing materials is an important step in concrete mixture. Three types of concrete mixes were prepared. All the concrete mixes were produced by same proportion.

Final mix portions:

C : FA : CA : Water
 424 : 712.3 : 1411.9 : 254.4
 1 : 1.68 : 3.31 : 0.60

4- Results and Conclusions

4-1 Slump test

The slump test conducted for all the batches shows that the slump is in the range of 120 – 150 mm, according to BS8500 [14], which is suitable for trench-fill foundations where a high flow is required. This is known as a "wet mix".

4-2 Concrete compressive strength

The compressive strength test was performed on the concrete cubes, tested at the curing age of 7, 28 and 60 days using the compression testing machine. The cube was placed between the compressive plates parallel to the surface and then compressed until failure occurred. The reported results are the average of five samples. The obtained results are shown in figure (3).

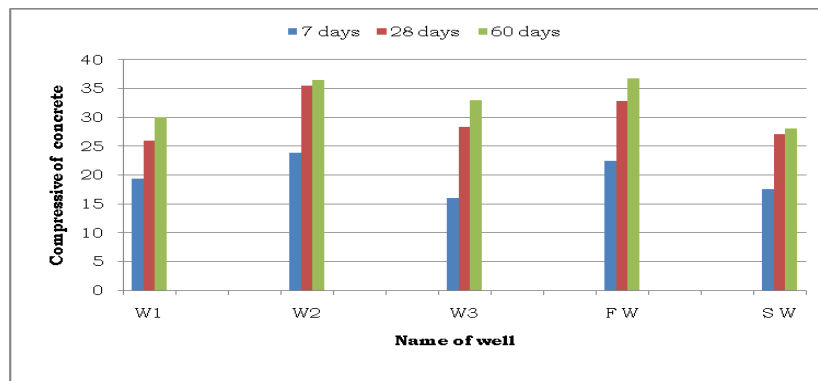


Fig. 3: Comparison of compressive strength for concrete mixes.

(W1,W2 and W3 are three wells salty water respectively and FW, SW are fresh and seawater respectively.)

The following conclusions are conducted from this study:

- 1- If we use salt water casting, the concrete has no reduction in the strength.
- 2- The strength of concrete increases with time.
- 3- Concrete can be made with water from sources other than potable water.
- 4- According to slump results, the source of water in mixing concrete doesn't affect the workability of concrete.
- 5- Due to water shortages and limited supplies, it is advised that other sources of water can be used to mix concrete in order to lessen the strain on potable water.

References

- [1] مصباح الصادق عبدالعزيز، ناصر مولود عبدالسلام. (2020). "تقييم الوضع المائي في المنطقة الممتدة من ساحل البحر بمدينة صبراتة إلى منطقة عفار". Alexandria . Journal of Agricultural Sciences, 65(1), page 15.
- [2] إسماعيل حمودة، محمد خوجة، عبدالرحمن بن زيد. (2021). "التغير في الأملاح الذائبة والكلورايد للمياه الجوفية في عدة مناطق بمدينة زليتن". الجامعة الأسمرية - CEST 2021 الإسلامية- كلية الهندسة – زليتن (14-16 ديسمبر صفحة 241 المؤتمر الرابع للعلوم الهندسية والتقنية.
- [3] جمعة علي المليان، موسى خليل سعيد. (2019). "تقييم تداخل مياه البحر لساحل منطقة زليتن- ليبيا". مجلة العلوم الإنسانية والتطبيقية جامعة الأسمرية. العدد 23 يونيو 2019. صفحة 338-339.
- [4] G. D. R. Naidu, A. Ram Prasad, S. Ramlal. (2019). " Effect of Sea Water on Strength of Concrete Made By River Sand and Sea Sand". International Journal of Recent Technology and Engineering (IJRTE). Volume-8 Issue-3, September 2019 . DOI: 10.35940/ijrte.C4831.098319. Page 2999.
- [5] Govalkar, M. A., & Lal, M. D. (2020). "A Review on Effect of Saline Water And Fresh Water on Concrete". Wutan Huatan Jisuan Jishu. Volume XVI . JUNE/2020. ISSN:1001-1749. Page 433.
- [6] Emmanuel, Akinsola Olufemi, Fatokun Ajibola Oladipo, and Ogunsanmi Olabode. "Investigation of salinity effect on compressive strength of reinforced concrete". Journal of Sustainable Development 5.6 (2012): 74.
- [7] Satish Kumar Vishwakarma., Anwar Ahmad., Syed Aqeel Ahmad and Rajiv Banerjee. (2018). EFFECT OF SALINE WATER ON CONCRETE WITH PARTIAL REPLACEMENT OF CEMENT WITH SILICA FUME AND FINE AGGREGATE WITH STONE DUST. International Journal of Recent Scientific Research . Vol. 9, Issue, 5(D), pp. 26715-26721, May, 2018. DOI: 10.24327/IJRSR . Page 26715.
- [8] E.M. Mbadike, A.U. Elinwa. (2011). "EFFECT OF SALT WATER IN THE PRODUCTION OF CONCRETE". Nigerian Journal of Technology. Vol. 30, No. 2, June 2011. Page 106.
- [9] Gawande, S., Deshmukh, Y., Bhagwat, M., More, S., Nirwal, N., & Phadatare, A. (2017). Comparative study of effect of salt water and fresh water on concrete. *International Research Journal of Engineering and Technology*, 4(4), 2642-2642-2643.
- [10] American Society for Testing and Materials ASTM C 136: Standard test method for sieve analysis of fine and coarse aggregates.
- [11] American Society for Testing and Materials ASTM C 127: Standard Test Method for specific gravity and the absorption of coarse aggregate.
- [12] American Society for Testing and Materials ASTM C 131: Standard Test Method for Resistance to Degradation of Small-Size Coarse Aggregate by Abrasion and Impact in the Los Angeles Machine.
- [13] American Society for Testing and Materials ASTM C 128: Standard Test Method for Relative Density (Specific Gravity) and Absorption of Fine Aggregate.
- [14] British Standard BS 8500-1:2006, Concrete- Complementary British Standard to BS EN 206-1, Method of specifying and guidance for specifier.

CO₂ INJECTION IN A CARBONATE RESERVOIR FOR EOR PROCESS

Omar Kalifa Hammuda Aluhwal

Oil and Gas Engineering Dep., Faculty of Engineering/Bani Waleed University, Libya

ABSTRACT: CO₂ injection is a mode that is used for enhanced oil recovery (EOR). The residual oil volume is left in porous media after the secondary recovery method of waterflooding operation which can be considered a remarkable and recoverable amount that must be extracted. Therefore, the tertiary recovery mode such as CO₂ injection may be a reliable method for this mission. A carbonate core holder CO₂ flooding trial method has been conducted at reservoir condition to investigate the oil recovery factor. Consequently, three experiments have run in the laboratory with three CO₂ slug sizes that have been injected into the carbonate reservoir after conventional secondary recovery. The results illustrated that oil flow rate increased after each injected CO₂ slug. Firstly, CO₂ slug size of 0.25 PV injected into reservoir which gained a recovery factor of 58.52 % with incremental recovery of 6.78 % over waterflooding process. Secondly, CO₂ slug size of 0.5 PV injected after waterflooding, so, the recovery factor reached up to 61.88 % and the incremental oil recovery was 8.88 %. Finally, the result has shown a significant final oil recovery of 64.49 % and additional recovery factor of 10.75 % when the system carried out CO₂ slug size injection of 1 PV. This might be attributed to good sweep efficiency, capillary force reduction, interfacial tension reduction as well as wettability alteration effectiveness. Consequently, the findings demonstrated that CO₂ displacement process is a remarkable method for EOR project.

Keywords: CO₂ injection, Carbonate reservoir, Oil recovery factor

INTRODUCTION

The oil pools are candidate for enhanced oil recovery (EOR) technique. Too many methods are available for this process such chemical (Honarvar, et. al., 2017; Aluhwal, 2008; Mohr, et. at., 2015; Aluhwal, 2019), steam, microbial, etc. CO₂ is considered an effective agent for enhanced oil recovery. CO₂ single phase flooding mode (Tuzunoglu and Bagci, 2000) substantially enhance oil mainly as a result of the following mechanisms (Al-Abri and Amin, 2010): Firstly, CO₂ may diffuse into crude oil phase and decreases the its viscosity. Secondly, CO₂ diffuses into oil phase cause to increase oil volume (swelling effectiveness) as well as reduces interfacial tension (IFT) between oil and water (Li and yang, 2013; Enayati, 2008). Therefore, the swelling and viscosity reduction are important factors which basically induce the oil through porous media to be recovered in which other enhanced oil recovery techniques is not applicable. A previous research shown that CO₂ can miscible with oil and cause swelling, reduce IFT as well as reduce oil viscosity (Badamchi-Zadeh, et al., 2009; Enayati, 2008; Yazdani and Maini, 2007). The CO₂ injection whether secondary or tertiary recovery method has received substantial attention in the petroleum industry as a result of its remarkable displacement efficiency and relatively not expensive (Stakup, 1978). The main major control mechanisms of CO₂ injection which impact on incremental light as well as heavy oil recovery are swelling effect and oil viscosity reduction. This process discovered in 1930s and had a high evolvment level in 1970s. so, during thirty yeas production work, CO₂ injection became the one of the most important enhanced oil recovery techniques for all types of oil (light, medium, heavy). CO₂ flooding can prolong production period and might increase oil recovery factor up to 25 % of oil initially in place (OIIP) (Yongmao, et. al., 2004). The previous experience of CO₂ flooding operations around oil fields in the world indicted that

improved oil recovery by CO₂ gas injection might cause ranging extra oil from 7 to 15 % of original oil in place (OOIP) (Mathiassen, 2003; Enayati, 2008). Furthermore, previous study illustrated that CO₂ flooding technique may cause formation permeability improvement, solution gas flooding and oil and water density change (Enayati, 2008; Yongmao, et. al., 2004). Additionally, this flooding mode may be applicable for sandstone and carbonate formation with different properties of hydrocarbon carrying zone such as thicknesses and permeabilities. The essential factors limit the CO₂ injection are CO₂ availability as well as cost to provide pipelines to bring it to the oil fields (Jessen, et. al., 2001). Several Alberta pools were subjected to the CO₂ flooding. So, the incremental oil recovery reached up to 13 % from the reservoir experience of carbon dioxide injection (Shaw and Bachu 2002; Enayati, 2008). Huazhou Li and his colleagues have reported that CO₂ flooding may enhanced heavy oil recovery where it can swell heavy oil and decrease its viscosity in presence other gases such as C₃H₈ or n-C₄H₁₀ (Li, et. al., 2013). CO₂ pure gas added to brine water flooding to improve oil recovery (Aluhwal, et. al., 2017; Fathollahi and Rostami, 2015; Gao, 2015; Aluhwal et. al., 2018). The CO₂ utilization for EOR methods can be CO₂ flooding, CO₂ huff and puff, and CO₂ – water alternating gas injection (WAG) (Zhao et. al., 2021).

1 TRIAL SETUP

1.1 Materials

The obtained grain dolomite rock sample from the laboratory originally contains calcium magnesium carbonate {Ca Mg (CO₃)₂} compound. The dolomite sample was packed into the core holder to simulate oil carbonate reservoir properties. In addition, the brine water was made from solution of sodium chloride (NaCl). The crude oil is available in the laboratory. The 99.99% purity of the analytical grade pressurized CO₂ gas was used for enhanced oil recovery process.

1.2 FLOODING SYSTEM

1.2.1 Apparatus

Injection pump: liquid (dual piston pump, model 12-6) is used to flow the mercury throughout stainless steel tubing to the accumulators of crude oil and saline water which are used for core holder injection trial at a particular flow injection rate.

Stainless steel core holder: The used column for injection system is made from grade 316 stainless steel with length of 34.5 cm and diameter of 3.8 cm.

Accumulators: The three accumulators withstand high pressure which one full of crude oil and another one full of saline water to saturate the carbonate reservoir core. The last one is full of CO₂ pure gas.

Backpressure regulator (BPR): The backpressure throughout injection trial regime is dominated by backpressure regulator (BPR) which is set up at outlet of the core holder. The backpressure regulator (BPR) may hold out high pressure till 4000 psi. Furthermore, all the accessories of fittings, BPR, stainless-steel tubes and valves have been purchased from Swagelok company. Figure 1 shows the trial set up assembly.

2 TRIAL METHODOLOGY

The core holder is set in the horizontal level in the oven to simulate oil recovery operations of secondary and tertiary recovery method. Initial oil and water saturations were performed firstly. Secondly, the water flooding method (secondary recovery) followed by the tertiary recovery method of

CO₂ injection. Furthermore, the CO₂ injection with various slug sizes of 0.25, 0.5 and 1PV were injected into the core holder at reservoir pressure, temperature and salinity of 2500 psi, 140 °F and 35,000 ppm, respectively.

2.1 Column Preparation

Prior to improve oil recovery, the grain dolomite rock sample of 150 μm size cleaned and dried, the fine grain is quietly inserted and pressed into the core holder while the core holder is continuously shacked. Moreover, distilled water is poured on the grain from the top side of core holder while the vacuum pump is running to pull the water from bottom side of core holder. Additionally, the both core holder sides supported by filter cloth of 5 μm size to forbade grain dolomite migration during displacement process.

2.2 Porosity and Permeability

The completely dried core holder is weight, filled with deionized distilled water and weight again, the different weight is equal to the space volume between grains. According to this rule, the porosity might be determined as next:

Porosity equation estimation as following:

$$\text{Porosity} = \frac{\text{DIW volume}}{\text{Bulk volume}} \quad (1)$$

The permeability was measured by transport Darcy equation. It is evaluated by the pressure difference between inlet and outlet portions of the core holder at various effluent rates.

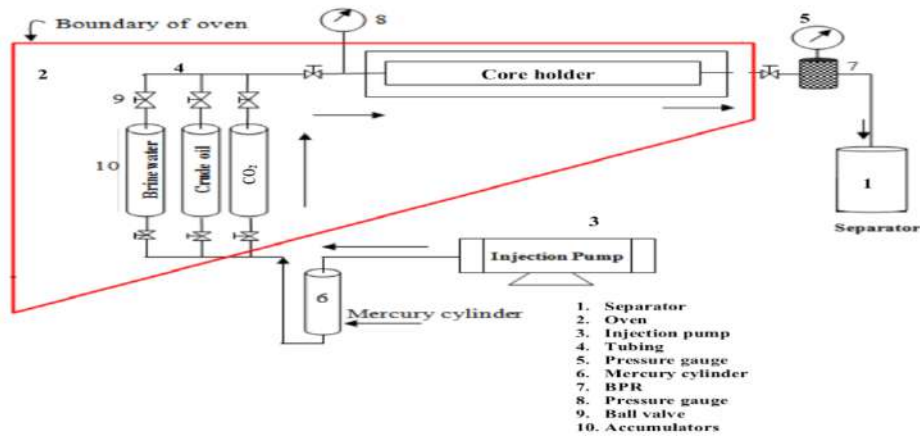


Fig. 1: Schematic diagram of injection system

$$\frac{Q\mu}{A} = K \frac{\Delta P}{L} \quad (2)$$

Where, Q is flow rate, μ is viscosity, A is area, ΔP is pressure difference and L is length. Consequently, $\frac{Q\mu}{A}$ is plotted versus $\frac{\Delta P}{L}$. The fitted line which passes the origin point is represent the data. Consequently, permeability constant of core holder is the slope of the straight line. Porosity and permeability data are shown in Table 1.

2.3 Saturation of Reservoir

The core holder is completely filled of artificial saline water, the crude oil is injected into the core holder in order to set up initial water saturation S_{wi} at high pressure and temperature of 2500 psi and 60 °C. The column was left to age at reservoir condition for 100 hours. The both valves at inlet and outlet portions have been completely shut off prolonged aging time.

Table 1. Fluid and grain rock properties

Brine water, viscosity, cp	0.70
38.5° API oil viscosity, cp	2.49
Grain dolomite, K, md	3221
Grain dolomite, \emptyset , %	40

3 RESULTS AND DISCUSSION

The impact of CO₂ injection on the oil flow rate was assessed at high pressure, temperature and NaCl salinity of 2500 psi, 60 °C and 35,000 ppm, respectively. The procured results shown that there is a substantially improving in cumulative oil production as a result of CO₂ displacement experiment. So, the oil recovery factor shown a remarkable increase during CO₂ injection compared to water flooding process for all CO₂ pore volume injection (Figure 2). Therefore, according to the processing data, the CO₂ slug size injection of 0.25 PV depicted a remarkable positive change in the recovery factor where it reached to 58.52 % with incremental recovery of 6.78 % over waterflooding. Similarly, the CO₂ slug size of 0.50 PV gained a substantial recovery factor of 61.88 % with incremental recovery of 8.88 %. Lastly, the productive of 1 PV CO₂ slug size injection illustrated a markedly recovery factor of 64.49 % and incremental recovery of 10.75 %. Moreover, the residual oil saturations after each experiment run were 32.45 %, 30.34 % and 25.85 % which were left by slug sizes of .25, 0.5 and 1 PV, respectively (Table 2). According to this analysis, the good CO₂ displacement process which reflects changes in rock wettability alteration, reduction of oil viscosity, reduction of interfacial tension (IFT) between oil and water, oil swelling, and appropriate CO₂ displacement efficiency. CO₂ gas can go through small pore space. It replaces the trapped oil and cause to oil flow towards production side. Therefore, all these parameters cause to reduce residual oil saturation. Figure 3 shows the various oil flow rates for all CO₂ slug sizes prolonged trials periods.

Table 2: RF of CO₂ inj. at inj. rate of .5 cc/min

Experiment No.	1		2		3	
	PV _{inj}	RF	PV _{inj}	RF	PV _{inj}	RF
Waterflooding	0.806	51.74	0.864	53	0.697	53.74
	PV _{inj}	RF	PV _{inj}	RF	PV _{inj}	RF
CO ₂ flooding	0.25	2	0.50	3.42	1	5.61
Final waterflooding	0.989	4.78	1.308	9.40	1.295	5.14
Total	2.04	58.52	2.683	61.88	3	64.49
Incremental oil recovery	6.78		8.88		10.75	
S _{or} , %	32.45		30.34		25.85	

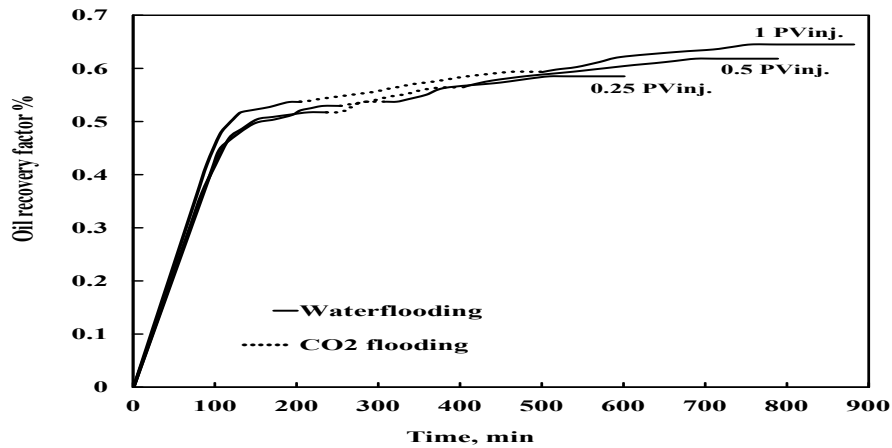


Fig. 2: CO₂ flood in carbonate reservoir

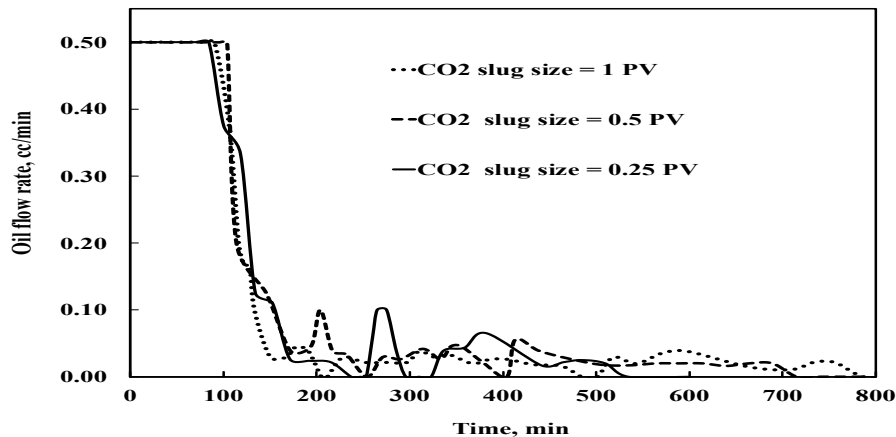


Fig. 3: Oil flow rate during CO₂ flood in carbonate reservoir

CONCLUSION

CO₂ injection can replace the trapped oil in the small pore space and displaces the oil towards production well. The large CO₂ slug size cause to high incremental oil recovery factor. Thus, this process shows a good outcome when the amount of CO₂ increases inside the rock formation.

References

- Honarvar, B., Azdarpour, A., Karimi, M., Rahimi, A., Afkhami Karaei, M., Hamidi, H., ... & Mohammadian, E. (2017). Experimental investigation of interfacial tension measurement and oil recovery by carbonated water injection: a case study using core samples from an Iranian carbonate oil reservoir. *Energy & Fuels*, 31(3), 2740-2748.
- Aluhwal, H. Kalifa, O. (2008). Simulation study of improving oil recovery by polymer flooding in a Malaysian reservoir. *Master's Thesis, University Technology Malaysia*.
- Mohr, S. H., Wang, J., Ellem, G., Ward, J., and Giurco, D. (2015). Projection of world fossil fuels by country. *Fuel*, 141, 120-135.
- Aluhwal, O. K. H. (2019). *Enhanced Oil Recovery By Surfactant Alternate Carbonated Water Injection* (Doctoral dissertation, Universiti Teknologi Malaysia).
- Al-Abri, A., & Amin, R. (2010). Phase behaviour, fluid properties and recovery efficiency of immiscible and miscible condensate displacements by SCCO₂ injection: experimental investigation. *Transport in porous media*, 85(3), 743-756.
- Aluhwal, O. K. H., Junin, R. B., and Nasri, N. S. B. (2018). Effect of CO₂ Content, Reservoir Temperature and Pressure of SACW on Oil Recovery. *Advanced Science Letters*, 24(6), 4232-4236.

- Aluhwal, O. K. H., Junin, R. B., and Nasri, N. S. B. (2017). Surfactant Alternating Carbonated Water Injection (SACW) is a New Process for Enhanced Oil Recovery. *Advanced Science Letters*, 23(9), 9085-9089.
- Badamchi-Zadeh, A., Yarranton, H. W., Svrcek, W. Y., & Maini, B. B. (2009). Phase behaviour and physical property measurements for VAPEX solvents: Part I. Propane and Athabasca bitumen. *Journal of Canadian Petroleum Technology*, 48(01), 54-61.
- Enayati, M., Heidaryan, E., & Mokhtari, B. (2008, June). New investigations into carbon dioxide flooding by focusing on viscosity and swelling factor changes. In *Canadian International Petroleum Conference*. OnePetro.
- Jessen, K., Sam-Olibale, L.C., Kavscek, A.R., Orr, F.M. (2001). Increasing CO₂ Storage in Oil Recovery, *First National Conference on Carbon Sequestration, sponsored by National Energy Technology Laboratory*, Washington DC, 2.
- Li, H., Zheng, S., & Yang, D. (2013). Enhanced swelling effect and viscosity reduction of solvent (s)/CO₂/heavy-oil systems. *Spe Journal*, 18(04), 695-707.
- Mathiassen, O.M., (2003). CO₂ as Injection Gas for Enhanced Oil Recovery and Estimation of the Potential on the Norwegian Continental Shelf, MSc. Thesis, *Trondheim*, 2.
- Shaw, J. C., & Bachu, S. (2002, June). CO₂ Flooding Performance Prediction for Alberta Oil Pools. In *Canadian International Petroleum Conference*. OnePetro.
- Stakup, F.I., (1978). Carbon Dioxide Miscible Flooding Miscible Flooding Past, Present and Outlook for the Future, *J. Pet. Tech.* 1102-1112.
- Tuzunoglu, E., and Bagci, S. (2000). Scaled 3-D model studies of immiscible CO₂ flooding using horizontal wells. *Journal of Petroleum Science and Engineering*, 26(1-4), 67-81.
- Yazdani, A., & Maini, B. B. (2007). Measurements and modelling of phase behaviour and viscosity of a heavy oil-butane system. In *Canadian International Petroleum Conference*. OnePetro.
- Yongmao, H., Zenggui, W., Yueming, J.B.Ch., Xiangjie, L., (2004). *Laboratory Investigation of CO₂ Flooding*, Paper SPE Presented at the 28th Annual SPE International Technical Conference and Exhibition in Abuja, Nigeria. 88883.
- Zhao, J., Wang, P., Yang, H., Tang, F., Ju, Y., & Jia, Y. (2021). Experimental Investigation of the CO₂ Huff and Puff Effect in Low-Permeability Sandstones with NMR. *ACS omega*, 6(24), 15601-15607.

Comparison of opening deep beam shapes under concentrated load

First Author^a, Ashraf M.L. Milad Second Author^b Nori.S.A. Ateig

Third Author Juhaynah .S. Alshukri Fourth Author Nooralden.A. Abubakr

^aDepartment of civil Engineerin , College of Engineering /Bain Waleed-University, Libya

Abstract: The objective of this study is to examine the deep beam opening behavior of lightweight reinforced concrete beams (LWC) with and without web openings, analyzed by the ansys19 software. The analysis included five samples of various shapes, a solid deep beam, a deep beam containing two square holes with sides length of 80 mm, a deep beam containing two circular holes with a diameter of 80 mm, a deep beam containing two vertical rectangular holes with dimensions of 140 * 80 mm, and a deep beam with two horizontal rectangular holes with dimensions of 80 * 140 mm. And each sample was subjected to a single point load. The effect of different gap shapes on the behavior of the sample was analyzed and compared. The results indicated that the shapes of the holes greatly affect the behavior of the deep beam, as it was found that the deep beams with circular gaps were the closest in terms of behavior to the deep solid beams among the four samples, and the deep beams with vertical rectangular gaps were the farthest for the behavior of the deep solid beams.

Introduction

Lightweight foam concrete is a new type of lightweight concrete, as it has the advantages of normal density concrete, aerated concrete and self-pressure concrete, by partially replacing the natural weight aggregates with polystyrene foam, which leads to reducing the weight of the concrete unit while maintaining the required strength. This, in turn, reduces the dead load by 15 to 20% and results in a reduction in the size of columns, bases and other bearing elements and reduces the total cost. Deep beams are members that are loaded on one side and supported on the opposite face so that pressure supports can develop between loads and abutments, and have either pronounced extensions (L_n), in, equal to or less than four times the depth of the total member (h). Or have areas of concentrated loads (A) within twice the depth of member (D) from the support face. In some facilities, deep beams with gaps of various shapes are needed, and these gaps affect the behavior of the deep beams and the basic services of the deep beams. In such cases, it is important to know the behavior of these beams and their ultimate strength. Many studies have investigated the effect of different gaps shapes on the behavior of the cameras, including that: (Nishitha Nair, Kavitha PE), University of Kerala, India, studied the effect of loads on seven different samples of deep beams (Deep beam without hole, deep beam with a circular hole one at centre, deep beam with a rectangular hole one at centre, deep beam with one circular hole one at side, deep beam with one square hole one at side, Deep beam with circular hole at two sides and Deep beam with rectangular hole at two sides) with ansys 14. It was found that the maximum tolerance was in the deep beam without hole, and the lowest tolerance was in the deep beam with rectangular hole at two sides [2]. Haider M. Alsaeq studied the effect of shapes and locations of gaps on the ability of endurance of deep beams. Haidar tested four gaps (circular, square, rectangular long sides in the horizontal and long rectangular from the vertical) .When investigating the effects of the shape of the gaps and its location on the structural behaviour of the hollow reinforced concrete beams, it was concluded that the use of a rectangular gap, long sides in the horizontal is considered to be the best among other forms of gaps, but it is often undesirable and does not do some purposes required [3]. Khattab Saleem Abdul-Razzaq, Hayder I. Ali and Mais M. AbdulKareem studied the effect of aperture shape on deep beams. Experiments were conducted to test thirteen deep beams under two point loads with square, circular, horizontal and vertical rectangular openings. Two holes were placed, one in each cut period. The creation of square, circular and

horizontal and vertical rectangular openings slots reduced the final capacity by about 20.5%, 18.3%, 24.7% and 31.7%, respectively, compared to the reference solid beam. In general, the opening size was found to be inversely proportional to the maximum capacity of the deep beam and the mid-section deviation because the reduction of the opening size resulted in less interruption in the compressive support connecting the loading and support points [4].

EXPERIMENTAL PROGRAM

The pilot study consisted of five simply supported reinforced concrete girders with mesh and no openings, and made of lightweight concrete. The packages were tested under the influence of a single concentrated payload by applying them to ANSYS19 software. All tested samples have the same geometry and the main upper and lower longitudinal reinforcement. The research sample was taken from the study (Amr Hassan Zahir, Wael Montaser and Muhammad Ramadan) entitled (An experimental study of the behavior of lightweight reinforced concrete deep beams with mesh holes)[1].

Geometry of the Deep Beam

The geometry of the full size beam is 1100mm x 400mm x 80mm. The beam is supported simply by providing a plate support on both sides. Single point loads are applied at the center of the beam. The concrete grade was 28.9 MPa and yield strength 550 MPa.

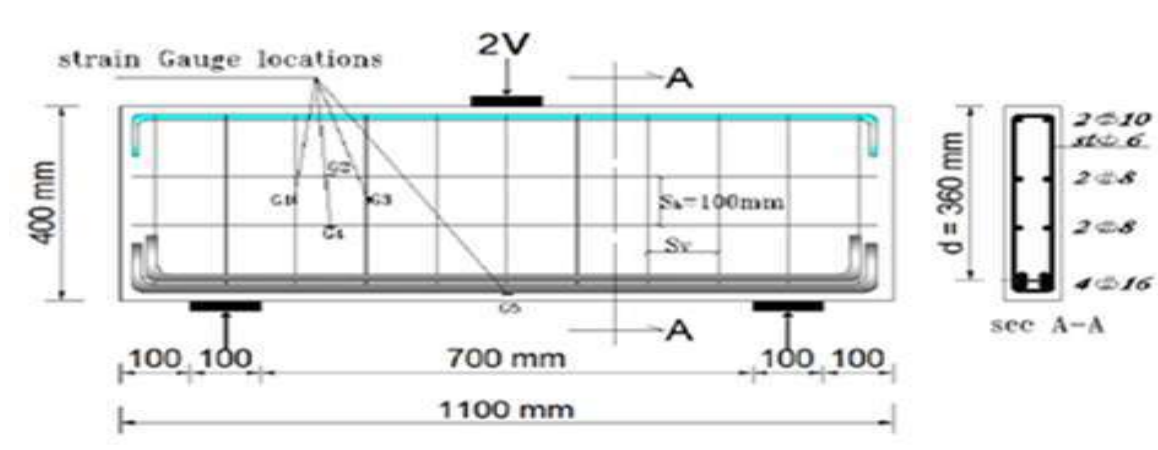


Figure (1): Reinforcement detail

Test Specimens

Table (1) shows samples of deep beams for treatment by research, its dimensions and the dimensions of the gaps in it.

Table (1): Typical dimensions of tested beams

Name	shape of specimen
BWOH	
BSHmS	
BCmHS	
BRHH	
BRHV	

Elements used for Modeling:

Table (2): shows the characteristics and identifications of the selected ANSYS finite element type representative of the main components for all beams.

Table (2): Characteristics and identifications of the selected ANSYS finite element types representative of the main components for all beams. (12)

Beam components	Selected from ANSYS library	Element characteristics
Reinforced Concrete Structural Solid	SOLID65	8-node Brick Element (3 Translation DOF per node).
1-Reinforcing bars (main, horizontal and vertical stirrups).	LINK180	2-node Discrete Element (3 Translation DOF per node).
Layered Structural Solid	SOLID186	20-node Brick Element (3 Translation DOF per node).

RESULTS

Evolutions of Crack and Load Capacity for RC **Deep Beam:**

The appearance of cracks begins when the samples are exposed to excessive loads or to more than they can bear, as when increasing loads more the samples reach the final breaking point and that varies from one sample to another due to the difference in the shapes of gaps, their dimensions and the distance between them.

First Crack:

The five samples were subjected to a single point load, and as the load increased, initial cracks appeared on the samples.

And it turned out that the BRHH sample was the one that showed the cracks first between the six hollow samples, so it started to crack when exposed to a 36.25 kN load, while the BCmHS was the one that showed the first cracks last between the four experimental samples. Where the cracks began when exposed to a load of 66 kN.

The result is closest to the BWOH reference sample that began cracking under 92 kN load.

The following figure shows all the results of the seven samples in terms of the first part:

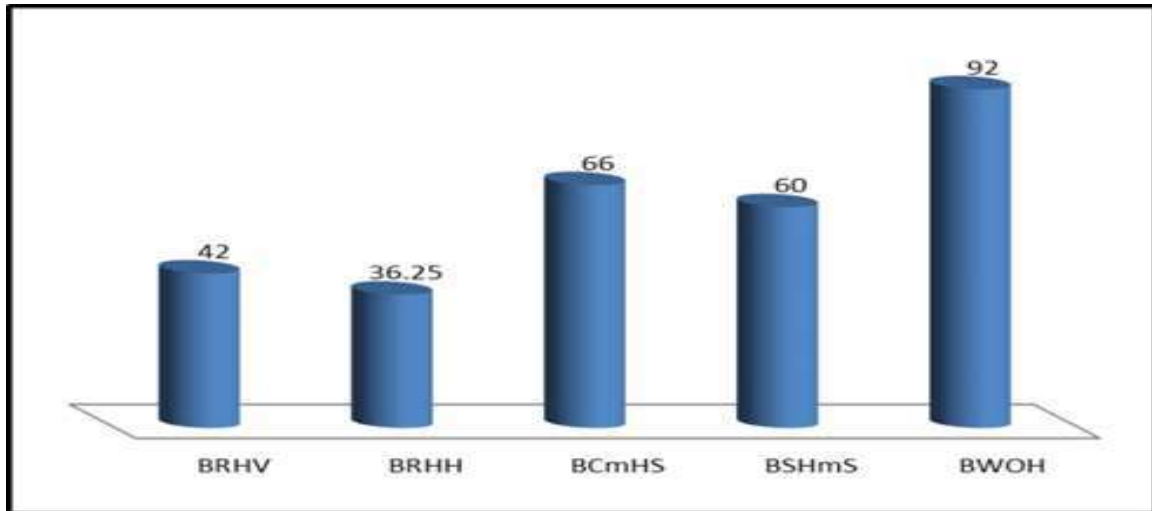


Figure (2): First Crack

Final load:

Samples reached collapse position when subjected to excessive loads. In the BWOH reference sample, it collapsed upon exposure to a load of 213 kN, the BCmHS sample was closest to the reference sample, and collapsed at a load of 205.25 kN, which means it requires a behavior very close to steel, at 96%.

The BRHV sample was the furthest in behavior compared to the BWOH reference sample, and collapsed at a 110.25 kN load, this indicates that it had only 51% of the power of the reference sample. The following figure (3) shows all the results of the five samples in terms of final pregnancy:

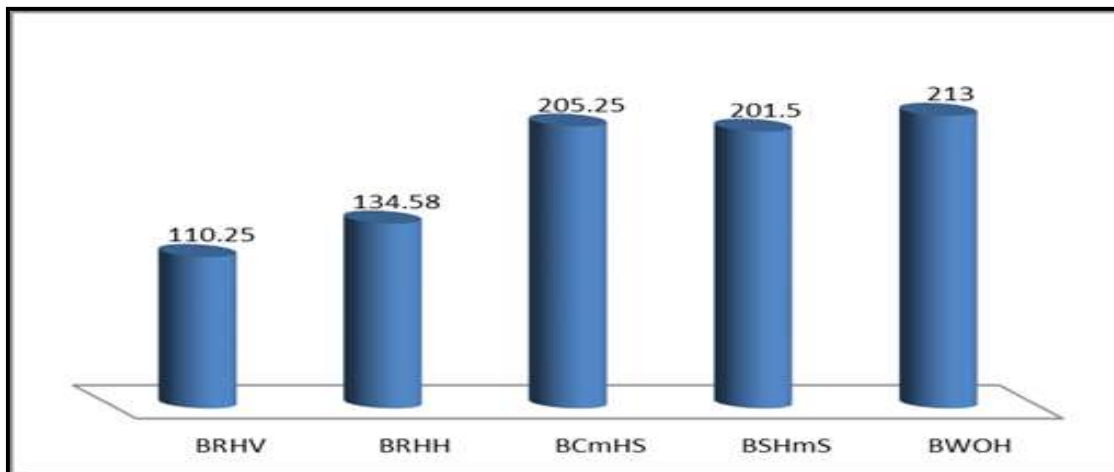




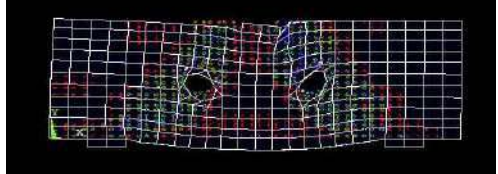

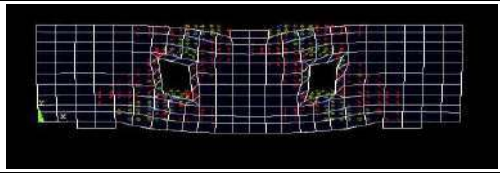
Figure (3): Ultimate load

Cracking Pattern and Mode of Failure:

The ANSYS program crack pattern records a crack pattern at each load step evolution of crack pattern developing for each beam at last loading step. ANSYS program display circles at locations of cracking or crushing in concrete elements. Cracking is shown with a circle outline in the plane of the crack, and

crushing is shown with an octahedron outline the first crack at an integration point is shown with a red circle outline, second crack with green outline, and third crack with a blue outline (ANSYS manual version 10.0).

Table (3) shows the evolution of cracks in the five experimental samples

	Cracks develop in the sample
BWOH	
BSHmS	
BCmHS	
BRHH	
BRHV	

Load Deflection Curve:

The following figure shows the deflection results for the five samples as a result of exposure to different loads:

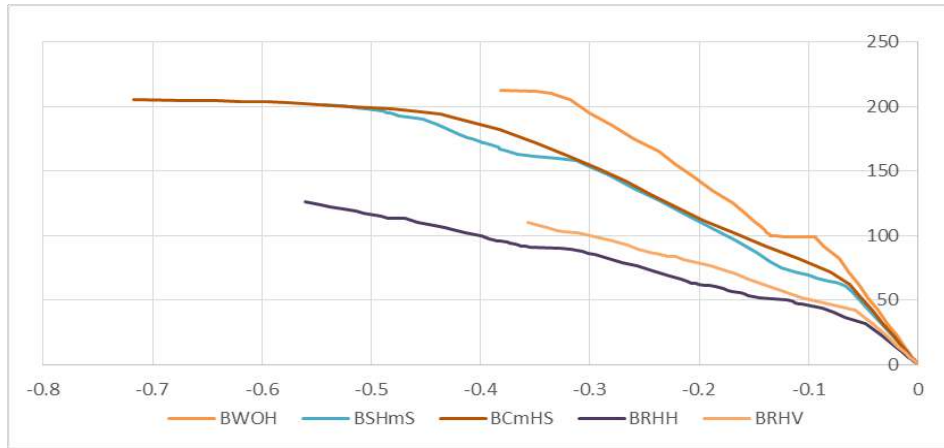


Figure (4): Comparison of load-deflection curve for specimens with different web opening type.

CONCLUSION

- 1- The behaviour of deep hollow beams varies with the shape of the gaps .
- 2- Deep beams containing a circular cavity contain the behaviour closest to the solid deep beam.
- 3- The deep beam which contains a vertical rectangular cavity has about 51% of the strength of the solid deep beam and this indicates its extreme weakness.
- 4- The deep hollow beams with a circular cavity are the best between round and square gaps.
- 5- The deep hollow beams with a horizontal rectangular bore are best between the horizontal rectangular gaps and the vertical rectangular gaps.
- 6- Deep beams with a circular cavity are the most flexible of the seven specimens.
- 7- The deep beams with a vertical rectangular cavity are the least flexible of the seven specimens.

REFERENCES

- 1- Amr H. Zaher , Wael Montaser & Mohamed Ramadan. Experimental Study of Behavior of Reinforced Light-Weight Concrete Deep Beams with Web Openings , 2017 .
- 2- Nishitha Nair, Kavitha P.E ,M.Tech Student, Civil Department EFFECT OF OPENINGS IN DEEP BEAMS USING STRUT AND TIE MODEL METHOD , 2015 .
- 3 - Haider M. Alsaq .Effects of Opening Shape and Location on the Structural Strength of R.C. Deep Beams with Openings , 2013 .
- 4 - Khattab Saleem Abdul-Razzaq , Hayder I. Ali and Mais M. Abdul-Kareem . A New Strengthening Technique for Deep Beam Openings Using Steel Plates , 2017 .
- 5 - K. S. Abdul-Razzaq, A. M. Jalil, and S. F. Jebur, "Behaviour of reinforced concrete deep beams in previous studies," *IOP Conference Series: Materials Science and Engineering*, vol. 518, ID 022065, 2019.
- 6 - M. Shariat, H. Eskandari-Naddaf, M. Tayyebinia, and M. Sadeghian, "Sensitivity analysis of reinforced concrete deep beam by STM and FEM (Part III)," *Materials Today Proceedings*, 2018.
- 7 - K. H. Tan, K. Tong, and C. Y. Tang, "Consistent strut-and-tie modelling of deep beams with web openings," *Magazine of Concrete Research*, vol. 55, no. 1, pp. 65–75, 2003.

- 8 - Yi T., Large-scale testing of a two-story URM structure, Ph.D. dissertation Georgia Institute of Technology, 2004.
- 9 - Yi T., Moon F.L., Leon R.T., Kahn L.F., Lateral load tests on a two-story unreinforced masonry building, ASCE J. Struct. Eng 2006.
- 10- slam, M. R., Mansur, M. A., & Maalej, M. (2005). Shear strengthening of RC deep beams using externally bonded FRP systems. Cement and Concrete Composites.

A review of the Microbiological Influenced on Corrosion rates in Oil seawater systems and three-phase transport pipelines

SALIM .O. MIFTAH

Petroleum Engineering Department , Engineering college/University Of BANI-WALEED, LIBYA

Abstract:

The development of corrosion management system (CMS) to manage and measure the mitigation of corrosion is now standard oilfield good practice, Nevertheless it is not unusual to find that the probability of MIC is not adequately addressed , despite the face that Microbiologically Influenced Corrosion (MIC) is identified as a corrosion risk. The result is that the mitigation of MIC is not measured or assured by the monitoring applied. Comparison of CMS documents illustrates that often there is no attempt to apply predictive models to assess the probability of MIC .The lack of a predication therefore makes measurement of mitigation impossible and this is often reflected by the face that MIC monitoring programmers. Actually measure biocide performance rather than MIC mitigation.

This paper is a review of the chemical treatment of microorganisms and their impact on corrosion rates in the oil industries, methods of controlling them, and how to resist them using chemicals or a change in the design of transport pipes and tanks to prevent their growth and describes how the application of even basic qualitative MIC predictions can greatly improve the management of MIC mitigation and raise the profile of MIC management within the CMS. Furthermore, the paper provides guidance as to the key monitoring parameter which are required to provide a meaningful statistical measure of MIC mitigation in pipelines transporting a range of oilfield fluids.

Keywords: (Bacteria , corrosion , Microbiologically , pipelines , seawater)

1.Introduction

Reports of corrosion failures implication bacterial activity – in particular the activity of Sulphate-reducing Bacteria (SRB) – continue to be published ensuring widespread appreciation that Microbiologically Influenced Corrosion (MIC) is a significant risk in oilfield operations [1,2,3]. Once any corrosion risk has been identified, controls ,should be applied to mitigate the corrosion mechanism and monitoring performed to confirm and measure the extent of the mitigation; I.e. the corrosion risk should be managed.

Despite being identified in many CMS documents , failures due to MIC continue to be reported, indicating that the MIC risk is not being effectively mitigated, Although reports vary widely , it not unusual to have the incidence of MIC being claimed to result in between 25 – 50 % of all internal corrosion events [4] as shown in figures 1` 2 3 ..

This paper presents an overview of the management of MIC in deferent pipeline systems and discusses how a full understanding of the impact of the pipeline environment on microbiological activity is required to firstly aid in the prediction MIC and subsequently design a mitigation strategy , implement controls and measure performance.

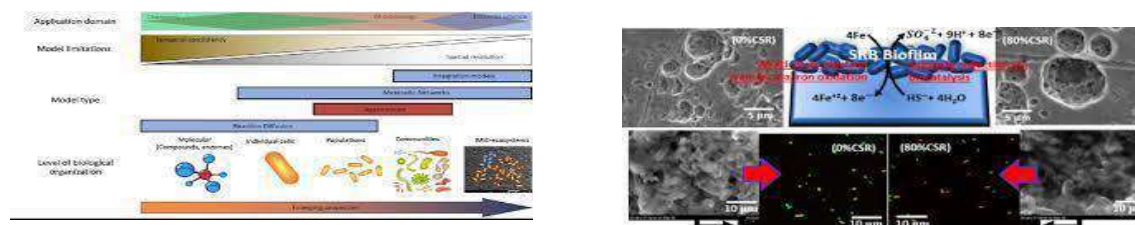


Fig.1 Accelerated corrosion of pipeline steel in the presence of *Desulfovibrio desulfuricans* biofilm due to carbon source deprivation in CO₂ saturated medium – ScienceDirect [sciencedirect.com](https://www.sciencedirect.com)

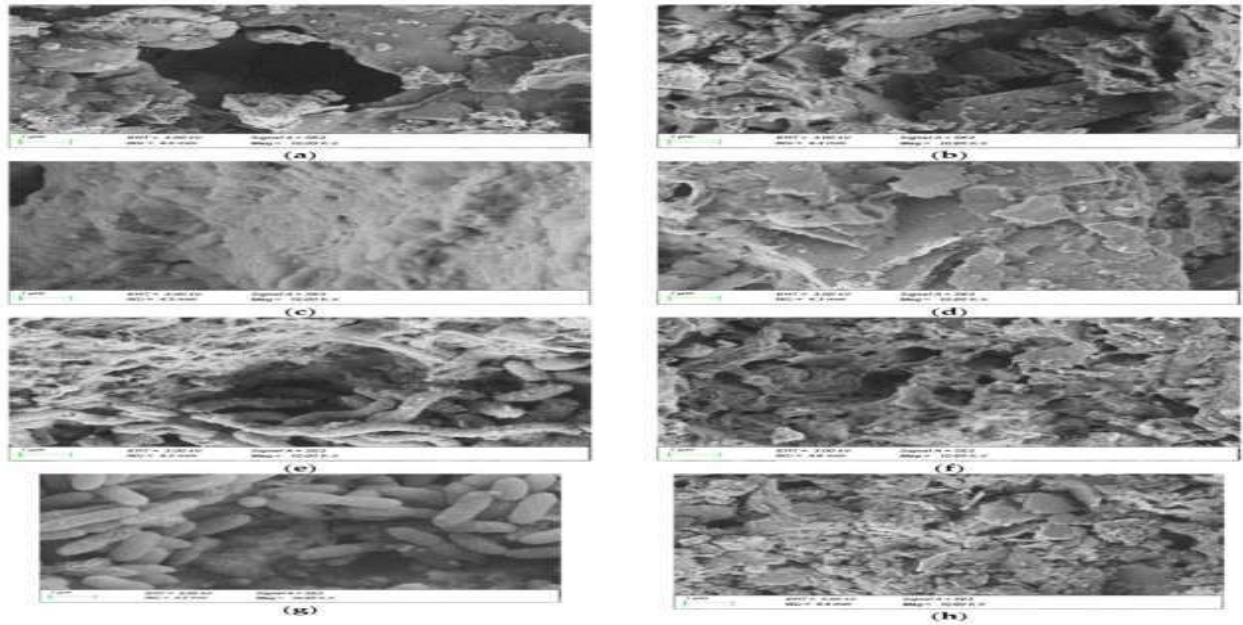


Fig.2 Microbially influenced corrosion—Any progress? – [sciencedirect.com](https://www.sciencedirect.com)

Current Common Practice

Controls to mitigate internal MIC in oilfield pipelines are currently all almost exclusively related to minimizing the numbers and/or activity of Sulphate-Reducing Bacteria (SRB) and to a lesser extent, organic Acid Producing Bacteria (APB). It is proposed that the corrosion mechanism for SRB is related to sulphide production and for APB the acid pH

resulting from carbon dioxide and organic acid production . The assumption is therefore that by maintaining low population numbers for these bacterial communities the production of hydrogen sulphide and organic acid will be minimized and MIC mitigated. A direct means of maintaining low numbers of bacteria is to kill any organisms present in the system by the application of biocides and therefore where controls are applied the injection of organic biocides is the predominant strategy. Determination of the effectiveness of the biocide treatment is most commonly attempted by enumerating the numbers of bacteria in samples of fluids collected from pipeline. Unfortunately this approach is over simplistic.

The effective mitigation of MIC is dependant on a wide number of biotic and abiotic factors many of which are specific to pipeline operations pipeline design and the nature of fluids and gases transported within the pipeline . Whilst the generic terms SRB and APB are common to all systems it is important to be aware that the SRB and APB present in a cold seawater pipeline will be very different from those present in a main oil pipeline or a hot 3-phase pipeline . Their response to system changes biocide treatments in terms of biocide formulation and injection criteria applied to pipeline transporting very different fluids. This approach is fundamentally flawed and this can be demonstrated by a simple consideration of even only a few of the key parameters controlling SRB or APB activity in different pipeline fluids pH temperature and water chemistry.

Current Prediction and Monitoring of MIC

Whilst the exact mechanisms which affect MIC associated with pipeline are still not clearly understood there is little argument that the rate and form of MIC is not related to the numbers of planktonic bacteria enumerated in synthetic bacterial growth media. However such analyses are by far the most commonly used tools employed to attempt to predict and monitor MIC. At best the enumeration of planktonic bacteria and the collection of fluid samples provides a qualitative measure only of biocide performance and in most cases provides no useful corrosion mitigation data whatsoever.

Of far greater importance are the following ;

- Bacterial activity in biofilms on the pipe walls.
- water content and water availability.
- water chemistry .
- flow velocity.
- Deposition of solids and scale.
- Concentration of dissolved gases (CO₂& O₂).
- Temperature, and pH

For this reason , the MIC model presented by Post[5] places emphasis on deposit formation and removal oxygen ingress , flow , velocity , and physicochemical conditions. This was modified by Maxwell [6] to include modules for biofilm development activity and its control.

2. CORROSIVE BIOFILMS

Corrosion is a surface phenomenon and as such the bacteria involved in MIC must also be associated with the surface, in complex community structures collectively known as biofilms [7]. In order to control MIC it is essential therefore , to prevent biofilm development or at least minimize the activity of corrosion related processes within the biofilm to low levels.

When a metal surface is exposed in an aqueous environment a conditioning film will develop almost instantaneously , followed quickly by bacteria cell. If suitable conditions allow , the cells will multiply and the biofilm will grow. Ultimately a multilayered complex mixed bacteria community is produced [8]. A wide number of physical , chemical and biological parameters will all impact on biofilm development ▪ including;

- Nature of substratum (mid steel , CRA, etc).
- Surface roughness and orientation.
- Flow velocity.
- Toxicity and stability of substratum .

heterognet

- Temperature ,pH , Eh.
- Solids.

It can be seen therefore, that biofilm development in oilfield process systems is likely to be heterogeneous due to the differing physicochemical conditions , mechanical design , etc, resulting in a variety of different environmental niches in different system and even in different parts of the same system . Furthermore even where there is consistency in system design and water chemistry , there can still be significant variability in biofilm heterogeneity , both on the macro and micro scale. On an apparently uniform surface , the density of bacterial cells and their activity within the biofilm can vary greatly within very small distance [9].

It is beyond the remit of this short paper to discuss in detail the complexity and heterogeneity of mature biofilms in oilfield systems. It is appropriate to highlight , however that it is this historic lack of

understanding of biofilm growth and activity that contributes greatly to the continued poor monitoring ineffective control and an inability to optimize MIC mitigation in the field

3. CLEANING AND SANITISING (DISINFECTION) STRATEGY (REMOVE, KILL OR INACTIVATE)

Microbiological control in other industries ; e.g. pharmaceutical drinking water, etc, often operates on a dual treatment philosophy; clean and sanitise . The treatments differentiate between cleaning (the removal of inorganic and organic debris , including bacterial cells) and sanitizing (the killing of bacteria cells). While the problems of bacterial growth in these other industries may be more related to human health and hygiene issues rather than MIC there remain the common feature that controls are applied to minimize bacterial activity in contaminating biofilms.

In oil field systems there is generally but not exclusively no separate cleaning treatment.

Where cleaning is applied this may be chemically with surfactants and/or scale solvers or physically with scrapers and cleaning pigs. In pipelines where the build up of surface attached deposits can result in restrictions in flow, several chemical and physical cleaning processes are commonly practical. Historically however these treatments were performed independently of bacterial control and were , therefore , not evaluated in terms of any antifouling effect or MIC mitigation .However , there is increasing anecdotal evidence that such cleaning procedures can provide significant benefit in MIC mitigation despite the fact that bacterial killing is not taking place.

The strategy for oilfield biocide application has historically been based on killing as many and as broad a spectrum of bacteria as possible whilst accepting that in an open ended flowing system sterilization is impossible . It was generally not highlighted that a disinfection philosophy would require the control of only those bacteria involved in MIC ; e.g, the SRB and/or APB .over the last year, however , this has been addressed as evidenced by the more recent move towards the application of alternatives to biocides; such as nitrite. Nitrite and anthraquinone [10,11,12]. These treatments are applied to achieve a total bacterial kill, but all are targeted at minimizing or preventing SRB activity.

A review of the strategy for bacterial control in the oil industry compared to to the strategies applied in other industrial demonstrates the apparent lack of consideration within oilfield systems for the requirement to physically or chemically clean the surfaces . In other industries there is an appreciation of the requirement to clean; i.e. remove deposits , apply detergents , mechanically abrade, etc. as key prerequisite or synergistic component of an effective antibacterial treatment. This paper includes cleaning when discussing the key parameters which must be evaluated and where possible controlled in order to effectively manage and mitigate MIC in pipelines transporting different oilfield fluids. Such an approach results in redefining the key performance Indicators (KPI,s) associated with MIC mitigation as an important first step in the effective management of corrosive biofilms.

4. MIC IN OIL PIPELINES

Due to the potential economic and environmental impact of a corrosion failure in an oil export pipeline. One might expect that MIC mitigation of such lines would receive significant attention both in terms of prediction and preventative treatment. However this is not always the case. Historically , poor risk assessments concluded that the probability of MIC was minimal and as a consequence there are many oil export pipelines which continue to receive little or no specific bacterial controls.

MIC prediction

Within a crude oil transportation pipeline a key parameter in determining the probability of MIC is water .Without water in the pipeline there will be no bacterial growth or activity. It is not possible to guarantee crude which is completely water free . However the idea that crude oil pipelines with less than 0.5 water will be at only minimal risk of MIC is erroneous.

Even at very low percentage of residual water in the export crude there is often the opportunity for water to settle out in low spots and low flow conditions. Over time therefore given the correct flow conditions the pipeline acts as a separator and ultimately significant volumes of water can become entrained within the line if adequate water removal pigs are not run. Control of contaminating water therefore , should be considered as key within the MIC mitigation strategy for oil lines. This allows the inclusion of parameters such as pigging, flow velocity and crude drying as components within MIC mitigation management.

Nevertheless whilst the role of free water in MIC and other corrosion mechanisms is not disputed a predictive model for MIC cannot rely on water control alone. If the metal surface remains oil wet due to wax deposition smearing of hydrocarbon deposits by the pig, etc. then this could have a very significant effect on the probability of MIC in crude oil pipelines. Thus the application of any qualitative modelling prediction would is not seen to provide any benefit. Rather than have no models however any attempt to apply even a semi-quantitative prediction tool should be supported.

Fluid Chemistry

Subsequent to water control the chemistry of the contaminating water should be considered Sulphate is required if an SRB corrosion risk is to develop. Low buffering capacity of the water is an important factor if APB corrosion mechanisms are considered. However neither of these parameters can be considered simplistically in terms of high and low concentrations of any particular molecule. For example the rate of sulphate reduction is unlikely to be affected by sulphate concentration until the concentration is below 10-20 mg/l. Above this concentration the rate of sulphate reduction and the concentration of sulphate generated are almost completely independent of sulphate concentration. Despite this fact semi-quantitative predictions for SRB mediate MIC appear to relate an increasing probability of MIC with increased sulphates concentration.

Biocide Treatment

The application of effective biocide treatments to oil pipelines is often poorly planned.

The biocide treatment can only effectively mitigate MIC if:

1. It reaches the targeted settled water and achieves a concentration bactericidal to the problematic organism in that water
2. bacterial activity in the water would has resulted in MIC . In most case biocide addition is based on the concentration of biocide in the fluids and does not consider the partitioning characteristics of biocide into the oil phase, It is important to determine therefore where the water is within the pipeline and the most appropriate chemistry to allow the biocide to be transported to that point. Currently in many cases the biocide selection is based solely on its ability to kill bacteria with no reference to partitioning and stability characteristics .

Batch biocide treatments are most commonly applied with a dose (concentration and exposure time) of biocide determined in a laboratory test and applied with a frequency to suit a calendar regulated regime ,I,e weekly , monthly quarterly . In order to apply an effective biocide treatment however a completely different strategy is required. The biocide dose needs to be determined base upon the ability of the biocide to effectively control a bacterial biofilm generated in the field. Secondly the frequency of the treatments needs to be determined considering the rate of water accumulation in the pipeline the persistency of the chemical at the points where the water is settling and the reinfection and regrowth rates of the surviving bacteria between biocide batches.

Biological Condition of Source Water

In some cases a KPI on the numbers of plancktonic SRB has been employed to accept or reject the fluids entering the pipeline system the strategy being that if the numbers of plancktonic SRP entering the system are maintained at low levels then this will retard the SRB activity in the system and thus mitigate MIC . A typically quoted KPI for such strategies is <100 SRB per ml. Consider however a

system pumping 10,000 Bbls fluid per day with a water content of 0.5 % . The numbers of planktonic SRB entering the system would be approximately 8.0×10^6 SRB cells per day. This in itself represents a very modest number of cells and when compared to the fact that an active biofilm can easily contain 10^6 SRB cells per cm^2 , it is demonstrable that the numbers of SRB introduced into the system whether higher or lower than the KPI – are irrelevant with regard to MIC mitigation once the system is contaminated.

5. MIC IN SEAWATER PIPELINES

Within a seawater pipeline the strategy formic management is very different to that described above for oil pipelines. Whilst water is still essential for corrosion its presence in the line is unavoidable and therefore water control would not be part of the strategy.

Furthermore there are a number of other factors which simplify the consideration of MIC in seawater injection system allowing perhaps the best opportunity to demonstrate the successful application of an MIC management strategy. These are;

- 1-Single aqueous phase only.
- 2-Commonality of water chemistry at numerous locations.
- 3-Commonality in system design.
- 4-Limited number of corrosion mechanisms.

A major drawback however is the lack of any correlation between SRB growth and activity and pitting corrosion rates. It is well documented in some systems that even in the presence of high numbers of SRB and the significant development of sulphidic biofilms that MIC pitting may not be encountered. Such observations highlight the role of deposits [13] and residual dissolved oxygen in stimulating MIC attack[14].

MIC Prediction

The Posts and Maxwell models can be applied directly to seawater systems the corrosion rate constant applied by Posts being based on seawater injection system case histories.

Given that the system is properly designed and operating within specification it could be argued that MIC is the predominate corrosion risk in a seawater injection which if nothing else , should highlight the requirement to optimize MIC management in these systems.

Seawater Chemistry

Whilst the inorganic chemistry of seawater may vary slightly in different parts of the world it is unlikely – except in extreme cases – that this would significantly affect the probability of MIC from location to location . Even gross changes to seawater chemistry may have little effect . This is exemplified by the application of sulphate removal as a means of scale control . In this process the sulphate concentration of seawater may be decrease from 2,700 mg/l to as low 25-100 mg/l. Whilst in a stagnant system this would limit the concentration of sulphide generated in a flowing system sulphide reduction activity would continue as sulphate was continuously supplied sulphide accumulation as iron sulphide at the metal surface would not be expected to significantly impacted even by this significant decrease in sulphate concentration.

Biocide Treatment

The application of biocide should in theory provide an effective means of bacterial control given that seawater presents an environment with supposed limited nutritional value . However the oil industry

record for mitigating MIC in seawater injection system is poor with many case histories of significant MIC pitting due to the activity of SRB being repeatedly reported over the past 40 years.

This lack of success can be related to many issues but it is certainly the case that the very large scale of seawater injection operation dictates that whilst concentration of nutrient are low the mass of nutrient throughput is very large . Furthermore the application biocides with treatment based on laboratory planktonic kill data and inappropriate batch frequencies have resulted in biocide treatment strategies which are not capable of achieving the required goal.

MIC Mitigation

Published reports and case histories of effective MIC mitigation are rare . There are several reports of bacterial numbers being significantly decreased by the application of more rigorous biocide treatments but this is almost never correlated and calibrated with improved corrosion inhibition . Where MIC mitigation has been reported the systems have complied with one or more of the following;

- Relatively small ($\leq 70,000$ BPD) system [15].
- Continuous biocide [16].
- Continuous nitrate.[17]
- Cleaning pigs employed [18].

The success in smaller water injection systems may simply be down to simplified logistic which allowed almost 100% availability of planned biocide treatment and an assurance that biocide soaks were performed during every planned shut-down.

In the large systems however biofilm and MIC control only by batch biocide treatments has proven extremely difficult . There are a number of case histories where once biofilm control had been lost it was proven impossible to cost effectively regain control . However as stated previously there is no evidence that MIC rates correlate with SRB or APB numbers and therefore whilst biofilm control might have been lost there was no evidence at what stage MIC was stimulated if at all.

One of the strategies which has been reported as successful is to re-inject a low residual chlorine downstream of the deaerator as an effective means of preventing biofilm development . The may not be application in all systems due to the additional general corrosion which can be encountered due to the presence of residual chlorine in a mild steel pipeline.

In the Norwegian sector of the North Sea several fields have replaced traditional batch biocide treatment with continues nitrate treatment. The addition of nitrate is well documented as a means of remediating sulphide systems and preventing further sulphate reduction activity. Statoil have reported a complete shift in bacterial activity in their water injection systems fro sulphate – reduction to nitrate reduction coupled with the removal of iron sulphide scales and an approximately three-fold decrease in corrosion rates following the introduction of continuous nitrate injection in the Norwegian North Sea fields [20].

Of very significant interest is the anecdotal of the significant impact of pigging in mitigating MIC . It has been reported that MIC mitigation was achieved by what was shown to be a sub-optimal biocide strategy in terms of minimizing sessile SRB numbers, when combined with cleaning pigs , even if these were run only infrequently [18]. The models for MIC in water pipelines place far more significance on the regularity of pigging than on the biocide treatment when predicting MIC mitigation.

One further very important parameter in the mitigation of MIC in seawater lines is oxygen control. It has been that the addition of even small concentration of dissolved oxygen into a system containing sulphide films can result in significantly aggravated pitting [14] . It is proposed that this is due to the

oxidation of parts of the iron sulphide film to elemental sulphur. Once again the models gives far more weighting to the presence of even small concentration of oxygen to stimulate MIC than they give to mitigating MIC with biocide treatment

Biological Conditions of Source water

In a seawater system the source water (open seawater) will provide approximately only one viable SRB cell per liter to the bulk phase . However in many seawater injection systems the deaeration tower acts as a large biological reactor and it is not uncommon to find SRB numbers of 10 per ml in the injection water exiting the tower . In a typical system injecting 10,000 BPD, this is equivalent to adding 1.6×10^{11} SRB to the bulk phase each day or 1.1×10^8 SRB per minute. Presenting the situation in this manner clearly demonstrates that a typical KPI of ≤ 10 SRB per ml for a water injection system does not assure minimal SRB activity as it actually allows for a contribution to the biofilm of 100 million SRB per minute.

6. MIC IN 3-PHASE PIPELINES

If the mitigation of MIC in oil pipelines with low water and seawater pipelines with 100% water proves difficult than the management of MIC in 3-phase- pipelines presents perhaps our greatest challenge.

MIC Prediction

Whilst the 3-phase system is more complicated than both the seawater and oil pipeline systems the application of the models previously mentioned does allow some screening of predicted corrosion rates due to the extremes of temperature , pH, flow velocity and total dissolved salts which can be encountered . Furthermore controls may be predominantly applied for other corrosive conditions such as CO₂ and H₂S due to their potential severity. The application of corrosion inhibitors and/or sulphide scavengers may have a secondary controlling effect on MIC.

Thus despite the completely it is probable that the potential for MIC in 3-phase pipelines may have be indirectly considered in more detail than for the other two pipeline systems previously discussed whilst the overall corrosion risk assessment is being performed.

Fluid Chemistry

The physicochemical environment in the water phase associated with 3-pipelines can vary significantly from field to field and even from well to well . In the worst case therefore each flow line will have to have a strategy developed specifically for that environment and this strategy will need to change as transported fluids change in water chemistry and solids content.

Once again water control is not generally an option and there will be parts of the line which will be almost continuously water wet. Furthermore the inorganic chemistry of produced water can vary significantly affecting the biology within the system and therefore varying the probability of MIC with location and time.

Biocide Treatment

The application of effective biocide treatments proves very difficult particularly where the situation is further complicated by the formation of inorganic scales (sulphate and carbonate or organic deposits and the continuous injection of potentially biostatic dependent on formulation and concentration , corrosion inhibitors . Determining the corrosion mechanism in such systems can also be very complicated and leads to frequent reporting of the cause of corrosion being MIC or Under Deposit Corrosion.

As mentioned previously MIC mitigation often becomes confused with other reasons for bacterial control. This can result in biocide being applied for no economic benefit. Commonly repeated errors include:

- Treating the system with biocide despite acceptable corrosion rates being confirmed.
- Applying very occasional treatment (ie one every three months) as just in case control.
- Monitoring for bacteria but using an inappropriate media (wrong TDS) or incubation temperature.

Biological Condition of Source Water

In a 3-phase pipeline carrying fluids directly or indirectly from a producing wells the biology of the system is the most complex of the three pipeline systems discussed in the paper.

The water associated with oil production can be formation water aquifer water or mixture of these with injection water . Each water source will have its own original microbiological populations including bacteria and archaea (the term which combines these two different microbial life forms is Prokaryotes). Which of these prokaryotes provide the source of sulphide producing organisms which might be predominant in MIC activity is an extremely complex problem to resolve. As a consequence many chose to ignore the complexity and continue to monitor for only sulphate –reducing bacteria (SRB) whereas strictly speaking if we hope to resolve MIC in 3-phase pipelines we should be studying sulphate reducing bacteria (SRB) and other prokaryotes capable of producing sulphide (or other corrosive environments) within the pipeline .

As the prokaryotes in the pipeline may be the result of microbiological activity within the oil reservoir it is often and possible to provide any control to their introduction into the system . This makes controlling their activity very difficult without to continuous treatment either into the well or directly downstream of the wellhead.

7.MIC MITIGATION MONITORING

Historically most attempts at MIC mitigation monitoring presented specifications for biocide efficacy determination based on limiting on limiting planktonic bacteria numbers to below set target limits. Whilst this strategy may be appropriate for bacterial control in a closed or batch process system it is not appropriate for continuous process systems as pipelines.

MIC Prediction

In order to prevent MIC it is essential to control sessile bacteria in biofilms together with other key parameters associated with MIC stimulation. However most corrosion management system do not have a philosophy of corrosion prevention but of corrosion mitigation . In order to mitigate MIC it is necessary to predict a corrosion rate against which any mitigation measures can be monitored . Currently there is a distinct lack of MIC prediction models. In part this is due to a reluctance within the industry to accept the introduction of qualitative MIC models despite the fact that discussion continues as to whether the commonly applied CO₂ corrosion prediction model are quantitative or qualitative.

As stated earlier the application of even a simple qualitative model for MIC is an essential first step in any MIC mitigation strategy .

Decision Trees

Decision trees are required to test the sensitively of model parameters exerting the greatest effect on MIC mitigation under different conditions. This will allow the greatest emphasis to be placed upon the most effective mitigation measure for that particular system . Within the decision tree it is important to include only those parameters that can be measured or predicted by modelling.

Implementation

Once the strategy has been developed from the model and decision trees this needs to be implemented. KPI's are required to manage and measure the extent to which the strategy to be implemented. Typically KPI's are required for application of controls biocide treatment, pig runs, removal, etc. as per any standard corrosion mitigation programmed.

Monitoring

It is key to a successful monitoring program is to monitor only those parameters where the data can be used either directly or indirectly to measure MIC mitigation. Pitting corrosion rates frequency of pitting etc, can be considered as direct analyses which could be used to measure MIC mitigation. Continuous on line measurement of temperature or pH and weekly counts on planktonic SRB is not uncommon but unless tied to an MIC prediction in some way this data serves to provide no useful purpose other than a comfort factor that something is being done.

Review and Learned for management

A continuous review of any management system is required to ensure that the effectiveness of the system is maintained. This must include a clear history of lessons learned and this is of particular relevance to MIC mitigation. This is no doubt that controls are being attempted and will continue to be applied with treatment regimes and strategies which have failed in similar systems at other locations. Particularly where this is the case with seawater pipelines where the transported fluids are very similar over a wide range of location a lessons learned database would help to fast track the strategy for MIC control in new projects.

It is widely recognized that maintaining a new system in clean condition to mitigate MIC is far more easily managed than remediating a system already contaminated with biofilms and exhibiting MIC pitting corrosion. [16].

Due to the problems involved in remediating dirty systems novel approaches were undertaken resulting in the development of nitrate treatments which are now widely practiced by several operators for MIC and SRB control in water injection systems. As yet however the industry has not developed a set of guidelines aimed at preventing the need to implement remediation treatment within the projected life of a water handling facility.

8. CONCLUSION

- Improved control of the development of corrosive biofilms and mitigation of MIC can be achieved by the application of a managed MIC mitigation strategy. This is particularly the case if MIC management is practiced from start-up in new systems.
- The strategy requires a modeled prediction of MIC which pays due cognizance to microbial kinetics system design and those operational parameters which exert the greatest effect on pitting corrosion rates.
- The strategy should be reviewed on an ongoing basis using properly interpreted data from a specifically designed routine monitoring program.
- The monitoring program should include only those abiotic and biotic analyses which are practical and which are actively employed in measuring MIC mitigation and reports should demonstrate measurement by KPI's.
- A remediation strategy will require very different treatments and controls in comparison to a mitigation strategy.

9. REFERENCES

1. Maxwell,S.(2002)In. Preceding of the corrosion 2002 Research Topical Symposim NACE Press, 2002,p 123.
- 2.Gaylate. P.M and Gaylarde.C.C (1994)In, Microbial Corrosion , Proceeding 3rd Int.EFC Workshop,pp,185.
3. NACE TM0194-94 (1994). Field Monitoring of Bacteria in Oil and Gas Systems . NACE.
- 4.Corrosion Management ,Are we doing the best we can?SPE Workshop, Lisbun ,June 2007.
5. Pots, B.F.M et al .(2002) Improvemwnt on Waard-Milliams corrosion and Applications to corrosion management , Corrosion 2002 , Paper .
6. Maxwell , S. (2006). Predicting Microbially . Influenced Corrosion (MIC) in Seawater Injection Systems.SPE.100519.
7. Costerton . J.W.and Lasbon,E.S. (1983).IN, Corrosion 83NACE paper NO 246.
8. Maxwell.S. (1984).The ecology of sulphate-reducing bacteria in biofilms on metal surfaces .PhD Thesis .University of Aberden.
9. Costerton, J.W.et al. (1987) Ann.Rev Microbiology .41,pp 464.
10. Thorstenson, T.et al . (2002).In, Corrosion 2002, NACE paper No 02033.
11. Hitzman , D.O .(1994). A new microbial technique for enhanced oilrecovery and sulfide prevention and reduction. SPE 22752.
- 12.Burger ,E.et al .(2001) .In Corrosion 2001. NACE paper No , 01274.
13. Maxwell , S. ,(2002).Microbially Influenced Corrosion (MIC) Resulting in Grrves in Subsea Water Injection Flowing. In, Proceeding of the Corrosion 2002 Research Topical Symposium . NACE Press.
14. Hardy, J,A and Bown ,J,L. (1984), Corrosion of mild steel by Biogenic sulphide films exposed to air. Corrosion 40,pp, 653.
15. Maxwell,S. et al ,(1987) In , Microbial Problems in the offshore Oil Industry .pp 209.
16. M ,. Maxwell,S. and Nice.P.I. (1988). Bacterial moitoring of the these Statfjord field water injection systems . Corrosion `88 pp,107.
17. Giangiacomo, L.A. and Dennis,M.(1997). Field Testing of the Biocompetative Exclusion Process for Control of Iron and Hydrogen Sulfides . SPE 38351.
18. Latifi,L. , Berry.M ,and Maxwell,S. (2007). Mitigation of MIC in water injection Flowlines .NACE.2007 .

Investigation of the effects of Wax Additives On the asphalt binder

Bashir M. Aburawi

Civil Engineering Department, College of Engineering / Elmergib University, Libya

Abstract: To reduce energy consumption and protect the environment, warm asphalt has been used widely in recent years. In this paper, Brookfield rotational viscometer test and dynamic mechanical analysis method are employed to investigate the effect of a kind of commercial wax named RH on the properties of two types of asphalt namely 60/70 and 80/100. It can be found that this kind of wax can increase the value of softening point, decrease complex modulus, and anti-rutting factor and increase the value of the penetration and the phase angle. The RH-modified asphalt has a lower viscosity, compared with the original sample.

Keywords: (WMA additive, Rheological property, Dynamic shear rheometer, Complex modulus, Rutting resistance factor)

Introduction

Asphalt is a pavement material that is brittle and hard in cold environments and soft at elevated temperatures. It has been historically employed as the most popular paving material for roadways [1]. Asphalt has been used in road construction and in many other applications for a long time. It can be produced from crude oils or found in nature as natural asphalt. The wax contained in crude oils will be still retained in the asphalt when the asphalt is produced through the distillation method. The wax may be the type of paraffin wax or microcrystalline wax. The presence of waxes in bitumen was usually considered detrimental to the performance of asphalt pavement, like increased sensitivity to cracking or rutting resistance in asphalt concrete pavements [2, 3].

This was mostly based on assumption that the melting of waxes at high temperatures reduced the asphalt mixture's resistance to rutting and that the crystallization of wax at low temperatures contributed to mixture cracking. It is also considered that the wax in asphalt will lead to physical hardening and poor binder adhesion to aggregate. However, from the literature review, it can be found that many studies have been done to evaluate the effect of wax as an additive to improve the performance of asphalt mixture, and it also can be found that the effects of waxes on asphalt quality and mixture performance are reported different. With the wax additive, the viscosity of asphalt is decreased at high temperatures (above approximately 80 °C), which improve the flow properties of asphalt.

The greatest benefit of this kind of effect is that the mixing temperature of the asphalt is reduced, and energy consumption and emissions are also reduced. Another benefit of using wax additive in asphalt is that the construction period can be extended; it has significant meaning in the cold region [3].

Paving the way for new technology. RH-WMA goes head-to-head with hot mix asphalt, steadily gaining acceptance throughout the asphalt paving industry. Over the last 5 years, numerous field validation trials of RH-WMA were established all over the world by private industry and road agencies. The

successful outcome of these field trials using RH-WMA suggests that WMA using RH-WMA may eventually be considered as a standard specification option for all pavement classes once contractors and asset owners gain confidence in the long-term performance of RH-WMA. In this paper, the effect of RH WMA, on the viscoelastic properties of asphalt is investigated.

WMA is an exciting development in asphalt technology, allowing the production and placement of asphalt paving at cooler temperatures than HMA. Compared with HMA, WMA technology can significantly reduce mixing temperatures of asphalt mixture by 20°C to 30°C [4]. Asphalt pavements make up an overwhelming majority of paved roads in the world.

The predominant technology for constructing these pavements is hot-mix asphalt (HMA), and it is currently the largest end-use of energy in most developed countries. HMA has been traditionally produced at a discharge temperature between 140°C and 180°C, resulting in high-energy (fuel) costs and the production of greenhouse gases. With growing environmental concerns and ever-increasing budgetary constraints, the use of Warm-Mix asphalt (WMA) is on the rise since it addresses both issues.

WMA allows the producers of asphalt pavement material to lower the temperatures at which the material is mixed and placed on the road. Reductions of 30 to 50°C have been documented. Such drastic reductions have the obvious benefits of cutting fuel consumption and decreasing the production of greenhouse gases. Engineering and construction benefits include better compaction of pavements; the ability to pave at lower temperatures, extending the paving season; and the potential to be able to recycle at higher rates. [5, 6]. Figure 1 shows the other advantages of the technology of warm mix asphalt.

RH-WMA is a unique, cost-effective, and environmentally friendly asphalt additive that eases the mixing process by reducing viscosity and enhancing flow. RH-WMA is a polyethylene wax-based asphalt binder additive produced from cross-linked polyethylene. It is designed to reduce the viscosity of asphalt binder at high temperatures while strengthening the asphalt crystalline structure at low temperatures. Unique Advantages of RH-WMA contains most of the benefits of Warm-Mix Technology in the industry; including a reduction in production temperature without compromising pavement performance.

Reduce Operating Cost			Reduce Harmful Emissions		
		30%			80%
Increase Compaction			Increase Production Rate		
		50%			25%
Longer Haulage Distance			Increase Recycling Rate		
		200%			75%





Reduce Burning Fuel Usage			Extend Paving Season		
		60%			70%

Fig. 1: Advantages of the technology of warm mix asphalt

RH-WMA can be used for all traditional hot-mix applications. With additional advantages identifiable with RH-WMA, it has been used in such demanding applications such as interstate highways, airfields, tunnels, and residential areas.

The RH-WMA additive would either reduce the viscosity of the binder or allow better workability of the mix at lower binder content. For this case, the optimum asphalt content of WMA is slightly lower than the optimum asphalt content for HMA. The Workability Index can be used effectively to assess the influence of production temperature [7]. Durability is one of the most important properties of a Hot Mix Asphalt (HMA). A key factor affecting the durability of asphalt pavements is moisture damage [8]. Moisture damage of an asphalt mixture generally called stripping potential is among the most important distresses of asphaltic pavements [9].

Cold region Asphalt pavement using rubber asphalt or stiffer binder: difficulty in compaction due to thin surface layer. Heavy traffic road that requires paving with WMA technology. Pavement construction under strict environmental controls. Reduced aging of asphalt during production to increase the service life of pavement and Pavement containing recycled asphalt pavement (RAP).

Moisture damage, occurring in several forms, can cause deterioration of asphalt pavements leading to a shortened service life of the pavement. Water or water vapour can affect the asphalt mixtures through the general 'theory' of water susceptibility (sensitivity) behaviour loss of adhesion (bond) between the aggregate surface and the asphalt cement; loss of cohesion softening and reduction in strength and stiffness of the asphalt mixtures; and/or fracture of individual aggregate particles with freezing. Keeping the moisture out or at least controlling the degree of moisture in the asphalt to avoid critical levels of saturation is a fundamental requirement. Design air voids and compacted density (insitu air voids) are important factors in the permeability of the asphalt mix. Grading and nominal size can also be contributing factors. Asphalt is rarely completely waterproof so some level of moisture is inevitable [10].

Materials and methods

Two types of neat asphalt binders namely: AC 60/70 and AC 80/100 are used in this study. The basic properties of binders are shown in Table (1).

Table 1: The test results of neat asphalt.

Test properties	Unit	Test results	
		60/70	80/100
Rotational viscosity @ 135°C	(Pa.s)	0.513	0.425
$G^*/\sin \delta$ @ 64°C	(kPa)	1.726	1.486
Penetration (25°C, 5s , 100g)	0.1 mm	64	81
Softening point	°C	47	44
Ductility at 25°C 5 cm/min	cm	> 100	> 100
$G^*/\sin \delta$ @ 64°C	(kPa)	3.262	2.830

RH is selected as a wax additive in this paper. RH, as a WMA additive, is a kind of white powder developed in China. RH forms a homogeneous solution with the base binder on stirring, and produces a marked reduction in the binder's viscosity. Figure 2 shows the RH-WMA that exists in the form of small white particles.

**Fig. 2:** RH-WMA as Additive for WMA

A Brookfield Rotational Viscometer (RV) test was used to measure the flow of binder to provide some assurance that it is fluidic enough when pumped and mixed in mixing plants and to determine the mixing and compaction temperatures. A Brookfield rotational viscometer is used to evaluate the effect of different temperatures on the viscosity after mixed with RH WMA.

Figure 3 shows the Brookfield RV that was used to determine the viscosity of the binder samples with and without RH-WMA. In this test, the temperature sweep was applied from 100°C to 170°C for PG 64 binder, at 10°C increments. For all the viscosity tests, 10 grams of asphalt binder sample was tested using spindle number 21. Three readings were taken for each test and the mean value was chosen as the final result.

**Fig. 3:** Brookfield Rotational Viscometer

Figure 4 shows the DSR machine used to characterize the viscous and elastic properties of the asphalt binder samples by measuring the complex shear modulus (G^*) and the phase angle (δ).



Fig. 4: DSR Equipment and Its Components

To estimate the rheological characterizations of the material, the dynamic mechanical analysis method is employed. The research of the Strategic Highway Research Program (SHRP) by the US suggests using complex modulus (G^*) and phase angle (δ) as the index of properties related to the performance of the asphalt on roads. Rheological measurements of the bitumen are performed with temperature sweeps using a Dynamic Shear Rheometer. The tests are carried out at 46–82 °C, and involved subjecting the bitumen of 1 mm thick in a pair of parallel plates of 25 mm diameter to alternating shear stress at a frequency of 1.59 Hz and measuring the resulting shear strain [11].

Results and discussion

The Brookfield rotational viscometer is used to study the viscosity properties of the binder AC 60/70 and AC 80/100 without/with RH WMA at different temperatures, both kinds of asphalt (AC 60/70 and AC 80/100) are usually used in the construction of roads. By this method, the viscosity properties of asphalt mixed with 2%, 3%, 4%, and 5% RH WMA by weight are evaluated under different temperatures. In this section, the viscosity characteristics of asphalt modified with RH are measured with Brookfield rotational viscometer when the test temperature is higher than 100 °C this step is to evaluate the workability of the asphalt mixture. The test results at temperatures 135°C and 165°C are shown in Figure 5 and Figure 6.

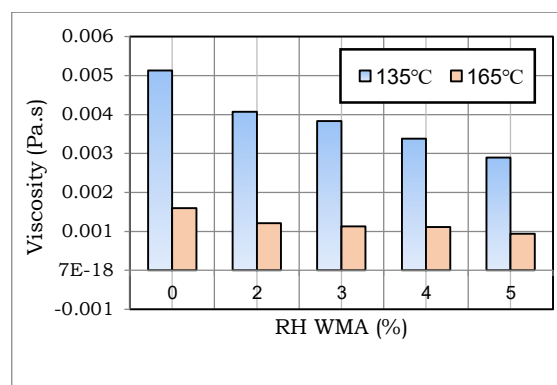


Fig. 5: The curve of viscosity–temperature for Bitumen AC 60/70

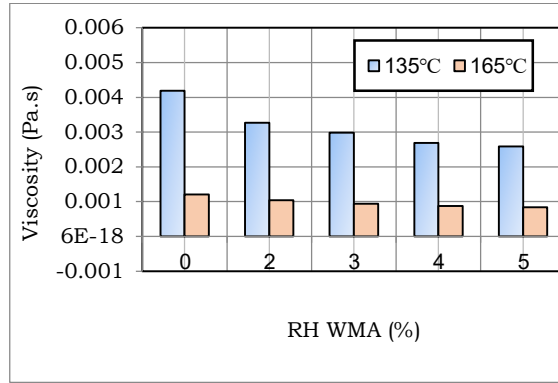


Fig. 6: The curve of viscosity–temperature for Bitumen AC 80/100

Analyzing Fig. 3 a and b it can be found that as to the two binders AC 60/70 and AC 80/100 without/with RH WMA, the viscosity decreases with temperature increasing, and when the temperature is higher than 135°C, RH modified asphalt has a lower viscosity, comparing with the original sample. It also can be found in Fig. 3 and 4 that the viscosity-temperature curve of the original asphalt is a nearly linear relationship, however, after mixing with RH, the relationship between viscosity and temperature is changed at about 135 °C, and after 135°C, the viscosity of RH modified asphalt is decreased significantly. When the temperature is higher than the entropy melting point, RH exists in asphalt as a liquid, which decreases the viscosity of asphalt. It means that RH-modified asphalt has better workability at low temperatures compared with neat asphalt.

The season that is suitable for asphalt pavement construction is short in cold regions (because the temperature is too low to construct). The properties of RH-modified asphalt make it possible to construct at relatively low temperatures, which means that the pavement construction period can be extended, which is meaningful for construction in cold regions. The mixing and compacting temperature can be determined by the viscosity-temperature curve of binders, 170 ± 20 centipoises and 280 ± 30 centipoise corresponding mixing temperature and compacting temperature, respectively [12]. The results are shown in Table (2) and Table (3).

From Tables 2 and 3, it can be found that after mixing with 2% RH, the mixing temperature and compacting temperature are decreased by about 5°C, compared with the original samples. These results indicate that the RH can decrease the construction temperature efficiently. However, this conclusion is just drawn from the viscosity-temperature curve, for some materials, such as polymer-modified asphalt, the mixing temperature and compacting temperature determined with the same method are not suitable.

Table 2: Construction Temperatures of bitumen AC 60/70 decided by viscosity–temperature curve.

Type of Bitumen	AC 60/70					
	% RH WMA	0%	2%	3%	4%	5%
Mix Temp. °C @ Viscosity = 0.17 Pa.s		160	155	155	150	150
Compaction Temp. °C @ Viscosity = 0.28 Pa.s		150	145	145	140	135

Table 3: Construction Temperatures of bitumen AC 80/100 decided by viscosity–temperature curve.

Type of Bitumen	AC 80/100				
% RH WMA	0%	2%	3%	4%	5%
Mix Temp. °C @ Viscosity = 0.17 Pa.s	155	150	150	145	145
Compaction Temp. °C @ Viscosity = 0.28 Pa.s	145	140	135	135	135

To study the rheological properties of the binder after mixing with RH, a DSR test is carried out. From the DSR test, complex modulus (G^*), phase angle (δ), and anti-rutting factor ($G^*/\sin \delta$) can be obtained. The phase angle measured the degree of viscosity of the bitumen; the complex modulus values and anti-rutting factor reflect the ability of rutting resistance. For materials of the same complex modulus value, the one, which has a higher phase angle value, will be more susceptible to viscous deformation and the higher complex modulus values and anti-rutting factor will have a better rutting resistance. The DSR test results are shown in Figures 6, 7, and 8.

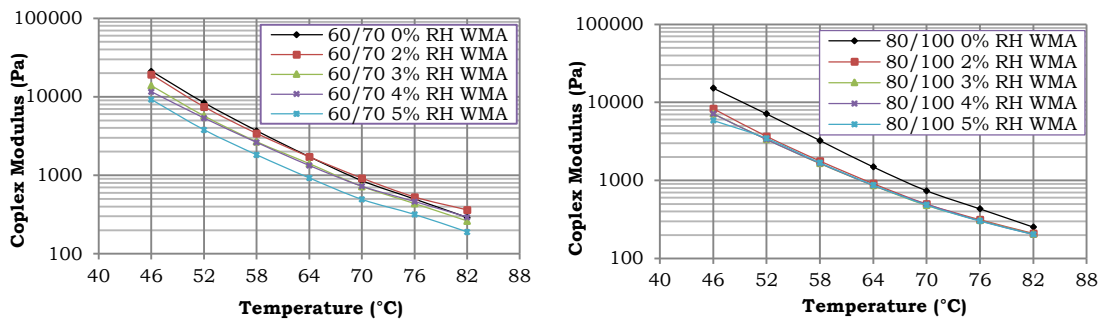


Fig. 6: The complex modulus of asphalt.

Figures 5 – 6 and 7 show the results of the temperature sweeps by the dynamic shear rheometer on the binders over the temperature range (46 – 82 °C) at the frequency of 1.59 Hz. They present the rheological behavior in graphic form for the RH-modified asphalt and original sample, respectively. In general, the original samples had relatively the highest complex modulus value and anti-rutting factor over the full temperature range.

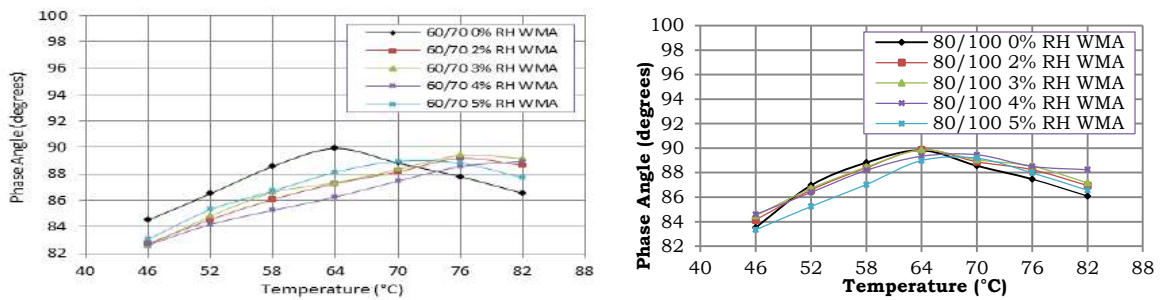


Fig. 7: The phase angles of asphalt.

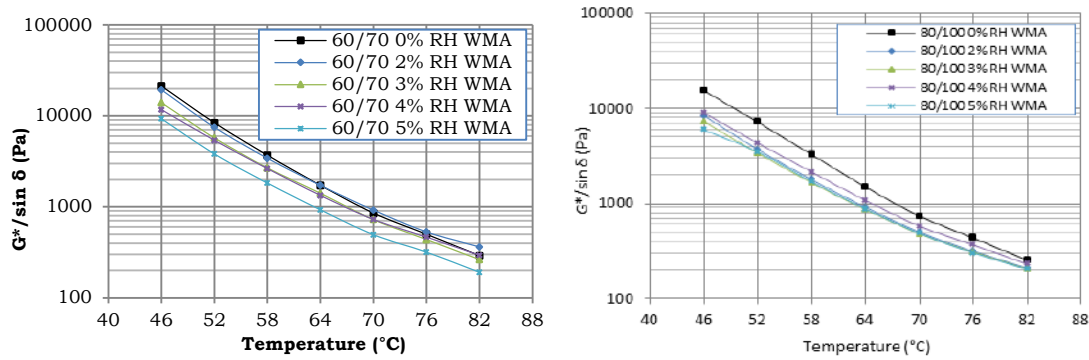


Fig. 8: The anti-rutting factor of asphalt.

From Figures 5 – 6 and 7 it can be found that with the content of RH increasing, the complex modulus and anti-rutting factor values decreased and the phase angles value increased. low binder complex modulus, together with high viscous deformation makes the asphalt pavement have low rutting resistance ability. These test results show that RH cannot improve the rutting resistance ability and decrease the temperature sensibility.

Conclusions

Based on the tests and analysis presented herein, the conclusions of the study are summarized as follows:

- (1) RH additive can increase the value of softening point and increase the value of the penetration. These properties are beneficial for improving asphalt pavement rutting resistance ability. When the content of the RH additive is higher than 4%, the increased rate of penetration and the increment rate of softening point becomes slow.
- (2) It is found from Brookfield rotational viscometer test that the viscosity decreases with temperature increase.
- (3) RH additive can decrease the value of complex modulus, and anti-rutting factor under the temperature range (46 - 82°C). It means that RH cannot improve the temperature sensibility of asphalt. That is beneficial for improving asphalt pavement rutting resistance ability.

Acknowledgements

The authors would like to acknowledge the Uni-versiti Sains Malaysia that has funded this research grant through the Research University Individual Grant Scheme (RUI Grant Number 1001/PAWAM/814231) which enables this paper to be written.

References

- [1] Sulyman, M., Sienkiewicz, M. and Haponiuk, J. Asphalt Pavement Material Improvement: A Review. *International Journal of Environmental Science and Development*, 5, 444-454, 2014.
- [2] Morea F, Marcozzi R, Castaño G. Rheological properties of asphalt binders with chemical tensoactive additives used in Warm Mix Asphalts (WMAs). *Construction and Building Materials*. 2012;29(0):135-41.

Investigation of the effects of Wax Additives On the asphalt binder

- [3] Mo L, Li X, Fang X, Huurman M, Wu S. Laboratory investigation of compaction characteristics and performance of warm mix asphalt containing chemical additives. *Construction and Building Materials*. 2012;37(0):239-47.
- [4] Wang, C., Hao, P., Ruan, F., Zhang, X. and Adhikari, S. Determination of the Production Temperature of Warm Mix Asphalt by Workability Test. *Construction and Building Materials*, 48, 1165-1170, 2013
- [5] Rubio MC, Martínez G, Baena L, Moreno F. Warm mix asphalt: an overview. *Journal of Cleaner Production*. 2012;24(0):76-84.
- [6] Yi-qiu T, Lei Z, Wei-qiang G, Meng G. Investigation of the effects of wax additive on the properties of asphalt binder. *Construction and Building Materials*. 2012;36(0):578-84.
- [7] Aburawi B. Effects of Reduction in Construction Temperature on Workability of Warm Mix Asphalt Incorporating Rh-WMA Additive. First Conference for Engineering Sciences and Technology (CEST-2018), September 25-27, 2018, vol. 2. DOI: <https://doi.org/10.21467/proceedings.4.6>
- [8] Grenfell, J., et al., (2014), Assessing asphalt mixture moisture susceptibility through intrinsic adhesion, bitumen stripping and mechanical damage. *Road Materials and Pavement Design*, 15(1): p. 131 -152.
- [9] Mehrara, A. and A. Khodaii, (2013) A review of state of the art on stripping phenomenon in asphalt concrete. *Construction and Building Materials*, 38: p. 423-442.
- [10] Aburawi B. Effects of Aging and Moisture Damage on Asphaltic Mixture. *Sebha University Journal of Pure & Applied Sciences*, vol. 21 No 4 2022. DOI: 10.51984/JOPAS.V21I4.2124.
- [11] Wang H, Dang Z, You Z, Cao D. Effect of warm mixture asphalt (WMA) additives on high failure temperature properties for crumb rubber modified (CRM) binders. *Construction and Building Materials*. 2012;35(0):281-8.
- [12] Mwanza AD, Hao P, Xongyonyar X. Determination of Mixing and Compaction Temperatures Shift for Asphalt Mastic at Different Type and Content of Mineral Fillers. *IJCEBM*. 2012:159.

Comparison between Non-linear and ANN Models for Prediction of Corrosion Inhibition Efficiency of Mild Steel

RAMZI JALGHAM*

Oil and gas department, College of engineering/Bani Waleed University, Libya

Abstract: QSAR can assist in the quick and low-cost identification of new corrosion inhibitor compounds. Early research revealed a connection between a molecule's quantum parameters and inhibition efficiency (IE). A possible nonlinear equation between experimental inhibition efficiencies (IE_{exp}) of corrosion inhibitors and some quantum parameters was sought for some Triazole derivatives in previous study. This work aims to compare nonlinear model from previous study and artificial neural network (ANN) used in this study to predict inhibition efficiency. The investigation shows that ANN is more efficient and accurate than nonlinear model to predict inhibition efficiencies, where correlation coefficient R (between IE_{exp} and predicted inhibition efficiency (IE_{pred})) increased from 0.95 to 0.99 and mean square error decreased from 4.0×10^{-3} to 6.1×10^{-5} respectively.

Keywords: (QSAR, neural network, corrosion inhibitors, Triazole, modelling, Quantum study)

Introduction

Pipelines are crucial pieces of machinery that are used to move gases and liquids over large distances. In the oil industry, corrosion occurs through procedures including acid cleaning, pickling, and etching, which calls for the use of corrosion inhibitors. The majority of pickling inhibitors are harmful substances. Due to increased global environmental awareness and new environmental protection requirements, these compounds must be replaced with more environmentally acceptable inhibitors. Inhibitors of mild steel corrosion in hydrochloric acid that are non-toxic, like Triazole derivatives, are the focus of this article. Triazole derivatives are among the various heterocyclic chemicals explored as corrosion inhibitors since they are regarded to be environmentally acceptable. Additionally, they are very thermally stable substances that are simple to synthesize, effective at low doses, and inexpensive. For this reason, the main methods for assessing the ability to block and adsorb are electrochemical technique and quantum chemical analysis [1-3].

Numerous approaches, including theoretical and experimental ones, have been used to study the inhibition efficiency of corrosion inhibitors. For instance, the most popular experimental techniques for evaluating the effectiveness of inhibition are electrochemical impedance spectroscopy (EIS), potentiodynamic polarization, and weight losses methodology. They are pricy and time-consuming. Theoretical techniques have overcome all of these challenges [1-3]. Most popular technique is QSAR.

Regression models is a set of statistical procedures for estimating the relationships (linear or nonlinear equations) between a dependent variable and one or more independent variables, that are utilized in the fields of chemical engineering and biological sciences are known as quantitative structure–activity relationship models (QSAR) [4].

Artificial neural networks (ANNs) have become effective tools for modeling links between quantum chemical parameters and IE . It is not always feasible to deal with many corrosion problems by the use of traditional analysis such as nonlinear repression technique. The limitations of traditional methods such multiple linear relationships, partial least squares, and principal component analysis are overcome by the capability of ANN techniques to describe nonlinear relationships [5].

The Triazole compounds that were employed in this work are depicted in Table 1 and Fig. 1 together with their chemical formulas, nomenclature, and structural details. Experimental research has shown these chemicals to be effective in inhibiting corrosion, with efficiencies ranging from 73 to 98.5% [4].

In previous work [4], the nonlinear technique was used to *IE*. Artificial neural networks (ANNs) were used in this study in an effort to forecast *IE*. At the end of this research, a comparison between nonlinear method and the application of ANN for predicting inhibition efficiency was made.

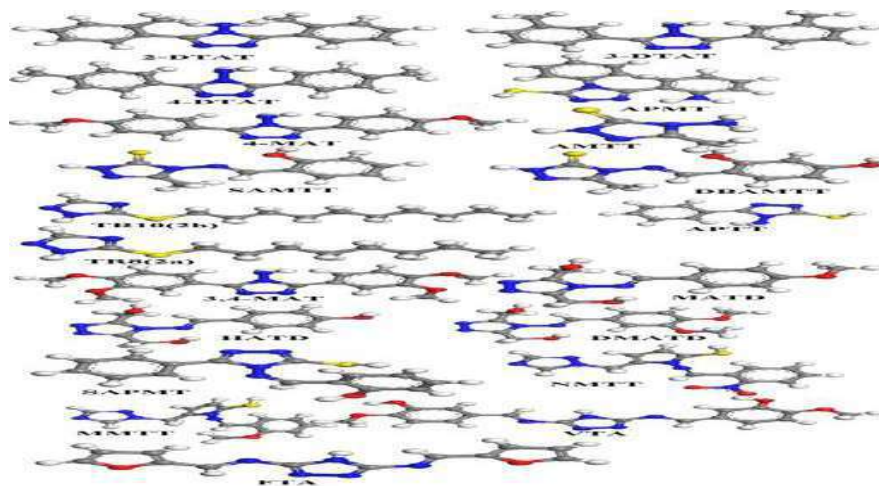


Fig. 1: Chemical structure of Triazole derivatives

Details of calculation methods

Quantum chemical computations were used to examine the molecular structures of the chosen inhibitors. All quantum calculations carried out in the Windows environment with of Material Studio 5.5 using AM1 semi-empirical method. Utilizing the default software parameters, all inhibitors were fully optimized geometrically without any limitations [6].

By the end of the quantum calculations, all calculated quantum parameters are tabulated in Excel file. A table with 20 rows and 10 columns was obtained. Each row corresponds to a certain inhibitor (from inhibitor1 to inhibitor 20) as shown if Fig.2. The columns correspond to quantum parameters: respectively inhibition efficiency *IE*, (energy of highest occupied molecular orbital (EHOMO), energy of lowest unoccupied molecular orbital (ELUMO), Total dipole (μ), surface area of molecule (SA), Energy gap (ΔE), Adsorption energy (E_{ads}), temperature (T), inhibitors concentration (C), and Log of the partition coefficient (AlogP)) [7]. After organization of quantum parameters in Excel file, these data are easily accessed by Matlab Software.

	A	B	C	D	Insert Function		G	H	I	J
1	IE	HOMO eig	LUMO eig	Total dipo	Molecular	ΔE	Adsorptio	T	Ci	AlogP (Fast)
2	0.921	-8.966	-0.414	5.779	306.798	-8.55214	-154.863	30	0.0005	4.856
3	0.883	-9.251	-0.283	5.379	303.578	-8.96852	-151.126	30	0.0005	4.856
4	0.957	-8.846	-0.443	5.511	307.409	-8.40328	-155.334	30	0.0005	4.856
5	0.834	-8.547	-0.432	3.672	278.850	-8.11478	-133.754	25	9.32E-05	3.657
6	0.98	-8.648	-0.388	4.541	324.768	-8.26051	-169.868	30	0.0004	3.416
7	0.73	-8.772	-0.129	3.098	143.402	-8.64292	-62.4055	27	0.0007	0.239
8	0.93	-8.507	-0.490	5.432	246.833	-8.01628	-125.568	27	0.0007	2.513
9	0.94	-8.496	-0.516	4.390	258.299	-7.98041	-127.465	27	0.0007	2.229
10	0.82	-8.692	-0.035	2.648	323.133	-8.65711	-146.651	30	0.000001	4.349
11	0.8	-8.692	-0.036	2.646	279.443	-8.65613	-127.475	30	0.000001	3.556
12	0.9181	-8.605	-0.447	4.423	203.762	-8.15852	-101.817	30	0.0008	2.499
13	0.985	-8.727	-0.580	2.113	384.059	-8.14718	-205.359	35	0.0001	2.910
14	0.9105	-9.259	-0.965	7.183	287.893	-8.29411	-143.797	30	0.001525	2.844
15	0.8824	-9.354	-1.019	6.490	267.400	-8.33546	-132.42	30	0.001611	2.812
16	0.9376	-9.126	-0.984	8.099	319.011	-8.14215	-160.597	30	0.001368	2.591
17	0.956	-8.595	-0.883	3.739	297.219	-7.71214	-159.295	25	0.001687	4.773
18	0.896	-9.094	-1.611	7.807	326.670	-7.48303	-167.276	20	0.001	4.049
19	0.901	-8.700	-0.663	6.853	337.046	-8.03744	-164.211	20	0.001	3.843
20	0.9005	-8.630	-1.321	6.400	278.139	-7.30884	-138.314	28	0.0003	2.982
21	0.93	-8.502	-1.156	1.420	394.798	-7.34609	-201.53	28	0.0003	3.652

Fig. 2: A screenshot of tabulated quantum parameters in Excel file

The excel file was called using xlsread command to load all parameters into Matlab workspace. The quantum parameters table is then presented to artificial neural networks using nftool command to prepare them for prediction of inhibition efficiency [8].

Table 1: Names, nomenclature and molecular properties of studied triazole derivatives

Full name	Nomenclature	Chemical formula	Net mol. mass
3,5-di(3-tolyl)-4-amino-1,2,4-triazoles	3-DTAT	C ₁₆ H ₁₆ N ₄	264.332
3,5-di(2-tolyl)-4-amino-1,2,4-triazoles	2-DTAT	C ₁₆ H ₁₆ N ₄	264.332
3,5-di(4-tolyl)-4-amino-1,2,4-triazoles	4-DTAT	C ₁₆ H ₁₆ N ₄	264.332
3-aminophenyl-4-phenyl-5-mercapto-1,2,4-triazole	APMT	C ₁₄ H ₁₂ N ₄ S	268.338
3,5-bis(4-methoxyphenyl)-4-amino-1,2,4-triazole	4-MAT	C ₁₆ H ₁₆ N ₄ O ₂	296.330
4-amino-5-methyl-4H-1,2,4-triazole-3thiol	AMTT	C ₃ H ₆ N ₄ S	130.169
4-salicylideneamino-3-methyl-1,2,4-triazole-5-thione	SAMTT	C ₁₀ H ₁₀ N ₄ O S	234.277
4-(2,4-dihydroxybenzylideneamino)-3-methyl-1H-1,2,4-triazole-5(4H)-thione	DBAMTT	C ₁₀ H ₁₀ N ₄ O ₂ S	250.276
5-decylsulfanyl-1,2,4-triazole	TR10(2b)	C ₁₂ H ₂₃ N ₃ S	241.397
5-octylsulfanyl-1,2,4-triazole	TR8(2a)	C ₁₀ H ₁₉ N ₃ S	213.343
4-Amino-5-phenyl-4H-1,2,4-triazole-3-thiol	APTT	C ₈ H ₈ N ₄ S	192.240
3,5-bis(3,4-dimethoxyphenyl)-4-amino-1,2,4-triazole	3,4-MAT	C ₁₈ H ₂₀ N ₄ O ₄	356.382
(4-(4-methoxybenzylideneamino)-4H-1,2,4-triazole-3,5-diyl)dimethanol	MATD	C ₁₂ H ₁₄ N ₄ O ₃	262.269
(4-(4-hydroxybenzylideneamino)-4H-1,2,4-triazole-3,5-diyl)dimethanol	HATD	C ₁₁ H ₁₂ N ₄ O ₃	248.242

(4-(3,4-dimethoxybenzylideneamino)-4H-1,2,4-triazole-3,5-diyl)dimethanol	DMATD	C13 H16 N4 O4	292.295
4-salicylideneamino-3-phenyl-5-mercapto-1,2,4-triazole	SAPMT	C15 H12 N4 O S	296.348
1-(2'-nitrobenzyl)methenylideneamino-2-mercapto-5-(1-(1',2',4'-triazol)) methenyl-1,3,4-triazole	NMTT	C14 H12 N6 O2 S	328.350
1-(2''-methoxybenzyl)methenylideneamino-2-mercapto-5-(1-(1',2',4'-triazol)) methenyl-1,3,4-triazole	MMTT	C15 H15 N5 O S	313.379
furfuraldine 3,5-diamino-1,2,4-triazole	FTA	C12 H9 N5 O2	255.237
Vanilidine 3,5-diamino-1,2,4-triazole	VTA	C18 H17 N5 O4	367.365

By default, nftool splits the table into three parts: 15% of the data are used for testing, 15% of the data are used for validation, and 70% of the data are used for training as shown in Fig.3. The algorithm modifies the network parameters throughout the course of 1000 epochs during the learning phase. The mean square error between the computed IE_{calc} and IE_{exp} is calculated during a time. Different training algorithms were tested. The points should ideally go closer to the identify line. The regression factor provides a quantitative evaluation of the overall performance. Also, the number of neurons in the hidden layer is one of ANN's most important characteristics. The network won't be able to model the complex data and the fit won't be good if there aren't enough neurons used. In this work, a small number of hidden layer (10 layer) was employed due to the size of data is large. The Schematically structure of the proposed ANN with 9 inputs (E_{HOMO} , E_{LUM} , μ , SA, ΔE , E_{ads} , T, Ci, and AlogP) and 1 output IE_{calc} is shown in Fig.4 [9-13].

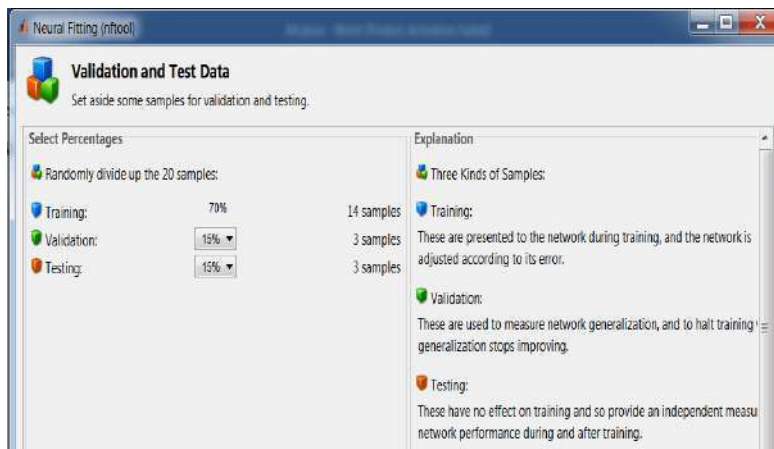


Fig. 3: splitting data into training, validation and tested data

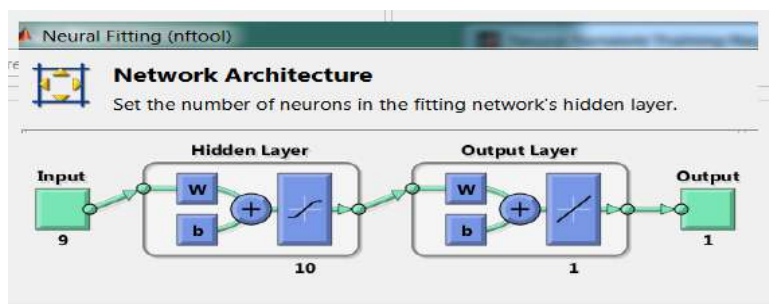


Fig. 4: ANN architecture with 9 input and one output

A statistical relationship between two variables is referred to as a correlation coefficient. There are a number of different kinds of correlation coefficients, but all of them will always fall between -1 and 1, where the strongest possible agreement is very close to 1. The linear relationship's strength and direction are measured by the Pearson product-moment correlation coefficient (R^2). A measure of how well and closely of two variables are related is the correlation coefficient (R) [4].

Results and discussion

The experimental data of inhibition efficacy (Electrochemical impedance spectroscopy (EIS)) were collected from references. This study used AM1 semi-empirical method and QSAR techniques. The compounds in Fig. 1 were subjected to semi-empirical quantum chemical computations, with the results shown in Table 2 [14].

Values for a few quantum chemical characteristics for molecules of Triazole derivatives are listed in Table 2. The HOMO and LUMO energies and how they are distributed across molecules have a crucial role in determining reactivity. The capacity of a molecule to give an electron is often linked to E_{HOMO} , whereas the ability to receive an electron is linked to E_{LUMO} . As a result, the adsorption process is facilitated by larger values of E_{HOMO} and lower values of E_{LUMO} . The results of Table 1 show, the estimated values of E_{HOMO} and E_{LUMO} are not similar to the measured values of IE_{exp} , and the measured quantum chemical parameters altered erratically with IE_{exp} inhibition. This suggested that the inhibitors might not be either the acceptor or the giver of the electrons [15-17].

Additionally, there must be a strong link between quantum parameters and corrosion inhibitor activity in order to derive reliable productivity assumptions. However, none of these parameters and inhibition efficiencies have a clear link. thus the need for new technique is necessary. In previous work, Lukovits non-linear model was employed to perform QSAR. In this study, The QSAR of the studied molecules in Fig. 1 as inhibitors for metal in HCl medium was performed using ANN [19-20]. Between IE_{exp} and IE_{calc} , a strong correlation coefficient R^2 of 0.985 has been obtained. In Table. 3, the calculated IE_{calc} and R^2 values for each approach are provided. In Fig. 4, the values of IE_{calc} and IE_{exp} for the derivatives of triazoles are plotted. A comparison between calculated and experimental values using nonlinear model and ANN is shown in Figure 4. Figures 5 showed a very high correlation coefficient of ANN than nonlinear model. This illustrates the close relationship between experimental and predicted values. The suggested ANN model is stable and predicative, as shown by the strong R^2 according to statistical parameters [21-23].

Comparison between Non-linear and ANN Models for Prediction of Corrosion Inhibition Efficiency of Mild Steel

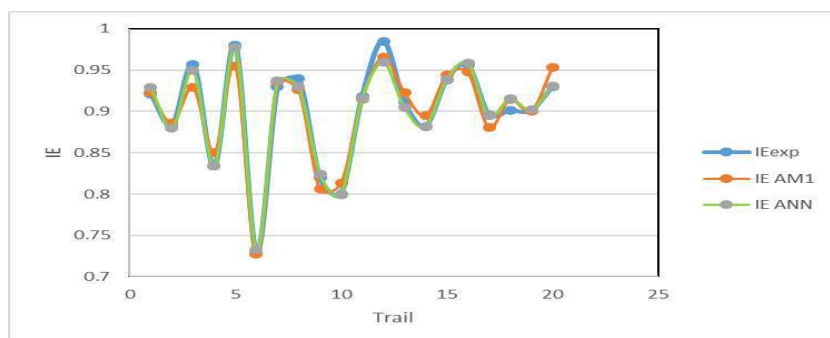


Fig. 5: IE_{calc} obtained by nonlinear method and ANN at different concentrations of compounds Triazole derivatives

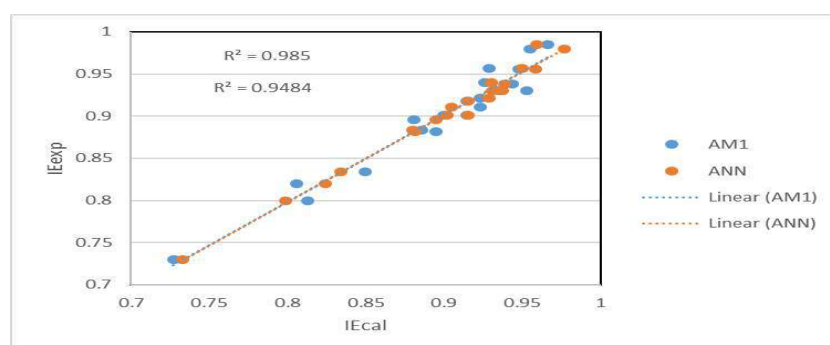


Fig.6: Correlation between IE_{exp} and IE_{calc} using nonlinear method and ANN

Conclusion

After the theoretical tests, it was discovered that the Triazole derivatives' inhibitory efficiency could be predicted using quantum parameters. The investigation shows that ANN is more efficient and accurate than nonlinear model, where correlation coefficient is higher and mean square error is lower. When corrosion measuring devices are not accessible, the ANN might be used to determine predict inhibition efficiency of Triazole derivatives. However, the inhibitory efficiency might be obtained when the quantum parameters are included in the ANN. ANN has higher correlation coefficients than nonlinear model from previous work, which indicate that the model's strength is good and that IE_{calc} and IE_{exp} are extremely close to one another. Following this comparative study, we concluded that ANN is the most appropriate algorithm for this kind of problems.

Table 3. IE_{exp} obtained using EIS of Triazole compounds and IE_{calc} obtained by the proposed equations and ANN method.

				IE_{calc}		
	R			0.974	0.992	Error= $(IE_{exp} - IE_{calc})^2$
	R ²			0.949	0.985	

RAMZI JALGHAM

	Compound	Ci (M)	$I_{E_{exp}}$	AM1	ANN	AM1	ANN
1	3-DTAT	5.00E-04	0.921	0.923	0.929	4.0E-06	6.7E-05
2	2-DTAT	5.00E-04	0.883	0.886	0.880	9.0E-06	1.1E-05
3	4-DTAT	5.00E-04	0.957	0.929	0.950	7.8E-04	4.9E-05
4	APMT	9.32E-05	0.834	0.850	0.834	2.6E-04	7.3E-08
5	4-MAT	4.00E-04	0.980	0.955	0.977	6.3E-04	8.1E-06
6	AMTT	7.00E-04	0.730	0.727	0.733	9.0E-06	7.5E-06
7	SAMTT	7.00E-04	0.930	0.935	0.937	2.5E-05	5.3E-05
8	DBAMTT	7.00E-04	0.940	0.926	0.930	2.0E-04	9.4E-05
9	TR10(2b)	1.00E-06	0.820	0.806	0.824	2.0E-04	1.8E-05
10	TR8(2a)	1.00E-06	0.800	0.813	0.799	1.7E-04	1.0E-06
11	APTT	8.00E-04	0.918	0.915	0.916	9.0E-06	6.2E-06
12	3,4-MAT	1.00E-04	0.985	0.966	0.960	3.6E-04	6.5E-04
13	MATD	1.53E-03	0.911	0.923	0.905	1.4E-04	3.9E-05
14	HATD	1.61E-03	0.882	0.895	0.882	1.7E-04	3.5E-08
15	DMATD	1.37E-03	0.938	0.944	0.939	3.6E-05	5.0E-07
16	SAPMT	1.69E-03	0.956	0.948	0.958	6.4E-05	5.4E-06
17	NMTT	1.00E-03	0.896	0.881	0.895	2.3E-04	8.4E-07
18	MMTT	1.00E-03	0.901	0.915	0.915	2.0E-04	2.1E-04
19	FTA	3.00E-04	0.901	0.900	0.902	1.0E-06	8.6E-07
20	VTA	3.00E-04	0.930	0.953	0.931	5.3E-04	1.3E-06
				mean squared error		4.0E-03	6.1E-05

References

1. Fang, J., & Li, J. (2002). Quantum chemistry study on the relationship between molecular structure and corrosion inhibition efficiency of amides. *Journal of Molecular Structure: THEOCHEM*, 593(1-3), 179-185. DOI: [10.1016/s0166-1280\(02\)00316-0](https://doi.org/10.1016/s0166-1280(02)00316-0)
2. Murmu, M., Saha, S. K., Murmu, N. C., & Banerjee, P. (2019). Effect of stereochemical conformation into the corrosion inhibitive behaviour of double azomethine based Schiff bases on mild steel surface in 1 mol L⁻¹ HCl medium: An experimental, density functional theory and molecular dynamics simulation study. *Corrosion Science*, 146, 134-151. DOI: [10.1016/j.corsci.2018.10.002](https://doi.org/10.1016/j.corsci.2018.10.002)
3. Fernandes, C. M., Alvarez, L. X., dos Santos, N. E., Barrios, A. C. M., & Ponzio, E. A. (2019). Green synthesis of 1-benzyl-4-phenyl-1H-1, 2, 3-triazole, its application as corrosion inhibitor for mild steel in acidic medium and new approach of classical electrochemical analyses. *Corrosion Science*, 149, 185-194. DOI: [10.1016/j.corsci.2019.01.019](https://doi.org/10.1016/j.corsci.2019.01.019)
4. Jalgham, R. T. (2021). Theoretical, Monte Carlo simulations and QSAR studies on some triazole derivatives as corrosion inhibitors for mild steel in 1 M HCl. *ES Energy & Environment*, 13, 37-49. DOI: [10.30919/ese8c476](https://doi.org/10.30919/ese8c476)
5. Alamri, A. H., & Alhazmi, N. (2022). Development of data driven machine learning models for the prediction and design of pyrimidine corrosion inhibitors. *Journal of Saudi Chemical Society*, 26(6), 101536. DOI: [10.1016/j.jscs.2022.101536](https://doi.org/10.1016/j.jscs.2022.101536)
6. Zhou, P., Yang, L., Hou, Y., Duan, G., Yu, B., Li, X., ... & Wang, F. (2021). Grain refinement promotes the formation of phosphate conversion coating on Mg alloy AZ91D with high corrosion resistance and low electrical contact resistance. *Corrosion Communications*, 1, 47-57. DOI: [10.1016/j.corcom.2021.05.001](https://doi.org/10.1016/j.corcom.2021.05.001)
7. Allam, N. K. (2007). Thermodynamic and quantum chemistry characterization of the adsorption of triazole derivatives during Muntz corrosion in acidic and neutral solutions. *Applied Surface Science*, 253(10), 4570-4577. DOI: [10.1016/j.apsusc.2006.10.008](https://doi.org/10.1016/j.apsusc.2006.10.008)
8. El Ashry, El Sayed & El Nemr, Ahmed & Essawy, Samy & Ragab, Safaa. (2006). Corrosion inhibitors part 3: quantum chemical studies on the efficiencies of some aromatic hydrazides and Schiff bases as corrosion inhibitors of steel in acidic medium. *ARKIVOC: archive for organic chemistry*. 205-220. DOI: [10.3998/ark.5550190.0007.b21](https://doi.org/10.3998/ark.5550190.0007.b21)
9. Khadom, A. A., Mahdi, M. S., & Mahood, H. B. (2020). Mathematical regression and artificial neural network for prediction of corrosion inhibition process of steel in acidic media. *Journal of Bio-and Tribo-Corrosion*, 6(3), 1-10. DOI: [10.1007/s40735-020-00390-7](https://doi.org/10.1007/s40735-020-00390-7)
10. Samide, A., Stoean, C., & Stoean, R. (2019). Surface study of inhibitor films formed by polyvinyl alcohol and silver nanoparticles on stainless steel in hydrochloric acid solution using convolutional neural networks. *Applied Surface Science*, 475, 1-5. DOI: [10.1016/j.apsusc.2018.12.255](https://doi.org/10.1016/j.apsusc.2018.12.255)
11. Boucherit, M. N., Amzert, S. A., Arbaoui, F., Boukhari, Y., Brahimi, A., & Younsi, A. (2019). Modelling input data interactions for the optimization of artificial neural networks used in the prediction of pitting corrosion. *Anti-Corrosion Methods and Materials*. DOI: [10.1108/ACMM-07-2018-1976](https://doi.org/10.1108/ACMM-07-2018-1976)
12. Al-Hazam, H. A. (2010). Prediction of corrosion inhibitor efficiency of some aromatic hydrazides and schiff bases compounds by using artificial neural network. *Journal of Scientific Research*, 2(1), 108-113. DOI: [10.3329/jsr.v2i1.2757](https://doi.org/10.3329/jsr.v2i1.2757)
13. Boukhari, Y., Boucherit, M. N., Zaabat, M., Amzert, S., & Brahimi, K. (2017). Artificial intelligence to predict inhibition performance of pitting corrosion. *Journal of Fundamental and Applied Sciences*, 9(1), 309-322. DOI: [10.4314/jfas.v9i1.19](https://doi.org/10.4314/jfas.v9i1.19)
14. Musa, A. Y., Mohamad, A. B., Takriff, M. S., & Jalgham, R. T. (2012). Electrochemical and quantum chemical studies on phthalhydrazide as corrosion inhibitor for mild steel in 1 M HCl

- solution. *Research on Chemical Intermediates*, 38(2), 453-461. DOI: [10.1007/s11164-011-0362-3](https://doi.org/10.1007/s11164-011-0362-3)
15. Ouchenane, S., Jalgham, R., Rezgoun, S., Saifi, H., & Bououdina, M. (2021). Experimental and theoretical studies of the corrosion inhibition properties of 2 amino, 4-6-dimethylpyrimidine for Mild Steel in 0.5 M H₂SO₄. *Chemistry Africa*, 4(3), 621-633. DOI: [10.1007/s42250-021-00239-7](https://doi.org/10.1007/s42250-021-00239-7)
 16. Musa, A. Y., Jalgham, R. T. T., & Mohamad, A. B. (2012). Molecular dynamic and quantum chemical calculations for phthalazine derivatives as corrosion inhibitors of mild steel in 1M HCl. *Corrosion Science*, 56, 176-183. DOI: [10.1016/j.corsci.2011.12.005](https://doi.org/10.1016/j.corsci.2011.12.005)
 17. Khaled, K. F. (2010). Experimental and molecular dynamics study on the inhibition performance of some nitrogen containing compounds for iron corrosion. *Materials Chemistry and Physics*, 124(1), 760-767. DOI: [10.1016/j.matchemphys.2010.07.055](https://doi.org/10.1016/j.matchemphys.2010.07.055)
 18. Khaled, K. F. (2010). Electrochemical behavior of nickel in nitric acid and its corrosion inhibition using some thiosemicarbazone derivatives. *Electrochimica Acta*, 55(19), 5375-5383. DOI: [10.1016/j.electacta.2010.04.079](https://doi.org/10.1016/j.electacta.2010.04.079)
 19. Musa, A. Y., Mohamad, A. B., Kadhum, A. A. H., Takriff, M. S., & Ahmoda, W. (2012). Quantum chemical studies on corrosion inhibition for series of thio compounds on mild steel in hydrochloric acid. *Journal of Industrial and Engineering Chemistry*, 18(1), 551-555. DOI: [10.1016/j.jiec.2011.11.131](https://doi.org/10.1016/j.jiec.2011.11.131)
 20. Álvarez, P. M., García-Araya, J. F., Beltrán, F. J., Masa, F. J., & Medina, F. (2005). Ozonation of activated carbons: Effect on the adsorption of selected phenolic compounds from aqueous solutions. *Journal of Colloid and Interface Science*, 283(2), 503-512. DOI: [10.1016/j.jcis.2004.09.014](https://doi.org/10.1016/j.jcis.2004.09.014)
 21. Dagdag, O., Berisha, A., Safi, Z., Dagdag, S., Berrani, M., Jodeh, S., Verma, C., Ebenso, E. E., Wazzan, N., & El Harfi, A. (2020). Highly durable macromolecular epoxy resin as anticorrosive coating material for carbon steel in 3% NaCl: Computational supported experimental studies. *Journal of Applied Polymer Science*, 137(34), 49003. DOI: [10.1002/app.49003](https://doi.org/10.1002/app.49003)
 22. Asadi, N., Ramezanzadeh, M., Bahlakeh, G., & Ramezanzadeh, B. (2019). Utilizing Lemon Balm extract as an effective green corrosion inhibitor for mild steel in 1M HCl solution: A detailed experimental, molecular dynamics, Monte Carlo and quantum mechanics study. *Journal of the Taiwan Institute of Chemical Engineers*, 95, 252-272. DOI: [10.1016/j.jtice.2018.07.011](https://doi.org/10.1016/j.jtice.2018.07.011)
 23. Lukovits, I., Kálmán, E., & Pálincás, G. (1995). Nonlinear Group-Contribution Models of Corrosion Inhibition. *CORROSION*, 51(3), 201-205. DOI: [10.5006/1.3294362](https://doi.org/10.5006/1.3294362).

Effect of salinity on seed germination and seedling growth of bread wheat

Amar Omran Alshmam

Crops Department, College of Agriculture/University of Tripoli, Libya

Abstract: At the Crop Physiology Lab, Faculty of Agriculture, University of Tripoli, Libya. (February 2022), Salinity effects were evaluated on seed germination and seedling growth bread wheat (*Triticum aestivum* L.) variety Utique. The seeds were grown in Petri dishes to five levels of electrical conductivity (Ec) 0, 2.5, 5, 7.5, and 10 ds/m, with three replicates. The data for the water uptake percentage, germination percentage, shoot length (cm), root length (cm), dry weight of root (g) and dry weight of shoot (g) was measured eight days after germination. The experimental statistical analysis was performed using one-way ANOVA ($P < 0.05$). Based on the ANOVA results, a DUNCAN test was performed to compare means.

The results show that the water uptake by seeds has a direct relationship with increases in NaCl levels. Where the highest water uptake level was recorded at low concentrations of NaCl. By increasing NaCl concentration, seed germination is delayed and decreased. Increasing NaCl concentrations adversely affected shoot length and root length and also, adversely affected shoot dry weight and root dry weight.

Probably, it was the delay in germination was mainly due to higher Na^+ accumulation in the seeds rather than osmotic stress in bread wheat.

Keywords: Salinity, NaCl, Germination, water uptake, Bread wheat.

Introduction

The Food and Agriculture Organization (FAO, 2009) indicated that the world population is envisaged to increase by 34 % in 2050 reaching about 9.1 billion, thus necessitating 70 % more food production. Meeting the nutritional requirements of the growing population remains a challenging task as climate changes threaten the sustainability and productivity of agricultural production systems (Hussain et al., 2014). Plants experience various abiotic stresses in the field. Modern agriculture also faces several abiotic stresses, such as sub-optimal levels of salinity, drought, chilling and temperature, as major constraints affecting crop yields (Saud et al. 2013). According to Wang et al., (2001), more than a 50 % reduction in the average yield of major crops has been attributed to abiotic stresses.

Plants use many strategies in response to abiotic stress, which ultimately improves plant growth and productivity in stressful environments. These phenomena include changes in morphological and developmental patterns (growth plasticity), also, physiological and biochemical processes against several stresses (Saud et al. 2014). The plant can try to escape or survive under stressful conditions that can reduce its growth so that the plant can concentrate its resources on stress resistance (Skirycz and Inze 2010).

In the world, soil salinity has adversely affected about 30 % of the irrigated, this represents about 6 % of the total land area (Chaves et al. 2009), which leads to a resultant monetary loss of 12 billion dollars (USD) in agricultural production (Shabala, 2013). According to FAO (2005), soil salinity is one of the major stressors affecting more than 831 million hectares of agricultural land worldwide.

Salinity is one of the most important abiotic stresses limiting crop production in dry and semi-dry regions, where soil salt content is naturally high and precipitation can be insufficient for leaching (Saboora and Kiarostami., 2006).

Increased incidence of salinity on arable lands suggests the need for a better understanding of the plant tolerance mechanisms in order to sustain crop productivity by modulating growth conditions to the best possible extent. Where under soil salinity, the plants have been inhibition of growth and

development, and reduction in photosynthesis, respiration and protein synthesis in sensitive species (Mustafa et al. 2014; Hussain et al. 2013).

Wheat (*Triticum aestivum* L.) is the staple food for more than 35% of the world's population (Jing and Chang., 2003). Wheat grain yield is depressed, by environmental stresses such as drought, heat, low temperatures, low fertility (especially nitrogen) and soil salinity (Mehmet et al., 2006). As with other crops, seed germination and wheat seedling growth have been negatively affected by drought (Passioura, 1988) and salinity stresses (Hampson and Simpson, 1990). According to Mehmet et al., (2006), any effect that drought might have should be most considerable under salt-stressed conditions because salinity can affect germination and seedling growth either by creating an osmotic pressure (OP) that prevents water uptake or by toxic effects of sodium and chloride ions on the germinating seed. The salt accumulation in soils affects plant growth to different degrees (Bernstein, 1975). However, in the same saline environment, different plant species may exhibit different growth responses (Mehmet et al., 2006).

Many studies are reported that several plants are sensitive to high salinity during germination and the seedling stage (Ghoulam and Fares., 2001). The source of the sensitivity to salinity is not fully understood. Where some researchers have indicated that the main reason for germination failure was the inhibition of seed water uptake due to a high salt concentration (Mehmet et al., 2006), whereas others have suggested that germination was affected by salt toxicity (Mehmet et al., 2006; Khajeh-Hosseini et al., 2003).

Wheat is cultivated over a wide range of environments, because of wide adaptation to diverse environmental conditions. It is a moderately salt-tolerant crop (Moud and Maghsoudi 2008; Saboora and Kiarostami., 2006).

The main goal of this study was to determine the effects of salinity on water uptake, seed germination, and seedling growth by seeds of bread wheat during germination at various concentrations of NaCl.

1. Materials and Methods

1.1. Seed Source

Seeds of bread wheat (*Triticum aestivum* L.) variety Utique was used for this study. The seeds were obtained from the Ministry of Agriculture. Before cultivation, seeds were sterilized in 1% sodium hypochlorite solution for 3 min, and then were rinsed with sterilized water and air-dried.

1.2. Preparation of NaCl solutions

The solutions were prepared based on methods by (Rhoades, et. al., 1992) with electrical conductivity (Ec) of 0 (as control), 2.5, 5, 7.5 and 10 ds/m.

1.3. Water uptake

Water uptake was recorded at 12 hours after planting. The water uptake percentage was calculated by the formula given below (Rahman et. al., 2008).

$$\text{Water uptake \%} = (W2 - W1/W1)100$$

Where:

W1 = Initial weight of seed

W2 = Weight of seed after absorbing water in a particular time.

1.4. Germination test

The experiment was carried out in three replicates where 10 seeds were separately germinated on two sheets of Whatman No.1 filter paper placed in 9-cm diameter Petri dishes. Priority, 10 ml of the respective test solution was poured into every dish. The papers were altered once every 2 days to

prevent salt accumulation (Rehman et al., 1996). The plates were incubated at $25 \pm 2^\circ\text{C}$ in darkness for 8 days (Rhoades, et. al., 1992). Germination percentages were recorded every 24 h for 4 days. Mean germination was calculated to assess the germination rate (Ellis and Roberts, 1980).

The data for the shoot length (cm), root length (cm), dry weight of root (g) and dry weight of shoot (g) was measured eight days after germination. Dry weights were measured after drying at 70°C for 48 h in an oven.

1.5. Data analysis

Statistical analysis was performed using one-way ANOVA (for $P < 0.05$). Based on the ANOVA results, a DUNCAN test to compare the averages, and test for significant differences among treatments by the GenStat program (Release; 19.3.0.9425; VSN International, Nottingham, UK). In the figures, different letters (a,b,c,...) between the columns express significant differences.

2. Results

2.1. Water uptake

A direct relationship was observed between water uptake by seeds and an increase in NaCl concentration ($P = 0.002$) (Figure 1). When NaCl concentration increases the water uptake ability decrease in comparison to the control. Maximum water uptake was recorded in (0, 2.5) NaCl concentration, where no significant effect between these concentrations.

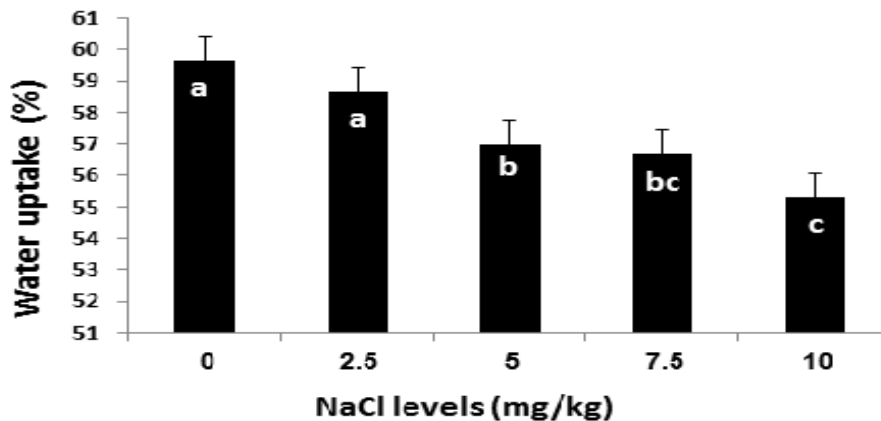


Figure 1: The effect of the different levels of NaCl concentration on water uptake by wheat seeds

2.2. Seeds germination (%)

The effect of increasing NaCl levels on germination percentage after 96 hours (final germination) is shown in (Figure 2). Results showed by increasing NaCl concentration, germination is delayed and decreased germination ($P < .001$). The maximum germination percentage was observed in the control compared with other levels of NaCl concentrations.

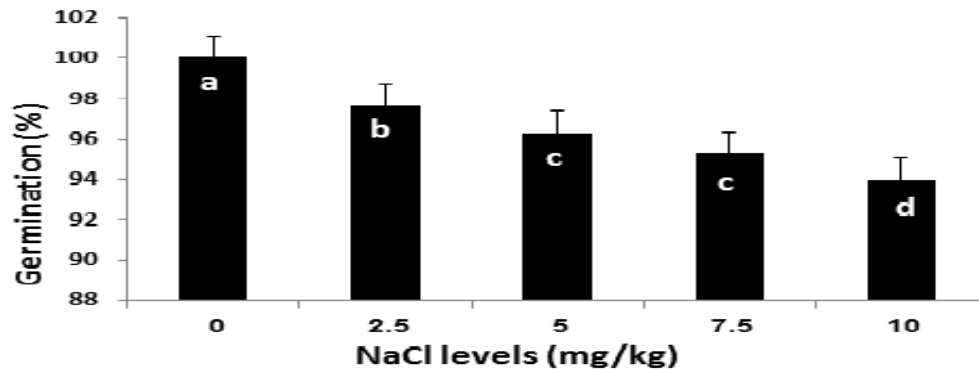


Figure 2: The effect of the different levels of NaCl concentration on seeds of wheat germination (%)

2.3. Shoot length (cm)

The mean of shoot length varied between 11.87 and 15.74 cm at various NaCl concentrations. The longest shoot length was observed in the control. Also, by increasing NaCl concentrations, the shoot length decreased. Results showed that the shoot growth was more affected by NaCl levels ($P < .001$) (Figure 3).

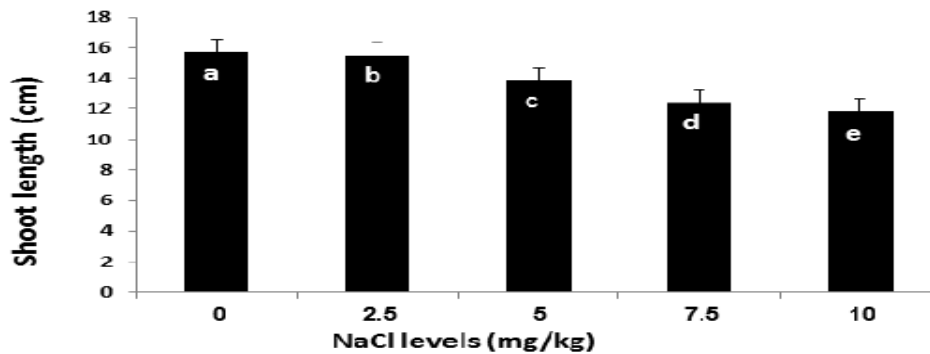


Figure 3: The effect of the different levels of NaCl concentration on shoot length (cm) of wheat

2.4. Root length (cm)

The mean root length varied between 9.39 and 12.31 cm in different NaCl concentrations. As was expected, the control (0 ds/m) and the highest (10 ds/m) NaCl concentration had the longest and shortest root length (12.31 cm & 9.39 cm) respectively. Generally, root length decreased as NaCl concentration increased significantly ($P < .001$) (Figure 4).

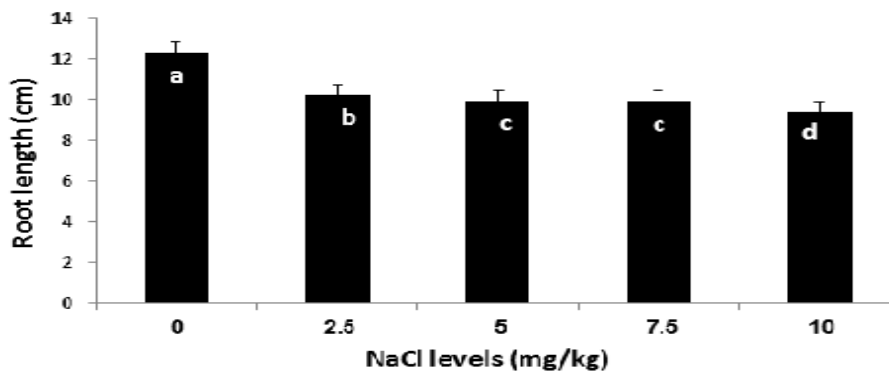


Figure 4: The effect of the different levels of NaCl concentration on root length (cm) of wheat

2.5. Shoot dry weight (mg/plant)

Increasing NaCl concentrations adversely affected significantly ($P < .001$) (Figure 5), shoot dry weight (mg/plant). Where the weight decreased with the increase in NaCl concentration. The control and the highest NaCl concentration had the longest and shortest shoot dry weight (0.128 mg/plant & 0.101 mg/plant) respectively.

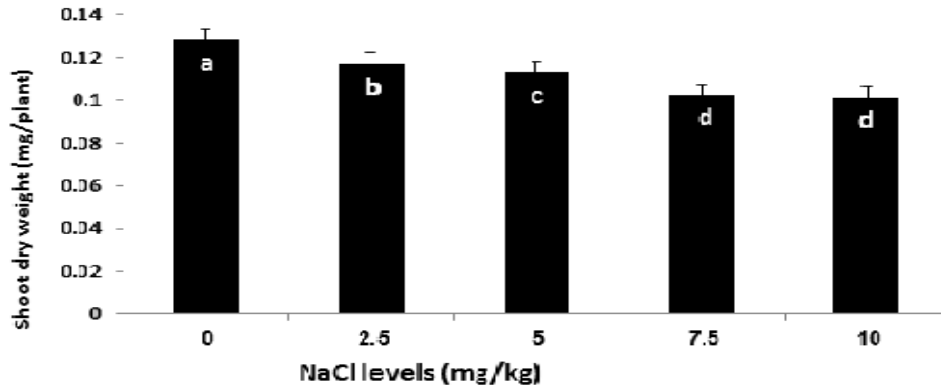


Figure 5: The effect of the different levels of NaCl concentration on shoot dry weight (mg/plant) of wheat

2.6. Root dry weight (mg/plant)

Higher NaCl concentrations resulted in a significant reduction in root dry weight ($P < .001$) (Figure 6). The results showed that the control and the highest NaCl concentration had the longest and shortest root dry weight (0.121 & 0.092 mg/plant) respectively.

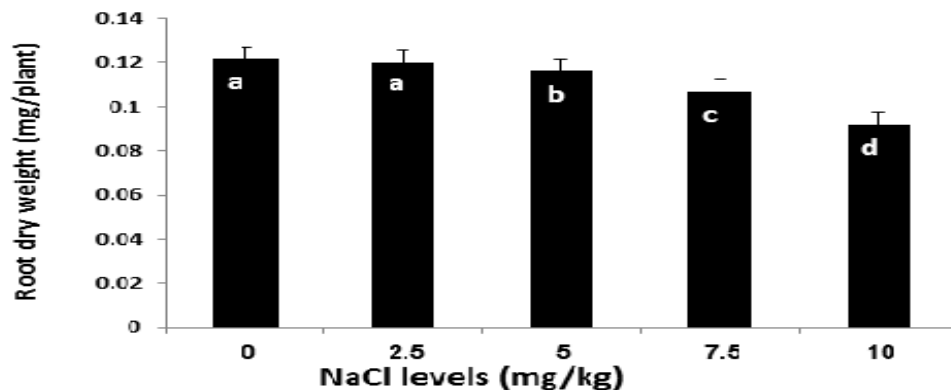


Figure 6: The effect of the different levels of NaCl concentration on root dry weight (mg/plant) of wheat

3. Discussion

This research was carried out to observe the effects of salinity on the germination and seedling growth of bread wheat. The maximum germination percentages were 100 % with control (0 sd/m). The results showed that by increasing NaCl concentrations, germination the delayed and decreased. Increasing salinity concentrations often cause osmotic and/or specific toxicity which may reduce germination percentage (Saboora and Kiarostami., 2006). A slight decrease in water uptake was observed by increasing NaCl levels. The osmotic barrier due to NaCl level affected water uptake and mean germination time but not final germination, this result was similar to the result of (Mehmet et al., 2006). Also, NaCl affected seed germination by creating an external osmotic potential preventing water

uptake. However, a number of studies have demonstrated that water uptake in plants is significantly reduced under salt or water stress conditions (Mehmet et al., 2006; Moud and Maghsoudi, 2008; Saboora and Kiarostami., 2006).

Root and shoot length decreased by increasing NaCl concentration. This result is similar to those reported by (Saboora and Kiarostami., 2006). As NaCl concentration increased, it antagonistically affected shoot and root dry weight. The reduction of dry weights relatively depended on the shoot or root lengths. Also, the wheat shoots were more severely affected by increasing NaCl concentrations than the roots.

In conclusion, it seems that the delay in seed germination was related more to Na⁺ accumulation in seeds rather than lower water uptake in wheat. Therefore, it is necessary to know the NaCl concentration in the shoots and roots in order to estimate the reasons for the delay in germination.

4. References

- 1) Bernstein, L., (1975). Effects of salinity and sodicity on plant growth. Annual Review of Phytopathology, 13(1), pp. 295–312.
- 2) Chaves, MM, Flexas J, Pinheiro C, (2009). Photosynthesis under drought and salt stress: regulation mechanisms from whole plant to cell. Ann Bot 103:551–560.
- 3) Ellis, R.H., Roberts, E.H., (1980). Towards a rational basis for testing seed quality. In: Hebblethwaite, P.D. (Ed.), Seed Production. Butterworths, London, pp. 605–635.
- 4) FAO (Food and Agricultural Organization), (2009). Land and plant nutrition management service. www.fao.org/wsfs/forum2050/.
- 5) FAO (Food and Agriculture Organization of the United Nations), (2005). Global network on integrated soil management for sustainable use of salt-affected soils. Rome, Italy: FAO Land and Plant Nutrition Management Service. <http://www.fao.org/ag/AGL/agll/spush>.
- 6) Ghoulam, C. and K. Fares., (2001). Effect of salinity on seed germination and early seedling growth of sugar beet (*Beta vulgaris* L.). Seed Sci. & Technol, 29: 357-364.
- 7) Hampson, C. and Simpson, G., (1990). Effects of temperature, salt, and osmotic potential on early growth of wheat (*Triticum aestivum*). I. Germination. Canadian Journal of Botany, 68(3), pp.524-528.
- 8) Hussain, S, Khaliq A, Matloob A, Wahid MA, Afzal I. (2013). Germination and growth response of three wheat cultivars to NaCl salinity. Soil Environ 32:36–43.
- 9) Hussain, S, Peng S, Fahad S, Khaliq A, Huang J, Cui K, Nie L, (2014). Rice management interventions to mitigate greenhouse gas emissions: a review. Environ Sci Pollut Res.
- 10) Jing, R.L. and X.P. Chang., (2003). Genetic diversity in wheat (*Triticum aestivum* L.) germplasm resources with drought resistance, Acta Botanica Boreal-Occident Sinica 23: 410-416.
- 11) Khajeh-Hosseini, M., Powell, A.A. and Bingham, I.J., (2003). The interaction between salinity stress and seed vigour during germination of soyabean seeds. *Seed Science and Technology*, 31(3), pp. 715–725.
- 12) Mehmet, A., M.D. Kaya and G. Kaya. (2006). Effects of NaCl on the germination, seedling growth and water uptake of triticale. Turkish Journal of Agriculture and Forestry 30: 39-47.
- 13) Moud, AM, Maghsoudi K., (2008). Salt stress effects on respiration and growth of germinated seeds of different Journal of Plant Interactions 95 wheat (*Triticum aestivum* L.) cultivars. World J Agric Sci. 4:351-358.

- 14) Mustafa, Z, Pervez MA, Ayyub CM, Matloob A, Khaliq A, Hussain S, Ihsan MZ, Butt M, (2014). Morpho-physiological characterization of chilli genotypes under NaCl salinity. *Soil Environ* 33:133–141.
- 15) Passioura, J., (1988). Root Signals Control Leaf Expansion in Wheat Seedlings Growing in Drying Soil. *Functional Plant Biology*, 15(5), p.687.
- 16) Rahman, M., U.A. Soomro, M.Z. Haq and S. Gul. (2008). Effects of NaCl salinity on wheat (*Triticum aestivum* L.) cultivars. *World Journal of Agricultural Sciences* 4: 398-403.
- 17) Rehman, S., Harris, P.J.C., Bourne, W.F., Wilkin, J., (1996). The effect of sodium chloride on germination and the potassium and calcium content of Acacia seeds. *Seed Sci. Technol.* 25, 45–57.
- 18) Rhoades, J.D., Kandiah, A. and Mashali, A.M., (1992). The Use of saline waters for Crop production. *FAO Irr. And Drain. Paper no: 48, p: 1 133, Rome, available at: https://www.ars.usda.gov/arsuserfiles/20361500/pdf_pubs/P1313.pdf* (Accessed: February 7, 2022).
- 19) Saboor, A., and Kiarostami, S., (2006). Salinity (NaCl) Tolerance of Wheat Genotypes at Germination and Early Seedling Growth. *Pakistan Journal of Biological Sciences*, 9(11), pp.2009-2021.
- 20) Saud, S, Chen Y, Baowen L, Fahad S, Arooj S, (2013). The different impact on the growth of cool season turf grass under the various conditions on salinity and drought stress. *Int J Agric Sci Res* 3(4):77–84.
- 21) Saud, S, Li, X, Chen Y, Zhang L, Fahad S, Hussain S, Sadiq A, Chen Y, (2014). Silicon application increases drought tolerance of Kentucky bluegrass by improving plant water relations and morphophysiological functions. *Sci World J*.
- 22) Shabala, S, (2013). Learning from halophytes: physiological basis and strategies to improve abiotic stress tolerance in crops. *Ann Bot* 112:1209–1221.
- 23) Skirycz, A, Inze´ D, (2010). More from less: plant growth under limited water. *Curr Opin Biotechnol* 21:197–203.
- 24) Wang, Y, Mopper S, Hasentein KH, (2001). Effects of salinity on endogenous ABA, IAA, JA, and SA in *Iris hexagona*. *J Chem Ecol* 27:327–342.

Thermal Energy Harvesting based Novel Wireless Sensor Node with Wired Measurement for Condition Monitoring of Gearbox

Badradin Elforjani^a, Samieh Abusaad^b, Dr Fung^c, Dr^d A Ball

^aDepartment of Electrical Eng., Higher Institute of Science and Technology Azizia, Libya

^bControl Department, College of Electronic Technology Tripoli, Libya

^{c,d}Centre for Efficiency and performance Engineering, University of Huddersfield

Abstract: during operation processes, industrial rotating machines revolve at variable speed under different loads. Under such operating conditions a heat would be generated within the internal components. Yet, temperature may increase within the machines when a fault is developing inside them. Therefore, the temperature of machines can be used effectively to monitor the condition of industrial equipment. This comparative study investigates the use of a novel wireless temperature node and compares the results obtained by wired measurement one. Both nodes are used to monitor the condition a gearbox transmission system under different operating circumstances. That is, the wireless temperature node was fabricated with a novel feature in that it is supplied by a thermoelectric generator module. The module is mounted on the gearbox without the need of using a wired power source or the requirement for recharging, or changing, batteries. Data collected by the node is transferred via a Low Energy Bluetooth and received by CC2540. The collected data is then analysed using a portable monitoring device, such as a PC. Results obtained show that the system can provides reliable monitoring information about the temperature of the monitored gearboxes. Experiments performed demonstrate an outstanding performance of the proposed system which make it suitable for wireless and wired condition monitoring purposes.

Keywords: (energy harvesting, wireless sensor networks, condition monitoring, temperature)

Introduction

Maintenance has become increasingly important to the industrial automated manufacturing processes. Meanwhile, the investment on maintenance has grown quickly with the increasing complexity of machines. Temperature monitoring is one of the most commonly and enormously known monitoring techniques used in the industrial machines. It is widely utilized for mechanical and electric machines. It also provides useful monitoring information about the condition of the components in machines. The gearbox is one of the most important components in the manufacturing. The maintenance cost for the gearbox is very high compared to other high failure rate components such as electric and hydraulic systems. With high and variable rotating speed under time varying load conditions, this bringing great challenges to the monitoring the conditions of gearboxes [1-3]. Cost performance is another factor that should be taken in to account in gearbox condition monitoring. Temperature is an important health indicator of mechanical equipment such as gearboxes [4, 5].

Thermoelectric modules are significant alternative to heat engines in the harvesting of waste heat. Precisely, temperature difference is used in thermoelectric systems based on micro converters exploiting Seebeck effects which are widely known as thermoelectric generators (TEGs). Many applications have been used with TEGs such as structural health monitoring applications [6-9].

The wireless sensor networks (WSN) are becoming widely adopted for many applications including complicated tasks like building energy management. However, one major concern for WSN technology is the short lifetime and high maintenance cost due to the limited battery energy. As lower power products have been used in WSN, energy harvesting technologies, due to their own characteristics, attract more and more attention in this area. Therefore, one of the solutions is to harvest ambient energy, which is then rectified to power the WSN [10,11].

Nowadays, smartphones employ major market of mobile phones than traditional cell phones. Smartphones with the development of wireless transmission technology, the researches on health management, telecommunication and monitoring of physiological signals have been important topics [12,13].

There are number of wireless protocols which can be utilised to establish a wireless sensor networks (WSN). Protocols like WiFi-HaLow, Bluetooth low energy (BLE), ZigBee and Thread are more suitable for long-term non-critical CM battery powered nodes due to inherent merits like low cost, self-organising network, and low power consumption. WirelessHART and ISA100.11a provide more reliable and robust performance but their solutions are usually more expensive, thus they are more suitable for strict industrial control applications [12].

It is particularly suitable for those devices that need transfer small quantity of data and within relatively short range such as medical instruments, health management devices and remote controllers. BLE technology can remove the inconvenience of wired transmission and eliminate the disadvantage of high power consumption in ordinary wireless transmission. In addition, more and more smartphones gain support for BLE, the possibilities of using the technology for new types of applications increase. In addition, WSN node appropriated for using in ultra-low power consumption and energy harvesting support has been developed for the purposes of environmental monitoring [11]-[14,15]

System Design

The block diagram of TEG powered sensor node is shown in Fig. 1, which includes a thermal energy harvester a DC-DC converter for boosting the voltage, a wireless sensor node for measuring temperature and transmitting data and received data by USB module, then monitored using portable monitoring devices, such as PC or smartphone. They will be introduced separately in the following four sub sections.

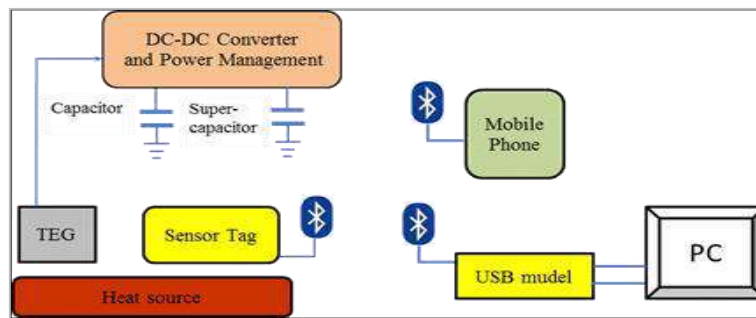


Fig. 1: Block diagram of TEG power sensor node

A. Thermal Energy Harvesting Generator Design

The thermal design is shown in Fig. 2; which consists of: TEG thermal insulation material, a heat sink, and two pieces of thin aluminium; the aluminium plates have been chosen due to the large thermal conductivity. One piece is to work as a heat collector for hot side, while the other one acts as a heat spreader for cold side. The design was built by using a commercially available TE module CP85438 [20]. The TEG is sandwiched between the two pieces of aluminium. Note that, some thermal insulation materials are stuffed between the two pieces of aluminium plates to reduce the heat transmission through the air flow from hot side to the cold side. A thermal insulating material, (thermal heat sink transfer double side adhesive) is designed to maintain temperature difference between hot and cold sides of TEG. Also, another insulation material is designed to surround the TEG module. It has been

worked in the thermal design to isolate the heat source from the heat sink. This is due to the fact that the heat source is close to the heat sink, so that is to reduce the heat transfer capability of the heat sink.

The heat sink plays an important role in the thermal energy harvester to maintain a temperature difference by radiating the heat on the cold side of the TEG module efficiently to the surrounding air. Here a medium size heat sink with thermal resistance of $1.5\text{ }^{\circ}\text{C}/\text{W}$ has been used.

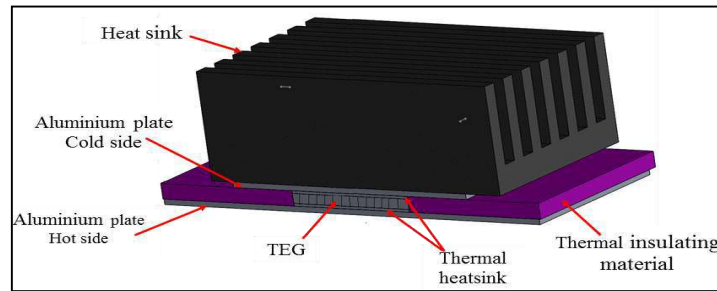


Fig. 2: Structure of the TEG Design

B. Wireless Temperature Node

To measure gearbox temperature, an integrated wireless sensor node named Sensor Tag is employed. As shown in Fig. 3, this compact sensor node integrates 10 low-power MEMS sensors and a two core BLE microcontroller CC2650 [21]. Two temperature sensors are available on the node with one for measuring object temperature and other for ambient temperature. Another benefit of this module is that its programs are open source, which enables to customize the data acquisition and embed intelligent signal processing algorithms on it.

The sensor Tag is specially designed for low power consumption applications and can be supplied by a coin battery [22,23]. Here, the coin battery is not used; instead the sensor tag is powered by the energy harvested from waste heat in order to avoid the inconvenience of changing the batteries during the lifetime of the system.



Fig. 3, Sensor tag CC2650K

C.USB Module

The The CC2540 USB evaluation module kit as shown in Fig. 4 contains one Bluetooth low energy USB dongle. The dongle can be used to enable Bluetooth low energy on our PC. The CC2540 combines an excellent RF transceiver with an industry- standard enhanced 8051 MCU, in system programmable flash memory and 8KB RAM. It is selected on the USB because it suitable for system where very low

power consumption is required. It also very low power sleep modes are available and low cost [16],[20,21].

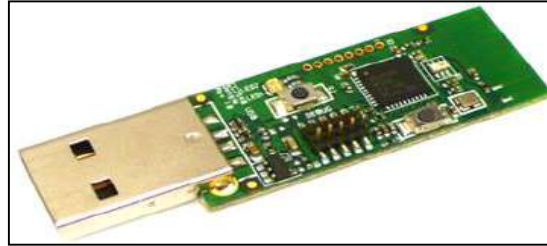


Fig. 4: The USB module.

The Experimental work

A. Performance Analysis on Gearbox

To evaluate the system to power up sensor node for condition monitoring, it is into a gearbox as shown in Fig. 5. The gearbox of test rig consists of three main parts: 15 KW three phase AC induction motor, two gearboxes connected back to back via flexible coupling and DC motor working as load. Therefore, to simulate a variable loads and variable speed operating conditions of common industrial machine the tests were carried out based on changing the AC motor speed while a fixed load applied. The test is designed to evaluate the transfer efficiency of the TE module [17-19].

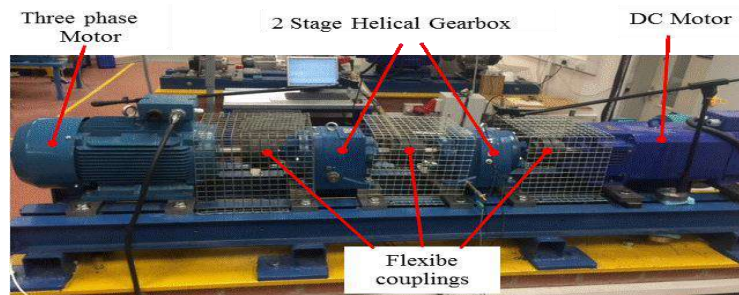


Fig. 5: The Test Rig

The TEG module is attached into the body of the gearbox by clamping it properly on vertical position as shown in Fig. 6. The body heat of the gearbox will be collected by the TEG module and converted to electricity to power the sensor tag. Meanwhile the working condition of the TEG module is monitored by an external data acquisition system to evaluate its performance. The monitoring parameter includes: temperature on the hot and cold side of the TEG module, open circuit voltage of the TEG module and its current over a 1 Ω resistor. Note that, the open circuit voltage and current are measured alternatively by using a relay. The time interval for these measurements is set as 6s.

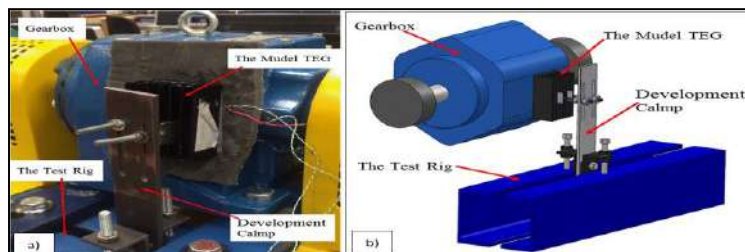


Fig. 6: The module TEG attached the gearbox a) picture of the module with gearbox, b) illustrated the development clamp in sold model

Results and Discussion

To evaluate the performance of the TEG module, set of comparison tests using Gearbox Test Rig were performed. Particularly, healthy gearbox operation condition and abnormal operation, i.e. low oil level with 40% tooth breakage as shown in Fig. 7. The AC motor is operated for one hour at the full speed (100% speed) under 70% of the full load. The readings from TEG module, including temperature, open circuit voltage and power over 1Ω resistor, are obtained by a data acquisition system and stored on a portable PC for further analysis. Fig. 8 represents the TEG module related readings during two sets of different test cases.

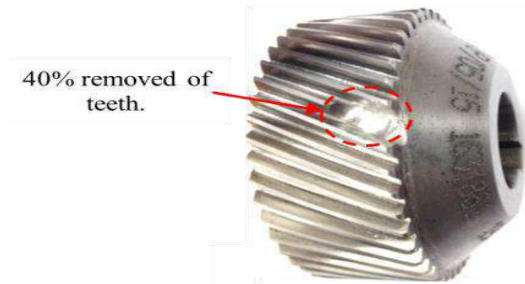


Fig. 7: Tooth breakage

It can be seen that both the hot side temperature T_h and cold side T_c of the TEG module under abnormal operation is higher than those of the healthy gearbox. This is reasonable since more heat is generated when gearbox under abnormal operation conditions. A temperature difference ΔT of around 12°C is maintained between the hot and cold sides. The ΔT of the abnormal operation case is higher than that of the healthy case, as indicated in Fig. 8 (a,b,c).

An open circuit ranging from 140 mV to 175 mV is generated from the TEG module, represented in Fig. 8 (d), which is sufficient for the input voltage requirement of the DC/DC booster circuit. By measuring the voltage of 1Ω resistor, the power consumption for this resistor, shown in Fig. 8 (e), indicates the power output capability of the TEG module ranging from 2mW to 5mV. It can be seen that the power consumed under abnormal operation case is higher than that of the healthy operation, as clear from Fig. 8 (e).

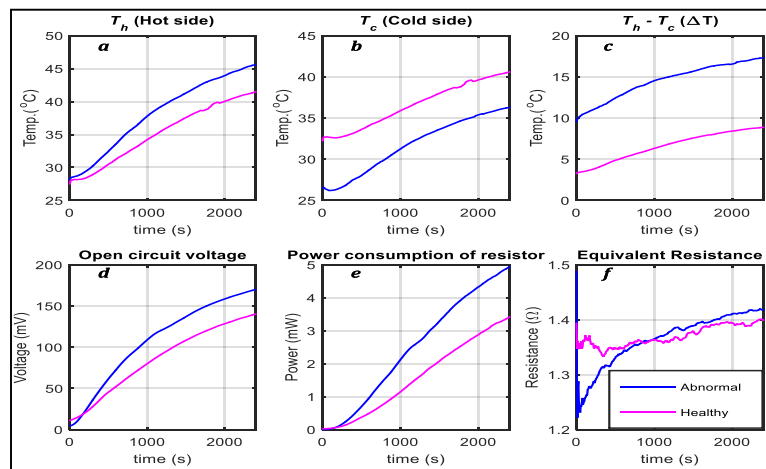


Fig. 8: TEG module related readings, including temperature, open circuit voltage and power over 1Ω resistor

Apart from temperature difference on its two sides, the power output capability of the TEG is also affected by the Seebeck coefficient, which is influenced by the temperature. Due to this phenomenon of the material, the internal resistance of the TEG module also changes with the temperature. By using the open circuit voltage and current over 1Ω resistor, the equivalent resistance for the TEG module is computed and represented in Fig. 8 (f). A resistance difference of about 0.1Ω can be observed for these two speed conditions. The results show that the resistance of the abnormal operation test is a bit higher than that of the health condition. This indicates that the internal resistance of the TEG module drops with the increase of the temperature.

WSN node described in this paper is designed for use in the field conditions to monitor industrial parameters as represented in Fig. 9. A super-capacitor is utilized as the main power source of WSN node. That is when there is no energy harvesting or if it is not sufficient for the continuous operation, the super capacitor would then supply the node. It also accumulates energy for a relative long time and then provides power to the sensor node for short period; during which signal is collected and transmitted to the central device. More details about the analysis and application of super-capacitor in WSN can be found in [25].

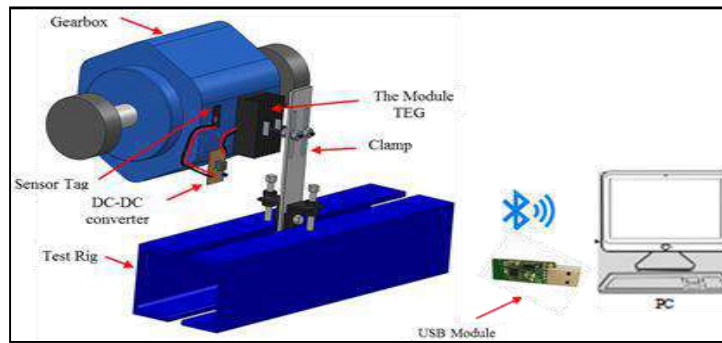


Fig. 9: The test system

By running the gearbox at 100% speed for two hours, the super capacitor can be fully charged, particularly is up to about 5.2V. By connecting the sensor tag to a DC-DC converter, the sensor information on the sensor tag CC2650 can be transferred via the Bluetooth low energy, and received By USB module CC2540. Signals are then monitored and analyzed using portable monitoring devices such as a PC as shown in Fig. 9.

The acquired signals from both TEG and wired sensor are represented in Fig10.

Where Fig. 10 (a) represents the results of temperature measurements obtained from the thermal designed system TEG. It shows changes of the rig gearbox temperature during the run. As clear from the figure, it represents a smooth and uninterrupted data. While Fig 10 (b) shows the wired signal without filtering. Both signals are superimposed in Fig. 10 (c) for better comparison and visualization. Though small differences in the two signals due to the noise from the wired signal, yet the difference is still acceptable for condition monitoring and diagnosis. Reasonably, TEG wireless system can provide accurate results with less noise and lower power requirements. It can be used effectively for gearbox monitoring by efficiently using energy harvesting technique.

Conclusion

Dependent about the experimental investigation results, it is viable to harvest thermo energy of a machine to power up the wireless temperature node and use to monitor the health and performance of the machine. Also the comparison study of thermal energy harvesting system has shown a slight different in the data of the different measurement, which leads following conclusion remarks:

- Thermoelectric generator (TEG) has been employed as the energy harvesting source to power up the wireless sensor node for condition monitoring. It can convert the widely available waste heat from machines to electrical energy. Meanwhile, its conversion efficiency is not high.
- Bluetooth Low Energy is employed as the wireless transmission protocol due to its low power consumption and it's widely availability on current portable smart phones and tablets. Third, the new generation low power consumption SOC CC2650 is selected on the sensor node because it integrates one processor for data acquisition and signal processing and also a specific processor for BLE communication.

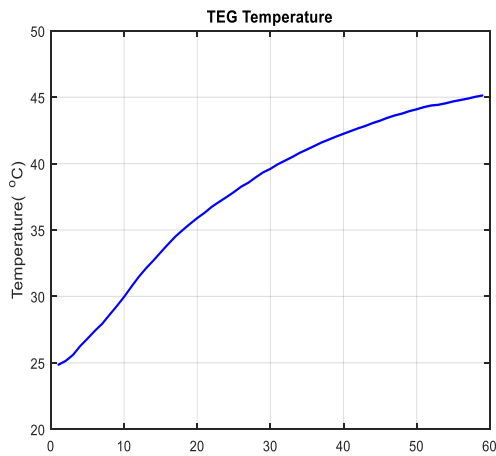


Fig. 10 (a): Results from the thermal design system

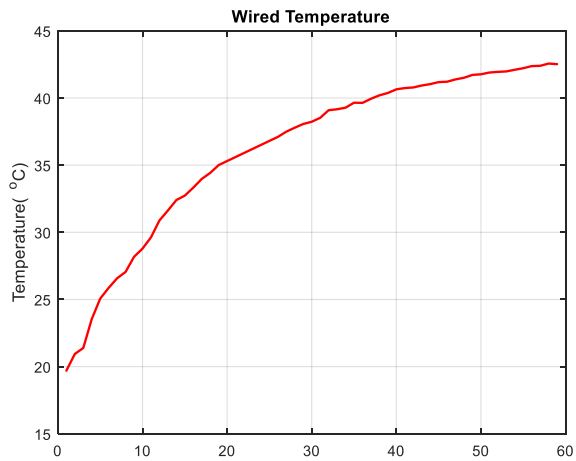


Fig. 10 (b): Results from wired signal

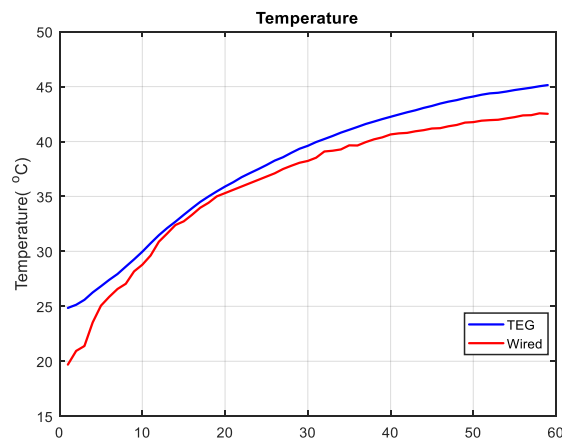


Fig. 10 (c): Comparison results between wired signal and TEG system

References

- [1] Crabtree, C., Y. Feng, and P. Tavner. Detecting incipient wind turbine gearbox failure: a signal analysis method for on-line condition monitoring. in Scientific Track Proceedings of European Wind Energy Conference. 2010.
- [2] Z.Hameed, Y.S.Hong, Y.M.Cho, S.H.Ahn C.K.Song, (2009), Condition monitoring and fault detection of wind turbines and related algorithms: A review. Renewable and Sustainable energy reviews,. 13(1): p. 1-39.
- [3] Y.Amirat, M.E.H.Benbouzid, E.Al-Ahmar, B.Bensaker S.Turri,.(2009), A brief status on condition monitoring and fault diagnosis in wind energy conversion systems. Renewable and sustainable energy reviews. 13(9): p. 2629-2636.
- [4] Guo, P. and N. Bai,(2011) Wind turbine gearbox condition monitoring with AAKR and moving window statistic methods. Energies. 4(11): p. 2077-2093.
- [5] Tavner, P., L. Ran, and J. Penman,(2008), Condition monitoring of rotating electrical machines. Vol. 56.: IET.
- [6] Bottner, H. (2002), thermoelectric micro devices: current state, recent developments and future aspects for technological progress and applications. in Thermo-electrics,. Proceedings ICT '02. Twenty-First International Conference on. 2002.
- [7] Mastbergen, D. and B. Willson,(2005), Generating light from stoves using a thermoelectric generator. in ETHOS International Stove Research Conference..
- [8] Palacios, R. and M.Z. Li. Electrical properties of commercial thermoelectric modules. in Fourth European Workshop on Thermoelectrics, ETS. 1998.
- [9] Mastbergen, D., B. Willson, and S. Joshi, (2012), Producing light from stoves using a thermoelectric generator.
- [10] Eakburanawat, J. and I. Boonyaroonate,(2006), A Thermoelectric Battery Charger System with Maximum Power Point Tracking Technique..
- [11] Xin, L. and Y. Shuang-Hua. Thermal energy harvesting for WSNs. in Systems Man and Cybernetics (SMC), 2010 IEEE International Conference on. 2010.
- [12] Lin, Z.-M., et al. Bluetooth Low Energy (BLE) based blood pressure monitoring system. in Intelligent Green Building and Smart Grid (IGBSG), 2014 International Conference on. 2014. IEEE.
- [13] Andersson, T., Bluetooth Low Energy and Smartphones for Proximity-Based Automatic Door Locks. 2014.
- [14] Paradiso, J.A. and T. Starner, Energy scavenging for mobile and wireless electronics. Pervasive Computing, IEEE, 2005. 4(1): p. 18-27.
- [15] Sardini, E. and M. Serpelloni, Self-powered wireless sensor for air temperature and velocity measurements with energy harvesting capability. Instrumentation and Measurement, IEEE Transactions on, 2011. 60(5): p. 1838-1844.
- [16] LTC3108 Ultralow Voltage Step-Up Converter and Power Manager, L.T.C. 2010.
- [17] Aneta P., Ljubomir V., Dušan V., Dejan M., Zoran P., (2015) Thermal Energy Harvesting Wireless Sensor Node in Aluminum Core PCB Technology. Sensors Journal, IEEE,. 15(1): p. 337-345.
- [18] M. Ferrari; V. Ferrari; M. Guizzetti; D. Marioli; A. Taroni (2009), Characterization of thermoelectric modules for powering autonomous sensors. Instrumentation and Measurement, IEEE Transactions on,. 58(1): p. 99-107.
- [19] Zivorad M., Vladimir M., Vladimir R., Milost Z., (2015), Energy Harvesting Wireless Sensor Node for Monitoring of Surface Water. in Proceedings of the 21 international conference on Automation& computing, University of Strathclyde Glasgow UK
- [20] Peltier.<http://www.alldatasheet.com/datasheet-pdf/pdf/307804/CUI/CP85438.html>].
- [21] Instruments,T.SensorTagCC2650STK.
http://processors.wiki.ti.com/index.php/CC2650_SensorTag_User's_Guidehttp://processors.wiki.ti.com/index.php/CC2650_SensorTag_User's_Guide.
- [22] Rgeai, M.N., Helical Gearbox fault detection using motor current signature, in Engineering and Physical Sciences., The University of Manchester, UK, 2007
- [23] Wahg, K., Vibration monitoring on electrical machine using vold-Kalman filter order Tracking, in The Department of Mechanical and Aeronautical., Pretoria: South Africa. p. 17. 2008
- [24] Toliyat, H.A.,(2013) Electric Machines: Modeling, Condition Monitoring, and Fault Diagnosis., GB: CRC Press Inc.
- [25] Kim, S. and P.H. Chou.,(2013), Size and topology optimization for supercapacitor-based sub-watt energy harvesters. Power Electronics, IEEE Transactions on, 2013. 28(4): p. 2068-.

A Cubic B-Spline Collocation Method for Solving Anomalous Sub-diffusion Equation

Faoziya S. Musbah^a

^aDepartment of Mathematics, Faculty of education/University of Bani Waleed, Libya

Abstract: In this paper, A cubic B-spline collocation method is proposed to solve one dimensional anomalous sub-diffusion equation. The fractional derivative is estimated by using right shifted Grünwald-Letnikov formula of order $\alpha \in (0,1)$. Numerical results are presented to confirm the feasibility and validity of this scheme.

Keywords: A Cubic B-spline collocation method, anomalous sub-diffusion equation, Grünwald-Letnikov formula.

Introduction

Paper must Diffusion equations are partial differential equations which model the diffusion and thermodynamic phenomena and describe the spread of particles (ions, molecules, etc.) diffusion not described by normal diffusion in the long time limit has become known as anomalous (unnatural) [1]. Fractional partial differential equations can be thought as generalizations of classical partial differential equations, which can give a better description of the complex phenomena such as signal processing, systems identification, control and non-Brownian motion [2] or so called levy motion which is a generalization of Brownian motion [3]. A comprehensive background on this topic can be found in books by [4] and [5].

In this article, a numerical scheme is constructed to obtain approximate solutions of the one-dimensional anomalous sub-diffusion equation. The Grünwald-Letnikov formula is applied to treat the fractional temporal derivative, while the cubic B-spline (CBS) is used to discretize the spatial derivative.

Consider the following model of anomalous sub-diffusion equation:

$$\frac{\partial^\alpha u(x,t)}{\partial t^\alpha} = D \frac{\partial^2 u(x,t)}{\partial x^2} + f(x,t), \quad (x,t) \in (0,1) \times (0,T], \quad (1)$$

with the initial condition

$$u(x,0) = g_1(x), \quad x \in [0,1], \quad (2)$$

and the boundary conditions

$$u(0,t) = g_2(t), \quad u(1,t) = g_3(t), \quad t \in [0, T], \quad (3)$$

where $u(x,t)$ is a concentration of a quantity such as mass, energy, etc., D is the diffusion coefficient (or diffusivity), f , g_1 , g_2 and g_3 are known functions. $\partial^\alpha u / \partial t^\alpha$ denotes the Riemann-Liouville fractional derivative. We consider the case when $0 < \alpha < 1$.

Definition 1.1 The fractional derivative ${}_0 D_t^\alpha$ of $f(t)$ can be defined by Riemann-Liouville formula as [6]

$${}_0 D_t^\alpha f(t) = \frac{d}{dt} \left[\frac{1}{\Gamma(1-\alpha)} \int_0^t \frac{f(t)dt}{(t-t)^\alpha} \right], \quad 0 < \alpha < 1, \quad (4)$$

where $\Gamma(\cdot)$ is the Gamma function and $0 \leq t \leq T$. The above derivative is related to the Riemann-Liouville fractional integral, which is defined as

$${}_0 I_t^\alpha f(t) = \frac{1}{\Gamma(\alpha)} \int_0^t \frac{f(t)dt}{(t-t)^{1-\alpha}}, \quad 0 < \alpha < 1, \tag{5}$$

Where ${}_0 D_t^\alpha {}_0 I_t^\alpha f(t) = f(t)$.

Definition 1.2 The right-shifted Grünwald-Letnikov formula of function f with respect to independent variable t is defined as [7]

$${}_0 D_t^\alpha f(t) = \frac{1}{\tau^\alpha} \sum_{k=0}^{n+1} \omega_k^{(\alpha)} f(t - (k-1)\tau) + O(\tau) \tag{7}$$

where $\tau = \Delta t$, $\omega_0^{(\alpha)} = 1$ and $\omega_k^{(\alpha)} = (1 - \frac{\alpha+1}{k})\omega_{k-1}^{(\alpha)}$.

The coefficients $\omega_k^{(\alpha)}$ are the coefficients of the power series of the generating function $\omega(z, \alpha) = (1-z)^\alpha$ and are also the coefficients of the two-point backward difference approximation of the first order derivative. The generating function $\omega(z, \alpha)$ with $0 < \alpha < 1$ can be written as a power series of the form

$$(1-z)^\alpha = \sum_{k=0}^\infty \binom{k-\alpha-1}{k} z^k = \sum_{k=0}^\infty \omega_k^{(\alpha)} z^k \tag{8}$$

Cubic B-spline functions

First, we introduce a uniform grid of mesh points (x_i, t_n) with $x_i = ih, i = 0, 1, \dots, M$ and $t_n = n\tau, n = 0, 1, \dots, N$, where M and N are positive integers, $h = 1/M$ is the spatial step size in the x direction and $\tau = T/N$ is the time step size in the t direction. The notations u_i^n and f_i^n are used for the exact values of u and f at the points (x_i, t_n) . An approximation U to the exact solution u can be expressed in terms of the cubic B-spline collocation approach as [8]

$$U(x, t) = \sum_{i=1}^M C_i(t) B_i(x), \tag{9}$$

where $C_i(t)$ are unknown control points and $B_i(x)$ are CBS functions defined as

$$B_i(x) = \frac{1}{6} \begin{cases} (x-x_{i-2})^3, & x \in [x_{i-2}, x_{i-1}] \\ h^3 + 3h^2(x-x_{i-1}) + 3h(x-x_{i-1})^2 - 3(x-x_{i-1})^3, & x \in [x_{i-1}, x_i] \\ h^3 + 3h^2(x_{i+1}-x) + 3h(x_{i+1}-x)^2 - 3(x_{i+1}-x)^3, & x \in [x_i, x_{i+1}] \\ (x_{i+2}-x)^3, & x \in [x_{i+1}, x_{i+2}] \\ 0, & \text{otherwise.} \end{cases}$$

The value of $B_i(x)$, $\dot{B}_i(x)$ and $\ddot{B}_i(x)$ at mesh point x_i are represented in Table 1.

Table 1: The value of $B_i(x)$, $\dot{B}_i(x)$ and $\ddot{B}_i(x)$ at mesh point x_i .

	x_{i-2}	x_{i-1}	x_i	x_{i+1}	x_{i+2}
$B_i(x)$	0	1/6	4/6	1/6	0
$B_i'(x)$	0	1/2h	0	-1/2h	0
$B_i''(x)$	0	1/h ²	-2/h ²	1/h ²	0

The set of B-spline functions $\{B_{-1}(x), B_0(x), \dots, B_M(x)\}$ is defined over $[a, b]$. Therefore, an approximation solution u_i^n at the point (x_i, t_n) over the subinterval $[x_i, x_{i+1}]$ is given as

$$u_i^n = \sum_{j=i-1}^{i+1} C_j^n B_j(x) \tag{10}$$

where $i = 1, 2, \dots, M - 1$. The approximated values of u and $\partial^2 u / \partial x^2$ are computed in term of the control points C_j^n as:

$$u_i^n = \frac{1}{6} (C_{i-1}^n + 4C_i^n + C_{i+1}^n) \tag{11}$$

and

$$\left. \frac{\partial^2 u}{\partial x^2} \right|_i^n = \frac{1}{h^2} (C_{i-1}^n - 2C_i^n + C_{i+1}^n) \tag{12}$$

Cubic B-spline collocation method for solving anomalous sub-diffusion equation

In this section, the CBS collocation method is constructed for anomalous sub-diffusion equation. The time fractional term of equation (1) is treated by using right shifted Grünwald-Letnikov formula (7) while its second spatial derivatives is replaced by applying the approximation formula (12), taking into the consideration that the estimation of truncation errors of this scheme are neglected. We set

$$\frac{1}{\tau^\alpha} \sum_{k=0}^n \omega_k^\alpha u_i^{n-k} = \frac{D}{h^2} \left. \frac{\partial^2 u}{\partial x^2} \right|_i^n + f_i^n, \quad i = 1, 2, \dots, M - 1, \tag{13}$$

$$n = 1, 2, \dots, N$$

Substitute equation (11) and (12) into equation (1), yields

$$\begin{aligned} \omega_0^\alpha (C_{i-1}^n + 4C_i^n + C_{i+1}^n) + \sum_{k=1}^n \omega_k^\alpha (C_{i-1}^{n-k} + 4C_i^{n-k} + C_{i+1}^{n-k}) \\ = 6r (C_{i-1}^n - 2C_i^n + C_{i+1}^n) + 6\tau^\alpha f_i^n, \quad i = 1, 2, \dots, M - 1, \end{aligned} \tag{14}$$

$$n = 1, 2, \dots, N$$

where $r = D\tau^\alpha / h^2$ is the fractional diffusion number. Simplifying the above equation, we obtain

$$\begin{aligned} (\omega_0^\alpha - 6r) C_{i-1}^n + 4(\omega_0^\alpha + 3r) C_i^n + (\omega_0^\alpha - 6r) C_{i+1}^n \\ = 6\tau^\alpha f_i^n - \sum_{k=1}^n \omega_k^\alpha (C_{i-1}^{n-k} + 4C_i^{n-k} + C_{i+1}^{n-k}), \quad i = 1, 2, \dots, M - 1, \end{aligned}$$

$$n = 1, 2, \dots, N \tag{15}$$

The system in (15) has $M-1$ linear equations involving $M+1$ unknowns. The two additional equations can be obtained from the boundary conditions of equation (1).

and the boundary conditions

$$u(0,t)=t^2, \quad u(1,t)=et^2, \quad t \in [0, T], \quad (21)$$

The exact solution of equation (19)-(21) is

$$u(x,t)=t^2 e^x. \quad (22)$$

We choose $\alpha = 0.5$. The numerical scheme discussed in this paper for solving the above example is implemented and its solution is compared with the exact solution. The computational results of Example 1 are illustrated in Table 2 along with the relative errors at $t = 6.25 \times 10^{-5}$, $\tau = 1.25 \times 10^{-5}$ and $h = 0.1$.

Table 2: Relative errors of the scheme at $t = 6.25 \times 10^{-5}$, $\tau = 1.25 \times 10^{-5}$ and $h = 0.1$.

x	Approx. soln.	Exact soln.	Errors
0.1	4.50256E-9	4.31707E-9	4.29649E-2
0.2	5.19015E-9	4.77110E-9	8.78295E-2
0.3	5.79088E-9	5.27289E-9	9.82365E-2
0.4	6.41295E-9	5.82744E-9	1.00475E-1
0.5	7.08946E-9	6.44032E-9	1.00793E-1
0.6	7.83142E-9	7.11765E-9	1.00282E-1
0.7	8.63749E-9	7.86622E-9	9.80476E-2
0.8	9.47852E-9	8.69352E-9	9.02977E-2
0.9	1.02425E-8	9.60782E-9	6.60633E-2

The comparison between the results of the CBS collocation method and the exact solution is plotted in Fig. 1 at $t = 6.25 \times 10^{-5}$, $\tau = 1.25 \times 10^{-5}$ and $h = 0.1$.

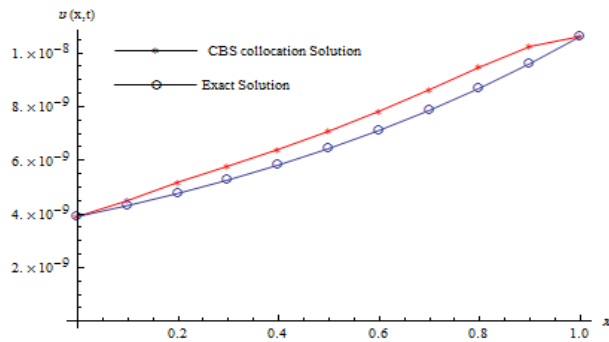


Fig. 1: Comparison between the results of CBS collocation method and exact solution at $t = 6.25 \times 10^{-5}$, $\tau = 1.25 \times 10^{-5}$ and $h = 0.1$.

From Fig. 1, we can observe that the numerical solutions of the CBS collocation method are close to the exact solutions. In Fig.2 the relative errors of the numerical CBS collocation method are presented at $t = 6.25 \times 10^{-5}$, $\tau = 1.25 \times 10^{-5}$ and $h = 0.1$.

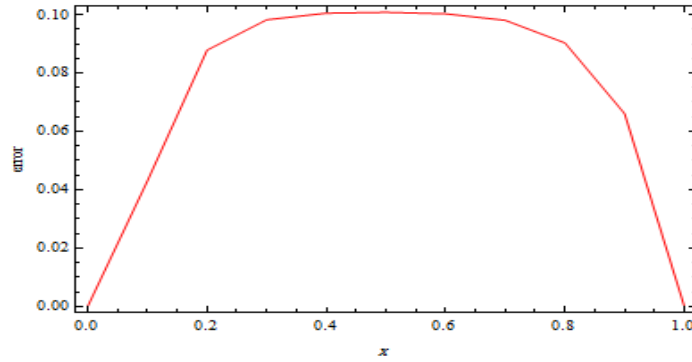


Fig. 2: The relative errors of the scheme at $t = 6.25 \times 10^{-5}$, $\tau = 1.25 \times 10^{-5}$ and $h = 0.1$.

Conclusion

In this paper, a numerical scheme based on CBS was presented for solving anomalous sub-diffusion equation. The time fractional derivative was estimated via Grünwald-Letnikov formula while the spatial derivative was utilized using the CBS approximation. The proposed algorithm was tested by a numerical example, which showed that the scheme is admissible, straightforward and produced reasonable results.

References

- [1] Al-Shibani, F. et al., (2012), The Implicit Keller Box method for the one dimensional time fractional diffusion equation., *Journal of Applied Mathematics & Bioinformatics*, **2**, 69-84.
- [2] Li, C. Chen, A., and Ye, J., (2011), Numerical Approaches to Fractional Calculus and Fractional Ordinary Differential Equation., *Journal of Computational Physics*, **230**, 3352-3368. DOI: 10.1016/j.jcp.2011.01.030.
- [3] Sousa, E., (2012), A Second Order Explicit Finite Difference Method for the Fractional Advection Diffusion Equation., *Computers and Mathematics with Applications*, **64**, 3141-3152. DOI: 10.1016/j.camwa.2012.03.002.
- [4] I. Podlubny, *Fractional Differential Equations*. Academic Press, San Diego, 1999, pp. 41-62.
- [5] S. Das, *Functional Fractional Calculus for system identification and controls*. Springer, New York, 2011, pp. 03-11.
- [6] R. Klages, G. Radons, and M. Sokolov, *Functional Anomalous Transport*. Wiley, Weinheim, 2008, pp. 110-118.
- [7] Meerschaert, M. Tadjeran, C., (2006), Finite Difference Approximations for Two-Sided Space-Fractional Partial Differential Equations., *Applied Numerical Mathematics*, **56**, 80-90. DOI: 10.1016/j.apnum.2005.02.008.
- [8] Latif, B. et al., (2021), New Cubic B-Spline Approximation for Solving Linear Two-Point Boundary-Value Problems., *Journal of Computational Physics*, **9**, 01-13. DOI: 10.3390/math9111250.
- [9] Takaci, D. Takaci, A., and Strboja, M., (2010), On the Character of Operational Solutions of the Time-Fractional Diffusion Equation., *Nonlinear Analysis*, **72**, 2367-2374. DOI: 10.1016/j.na.2009.10.037.

Modeling and simulation of Polysiloxane diaphragm pressure sensor whit grapheme beam

Mohamed Elmahdi Ali

Electrical Department, Engineering College/Sirte University, Libya

Abstract:

This paper studies a resonant pressure sensor whose elementary sensing component is the polysiloxane circular diaphragm, and the final sensing component is the graphene beam resonator attached to the polysiloxane circular diaphragm. The relationship between the fundamental natural frequency of the beam resonator and the measured pressure is calculated. As the beam is located at different positions of the upper plane of the polysiloxane circular diaphragm along its radial direction is a simulation, analyzed, and investigated. Some significant results are obtained. . Based on the differential output frequencies, a set of optimum parameters of the proposed Pressure Sensor is determined. The performed pressure range is 0~10Kpa. Keywords: polysiloxanee , beam, pressure; graphene; Frequency.

Introduction

Microelectromechanical systems are systems that consist of small-scale electrical and mechanical components for specific purposes. MEMS were translated into systems with mechanical and electrical components but have extended their boundaries to include optical, radio-frequency, and Micro devices [1].

The resonant sensor is based on a special sensing structure, which is operating at its resonating state. And the measured quantities can be detected by using the resonant frequency (or the natural frequency), phase shift, or amplitude of the vibrating output signal for the sensing component [2].

resonant pressure sensors have been widely used in the automotive industry, medical instrument, aerospace, and military fields due to their high accuracy, long-term stability, direct digital output (without A/D conversion), low hysteretic, and high repeatability[3].

Polysiloxane is composed of atoms arranged in a diamond structure with a cubic symmetry. Although Polysiloxane has a tendency to cleave along crystallographic planes because of the bulk defects in the crystal, it is a mechanical material with high strength [4].

Graphene is a one-atom-thick layer of carbon atoms arranged in a hexagonal lattice. Graphene is the thinnest material known to man at one atom thick, and also incredibly strong - about 200 times stronger than steel. On top of that, graphene is an excellent conductor of heat and electricity[5].

Sensors are devices used to measure physical or chemical states. They deliver a signal that can be received by a machine or person. As a rule, the measurements (the reactions of the sensor element to the states to be measured) are converted into electrical or optical signals and, namely, increasingly into digital signals. Optical glass fibers are gaining growing importance in the transmission of signals [6].

Circular diaphragm sensors are one of the more sophisticated elementary sensing components of Polysiloxane microstructure resonant sensors when compared to square diaphragm sensors. The following are its main benefits: stress concentration on the useful ring sensing area, adjustable stress distribution design, simpler attainment of a differential measurement scheme to boost sensitivity and minimize some disturbances, such as temperature, etc. This paper's goal is to demonstrate a sophisticated Polysiloxane resonant pressure sensor model created using the finite element technique

(FEM). The link between the output frequency and the applied pressure is simulated and calculated using the model [7].

SENSOR STRUCTURE AND OPERATING PRINCIPLE

Fig. 1 shows the structure of a Pressure sensor. The preliminary sensing unit is a polysiloxane circular diaphragm. The pressure being measured acts perpendicularly on the lower plane of the circular diaphragm and yields circumferential and radial stresses. The final sensing unit is a graphene beam attached to the upper plane of the circular diaphragm. The thickness of the diaphragm H should be much greater than the Thickness of the beam h .

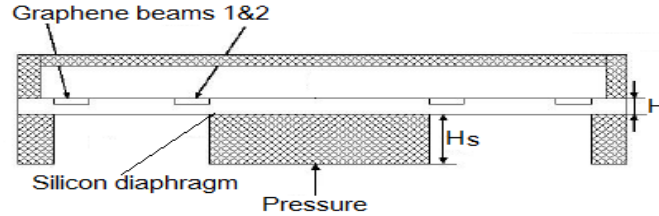


Fig.1 sensing structure of the pressure sensor

Based on the structural characteristics, the beam's axial direction is subjected to an appropriate beginning stress that is equal to the radial stress of the circular diaphragm at the same location. The natural frequency of the graphene beam varies with the radial stress on the upper plane of the polysiloxane circular diaphragm because the primary vibration of the beam occurs along its normal direction (direction of the beam's thickness) and the initial stress is applied along the axial direction of the beam (direction of the beam's length). Therefore, the change in the beam's inherent frequency will be used to determine the applied pressure.

STRESSES ON THE UPPER PLANE OF POLYSILOXANE CIRCULAR DIAPHRAGM

The circular diaphragm loaded by pressure at its center has the following differential equation: [8].

$$\frac{d}{dr} = \left[\frac{1}{r} \frac{d}{dr} \left(r \frac{dw}{dr} \right) \right] = \frac{G}{\lambda} \quad (1)$$

$$\lambda = \frac{EH^3}{12(1-\mu^2)}, \quad G = \frac{rP}{2}$$

Where:-

P - the applied Pressure ($P \geq 0$).

Λ - the flexural rigidity of the diaphragm.

W -the normal displacement of the circular diaphragm.

E -The Young's modulus.

μ -the Poisson ratio of the sensing structure.

G = the shearing force at the circumference of radius r of the diaphragm.

The boundary conditions at the inner and outer edges of the circular diaphragm are as follows

$$\left\{ \begin{array}{ll} r = R_1 & \frac{dw}{dr} = 0 \\ r = R_2 & w \frac{dw}{dr} = 0 \end{array} \right. \quad (2)$$

Where:-

r - radial coordinate of the circular diaphragm in polar.

From Eqs. (1) and (2), the normal displacement of the circular diaphragm W can be obtained. Then the radial stress $\sigma_r(r)$ and circumferential stress $\sigma_\theta(r)$ of the circular diaphragm can be obtained as follows [8].

$$\begin{cases} \sigma_r(r) = \frac{-3PA^2}{8H^2} \left[(3+\mu)R^2 - (1+\mu)(K^2+1) - \frac{(1-\mu)K^2}{R^2} \right] \\ \sigma_\theta(r) = \frac{-3PA^2}{8H^2} \left[(1+3\mu)R^2 - (1+\mu)(K^2+1) + \frac{(1-\mu)K^2}{R^2} \right] \end{cases} \quad (3)$$

$$R = \frac{r}{R_2}, \quad K = \frac{R_1}{R_2}$$

ANALYTICAL ANALYSIS AND SIMULATION OF GRAPHENE BEAM

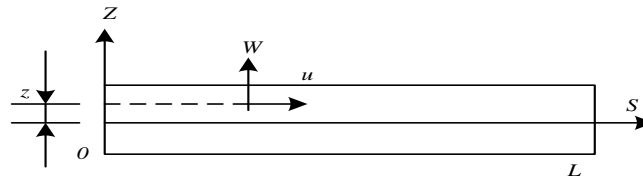


Fig.2 The model of graphene beam

Fig. 2 shows the mathematical model of the beam. The axial and normal vibrating displacements $u(s,z,t)$ and $w(s,t)$ of the beam at an arbitrary point in Cartesian coordinates can be written as[9].

$$\begin{cases} u(s, z, t) = -z \frac{dw(s)}{ds} \cos \omega t \\ w(s, t) = w(s) \cos \omega t \end{cases} \quad (4)$$

Where:-

s, z - the axial and normal coordinates of the beam in Cartesian coordinates.

ω [rad/s] - the natural frequency.

$w(s)$ - Corresponding vibrating shape along the axial direction of the beam.

Then the finite element equation is as follows

$$(\mathbf{K} - \omega^2 \mathbf{M})\mathbf{a} = 0 \quad (5)$$

Where:-

K- assembly stiffness Matrix.

M- assembly Mass Matrix

\mathbf{a} - the assembly nodal vector, consisting of all a_j .

For the actual structural features of Fig.2, the boundary conditions of the beam are as follows

$$\begin{cases} s = 0: & w(s) = w'(s) = 0 \\ s = L: & w(s) = w'(s) = 0 \end{cases} \quad (6)$$

Eq.(5) is the FEM model for the microstructure polysiloxane resonant Pressure sensor shown in Fig. 1. From Eqs. (5) and (6) the natural frequencies and their corresponding vibrating shapes can be obtained.

SENSOR PRESSURE DETECTION CIRCUIT SYSTEM

The pickup signals is very weak and lost in the loud background noise because the size of the resonant beam and vibration amplitude is so small [9]. A detection circuit system is created based on the lock-in amplify principle to extract the weak vibrating signal. It carries out tests for the pressure sensor's characteristics. The circuit system's block diagram is shown in Figure 3.

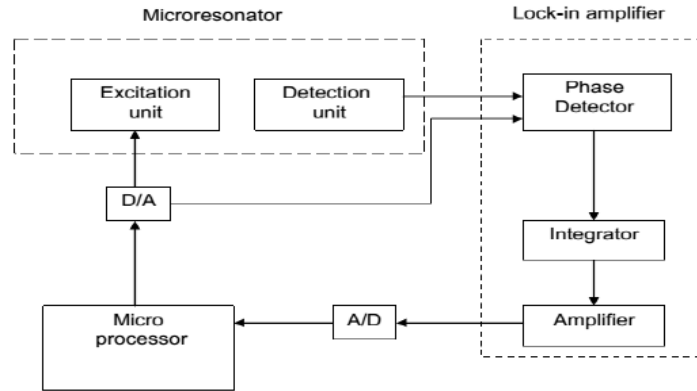


Fig.3. The block diagram of the detection circuit system

CALCULATION AND DISCUSSION

In this paper, the main investigations are the varying laws of the Pressure-frequency relationship for the graphene beam resonator as the thickness H , inner radius R_1 for the polysiloxane circular diaphragm and the corresponding lengths of the graphene beam L are varied. In order to get some generalized results of the pressure -frequency relationship for the graphene beam resonator, some related parameters are selected as follows:

The Reference value for the outer radius of the circular diaphragm is $R_2 = 4 \times 10^{-3} \text{m}$. Reference values for the width and thickness of the beam are $b = 10 \times 10^{-5} \text{m}$ and $h = 1 \times 10^{-5} \text{m}$.

INVESTIGATION OF THE FREQUENCY-PRESSURE RELATIONSHIP

Define $f(P)$, $f(0)$ the basic natural frequency of the beam for pressure P and for pressure; $P = 0$; $\Delta f = f(P) - f(0)$ as the variation of the basic natural frequency of the beam within $(0, P)$ and $\beta = [f(P) - f(0)] / f(0)$ [%] as the relative variation or the sensitivity of the basic natural frequency for the beam within $(0, P)$ the interval.

LOCATION OF BEAM ON THE UPPER PLANE OF THE CIRCULAR DIAPHRAGM

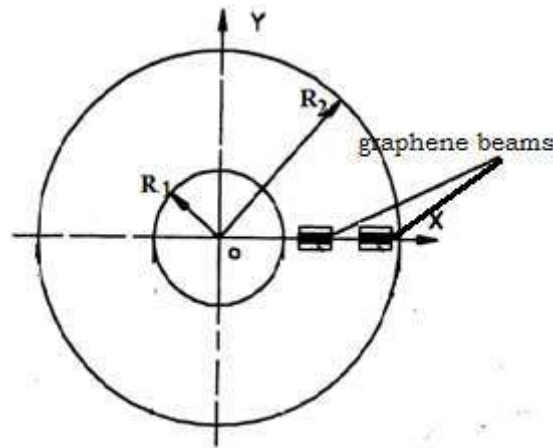


Fig.4 the upper plane of the polysiloxane circular diaphragm

The frequency changes of the two graphene beams are opposite, one is positive, and the other is negative. Therefore, the differential output scheme can be realized, and the measured Pressure can be determined by the frequency difference between beam 2 and beam 1.

The distance $R_2 - R_1 - 2L$ (fig 4) between beam2 and beam1 could not be selected as too small compared with the length of the beam L . On the other hand, in order to make use of the effective annular sensing area of the polysiloxane circular diaphragm, the distance $R_2 - R_1 - 2L$ could not be selected too big. In this paper, the relationship for R_2, R_1 , and L is selected as

$$R_2 - R_1 = 2.3L \quad (7)$$

In such a case, the length of the beam L is dependent on the inner radius of the polysiloxane circular diaphragm R_1 .

Table1 gives the beam's relationships between frequency and measured Pressure within 0-10Kpa, as the beam is located at different positions.

Table2 gives the frequency variation and sensitivity of the beam corresponding to Table

Table 1: The frequency of graphene beam within 10KPa

Pressure M Pa	Location of the beam		
	1.4 ,2.47	2.21,3.2	2.98,4
0.0	645.714	645.714	645.714
1	661.484	639.799	615.276
2	684.188	641.532	591.674
3	706.198	643.241	567.126
4	727.472	644.834	541.448
5	748.148	646.483	514.426
6	768.272	647.997	486.004
7	787.787	649.452	456.074
8	806.933	650.914	423.938
9	825.499	652.300	389.409
10	856.479	665.719	364.604

Table 2: The variation frequency and sensitivity of graphene beam within 10K pa

Position	1.4 ,2.47	2.21,3.2	2.98,4
Sensitivity	32.6 %	3.1 %	-43.5 %
Variation(kHz)	210.765	20.005	-281.110

From the Tables, some results can be obtained as follows:

As the beam is located at different positions of the upper plane of the diaphragm along its radial direction, the sensitivity of the beam resonator is different.

The best location for the beam resonator is at the inner edge and the outer edge for the circular diaphragm, where the beam's sensitivity reaches the biggest.

The beam resonator is defined as beam1 as it is located at the outer edge, and defined as beam2 as the beam located at the inner edge.

THE THICKNESS OF THE POLYSILOXANE CIRCULAR DIAPHRAGM

The thickness of the polysiloxane circular diaphragm H should be much greater than the Thickness of the graphene beam h., fig. 5 shows the relationships between the frequency of beam1 and the pressure for the different thicknesses of the diaphragm H. Fig. 6 shows the relationships between the frequency of beam2 and the pressure for the different thicknesses of the diaphragm H.

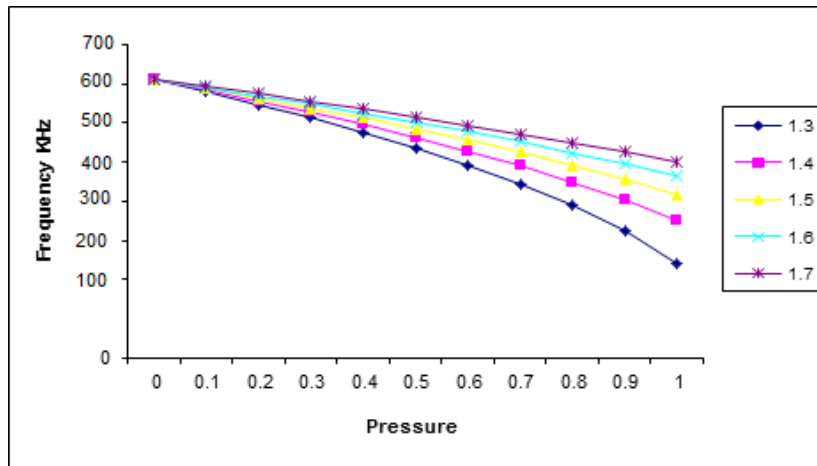


Fig. 5:The relationships between the frequency of beam1 and the pressure

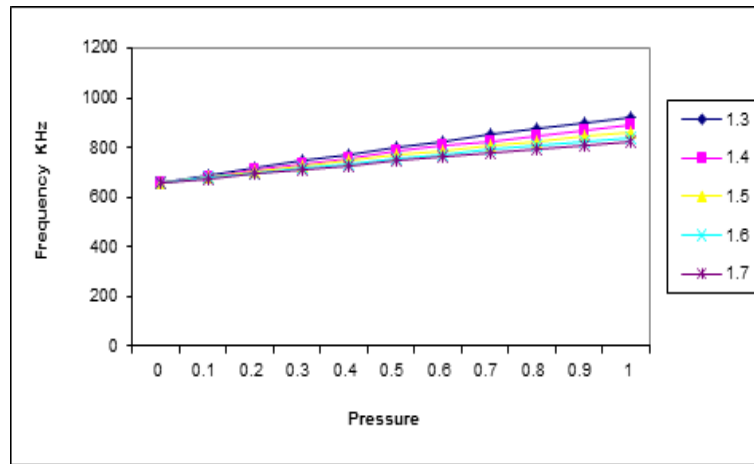


Fig.6: The relationships between the frequency of beam2 and the pressure

Table 3: The variation frequency (kHz) of Beam1 and Beam2

<i>H</i> ($\times 10^{-4}$ m)	$(R_1 \times 10^{-5}$ m, $L \times 10^{-4}$ m)			
	<i>Beam1</i>		<i>Beam2</i>	
	(1.35,1.06)	(1.4,1.04)	(1.35,1.06)	(1.4,1.04)
1.3	-503.261	-472.812	275710	281.228
1.4	-381.451	-365.721	251.842	246.003
1.5	-302.217	-294.789	206.508	206.236
1.6	-251.103	-245.781	189.463	185.125
1.7	-219.493	-213.681	167.530	165.372

Table 4:The Sensitivity of Beam1 and Beam2

<i>H</i> ($\times 10^{-4}$ m)	$(R_1 \times 10^{-5}$ m, $L \times 10^{-4}$ m)			
	<i>Beam1</i>		<i>Beam2</i>	
	(1.35,1.06)	(1.4,1.04)	(1.35,1.06)	(1.4,1.04)
1.3	-70.7 %	-69.5 %	40.3 %	39.7 %
1.4	-55.2 %	-51.9 %	37.4 %	34.8 %
1.5	-45.5 %	-43.7 %	31.3 %	28.9 %
1.6	-37.9 %	-36.6 %	26.3 %	26.2 %
1.7	-32.6 %	-30.1 %	25.2 %	24.5 %

From the tables and figures, we can get the following results:

The relative frequency variation (sensitivity) is increased as the thickness of the polysiloxane circular diaphragm H decreases for beam1 and beam2.

The relative frequency variation (sensitivity) is increased as the inner radius of the polysiloxane circular diaphragm R_1 decreases or the length of the beam increases for beam1 and beam2.

DESIGN AND OPTIMIZED PARAMETERS FOR PRESSURE SENSOR

Based on the differential output scheme of the Pressure Sensor and some related criteria, a set of appropriate parameters for the sensing structure of the sensor is determined for measuring the Pressure within 0-10 K Pa.

Outer radius R_2	$4 \times 10^{-3} \text{m}$
Inner radius R_1	$1.35 \times 10^{-3} \text{m}$
Thickness H	$1.4 \times 10^{-4} \text{m}$
Length of beam L	$1.06 \times 10^{-4} \text{m}$
Width of beam b	$10 \times 10^{-5} \text{m}$
Thickness of beam h	$1 \times 10^{-5} \text{m}$
frequency range for beam 1	(645.714-364.604)khz
frequency range for beam 2	(645.714-856.479)khz

CONCLUSIONS

The modelling and simulation for a Pressure Sensor are carried out in this paper. The elementary sensing component of the Pressure Sensor is the Polysiloxane circular diaphragm, and its final sensing component is the graphene beam resonator which is attached to the Polysiloxane circular diaphragm. The sensitivity of the basic natural frequency to measure Pressure for the beam resonator will be increased as the thickness of the circular diaphragm H being decreased, or the inner radius of the circular diaphragm R_1 is decreased, as the outer radius keeping constant, or the length of the graphene beam being increased. It is the best selection for a pair of beams (beam 1 and beam 2) to be located at the outer and inner edges of the circular diaphragm, respectively.

References

- [1] S, Shanky, R Sharma, B. D. (2021). Design and development of MEMS based guided beam type piezoelectric energy harvester. Springer Singapore. . online]. Available at: www.libgen.io
- [2] Duqi, Enri, Giorgio Allegato, and Mikel Azpeitia. "Pressure Sensors." *Silicon Sensors and Actuators*. Springer, Cham, 2022. 523-541.
- [3] Y , Zhuoqing. (2021). Advanced MEMS/NEMS Fabrication and Sensors. Springer International Publishing AG. Available at: www.libgen.io
- [4] Osipov, Artem A., et al. "Silicon carbide dry etching technique for pressure sensors design." *Journal of Manufacturing Processes* 73 (2022): 316-325.
- [5] Liu, Jihong, Siyu Bao, and Xinzhe Wang. "Applications of Graphene-Based Materials in Sensors: A Review." *Micromachines* 13.2 (2022): 184.
- [6] ZHAO, Wen-sheng, et al. "A Review on Microwave Resonant Sensors." *ACTA ELECTONICA SINICA* (2022): 1.
- [7] E, Masayoshi, ed, (2021). 3D and Circuit Integration of MEMS. online]. Available at www.libgen.io
- [8] M. Shaglouf, A. Abugalia, Finite Element Modeling and Simulation of A Microstructure Quartz Beam Resonant, Sirte University Scientific Journal (Applied Sciences), Vol. 8 (1), 113–120 June 2018
- [9] M. Shaglouf s.omer. Modeling and simulation and fabrication of resonant pressure sensor with silicon nitride beam. Third International Conference on Electrical Engineering and Information technology (ICEEIT 2021), 30 31 October 2020, Benghazi – Libya.
- [10] Dhanaselvam, P. Suveetha, et al. "Pressure Sensors Using Si/ZnO Heterojunction Diode." *Silicon* 14.8 (2022): 4121-4127.
- [11] Belwanshi, Vinod, Sebin Philip, and Anita Topkar. "Performance Study of MEMS Piezoresistive Pressure Sensors at Elevated Temperatures." *IEEE Sensors Journal* 22.10 (2022): 9313-9320.
- [12] Tai, Guojun, et al. "Force-Sensitive Interface Engineering in Flexible Pressure Sensors: A Review." *Sensors* 22.7 (2022): 2652.
- [13] Ha, Kyoung-Ho, et al. "Soft Capacitive Pressure Sensors: Trends, Challenges, and Perspectives." *ACS nano* 16.3 (2022): 3442-3448.
- [14] Wang, Lukang, et al. "Development of Laser-Micromachined 4H-SiC MEMS Piezoresistive Pressure Sensors for Corrosive Environments." *IEEE Transactions on Electron Devices* 69.4 (2022): 2009-2014.
- [15] Kim, Youn, et al. "Fabrication of highly conductive graphene/textile hybrid electrodes via hot pressing and their application as piezoresistive pressure sensors." *Journal of Materials Chemistry C* 10.24 (2022): 9364-9376.

Identification of Measles Rash spots by Image Contrast Enhancement

Atigah A. Karnaf
College of Electronics Technology, BaniWalid

Abstract: Measles is classified as contagious and fatal disease in both developing and poor countries. In developing countries, the number of deaths reaches more than 100.000 each year. After decade of successful vaccination for measles in 2000, US declared that the eliminated of measles. As result, the health care and the public have never seen any measles states. Unfortunately, measles came back in US in 2019 with more than 1000 confirmed cases. To give our assisting in diagnosing measles, we studied a color image from the Measles Rash patient's skin in an aim to create a computer or phone application in future and then we identified the token image by using matlab simulation codes. Our method shows better contract enhancement and the clear visual image of low contrast measles images has been achieved.

Keywords: (Medical imaging, Measles Rash, Digital Image Processing, Image Enhancement, Contrast Images)

Introduction

Several medical imaging forms have been applied for enhancing such as eyes, bones, heart, and brain...etc[1]. Therefore, our focus in this research is enhancing Measles Rash images for its negative effect. Here, brief information about why we choosing this disease will be noted. Measles is strong viral reparatory illness [2] [3]. It is serious contagion disease [7]. Measles Rash illness symptom starts in appearing three to five days after high fever, running nose, water eyes and cough. These symptom seems mimic other illnesses such as normal flu, but afret three to five days symptoms begin, Measles rash appears as a flat dray red spots which it starts from the up of the head until down to the feet. These symptoms can be dangerous for chiders more than adults. Measles is very danger contagion diseases that end to death before starting measles vaccination program [7]. Globally, Measels cases increased with more than 500,000 confirmed cases of measles and an estimated of 140,000 cases resulted in death [8]. The World Health Organization comes to terms that people can be protected by giving the vaccine to reduce the harmful of measles [3].

The purpose of this research is reducing the infection of measles by preventing patients of spreading of measles disease among of people. Our objective is processing Measles Rash images which are received from the patients because the received images may not have a good quality. Measles Rash images should have high end of contrast because it is a small spots on a skin as shown in fig. 1.



Fig. 1: Image of Measles's Rash [6]

Method

The proposed method as show in the block diagram fig.2 was processing the given measles rash color image by histogram algorithm techniques after two steps.

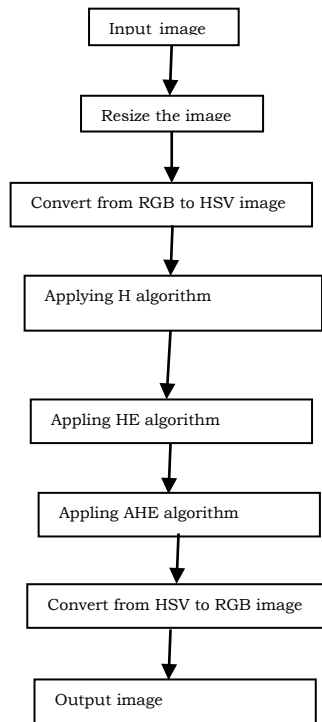


Fig. 2: Image of Measles's Rash patient and it's histogram

First step, the measles rash color image was resized to make sure that the image has the same number of rows and columns.

Second step, the measles rash color image has been converted from Red, black and blue (RGB) system to hue, saturation, and value (HSV) system for appearing image color under light. Now, measles rash resized and converted image passed by three histogram algorithms techniques which are H, HE and AHE in order.

Generally, histogram defined as a graphical representation of the image which has X and Y axis .Where X axis represents the gray level of brightness to darkness and Y axis represents the pixels' number.

1- Histogram

Fig.2 shows Measles's rash image as revised from the patient and its histogram. The histogram provides clear information regarding the contrast of the image in darkness side. However, we cannot get any information from the patient's image about the disease as we supposed to see.

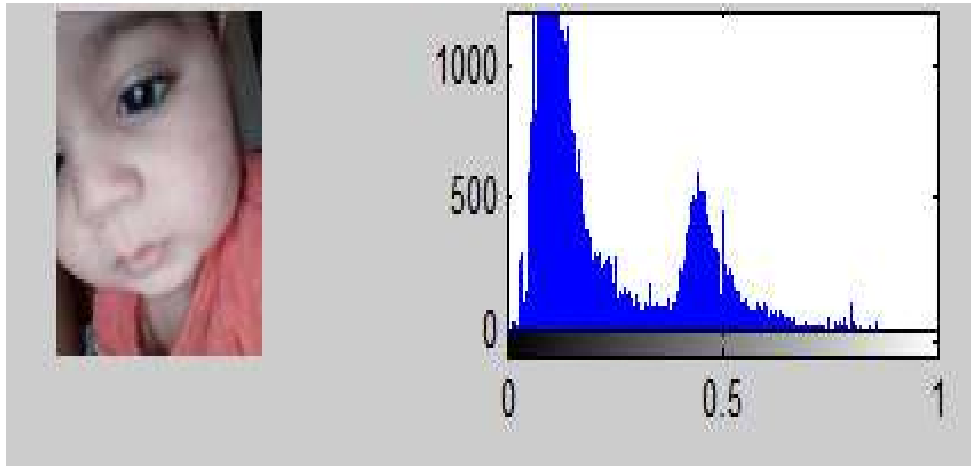


Fig. 3: Image of Measles's Rash patient and it's histogram

2- Histogram Equalization

To increase the contrast in the image, HE has been used. HE spread the intensity values. Also, HE stretch out rang of intensity image [4] [5]. HE technique changed the distribution of pixel values and compress the dynamic range of image, thus the image archived increasing in its contrast as shown in Fig 3.

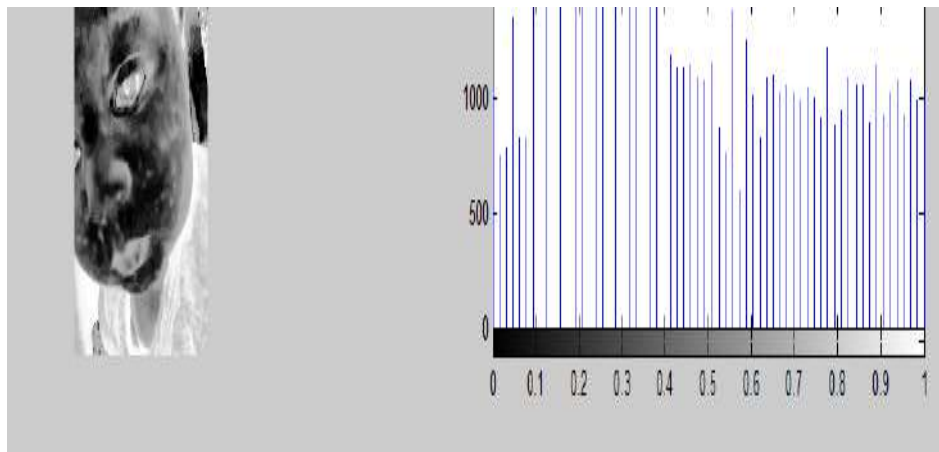


Fig. 4: Measles's Rash patient image and it's HE

3- Adaptive Histogram Equalization

AHE differs from the previous histogram in way that AHE computes several histograms, each identical to a distinct part of the image. After that the parts can be used to redistribute the lightness pixels of the image. Therefore, the local contrast and enhancing the details of the edges in each region of the image.

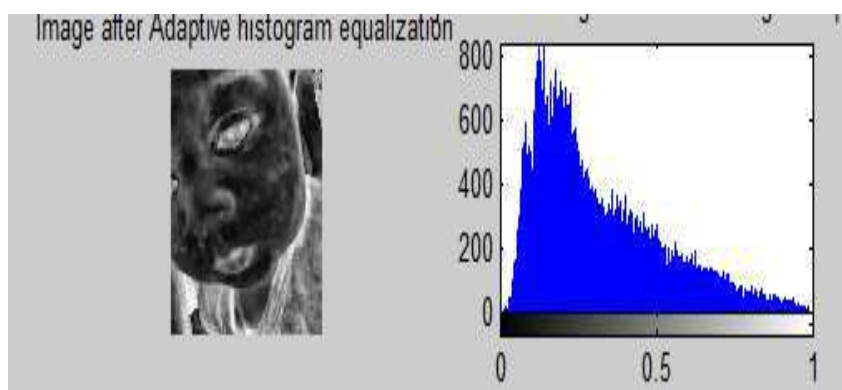


Fig. 5: Image of Measles's Rash patient and it's AHE

Results and Discussion

In this paper, we have identified the harmful of Measles Rash disease. We noted that vaccinations are very crucial in protecting people specially children against preventable disease. We worked on medical image processing enhancement be effective to against spread the disease among people. The simulation was perform based on MATLAB2013a. Our implantation of contrasting the image by histogram algorithm technique gave an excellent result. Several of image enhancement techniques and algorithms such as resize, convert, Histogram (H), Histogram Equalization (HE), and Adaptive Histogram Equalization (AHE) were proposed to get a good contrast, and the function of H was giving information of colour level and clarifies the contrast of the image form brightness or darkness as shown in fig 3. After that, HE stretch and spread the intensity of the image to increase the contrast as shown in fig 4. Additionally, AHE used to redistribute the lightness pixels of the image and clarify the local edges of the image. The specific goal was improve the image contract. AHE is very effective at enhancing contrast of Measles rash image as shown in fig 5.

Conclusion

Our result of enhance the measles rash image as shown in fig 6 were privilege schussed. The figure shows that the small red tiny spots are very clear on the patient's face. So the doctors noted his prescription according to the output image and other indication. The aim of this research was help medical care to uses more and more technology to save human life. We get our objective from this paper and we are looking for create a computer and phone application to could serve as a powerful tool in the diagnosis of the measles disease.



Fig. 6: Image of Measles's Rash patient image before and after enhancement

Acknowledgment

We would like to thank College of Electronics Technology, BaniWalid for the support of this work.

References

- [1] Abdullah, Y.M.Y., &Alqahtani, T. (2019).Research in Medical Image Using Image Processing Techniques. In (Ed.), Medical Image – Principles and Applplication.IntechOpen. <https://doi.org/10.5772/interchopen.8436>.
- [2] Alkoshi, S. (2022). Measles disease outbreak and genotype identification in Libya, 2018. Sri Lankan Journal of Infectious Diseases, 12(2).
- [3] World Health Organization. Measles elimination poster 2020 Available from: <https://apps.who.int/iris/handle/10665/260503>. Accessed on 5.02.2020
- [4] Cheng, H. D., & Shi, X. J. (2004). A simple and effective histogram equalization approach to image enhancement. Digital signal processing, 14(2), 158-170.
- [5] Ran, H. L., Dong, J. L., Zhang, K., Xi, S. B., Huang, J., & Peng, H. (2022, October). Detection of welding cavity defects in x-ray images based on digital image processing technology. In *5th International Conference on Computer Information Science and Application Technology (CISAT 2022)* (Vol. 12451, pp. 367-371). SPIE.
- [6] Source: Center for disease Control and Prevention (CDC). All rights reserved.Available online: www.cdc.
- [7] Centers for Disease Control and Prevention. (2018, February 5th). Measles (Rubella) Pre-vaccine Era [Online]. Available: <https://www.cdc.gov/measles/about/history.html>
- [8] Centers for Disease Control and Prevention. (2020, June 9th). Measles (Rubeola) Measles Cases and Outbreaks [Online]. Available: <https://www.cdc.gov/measles/casesoutbreaks.html>.

Engagement of marble powder in self compacting concrete

Dr. Abdelhamed I. Ganaw

Civil Engineering, Faculty of Engineering /Elmergib University-Libya

Abstract: This study explores the outcome of using marble powder in the production of self-compacting concrete (SCC) by partial replacement of cement. Waste marble was collected from local workshops and crushed to small particle sizes then sieved on 75 microns. A percentage of cement of 5, 10 and 15 % was replaced by marble powder at w/c ratio of 0.5, 0.55 and 0.6. Super-plasticizer was employed for all mixes with addition of sand and coarse aggregate. Fresh concrete workability then measured and compressive strength of self-compacting concrete was determined at 7 and 28 days, finally permeability of 28 days hardened concrete was tested. The results indicated that marble powder can be used as partial replacement of cement in self-compacting concrete with good concrete properties

Keywords: marble powder, super plasticizer, self-compacting concrete, compressive strength.

Introduction

Self-compacting concrete (SCC) is produced by engagement super plasticizers in concrete, the resulted high flow concrete sometimes called flowing concrete Neville, (1995), Due to the wide use of SCC in construction is essential to produce high quantity of cement which impacts on the environment by gas emission. And bad effect on land. Due to the large amount of waste materials like marble waste which become an issue in many countries, for example as what happened in the EU. The European parliament and the European union (2018) decided that waste management should be improved and transformed into sustainable material management. They felt the problem of waste material, especially on the environment and human health which should be protected, at the same time the Union decided to reduce the dependency on the imported resources, according to that, EU published a legislation report to reuse waste materials in the industry. The Partial replacement of cement by some waste materials like marble dust or glass powder is beneficial as that helps in reducing the waste material and minimizes gas emission from cement production, Ganaw et al.(2016). Marble powder was also employed in concrete as a mineral additive and resulted in good concrete mechanical properties as reported by Belouadah et. al.(2014) . Moreover, Khatib and others (2012) replaced cement by waste material powder and reported that concrete slump increases by powder increase with high strength at 10% replacement. Ural and Yaksi (2020) were employed waste marble particles to road construction with other materials and reported that the result is suitable as a base material according to the Technical Specifications of Turkish Highways. Ganaw et al. (2018) also replaced a part of cement by marble powder and proved that concrete strength was satisfied to many applications. Gulmez (2021) was employed waste marble powder and waste steel pieces to concrete and reported that flexural strength of concrete was improved until the powder percentage of 10%. Consequently, the use of waste materials like marble powder can be added to concrete to improve its properties and reducing the quantities of waste materials.

2. Used Materials

Ordinary Portland cement from Elmergib factory- Alkhums was used in concrete production with Blain fineness of 2950 cm²/gm and its initial and final setting times are satisfying to BS EN 196 – 3 (1995).

Water used in all mixes was taken from the school of engineering water network. It is suitable in the production of concrete. Fine aggregate used was imported from Zliten quarries. It was

clean and its gradation satisfied the requirements of British standard BS 812:1992. Coarse aggregate was imported from local quarry in Alkhums with max aggregate size of 14 mm. Specific gravity and absorption of aggregate were 2.58 and 0.023 respectively.

All used marble in the research was collected from local marble workshops. Waste marble was collected and crushed in los angles drum machine, then sieved to pass 75 micron. After that all sample was collected and mixed again with the mixer for homogeneity. The material then kept in containers to the time of mixing. Marble powder Blaine surface area was 3500 cm²/gm. Super plasticizer (Sika-Viscocrete) for SCC was used at 1% for all mixes.

3- Methodology

Concrete mix was first produced at w/c ratios of 0.45, 0.50 and 0.55 without any addition of marble powder, then cement was replaced by marble powder of 5%, 10% and 15% at the same w/c ratios and constant quantity of sand and coarse aggregate and 1% superplasticizer (SP) . Fresh concrete was mixed by the mixer and its workability was measured by the slump flow test according to the EFNARC 2002. Fresh concrete was casted in 150mm cubic moulds. After 24 hours concrete samples then removed from their forms and put in water for 7 and 28 days for permeability and compressive strength tests.

4. Discussion of test results

4.1 SCC workability

Figure 1 shows the relation between fresh SCC seepage and w/c ratio at different marble powder contents. It is clear that concrete seepage decreases with the increase of marble powder content for the same water content. Percentage of 15% marble dust at w/c ratio of 0.45 resulted in the lowest value of diameter of 655 mm and this still in the requirements of self-compacting concrete specifications EFNARC 2002 with (650 mm to 800mm) diameter.

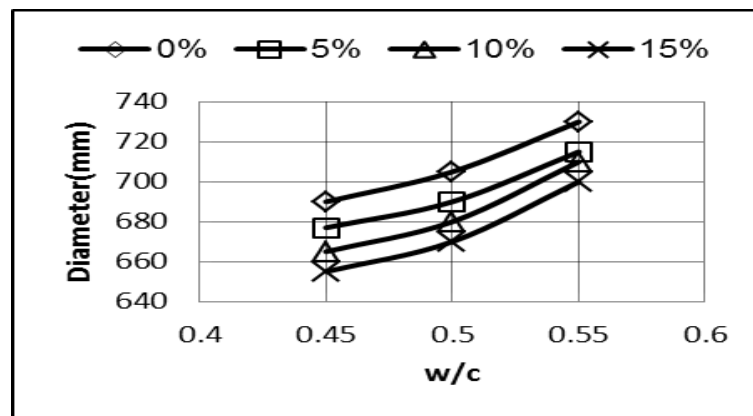


Fig. 1 Concrete seepage at different w/c ratios

4.2 Compressive strength of concrete

Figures 2 and 3 show the relation between hardened concrete compressive strength and w/c ratio at 7 and 28 days respectively for different marble powder contents. SCC compressive strength decreases with the increase in w/c ratio at both ages. Although both graphs show that as the powder content

increases the strength decreases for all w/c ratios. It is well observed that compressive strength decreases with the increase in powder content for both ages with good strength especially at 28 days. Figures also show that as the w/c ratio increases the strength of concrete decreases due to the gel voids increase in hardened state.

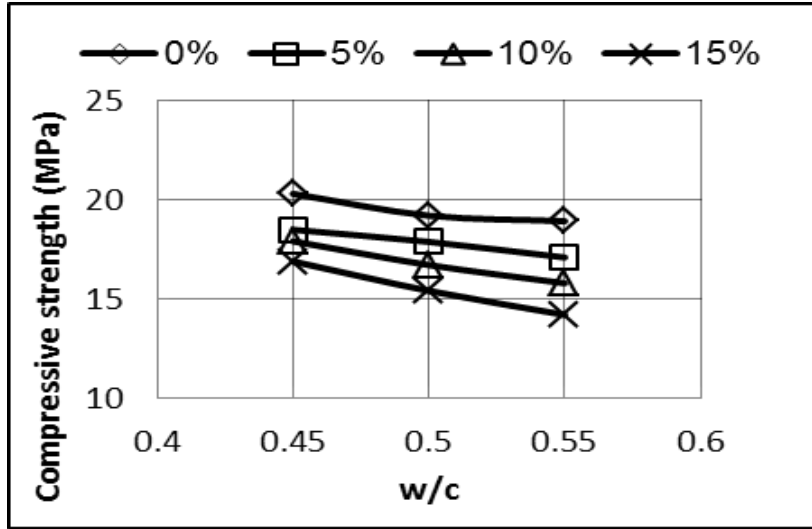


Fig. 2 Compressive strength vs w/c ratio at 7 days

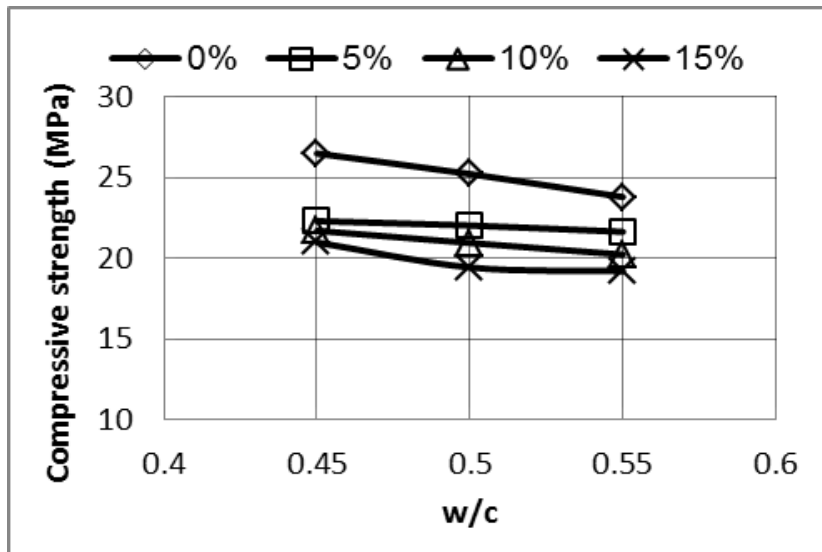


Figure 3 Compressive strength vs w/c ratio at 28 days

4.3 Water permeability depth

Figures 4 shows the relation between permeability depth in concrete and w/c ratio for different marble powder contents. It is very important to notice that water permeability depth decreases with the increase in marble powder content at all w/ ratios. From the relations it can be also noticed that

permeability increases with the increase in w/c ratios for all samples. This result can be very useful when durability of SCC for durability is necessary.

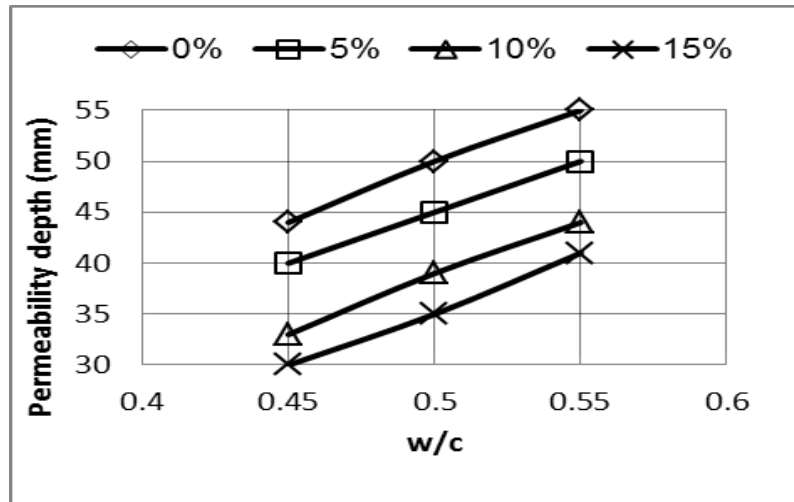


Fig. 4 Water permeability vs w/c ratio

5. Conclusions

From the investigation, it can be concluded that;

- 1- SCC with satisfied workability can be reached by the use of super plasticizer and a part of cement replaced by marble powder during concrete production.
- 2- Satisfied compressive strength was obtained even when replacement percentage reached 15% and production.
- 3- It is very useful to get lower permeability especially when durability is important and this was achieved by cement replacement by marble powder.

As a result, the replacement of cement by part of waste marble powder cement will minimize the cost of concrete production and results in low gas emission during cement production and protect the land from pollution.

6. References

- 1- A. M Neville, Properties of concrete. Fourth edition, Pearson Education Ltd., 1995
2. British Standards BS 812, Methods of Sampling and Testing of Minerals Aggregates, Sand, and Fillers, 1992.
3. BS EN 196 – 3, Method of Testing Cement. Determination of Setting time and Soundness, 1995.
4. EU,(2018), DIRECTIVE (EU) 2018/851 OF THE EUROPEAN PARLIAMENT AND OF THE COUNCIL, Official Journal of the European Union, May 2018
- 5-. EFNARC, Specification and Guide Lines for Self Compacting Concrete,2002, UK
- 6- G. Abdelhamed, A Mhmud, S., Salah and E., Jamal, Partial replacement of cement by marble powder on concrete properties, Archives of civil engineering department, Alkhums, 2018

- 7- G.,Abdelhamed. Jabballa & R. Sultan, (2016) Effect of waste glass as partial replacement of cement on mortar properties, Proceeding of the 5th conference of the high professional institute for comprehensive professions, AlKhums.
8. M. Belouadah, Z. Rahmoni & N. Tebbal, (2014), Effect of incorporation of local mineral additions on the mechanical behaviour of concrete. Proceeding of the conference of CONST ENG 14 on structures, materials and construction engineering, Turkey.
9. J.M. Khatib, E.M. Negim, H.S.Sohl and N.Chileshe, (2012), Glass Powder Utilization in Concrete Production., European Journal of Applied Science, vol. 4, no. 4, 173-176.
- 10- N., Gulmez, Performance of marble powder on cementitious composites including waste steel chips as an additive, Construction and building materials, V312, December
- 11- Sika ViscoCrete-3425, High Performance Superplasticizer concrete admixture., commercial samples, Tripoli. 2015.
- 12- U. Nazile and G Yaksi,(2020), Utilization of marble piece wastes as base materials, Journal of open Geoscience.

Theoretical studies on the efficiencies of some thio compounds as corrosion inhibitors of mild steel in HCl using PM6

Waleed Ahmoda^a, Allam Musbah Al Allam^b,

^aCollege of Technical Sciences, Bani Walid, Libya

^bEngineering and Information Technology Research Centre, Bani Walid, Libya

Abstract

Quantum chemical calculations were performed on 19 thio compounds using semi-empirical method PM6 within program package of Material Studio 5.5. The effect of molecular structure on the corrosion inhibition efficiency was investigated using the quantum chemical calculations. The electronic properties such as highest occupied molecular orbital (HOMO), lowest unoccupied molecular orbital (LUMO) energy levels, (LUMO – HOMO) energy gap, dipole moment (λ) and fraction of electron transfer (ΔN) were calculated and discussed.

Keywords: PM6, Corrosion Inhibition, Quantum Chemical Parameter

Introduction

Corrosion is the destructive attack of metal or alloy chemically or electrochemically against its environment which leads to loss of useful properties of materials. The protection of metals against corrosion can be achieved by adding inhibitors in small concentrations to its environment [1]. Corrosion inhibitors are either synthesized from cheap raw materials or are chosen from organic compounds containing electronegative functional groups and p-electrons, triple or conjugated double bonds. The presence of heteroatoms (such as sulfur, oxygen, nitrogen) as well as aromatic rings in organic compounds facilitates the adsorption of the inhibitor on the metal surface in which the initial mechanism for the corrosion inhibition of the metal [2]. Some organic compounds are found to be effective corrosion inhibitors for many metals and alloys. It has been commonly recognized that organic inhibitor usually promotes formation of a chelate on the metal surface, which includes the transfer of electrons from the organic compounds to metal, forming coordinate covalent bond during such chemical adsorption process [3-5]. Some thio compounds are found to be good inhibitors for mild steel in acid [6-8]. Recently, theoretical chemical calculations have been used, such as quantum chemical calculations, to explain the mechanism of corrosion inhibition [9]. Quantum chemical calculations are proven to be a very powerful tool to understand the inhibition mechanism [10].

The present study is aimed to determine the relationships between molecular structures of 19 thio (sulfur) containing compounds namely: 6-thioguanine (TG) [5], 2,6-dithiopurine (DTP) [13], 4-amino-5-phenyl-4H-1, 2, 4-triazole-3-thiol (APTT) [6], N'-(3,4-dihydroxybenzylidene)-3-[[8-(trifluoromethyl)quinolin-4-yl]thio]propanohydrazide (DHBTPH) [7], 3-[[8-(trifluoromethyl)quinolin-4-yl]thio]-N'-(2,3,4-trihydroxybenzylidene)propane hydrazide (TQTHBH) [8], 5-(1H-1,2,4-triazole-1-alkyl)-1,3,4-oxadiazole-2-thiol (TAOT) [9], N'-[4-(diethylamino)benzylidene]-3-[[8-(trifluoromethyl)quinolin-4-yl]thio]propane hydrazide (DEQTPH) [10], Quinolin-5-ylmethylene-3-[[8-(trifluoromethyl)quinolin-4-yl]thio]

propanohydrazide (QMQTPH) [11], 3,5-bis(4-methylthiophenyl)-4H-1,2,4-triazole (4-MTHT) [12], N-(2-Thio benzimidazolyl methyl) isatin-3-isonicotinoyl hydrazone (TBIH) [13], thiourea (TU) [22], thioacetamide (TAcA) [22], 4,4-dimethyloxazolidine-2-thione (DMT) [23], N-methylthiocarbamide (N-MTU) [22], tetramethylthiocarbamide (TMTU) [22], 2-imidazolidinethione (ETU) [22], thiobenzamide (TBA) [22], N-ethylthiocarbamide (N-ETU) [22] and Schiff base furoin thiosemicarbazone (FTSC) [24] and their inhibition efficiencies. The selected thio compounds were previously reported as corrosion inhibitors for mild steel in 1.0 M HCl solution at 30°C. Through the method of quantum chemical calculations, the structural parameters, such as the frontier molecular orbital (MO) energy HOMO (highest occupied molecular orbital) and LUMO (lowest unoccupied molecular orbital) and the fraction of electrons (ΔN) transfer from inhibitors to metal surface were calculated and correlated with corrosion inhibition efficiencies. The molecular structures for the selected thio compounds are shown in Figure 1.

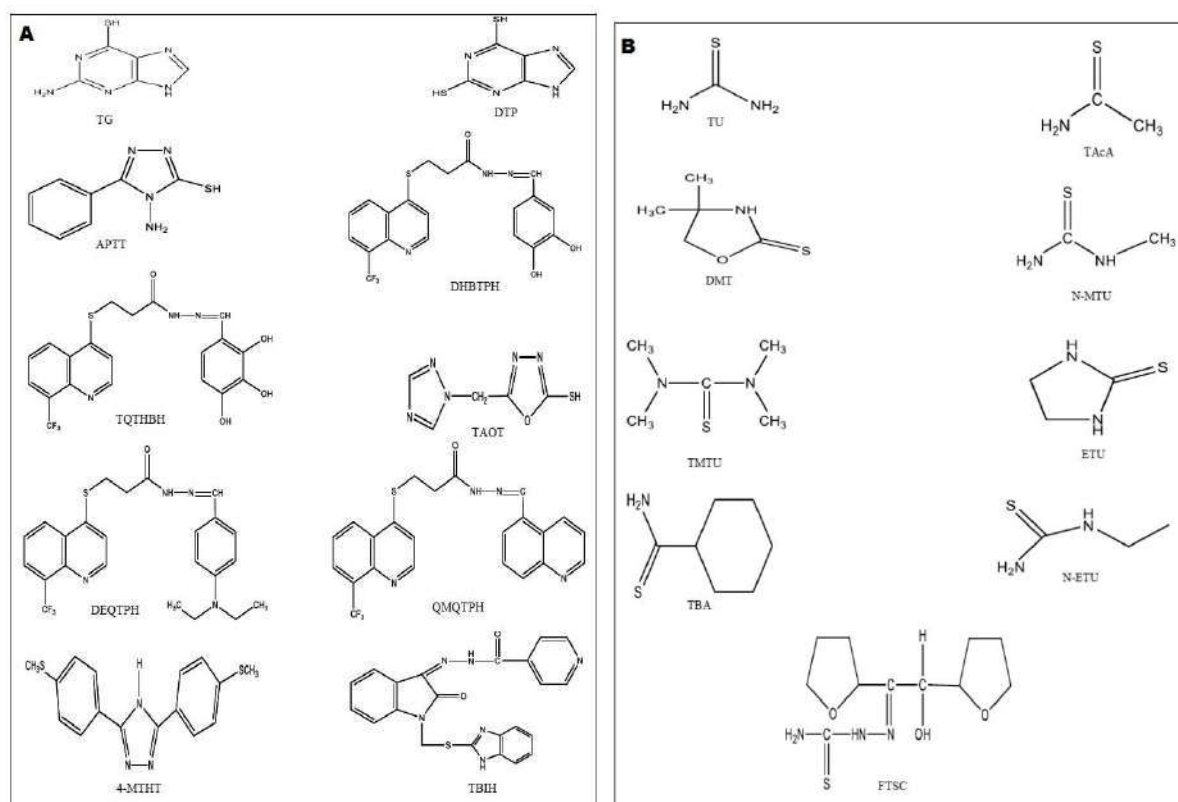


Fig.1. Molecular structure of studied molecules

Method of calculations

The quantum chemical calculations were performed using the VAMP 10.0 in Materials Studio 5.5 software. Parametric Method (PM6), semi-empirical method was employed to obtain the quantum chemical parameters and to optimize the molecule geometry. Complete geometry optimization of the molecules was carried out at ab initio level RHF (Restricted Hartree Fock theory) and SCF mode (self-consistent field). This basis set is known to provide accurate geometries and electronic properties for wide range of organic compounds. The optimization was repeated until minimum energy reached. The following quantum chemical indices were calculated: the energy of the highest occupied molecular orbital (E_{HOMO}),

the energy of the lowest unoccupied molecular orbital (E_{LUMO}), dipole moment (λ), Mulliken atomic charges and number of transferred electrons (ΔN).

The numbers of transferred electrons (ΔN) were calculated based on the following quantum chemical method [15]:

$$\Delta N = \frac{(X_{Fe} - X_{inh})}{[2(\eta_{Fe} + \eta_{inh})]} \quad (1)$$

Where X_{Fe} and X_{inh} denote the absolute electronegativity of mild steel and the inhibitor molecule, respectively; η_{Fe} and η_{inh} denote the absolute hardness of mild steel and the inhibitor molecule, respectively. These quantities are related to electron affinity (A) and ionization potential (I).

$$X_{inh} = \frac{I + A}{2} \quad (2)$$

$$\eta_{inh} = \frac{I - A}{2} \quad (3)$$

I and A are related in turn to E_{HOMO} and E_{LUMO} via

$$I = -E_{HOMO}$$

$$A = -E_{LUMO}$$

The fraction of electrons transferred (ΔN) from inhibitor to the mild steel molecule was also calculated using a theoretical X_{Fe} and η_{Fe} values for mild steel of 7 eV/mol and 0 eV/mol, respectively [16].

Results and Discussion

Quantum chemical calculations

The optimized molecule structure of the selected thio molecules are shown in Figure 2.

The calculated quantum parameters of the HOMO, LUMO and dipole moment for selected thio compounds were presented in Table 1.

Frontier orbital theory is useful in predicting adsorption centers of the inhibitor molecules responsible for the interaction with surface metal atoms [17]. The terms involving the frontier molecular orbital could provide dominative contribution, because of the inverse dependence of stabilization energy on orbital energy difference. Studies by Fang and Li [3] have suggested that excellent corrosion inhibitors are usually those organic compounds which not only offer electrons to the unoccupied orbital of the metal but also accept the free electrons from the metal.

It can be seen from Table 1 that the obtained quantum chemical parameters changed irregularly with inhibition efficiency. The inhibition efficiency is misrelated with neither the changes of the E_{HOMO} and E_{LUMO} , which suggested that the inhibitors were perhaps neither the acceptor nor the donor of the electrons. This indicates there was no electron transferring in the interaction between the inhibitor molecules and the metal surface. Thus, the interactions are probably physical adsorption, and the interactions between the inhibitors and the metal surface might be ascribed to the hyper conjugation interactions- π stacking [18]. The frontier molecule orbital density distributions of thio compounds were presented in Figure 2.

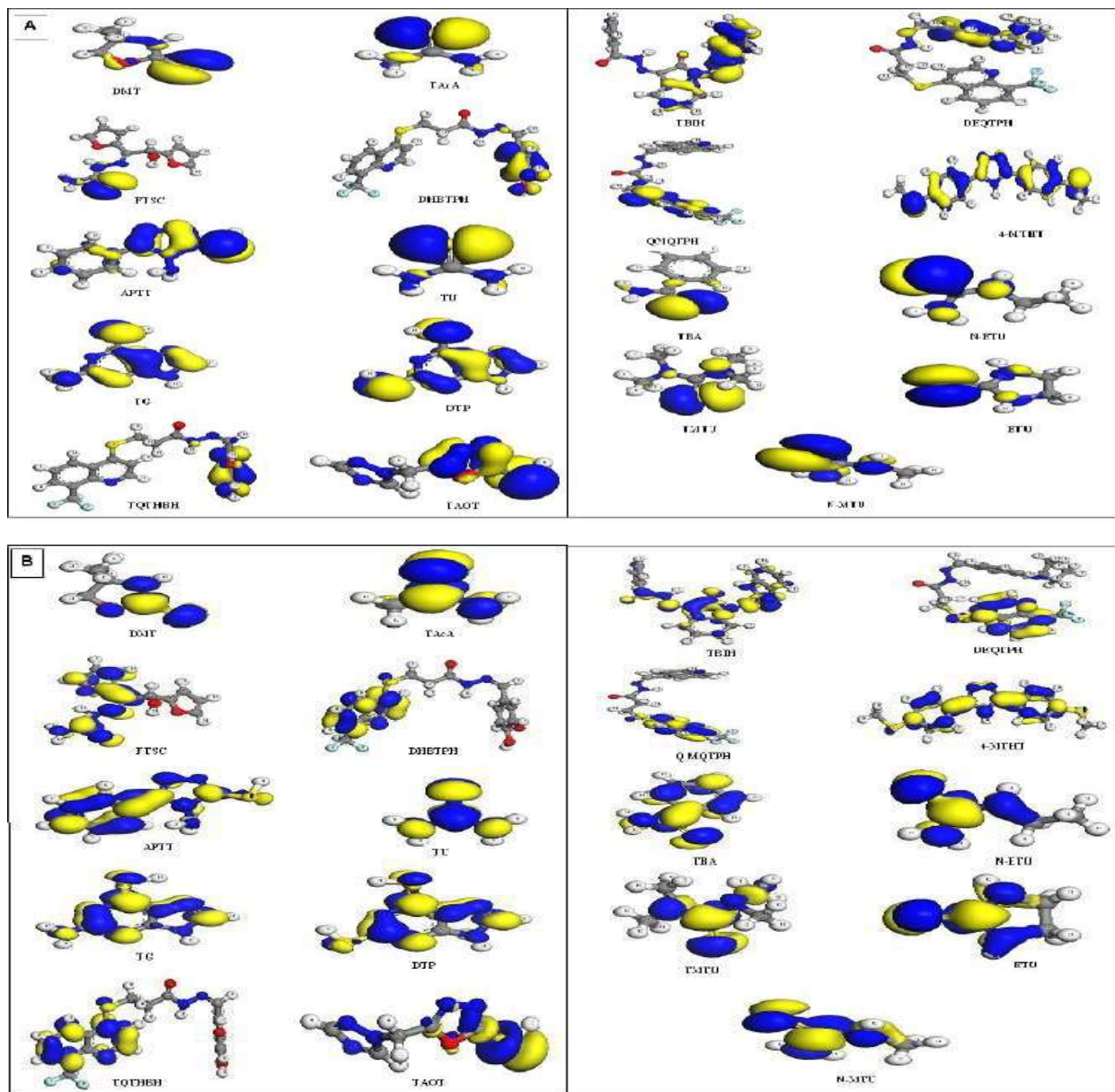


Fig. 2. The frontier molecule orbital density distributions of this compounds: **(A)** HOMO and **(B)** LUMO.

As seen from the figure, the populations of the HOMO and LUMO focused around the sulfur and nitrogen atoms. The condition of physical adsorption is the presence of both electrically charged surface of the metal and charged species in the bulk of the solution; the presence of a metal having vacant low-energy electron orbital and of an inhibitor with molecules having relatively loosely bound electrons or heteroatom with lone pair electrons. Thus in the HCl acid medium, thio compounds may be protonated predominantly affecting the nitrogen atoms [18]. Thus, they become cations, existing in equilibrium with the corresponding molecular form. The protonated thio compounds, however, could be attached to the mild steel surface by means of electrostatic interaction between Cl^- and protonated thio compound since the mild steel surface has positive charges in the acid medium [19]. This could further be explained based on the assumption that in the presence of Cl^- would attach to positively charged surface. When thio

compound adsorbs on the steel surface, electrostatic interaction takes place by partial transference of electrons from the polar atom (S and N atoms and the delocalized π electrons around the heterocyclic rings) of thio compound to the metal surface. In addition to electrostatic interaction (physisorption) of thio compound molecules on the mild steel surface, molecular adsorption may also play a role in the adsorption process. Thus the adsorption of thio compounds on the mild steel surface in HCl may be achieved by the interaction between iron atoms and heteroatom of sulfur. The electronic configuration of iron is $[\text{Ar}]4s^23d^6$, 3d orbital is not fully filled with electrons. The unfilled orbital of iron could bond with the highest occupied molecular orbital (HOMO) [20] of thio compound, while the filled 4s orbital of the former could interact with the lowest unoccupied molecular orbital (LUMO) of the latter.

Table 1. Molecular properties of the optimize thio compounds using PM6.

Compound	Inhibitor conc. (mM)	E_{HOMO} (eV)	E_{LUMO} (eV)	$E_{\text{LUMO}} - E_{\text{HOMO}}$ (eV)	λ	ΔN	IEexp%
TU	0.4	-8.69	0.234	-8.924	5.622	0.311	48.6
DMT	4	-8.726	0.164	-8.89	7.121	0.306	82.5
TBA	10	-8.686	-0.989	-7.697	4.779	0.281	97
N-ETU	10	-8.504	0.355	-8.859	6.43	0.330	95
TMTU	10	-8.282	0.181	-8.463	5.201	0.349	95
ETU	10	-8.601	0.179	-8.78	6.329	0.318	92
N-MTU	10	-8.541	0.342	-8.883	6.798	0.327	92
TAcA	10	-8.643	-0.126	-8.517	5.044	0.307	67
FTSC	3	-8.712	-1.002	-7.71	7.14	0.278	97.7
TG	1	-8.888	-0.778	-8.11	3.155	0.267	77.9
DTP	1	-9.063	-1.196	-7.867	1.524	0.238	85.9
TQTHBH	1.1	-9.332	-1.489	-7.843	2.851	0.203	88.9
TAOT	1	-9.967	-1.308	-8.659	4.085	0.157	89.1
TBIH	1.1	-9.187	-1.476	-7.711	1.062	0.216	98.04
QMTPH	0.5	-9.337	-1.473	-7.864	4.312	0.203	93.1
APTT	0.4	-8.993	-0.683	-8.31	5.547	0.260	86.1
DHBTPH	1.15	-9.12	-1.477	-7.643	2.7	0.223	88.4
DEQTPH	1.05	-8.365	-1.542	-6.823	3.746	0.300	91.8
4-MTHT	0.5	-8.459	-0.883	-7.576	5.128	0.307	96.8

Mulliken charge and adsorption mechanism

The Mulliken charge distributions of the inhibitors are presented in Figure 3. It can be readily observed that sulphur, nitrogen atoms and the some carbons atoms have higher charge densities. The regions of highest electron density are generally the sites to which electrophiles attacked [34]. Therefore S, N and C atoms were the active centre, which have the strongest ability of bonding to the metal surface. On the other hand, HOMO (Figure 2A) was mainly distributed on the area containing sulphur and nitrogen atoms. Thus, this area is probably the primary site of the bonding. It was found that the studied inhibitors apart from existing in the cationic form which can interact with mild steel surface by

electrostatic attraction. This interaction with the mild steel surface using a number of active centres is forming a good protective layer on the mild steel surface. The inhibition of acid corrosion by such organic cations is strongly influenced by the nature and charge of the metal surface.

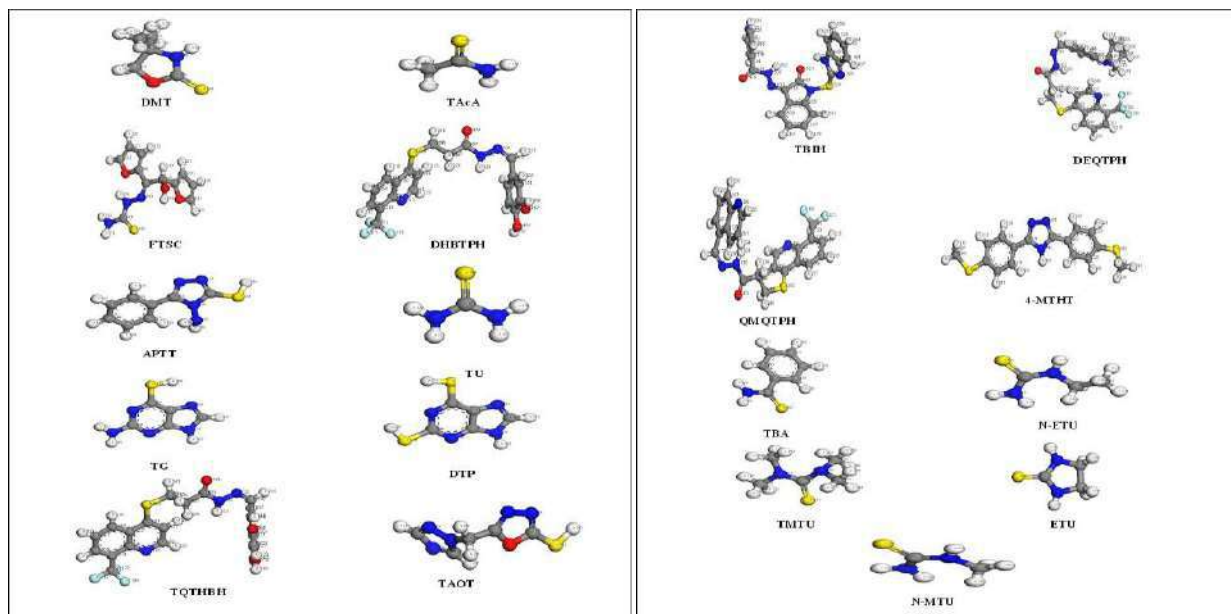


Fig. 3. Mulliken charges of thio molecules.

Conclusion

The relationships between inhibition efficiency of mild steel in 1M hydrochloric acid and the energy of the highest occupied molecular orbital (E_{HOMO}), the energy of the lowest unoccupied molecular orbital (E_{LUMO}), energy gap ($E_{LUMO} - E_{HOMO}$), dipole moment (λ), Mulliken atomic charges and number of transferred electrons (ΔN) of the thio compounds were calculated using the PM6-SCF method. Quantum chemical calculations have shown that apart from thio molecules adsorbing as cationic species on the mild steel surface, the adsorption of the molecule is take place through S atoms. The locations containing S and N atoms with high electron density is the most possible site for bonding the mild steel surface through electron donations to the metal surface.

References

- [1] R. M. Issa, M. K. Awad, F. M. Atlam, Quantum Chemical Studies on the Inhibition of Corrosion of Copper Surface by Substituted Uracils. *Appl. Surf. Sci.* 255 (2008) 2433.
- [2] A. Y. Musa, A. Mohamad, A. H. Kadhum, M. S. Takriff, W. Ahmoda, Quantum chemical studies on corrosion inhibition for series of thio compounds on mild steel in hydrochloric acid, *J. Ind. Eng. Chem.* 18 (2012) 551.
- [3] J. Fang, J. Li, Quantum chemistry study on the relationship between molecular structure and corrosion inhibition efficiency of amides, *J. Mol. Struct. (THEOCHEM)* 593 (2002) 179.
- [4] M. Ajmal, A.S. Mideen, M.A. Quaraishi, 2-hydrazino-6-methyl-benzothiazole as an effective inhibitor for the corrosion of mild steel in acidic solutions, *Corros. Sci.* 36 (1994) 79.
- [5] M. Elayyachy, A. El Idrissi, B. Hammouti, New thio-compounds as corrosion inhibitor for steel in 1 M HCl, *Corros. Sci.* 48 (2006) 2470.

- [6] S.M.A. Hosseini, A. Azimi: The inhibition of mild steel corrosion in acidic medium by 1-methyl-3-pyridin-2-yl-thiourea, *Corros. Sci.* 51 (2009) 728
- [7] A.Y. Musa, A.H. Kadhum, A. Mohamad, M.S. Takriff, A. Daud, S.K. Kamarudin, On the inhibition of mild steel corrosion by 4-amino-5-phenyl-4H-1, 2, 4-triazole-3-thiol, *Corros. Sci.* 52 (2010) 526.
- [8] B. Joseph, S. John, A. Joseph, B. Narayana, Imidazolidine-2-thione as corrosion inhibitor for mild steel in hydrochloric acid, *Ind. J. Chem. Technol.* 17 (2010) 366.
- [9] S.G. Zhang, W. Lei, M.Z. Xia, F.Y. Wang, QSAR study on N-containing corrosion inhibitors: Quantum chemical approach assisted by topological index, *J. Mol. Struct. (THEOCHEM)* 732 (2005) 173.
- [10] G. Bereket, C. Öğretir, Ç. Özşahin: Quantum chemical studies on the inhibition efficiencies of some piperazine derivatives for the corrosion of steel in acidic medium, *J. Mol. Struct. (THEOCHEM)* 578 (2002) 79.
- [11] Chakrabarti A. Quantum-chemical study of the corrosion inhibition of mild steel in 6 % (wt/wt) HCl by means of cyanoguanidine derivatives. *Br. Corros. J.*, 19 (1984) 124
- [12] F. B. Growcock. Inhibition of steel corrosion in HCl by derivatives of cinnamaldehyde. Part I. Corrosion inhibition model. *Corrosion*, 45 (1989) 1003.
- [13] Yan, Y., Weihua W. Li, L. Cai, B. Hou. Electrochemical and quantum chemical study of purines as corrosion inhibitors for mild steel in 1M HCl solution. *Electrochimica Acta*, 53 (2008) 5953.
- [14] Ahmed Y. Musa, A. A. H. Kadhum, A. B. Mohamad, M. S. Takriff, A. R. Daud, S. K. Kamarudin. Adsorption isotherm mechanism of amino organic compounds as mild steel corrosion inhibitors by electrochemical measurement method. *Jour. of Centr.Sou.Univer.of Techn.*, 17 (2010) 34.
- [15] Saliyan, R., A. V. Adhikari. Inhibition of corrosion of mild steel in acid media by N'-benzylidene-3-(quinolin-4-ylthio)propanohydrazide. *Bull. of Mater. Scie.* 31 (2008) 699.
- [16] Saliyan, R., A. V. Adhikari. Corrosion inhibition of mild steel in acid media by quinolinyl thiopropano hydrazone *Ind. Jour. of Chem. Techn.* 16 (2009) 162.
- [17] Ying, Y., L. Wei-hua, X. Shao-hua, H. Bao-rong. Corrosion inhibition of mild steel by novel heterocyclic compound in 1 mol/L HCl solution. *Corros. Scie. and Protec. Techn.*, 19 (2007) 414.
- [18] R. Saliyan, A. V. Adhikari. N'-[4-(diethylamino)benzylidene]-3-[[8-(trifluoromethyl)quinolin-4-yl]thio]propano hydrazide) as an effective inhibitor of mild steel corrosion in acid media. *Mater. Chem.y and Phys.* 115 (2009)618
- [19] Saliyan, R., A. V. Adhikari. Quinolin-5-ylmethylene-3-[[8-(trifluoromethyl)quinolin-4-yl]thio]propanohydrazide as an effective inhibitor of mild steel corrosion in HCl solution. *Corros.Scie.* 50 (2008) 55.
- [20] Lagrenee, M., B. Mernari, M. Bouanis, M. Traisnel, F. Bentiss. Study of the mechanism and inhibiting efficiency of 3,5-bis(4-methylthiophenyl)-4H-1,2,4-triazole on mild steel corrosion in acidic media. *Corros. Scie.* 44 (2002) 573.
- [21] Ashish K., M. Quraishi. Investigation of adsorption of isoniazid derivatives at mild steel/hydrochloric acid interface: Electrochemical and weight loss methods. *Mater. Chem. and Phys.* 123 (2010) 666.
- [22] Stoyanova, A. E., E. I. Sokolova, S. N. Raicheva. The inhibition of mild steel corrosion in 1 M HCL in the presence of linear and cyclic thiocarbamides—Effect of concentration and temperature of the corrosion medium on their protective action. *Corros. Scie.* 39 (1997) 1595.
- [23] W. Ahmoda, QSAR for Series of Thio Compounds as Corrosion Inhibitors in 1M HCL, *IJSETR*, 7 (2018) 1971.

Thermal stability and mechanical properties of alkaline activated mortars synthesized from POFA after exposure to elevated temperatures

Otman M. M. Elbasir

Department of Civil Engineering, High institute of Science and Technology, Qaser Bin gashear , Libya.

Abstract: This paper presents results from experimental studies on the Thermal stability and mechanical properties of alkaline-activated mortars, which that prepared by alkaline solution activating POFA. The compressive strength test and characterization, employing XRD and, FESEM were conducted on geopolymer mortar specimens at ambient temperature and after exposure to elevated temperatures from 200°C - 1000°C. Results from these tests show that geopolymer mortar exhibits higher temperature-induced degradation in compressive strength and body at 1000°C. The mixture of POFA experienced no thermal cracks, its deformation occurred at 1000°C which resulted in extensive shape changes. measure the compressive strength of the exposed alkaline-activated mortars. The relative residual compressive load for the mixture (a) decreased from 77% to 40% after exposure to temperatures from 200°C to 800°C

Keywords: POFA; Compressive strength ; Thermal stability ; XRD ; FESEM

Introduction

Geopolymer or alkaline activated is a type of new cement, and a new environment-friendly inorganic binder, obtained by alkaline solution activating aluminosilicate source material (such as POFA, fly ash, and slag), has attracted significant interest in recent years as a practical alternative to Portland cement [1–4]. Issues related with the utilization of conventional supplementary materials such as (FA), slag (GGBFS), (SF), etc. are due to restricted accessibility locally and higher transport costs imported from somewhere else [5-7]. Palm oil produces plentiful waste squander in Malaysia. The palm oil industry produces about 80% of squandered materials such as product fruit bunches and shells which make genuine issues for the environment [8]. This agricultural squander has been utilized as a substitute for fuel [9]. to turn on generators for electrical energy technology in palm oil mills. After the burning process, the closing residues are both dumped into the soil or left in open land. This waste fabric leads to environmental air pollution and contaminates groundwater [10]. and exchange the normal composition of the soil. Moreover, the addendum of waste as a supplementary material in concrete or mortar reduces the compressive power as a result of decreasing the concentration of portlandite due to the dilution effect [11 –13]. The effect of thermal stability on geopolymer mortar from properties of physical, chemical, and morphology change of minerals, and their influence on compressive strength development is a motivation for this study. some researchers incorporated fly ash, slag, and metakaolin in concretes at ratios of 10% and 20% in the form of either cement added or replaced without affecting the cement content and concrete samples to which they are exposed to 200, 400, 600, and 800 °C for 3 hours. The results indicated that FA concretes exhibited the highest relative strength at temperatures of 600 and 800°C. On the other hand, the neat MK system showed a much higher residual strength upon cooling from 1000°C to room temperature, indicating that the extent of glass formation from the geopolymer gel at 1000°C is reduced by the incorporation of Ca into the gel, which occurs as a consequence of the formation of C-S-H type gel that coexisted with the

aluminosilicate geopolymer gel [14]. Ranjbar et al. (2014a [15] reported low thermal stability of mixtures of POFA/FA-based geopolymer mortar when this mixture is exposed to above 300 °C. However, in the case of the increased content of fly ash, the results revealed an increase in the high-temperature thermal stability in strength rather than increasing in POFA content (decreased compressive strength) in the mixtures investigated. This was linked to the beginning of pore formation upon exposure to elevated temperature. This finding is basically due to the combustible compounds such as carbon in the untreated POFA which decomposed in the vicinity of 500°C. The objective of this research is to investigate the effect of thermal stability on physical properties, chemical composition, morphology, and their influences on the compressive strength development of geopolymer mortar. The resulting of geopolymer were extensively characterized, employing XRD and, FESEM

2. Materials and methods

2.1 Materials

2.1.1 Palm oil fuel ash

Palm oil fuel ash (POFA) was obtained from United Oil Palm Industry in the state of Penang, Malaysia. The first step involves drying the ashes within an oven for 24 h at 105°C to take out the POFA's inherent moisture since the POFA was placed outside the mill. POFA was thereafter sieved through 300 mesh to take out coarser particles of partially burnt ashes from fibers and palm kernel shells, following the work of Elbasir et al. (2017). Then the POFA was grounded into particles of size 10 µm by utilizing a ball mill fitted with 150 steel balls that rotate about 180 rpm for 8 hours. The unburnt carbon was then removed by heating the grounded POFA in a furnace at 550 °C for 90 minutes. The resulting POFA was specified as treated t-POFA. Fine POFA, designated as f-POFA, was fabricated by grounding the t-POFA for an additional 8 hours to enhance its fineness. Then, the f-POFA was grounded another 8 hours to obtain u-POFA (ultrafine POFA) with an average particle size of 1.1 µm.

2.1.2 Aggregates

Total fine aggregates content of 100 percent river sand along with properties of 1.85 fineness modulus as well as specific gravity 2.62 under saturated and surface dry (SSD) conditions. The ratio of sand to raw materials (FA, u-POFA, and GBFS) was maintained at 1.5.

2.1.3. Alkaline activator

10 M concentration NaOH and sodium silicate with initial silica modulus 2.2 ($M_s = \text{SiO}_2/\text{Na}_2\text{O}$) were utilized to synthesize the alkali activators for the purpose of mortar mixtures). This contains sodium silicate with sodium hydroxide 10 M.

2.2 Design and preparation

Delay time before heat application had no adverse effect on compressive strength development. In addition to this, a longer delay time is required to provide ample time during the manufacturing process. In this study, selected single binders fabricated from POFA mixtures for thermal stability analyses were chosen from the base material (POFA) (as shown in Table 1).

Table 1: Mix proportions for thermal stability

Type of Mix materials (kg) m ³		Sand (kg)/m ³	Na ₂ SiO ₃ (kg)/ m ³	NaOH (kg)/ m ³	Water (kg)/ m ³	Added water (kg)
POFA	856	1280	293	40	80	60

2.2.1 Test Procedure

To examine the significant effect of the single binder of (POFA) on thermal stability as shown in Figure (1), the alkali-activated mortar specimens from the mixture were exposed to various elevated temperatures. The testing procedure was the same as previous researchers [14]. Specimens were cured at ambient temperature for 28 days, prior to exposure at various elevated temperatures (from 200°C to 1000°C) in increments of 200°C at a heating rate of 10 °C/min. The specimens were placed inside the electrical furnace, as shown in Figure (1). As soon as the target temperature was attained, it was maintained for an additional 1 hour before the furnace was shut down to allow the specimens in the furnace to cool down to room temperature.



Fig 1: Samples placed inside the electrical furnace after heating

2.2.2 Specimen Analysis

The compressive strengths after cooling were determined according to ASTM C109/C109M (ASTM, 1999a) test [16]. The residual compressive strength was measured in triplicate samples. The behaviour of the hardened geopolymer mortar mixtures after exposure to different thermal loads was evaluated quantitatively by measuring the retained residual compressive strengths after the heat exposure. Detailed XRD and physical appearance analysis were undertaken to observe the effects of high temperatures on specimens exposed at 1000°C. From the XRD analysis, only the specimen with the highest thermal stability was investigated for their phases, physical, and microstructure changes (from ambient temperature to 1000°C) using FESEM. To further confirm the results of XRD analysis and microstructure changes.

3. Results and discussion

3.1 Visual observation

The main visual observation of the selected hardened mortars before and after exposure to elevated temperatures is shown in Figure (2). The specimens (a - d) before exposure to elevated temperatures reveal that at ambient temperature all mixtures have a dark grey colour. However, after being exposed to elevated temperatures from 200°C - 1000°C, all mixtures changed from grey to light sand and light pink. Although mixture (a) contained u-POFA experienced no thermal cracks, its deformation occurred at 1000°C which resulted in an extensive shape changes.

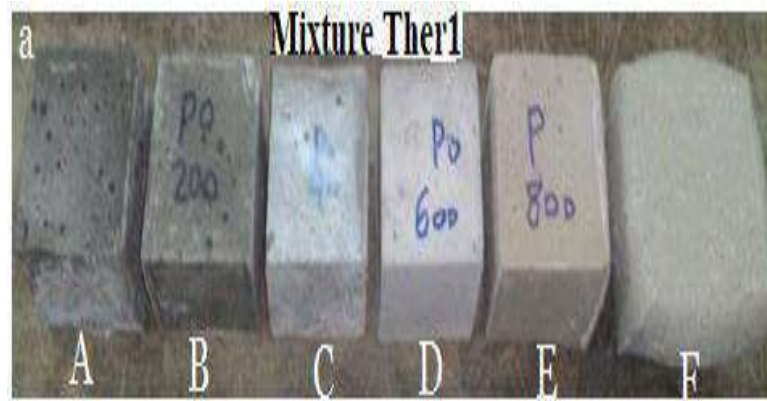


Figure 2 : Photographs of hardened single alkali activated mortars containing u-POFA Ther1, before and after being exposed to elevated temperature of (A) 28°C, (B) 200°C (C) 400°C (D) 600°C (E) 800°C (F) 1000°C

3.2. Compressive strength (CS)

Figure 3. and Figure 4. show the residual compressive strength results of single alkaline-activated mortars containing u-POFA at 28 days (as the reference) and after being exposed to elevated temperatures ranging from 200°C to 1000°C with an increment of 200°C. Figures 3 and 4 reveal that the strength of all alkaline activated u-POFA-based mortar steadily decreased as temperature increased from 200°C to 1000°C. On the other hand, for the specimens of alkaline activated u-POFA mortar after being exposed to 1000°C, the deformation in the form of sharp swelling was indicated. As shown in sample F given in Figure 2 , there is a change in the specimen's size and shape, which made it impossible to measure the compressive strength of the exposed alkaline activated mortars. The relative residual compressive load for the mixtures decreased from 77% to 40% after exposure to temperatures from 200°C to 800°C, respectively

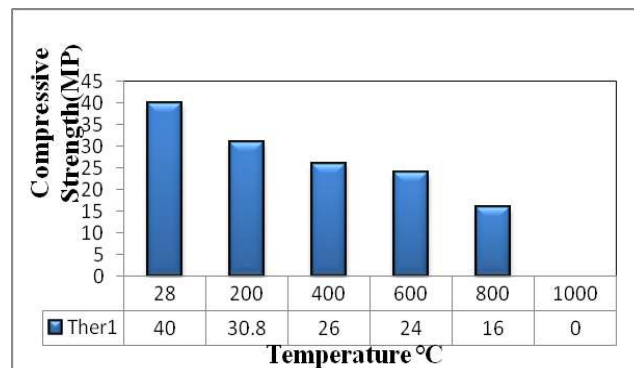


Fig 3: Residual compressive load of alkaline activated mortars

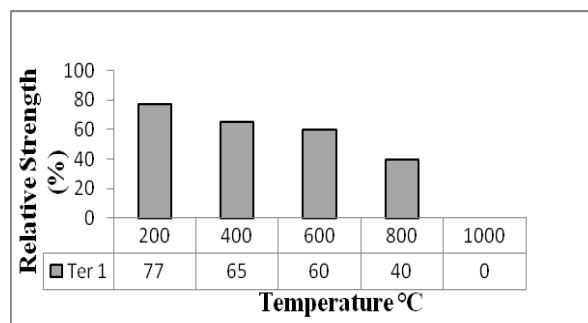


Fig 4: Relative residual compressive load alkaline activated mortars

3.3 Mineralogical analysis

X-ray diffraction tests were performed to identify the phases of the geopolymer mortar specimens. As shown in Figure 5, the XRD patterns have similar crystalline phases for mixture Ther1 made from u-POFA at 28 days and being exposed to elevated temperatures of 200°C to 400°C. It should be noted that the calcite phases remained. After exposure to 600°C, no calcite phase was retained in the structure. While, the quartz and jadeite phases remained the same after exposure to 800°C, however, after exposure to 1000°C no calcite phase was retained in the structure. The new phase was identified as nepheline with chemical formula $\text{NaAl}(\text{SiO}_4)$. Nepheline starts to form at high temperatures (800°C) from the decomposition of amorphous aluminosilicates [17]. The collapse of the tetrahedral framework at about 800°C, just before melting (about 1000°C), may explain the higher rate of expansion observed with nepheline).

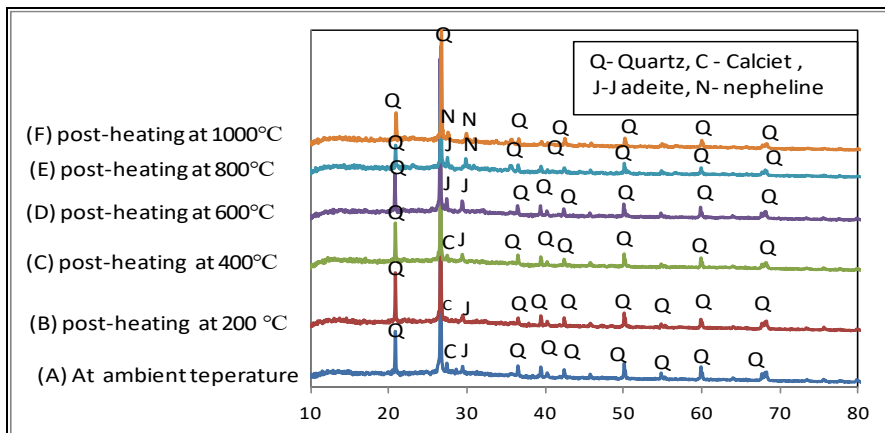


Fig 5: XRD diffractograms of u-POFA based alkali activated mortar before and after being exposed to elevated temperature of (A) 28 °C (B) 200 °C (C) 400 °C (D) 600 °C (E) 800 °C (F) 1000 °C

3.4 Field emission scanning electron microscopy analysis

The FESEM microscopy images of the alkali activated mortar mixtures which are prepared from POFA waste before and after exposure to elevated temperature are shown in Fig 6. The specimens demonstrated the effects of high temperatures up to 1000°C. The FESEM micrographs (exposure temperatures from 200°C to 1000°C) for the specimens of POFA. The selection of the mixture was based on physical appearance, relative residual compressive strength, and XRD analyses. The micrographs showed that when exposed to elevated temperatures from 200°C to 600°C (Fig 6), the cracks observed on the surface were wide and larger. Similarly, the number of pores also increased. However, when heated at 800°C, a number of microcracks appeared besides the uniformly dispersed pores with similar diameters (Duxson et al., 2006). The microstructure of POFA samples before and after heating is characterized by the presence of unreacted materials in POFA samples embedded in the reaction product of geopolymerization of the POFA. As shown in Fig 5, the results of XRD analysis of the reaction product indicate the formation of C-S-H gel with a low Ca content along with geopolymer-type gel (N-A-S-H), as observed previously by [18]. Heating from 600°C to 1000°C has formed some pores also decreased the compressive load significantly. Martin et al. (2015) [15] reported that it disappeared at 800°C, giving way to nepheline (NaAlSiO_4).

Thermal stability and mechanical properties of alkaline activated mortars synthesized from POFA after exposure to elevated temperatures

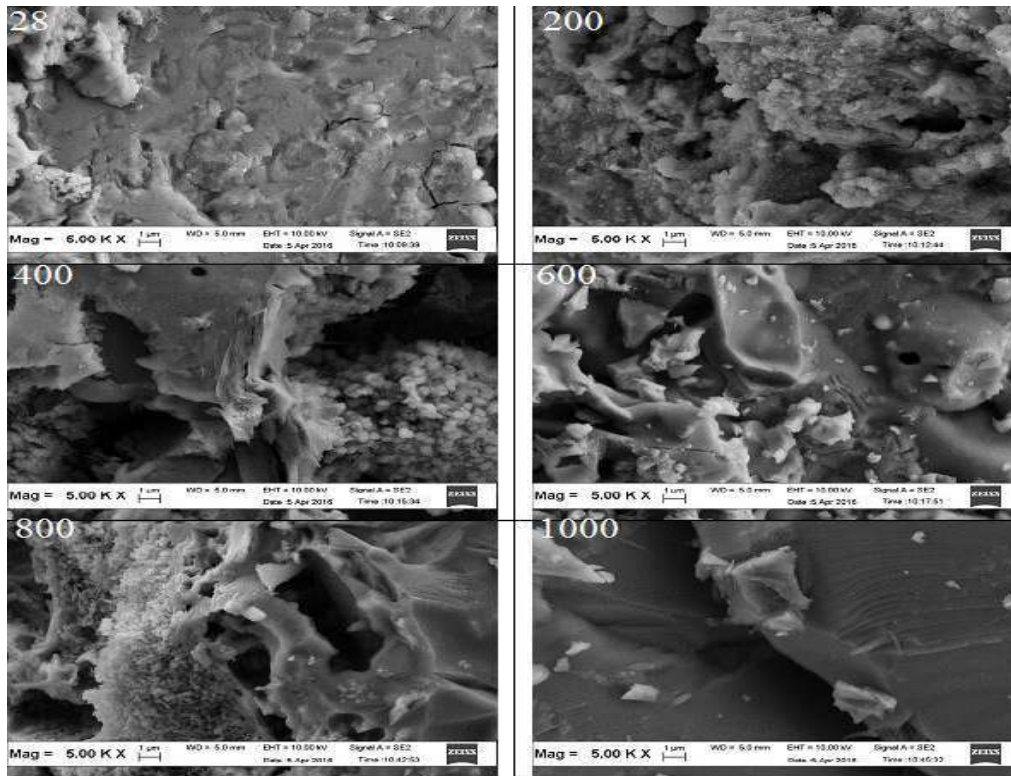


Figure 6: FESEM for mixture of u-POFA based alkali activated mortar before and after being exposed to elevated temperature of 200 C to 1000 C

Conclusion

In this research, the effect of Thermal stability and mechanical properties of alkaline-activated mortars, which that prepared from, Waste of palm oil full ashes. The change in the compressive strength was also investigated. Based on the results, the following conclusion can be drawn:

1. The main finding of the strength of all alkaline activated POFA-based mortar steadily decreased as temperature increased from 200°C to 1000°C.
2. After being exposed to 1000°C, the deformation in the form of sharp swelling was indicated. As shown in sample F given in Figure 2 , there is a change in the specimen's size and shape, which made it impossible to measure the compressive strength of the exposed alkaline activated mortars.
3. The relative residual compressive load for the mixtures decreased from 77% to 40% after exposure to temperatures from 200°C to 800°

References

- [1] J. Davidovits, Geopolymers and geopolymeric materials, J. Therm. Anal. 35 (2) (1989) 429–441.
- [2] F.U.A. Shaikh, Review of mechanical properties of short fibre reinforced geopolymer composites, Constr. Build. Mater. 43 (2013) 37–49.
- [3] P. Duxson, A. Fernandez-Jimenez, J.L. Provis, G.C. Lukey, A. Palomo, J.S.J. van Deventer, Geopolymer technology: the current state of the art, J. Mater. Sci. 42 (9) (2007) 2917–2933.
- [4] S.A. Bernal, E.D. Rodriguez, R.M. de Gutierrez, M. Gordillo, J.L. Provis, Mechanical and thermal characterisation of geopolymers based on silicat eactivated metakaolin/slag blends, J. Mater. Sci. 46 (16) (2011) 5477–5486.
- [5] S. Alam, S. Gul, Correction: assessment of pozzolanic activity of thermally activated clay and its impact on strength development in cement mortar, RSC Adv. 5 (14) (2015) 10680.

- [6] Topala Ö, Karakoç MB, Özcan A. Effects of elevated temperatures on the properties of ground granulated blast furnace slag (GGBFS) based geopolymer concretes containing recycled concrete aggregate. *Eur J Environ Civ Eng.* 2022;26(10):4847-62.
- [7] Hasnaoui A, Ghorbel E, Wardeh G. Optimization approach of granulated blast furnace slag and metakaolin based geopolymer mortars. *Constr Build Mater.* 2019;198:10-26.
- [8] H. Chong, P. Chia, M. Ahmad, The adsorption of heavy metal by Bornean oil palm shell and its potential application as constructed wetland media, *Bioresour. Technol.* 130 (2013) 181–186.
- [9] C. Di Blasi, Combustion and gasification rates of lignocellulosic chars, *Prog. Energy Combust. Sci.* 35 (2) (2009) 121–140.
- [10] J. Kanadasan, H.A. Razak, Mix design for self-compacting palm oil clinker concrete based on particle packing, *Mater. Des.* 56 (2014) 9–19.
- [11] S. Ferreiro, M. Frías, R.V. de la Villa, M.S. de Rojas, The influence of thermal activation of art paper sludge on the technical properties of blended Portland cements, *Cement Concr. Compos.* 37 (2013) 136–142.
- [12] M. Karim, M. Zain, M. Jamil, F. Lai, M. Islam, Strength of mortar and Concrete as influenced by Rice husk ash: a review, *World Appl. Sci. J.* 19 (10) (2012) 1501–1513.
- [13] S. Lee, M.-D. Seo, Y.-J. Kim, H.-H. Park, T.-N. Kim, Y. Hwang, S.-B. Cho, Unburned carbon removal effect on compressive strength development in a honeycomb briquette ash-based geopolymer, *Int. J. Miner. Process.* 97 (1) (2010) 20–25.
- [14] Bernal, S. A., Rodríguez ‘E. D., de Gutiérrez, R. M., Gordillo, M. & Provis, J. L. (2011b). Mechanical and thermal characterisation of geopolymers based on silicate-activated metakaolin/slag blends. *Journal of materials science*, 46(16), 5477-5486 .
- [15] Ranjbar, N., Mehrali, M., Alengaram, U. J., Metselaar, H. S. C. & Jumaat, M. Z. (2014a). Compressive strength and microstructural analysis of fly ash/palm oil fuel ash based geopolymer mortar under elevated temperatures. *Construction and Building Materials*, 65, 114-121
- [16] ASTM, C. (1999a). 109 Standard Test Method for Compressive Strength of Hydraulic Cement Mortars (using 2-in. or [50-mm] Cube Specimens). *Philadelphia, PA: American Society for Testing and Materials*, 318 .
- [17] Murri, A. N., Rickard, W., Bignozzi ‘M. & Van Riessen, A. (2013). High temperature behaviour of ambient cured alkali-activated materials based on ladle slag. *Cement and Concrete Research*, 43, 51-61 .
- [18] Islam, A., Alengaram, U. J., Jumaat, M. Z. & Bashar, I. I. (2014a). The development of compressive strength of ground granulated blast furnace slag-palm oil fuel ash-fly ash based geopolymer mortar. *Materials & Design*, 56, 833-841.

Applications of EOR Azzaytuna Analysis as a New Tool for Screening of Enhanced Oil Recovery Methods

Mohamed Baqar^{a*}, Hamza Meelad^b, Hana Sheikh^c, Ayman Allsaed^d, Mohammed Mohammed^e, Bader Awedat^f

^{a,b,c,d,e}Department of Petroleum Engineering, College of Engineering/Azzaytuna University, Libya

^fCollege of Information Technology/Azzaytuna University, Libya

Abstract: The production of oil through reservoirs generally run through series of production stages. It can be classified as primary, secondary and tertiary (enhanced oil) recovery techniques. In the EOR stage, several processes and technologies are used to increase or uphold recovery from existing fields. These processes often involve the injection of fluid(s) and most recently microbes into a reservoir. Therefore, maintaining and increasing oil production from existing fields require proper selection, design, and implementation of EOR methods. One of the most used method for quick screening of the different EOR techniques is considering the successful previous experiences from the methods that have been applied in other fields. In this paper, an EOR screening tool has been designed using visual basic studio based on the recently reported EOR projects over the world. The developed tool, which is named " EOR Azzaytuna Analysis", is applied for one of the partially depleted reservoir that is located in Al-Zenad Farrud oil reservoir in Libya. The obtained results from "EOR Azzaytuna Analysis" have been compared to the obtained ones from the most common EOR screening tool known as EORgui. Both results were in-agreement and concluded that immiscible and CO₂ injection method, are the most viable options for the selected field understudy.

Keywords: (Enhanced Oil Recovery, Oil Reservoir, Screening Criteria, Screening Tool)

Introduction

The production of oil and gas from hydrocarbon fields are generally divided into three stages. In the initial stage, the production occurs naturally, whereas, the next stage when the reservoir pressure is not enough for supporting the production from the formations, other techniques such as water flooding and gas injection are applied. Generally, water flooding is the main driving mechanism for maintaining reservoir pressure because of availability and low cost of injection fluid. However, oil recovery using this flooding process is not high enough [1]. In the tertiary recovery stage, commonly known as enhanced oil recovery (EOR), it is possible to recover almost 30-60% of the field's original oil in place (OOIP) which is high compared to primary and secondary recovery methods where recovery factor is equal to 20-40% [2]. Despite that the main goal of EOR is to mobilize the remaining oil after primary recovery, no single process can be considered an optimal oil recovery from every reservoir. In addition, every well has to be treated differently according to the nature of that well. Therefore, screening must be carried on to determine which EOR method is the best and most efficient to be used on the selected well. Data of the well such as petro-physical, chemical, geological, environmental and fluid properties (density and viscosity which are dependent on temperature) must be taken into consideration and this will be the criteria of the screening process. Selecting the suitable EOR method by screening the reservoir and fluid properties can ultimately reduce the risk by eliminating inefficiencies.

Problem of Statement

Al-Zenad Farrud oil reservoir is located in the western Sirte Basin of Libya. Solution gas drive was considered to be the predominant mechanism for the primary depletion. Recent data indicate the partially depletion of the reservoir which suggests the use of any suitable EOR methods.

Study objectives

In continuation of our study regarding the development of a new tool for screening criteria. The tool, which is known as "EOR Azzaytuna Analysis", was designed using visual basic studio and the database is based on the successful previously reported EOR projects. The tool will be used for Al-Zenad Farrud as a screening criteria of EOR techniques according to the data provided. The applicability of using this tool will be tested and the obtained results will be compared with the results obtained from the commercially well known tool named EORgui. The output data for both tools will be highlighted.

Methods

The methodology used in this paper include

- 1- The EOR Azzaytuna Analysis tool has been programmed according to the reported method in Azzaytuna University circles [3].
- 2- The data required for the Al-Zenad Farrud oil reservoir have been collected.
- 3- Input data has been proceeded as requested from the EOR Azzaytuna Analysis tool.
- 4- Screening criteria for Al-Zenad Farrud oil reservoir has been processed using the developed tool.
- 5- The same data of Al-Zenad Farrud oil reservoir have been acquired using the "EORgui" for comparison purposes.
- 6- The results of both tools have to carefully be further analyzed.

Data of Studied Reservoir

The data of Al-Zenad Farrud oil Reservoir is gathered and tabulated as shown in Table 1.

Table 1: Input data for the screening

Reservoir and fluid properties	Value
API gravity	38.57
Oil viscosity (cP)	0.61
Temperature	180 °F
Permeability (md)	72.93
Formation	Carbonate
Oil saturation (%)	0.724
Oil composition	C1-C7%
Reservoir thickness (ft)	>20
Reservoir depth (ft)	6170

Development of EOR Azzaytuna Analysis tool

Previously, the selection of the most applicable technique for EOR method was achieved manually using SPE format. This format is based on field experience and project execution worldwide. Therefore, this format was the beginning of all tools regarding the EOR screening. The format consists of five plots which are the viscosity plot, the permeability plot, the depth plot, the plot of reservoir pressure vs. oil viscosity and the plot of reservoir depth vs. viscosity, and the oil gravity range for EOR methods. Recently, several techniques have been designed for EOR screening [4,5]. In common of these tools, a user can screen oil fields directly and quantify incremental production for potentially applicable EOR techniques.

EOR Azzaytuna Analysis is a tool, which was developed using C++. The routine of the tool taking into consideration the already published screening criteria by Taber et al. in 1997 [6,7]. It is based on the EOR screening criteria, which were updated by A. Aladasani and B. Bai [8]. In this tool, the user can quickly screen an oil field in order to determine which EOR method(s) is/are more suitable to be applied. Eight methods of EOR are available using nine reservoir and oil properties, such as API gravity, viscosity, hydrocarbon composition, thickness, permeability, and oil saturation, type of the reservoir formation, thickness, depth and temperature, resulting in the most suitable EOR method for each oil field [9]. EOR Azzaytuna Analysis is designed and developed in order to make the selection of EOR methods easier and faster. A simple flow chart of the tool is described in Fig 1.

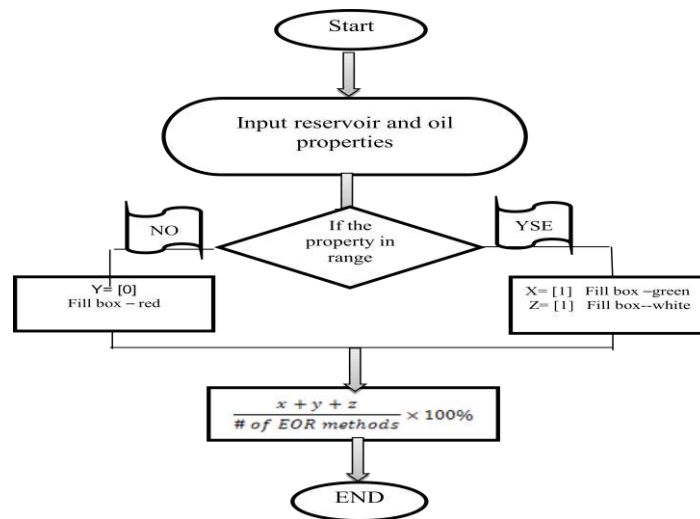


Fig. 1: Flow chart of EOR Azzaytuna Analysis

The database has been designed according to the successful previous experiences from the methods that have been applied in other fields. Gravity, as an example of the entry code for the eight EOR methods are shown in Fig. 2. The overall matching percentage for the selected EOR method is then calculated according to the following equation :-

$$P(x) = \frac{x + y + z}{\# \text{ of EOR methods}} * 100\%$$

Where P(x) = overall matching percentage for the selected EOR method

x = the amount of matching properties

y = the amount of mismatching properties

z = the amount of neglected properties (not critical entry)

```

End Sub
Private Sub Button1_Click(sender As Object, e As EventArgs) Handles Button1.Click
    Try
        Clear_All()
        DGVI.Rows(1).Cells(0).Style.BackColor = Color.Green
        If Val(txt_Gravity.Text) >= 29 And Val(txt_Gravity.Text) <= 54 Then
            DGVI.Rows(0).Cells(2).Style.BackColor = Color.Green
            A_Nitrogen += 1
        Else
            DGVI.Rows(0).Cells(2).Style.BackColor = Color.Red
        End If
        If Val(txt_Gravity.Text) >= 23 And Val(txt_Gravity.Text) <= 57 Then
            DGVI.Rows(0).Cells(3).Style.BackColor = Color.Green
            A_HydroCarbon += 1
        Else
            DGVI.Rows(0).Cells(3).Style.BackColor = Color.Red
        End If
        If Val(txt_Gravity.Text) >= 22 And Val(txt_Gravity.Text) <= 45 Then
            DGVI.Rows(0).Cells(4).Style.BackColor = Color.Green
            A_CarbonDioxide += 1
        Else
            DGVI.Rows(0).Cells(4).Style.BackColor = Color.Red
        End If
        If Val(txt_Gravity.Text) >= 12 Then
            DGVI.Rows(0).Cells(5).Style.BackColor = Color.Green
            A_Immiscible_Gases += 1
        Else
            DGVI.Rows(0).Cells(5).Style.BackColor = Color.Red
        End If
        If Val(txt_Gravity.Text) >= 20 And Val(txt_Gravity.Text) <= 44 Then
            DGVI.Rows(0).Cells(6).Style.BackColor = Color.Green
        End If
    Catch ex As Exception
    End Try
End Sub
    
```

Fig. 2: Coding of the Gravity

The database entry into the tool are shown in Fig. 3.

Fig. 3: Database of EOR Azzaytuuna Analysis

Application of EOR Azzaytuna Analysis

It should be noticed that the database in the EOR Azzaytuna Analysis contains input as screening criteria by (Al-adasani and Bai, 2010). After entering the acquired information data, the tool was performed and the results were extracted as shown in Fig. 4.

Fig. 4: Quick and database screening using EOR Azzaytuna Analysis

It can be seen that the ratio of matching each EOR methods were represented as a percentage of entered data of Al-Zenad Farrud oil Reservoir to the database of the reported ones. It is clear that the highest percentage was for Immiscible and Carbon Dioxide methods with (100%). The Nitrogen and Hydrocarbon and Polymer methods are (89%). The Combustion and Polymer-ASP methods with (67%), whereas the Steam method shows the least ratio percentage of (44%).

For clarity purposes, the tool is performed in a color coded mode. A dark green color in the codes represents the match conditions. However, the white color, means value is neglected (not critical). The red color means it does not meet the conditions of the table. The results for the two methods (Immiscible and Carbon Dioxide) show four codes in dark green. Since there are no red codes for the two methods, they considered the best applicable EOR methods. The second choice is the methods Polymer and Hydrocarbon, Nitrogen where each method has one red code. In methods of Combustion and Polymer-ASP, the software shows three red codes. Lastly, a Steam method is not recommended due to more codes in red.

EORgui screening Tool:

EORgui tool [10] has been used to select the optimum EOR method for Al-Zenad Farrud oil reservoir. Fig. 5 graphically represents the recommended methods. The screening shows immiscible gas to be the most suitable EOR method for " Al-Zenad Farrud oil reservoir" with a high percentage matching of 83%. The ability to applying Carbon dioxide Miscibility flooding for this field is about 78%. The SP/ASP and Combustion methods are ranked next with a matching of 73% and 67%, respectively. Nitrogen and hydrocarbon flooding are not strongly recommended for this case as they are ranked last.

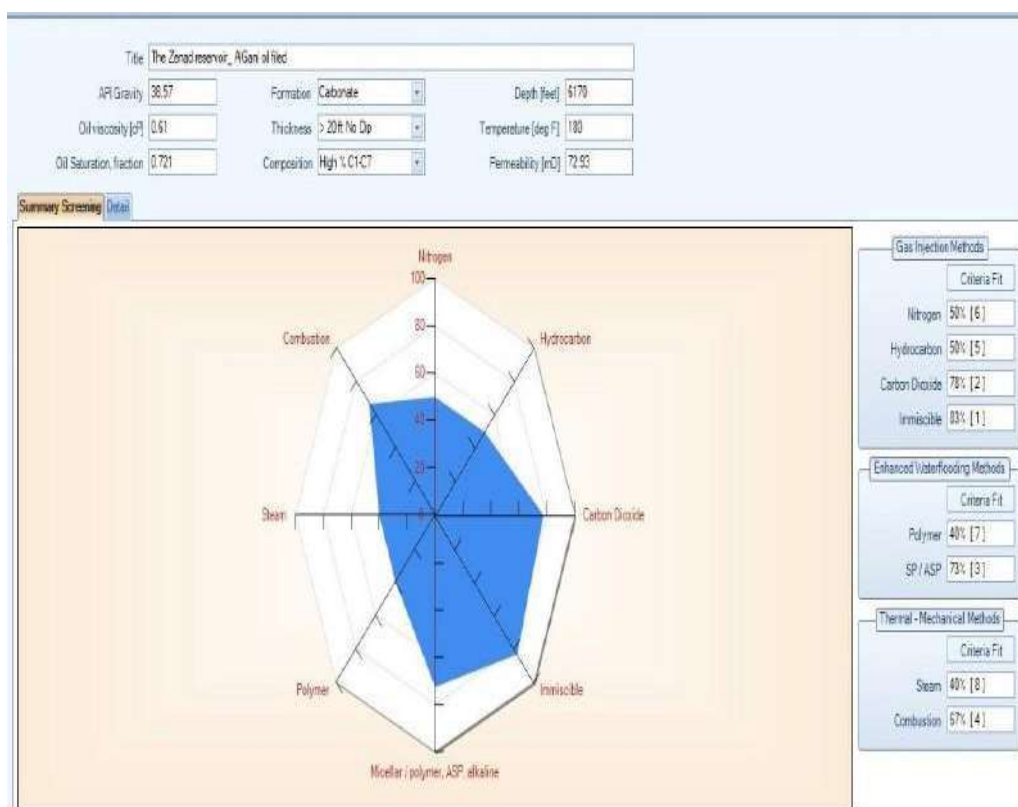


Fig. 5: Quick screening using EORgui

Fig. 6 shows the database and the obtained screening results of Al-Zenad Farrud oil reservoir using EORgui.



Fig. 6: Database screening using EORgui

Comparative analysis for the case study

The obtained results, as the best applicable EOR methods, from both tools (EORgui and EOR Azzaytuna analysis) are shown in Table 2.

Table 2: The best applicable EOR methods

Screening tool	Suitable EOR methods
EORgui	-Immiscible method (83%).
	-Carbon dioxide_CO2 Miscibility flooding (78%).
EOR Azzaytuna Analysis	-Immiscible method (100%).
	-Carbon dioxide_CO2 Miscibility flooding (100%).

It is clear that the suitable EOR methods based on the screening results for Al-Zenad Farrud oil reservoirs are: the immiscible and the CO₂ injection. However, the use of enhanced oil recovery techniques will not be initiated unless they have an economic return. This result considering the application of CO₂ in enhanced oil recovery and because it is a preferred technology for reducing carbon dioxide emissions into the atmosphere.

Conclusions

The use of EOR Azzaytuna Analysis as a newly developed tool for EOR screening makes it faster than just using a time consuming manual screening method. The results through "Al-Zenad Farrud oil reservoir" showed that the developed tool has the capability to do selection of suitable EOR based on

the data provided. The recommended EOR methods are both immiscible and carbon dioxide flooding. The obtained results was in agreement with the results obtained using EORgui as a screening tool.

Recommendations

The following recommendations could be taken into account

1. The results of applying any EOR methods do not start to appear quickly, as years may pass before judging the success or failure of the technology used. Therefore, the risk factor is high, whether technically, environmentally or economically. This means that frequent update of these developments is an important step of this tool.
2. Another analysis methods, such as the calculation of recovery factor, economical analysis calculations, the most cost effective method, cost of facilities and equipment and the availability of the injected fluid have to be implemented as a package in this tool.

References

- 1- Pwaga, S., "Comparative Study of Different EOR Methods". Trondheim: Norwegian University of Science and Technology, 2010.
- 2- Hama, M. Q. "Updated screening criteria for steam flooding based on oil field Updated screening criteria for steam flooding based on oil field projects data", Masters theses, Faculty of the Graduate School of the Missouri University of Science & Technology, Spring (2014).
- 3- A. Alhadi, H. Mohamed, H. Saleh, M. Mohamed, "Development of a new software for screening of enhanced oil recovery methods", BSc thesis (2022)
- 4- Urayet ; A.A. "Advanced Topics in Petroleum Engineering". University of Tripoli. Tripoli, Libya (2004).
- 5- Mohamad Faizzudin B Mat Piah, "*Enhanced Oil Recovery Field Development: Process Flow of EOR Selection for Sandstone Formation*". B.Sc. Project, Dept. Pet. Eng., University Technology. PETRONAS. SEPTEMBER 2012.
- 6- Taber, J.J., Martin, F.D., Seright, R.S. (1997), EOR Screening Criteria Revisited – Part 1: Introduction to Screening Criteria and Enhanced Oil Recovery Field Projects., Society of Petroleum Engineers Reservoir Evaluation & Engineering SPERE, doi:10.2118/35385-PA, pp. 189-198.
- 7- Taber, J.J., Martin, F.D. Seright, R.S., (1997), EOR Screening Criteria Revisited – Part 2: Applications and Impact of Oil Prices", Society of Petroleum Engineers Reservoir Evaluation & Engineering SPERE, doi:10.2118/39234-PA, pp. 199-206.
- 8- Al-Adasani, A., Bai, B. (2010), Recent Developments and Updated Screening Criteria of Enhanced Oil Recovery Techniques., SPE-130726-MS. Presented at the International Oil and Gas Conference and Exhibition, Beijing, China, 8 – 10 June 2010.
- 9- T. Ahmed, Reservoir Engineering Handbook. (4th ed.) Houston: Gulf Professional Publishing, 2010.
- 10- EORgui 1.1 Software, Technical Manual, [online] available at: www.Petroleumsolutions.com, Co. UK, Petroleum Solutions Ltd, 2005–2010.

An overview: Environmental influence of wastewater

Allam Musbah Al Allam^a, Waleed Ahmoda^b Khaled Omar Mohamed Oraibi^a, Mohamed Alfitouri Masoud^a, Mohammed Ahmed Ahbil^a,

^aEngineering and Information Technology Research Centre, Bani Walid, Libya

^bCollege of Technical Sciences Bani Walid, Libya

Abstract

Nowadays, environmental law has become strict on health such as a decrease in pollution and the economy. Thus, the pollution is a result of the emptying of different organic and inorganic substances into the environment traditional methods such as chemical sedimentation, carbon adsorption, ion exchange, evaporations, and membrane processes are found to be influential in wastewater treatment. Currently, biological treatments have acquired popularity to remove toxic and other harmful materials. The aim of this search is to make an overview including the performance of each technique in the treatment of wastewater. Moreover, this research aims to study the possibility of using treated wastewater sewage water station for irrigation. Also, this paper concentrated on the currently developed and newly applicable different treatments operated for the disposal of heavy metals from industrial wastewater.

Keywords: Volumatic Properties, Superpave Mix Design, Stiffness, Soft Clay, Aging Method

1. INTRODUCTION

Actually, the world's chemical industries face massive Environmental regulatory demanding situations in handling their wastewater effluents [1]. Crini, G & Lichtfouse found that [2], during the last 30 years, environmental problems about the biological contaminations and chemicals of water have become the main worry for society, public authorities, and the industry. Even though it appears to be that, the present knowledge about the environmental effect and public health risks connected with wastewater irrigation over the world [3]. On the other hand, the systematic processing of wastewaters started in the late 1800s and early 1900s. Also, for the last two centuries, wastewater treatment has continuously been progressing to meet strict disposal standards [4]. Newly, wastewater is increasingly used and confirmed as a strategy for preservation. However, there is a directory of increased spread of parasitic infections among agriculture workers exposed to irrigate with raw wastewater Negativity Environmental impact might outcome from long-term wastewater implementation. Moreover, emphasis is placed on future research priorities and procedure that must be taken for reducing public health risks and environmental pollution. Based on the study of Siebe C & Cifuentes, urban sewage and wastewater disposal is the main concern in our society [5]. In many countries, land clearing is an increasing practice, since river pollution is prevented. Wastewater represent also an importance irrigation resource and nutrient supply in agricultural production. Furthermore, Abou-Seeda et,l [6] found that, the requirement to identify their contents prior utilizing them in irrigation process due to some have high concentrations of some elements beyond its natural limits in some cases they cause pollution. In terms of wastewater treatment, the increasing volumes of waste being created would not be an issue if waste was looked as a managed properly and resource [7]. In recent years, domestic solid waste is the most complex solid waste stream [8], as opposed to more homogeneous waste streams resulting from agricultural activities. Otherwise,

environmental laws have become strict toward the economy, health, and decreased pollution [9]. Therefore, the pollution is an outcome of the discharge of different organic and inorganic materials into the environment. Nonetheless, Ye, Xin, et al. found that, the ways of wastewater treatment were first developed in response to the different circumstances used by the evacuation of wastewater to the environment and concern for public health [10]. According to the study of Alshammari, M. S [11], reported that, the population of the world has been grown and it has never been more primary to maintain water supplies to our maximum range capacity and to make sure that the water at our removal is clean and free from pollutants. The disposal of such contaminants in wastewater is one of the major targets in waste management. However, El-Khateeb, Mohamed A., et al, reported that, the extent of methods applied for the treatment of different sorts of waste treatment technologies is expensive [12]. Meanwhile, wastewater treatment could be utilized to irrigate the trees, which applies to save soils from corrosion and sand dunes settlement [13]. In general, through the operation of wastewater treatment, main specific and quantitative changes happen in the allocation of the bacterial population. It is commonly supposed that treatment determines a marked decrease in the bacterial numbers, inclusive the overall numbers of resistant bacteria [14]. Based on the study of Wang, Y., Fenner, K., & Helbling, D. E [15], the wastewater has been specified as a key source of micropollutants and their disposal residues a key challenge for treatment operation.

2. USING WASTEWATER TREATMENT IN IRRIGATION

Water is one of the most important materials on the earth. Therefore, all plants and animals have to get water to survive [16]. Also, the water covers about 71% of the Earth's Surface, and only 2.5% of the Earth's Water is fresh water. On the other hand, the important of water for life cannot be denied [17]. Thus, one of the most public ways for that is the reuse of treated sewage and agricultural drains. Moreover, processing procedures to fulfil the desired quality of sewage effluent for irrigation contain primary treatment, secondary treatment, oxidation, denitrification, phosphate precipitation, filtration, lime precipitation, ammonia volatilization, disinfection, and soil-aquifer treatment [18]. Therefore, most of the researchers emphasize its different nature and content rely on their sources. On the other hand, poor quality water is applying for irrigation purposes in the dry and semi-dry areas [19]. Also, sewage water is a very high proportion of this poor-quality water and may be an importance source of water that might be utilized for irrigating agricultural crops. For instance, the content of salts is an importance index to be considered when utilizing this water for irrigation [20]. In addition, sewage irrigation has possible benefits of meeting the water requirements, the sewage irrigation can be messed up to harm the soil health [21]. According to Fejgin A & Shalhevet, the use of sewage effluents for irrigating agricultural land is a worldwide practice [22]. Rattan, R. K., et al, stated that the particularly common in developing countries, where water treatment cost is high. However, there is a gradual rejection availability of fresh water for irrigation in India [23]. Friedel, J. K., et al, stated that there is a powerful possibility of agriculture and economic benefits of wastewater irrigation [24]. Therefore, in the long-term pollutants can be slowly introduced and accumulated in the soils and cause a potential risk to soil quality and productivity. Masto, Reginald Ebhin, et al,[25] reported that the impacts of sewage water irrigation on soil physical and chemical parameters have been studied in more detail. Furthermore, the irrigation fields of some countries have been used for 100 years. Thus, their soils fundamentally contain heavy metals in the topmost layer [26]. Nowadays, because of the constraint in the availability of fresh water for irrigation,

wastewater particularly sewage water is being utilized for irrigation of cultivation fields [27]. Moreover, Gregory, [28]. A reported that the reuse of wastewater for agriculture irrigation purposes decreases the amount of water that requirements to be removed from water resources. Also, it might be the potential solution to decrease the freshwater demand for zero water to avoided the pollution load in the receiving sources.

3. HEAVY METALS

Heavy metals present in wastewater do not appear to affect soil so far, because of their low availability. Due to the accumulation of heavy metals in soils, increasing the quantities of mobile metal fractions instantly can be easy to transport [29]. On the other hand, ways of treating industrial wastewater containing heavy metals often include technologies for a decrease of toxicity for meeting technology-based treatment standards. Moreover, heavy metals have contaminated many sites in industrial countries and affect risks to ecosystems [30]. Following techniques have been applied by different researchers for the disposal of heavy metals. In the same way, physical separation techniques are firstly applicable to particulate forms of metals, discrete particles. Meanwhile, heavy metal pollution has become today the most serious environmental problems. Hence, the treatment of heavy metals is of special concern because of their insistence in environmental. Recently, different ways for heavy metal disposal from wastewater have been widely found. Consequently, the traditional chemical operates for removing heavy metals from wastewater include processes such as, flotation, chemical precipitation, ion exchange, and adsorption [31].

4. SEWAGE TREATMENT

The important of sewage water treatment plant to provide a certain degree of treatment for wastewater before it is used in agriculture or landscape irrigation or aquaculture [32]. Therefore, the main objective of wastewater treatment is generally to allow human effluents to be disposed of without endangering human health or causing unacceptable harm to the natural environment. Moreover, there are some sources of wastewater such as human waste, washing water, rainfall collected on roofs, and highway drainage [33]. Generally, sewage contains all the water used from a household that is utilized for washing and toilet wastes [34]. Hence, wastewater is especially water and contains little particle matter, probably only 0.03%. Thus, in big cities, the solid fraction of wastewater can overall more than 1000 tons of solid material per day. Nevertheless, water is considered the most important for every human being but nowadays, it is becoming polluted because of the increased level of pollution. The waste treatment plant is known as the best alternative that cleans the water in an effective way [35]. Likewise, the best portion of applying this wastewater is that has the capability to remove the harmful contaminants and smells from the water [36]. However, wastewater treatment is the operation of removing contaminants from wastewater and household sewage [37]. Also, it includes physical-chemical, and biological processes to remove chemical and biological contaminants. Naidoo, S., & Olaniran, A. O. [38] reported that the topical of wastewater treatment is to make a disposable effluent without causing harm to the surrounding environment and prevent pollution. Wastewater contains more than 99% of water and is a mixture of domestic and industrial waste. Sewage is produced by residential, institutional, commercial, and industrial enterprises. Sewage treatment is the process of removing contaminants from sewage, mainly from domestic sewage [39]. It includes physical, chemical, and biological processes to remove these

pollutants and produce environmentally treated wastewater. Figure 1 present simple flow diagram of sewage treatment.

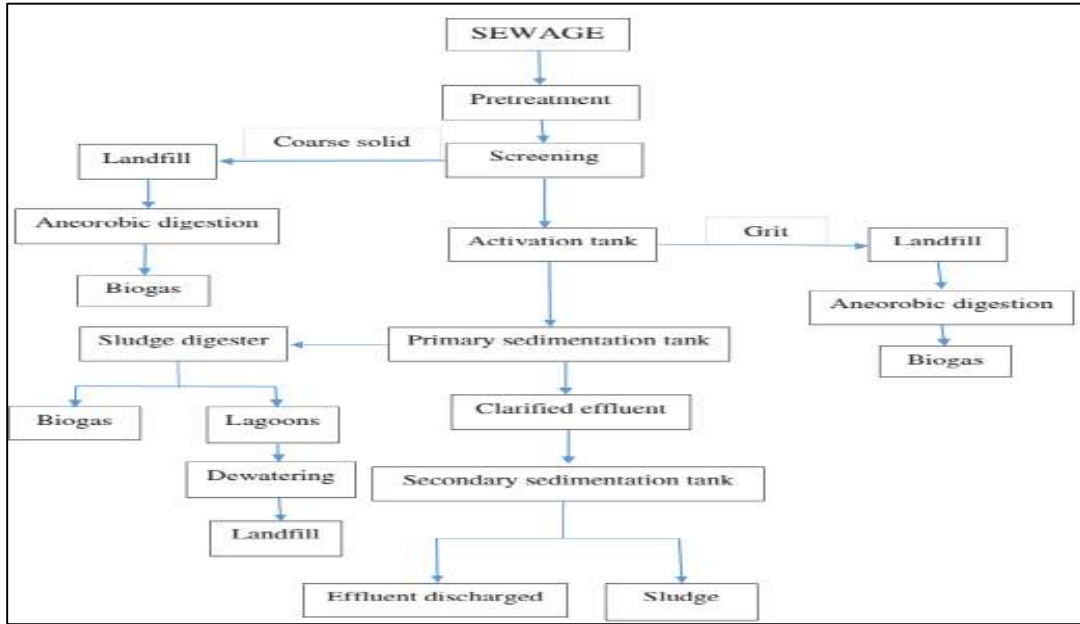


Fig 1: Simple flow diagram of sewage treatment

The primary treatment might include sand, which the velocity of the coming wastewater is modified to allow the adjustment of sand, grit, stones, and broken glass. Thus, these coarse solids are removed because they might harm the pumps and other equipment. The influent in sewage water passes during a bar screen to remove all large objects such as rags, cans, sticks, and plastic packets carried in the sewage stream. After that, bar screens of varying sizes might be utilized to improved solids disposal as shown in Figure 1. The main purpose of treatment is to dispose of contaminants from waste water [40]. It also contains chemical, and biological processes to remove the pollutants. Accordingly, the wastewater treatment is divided into three stages: pretreatment, primary, secondary and tertiary treatment. The term sewage treatment plant is often replaced nowadays by the term sewage treatment plant. Sewage treatment is mainly divided into three stages: preliminary treatment or pretreatment, primary treatment, and secondary treatment [41]. Sewage water treatment generally includes three stages, as described below:

5. PRIMARY SEWAGE TREATMENT

Pretreatment removes materials that can be easily collected from raw sewage before they damage or clog the pumps and sewage lines to pretreatment filters litters, tree limbs, leaves, and branches [42]. It includes the physical processes of sifting, cutting, degeneration, and sedimentation [43]. The settled and floating material is removed and the remaining liquid may be discharged or subjected to secondary treatment. Figure 2 shows the steps of primary sewage treatment.

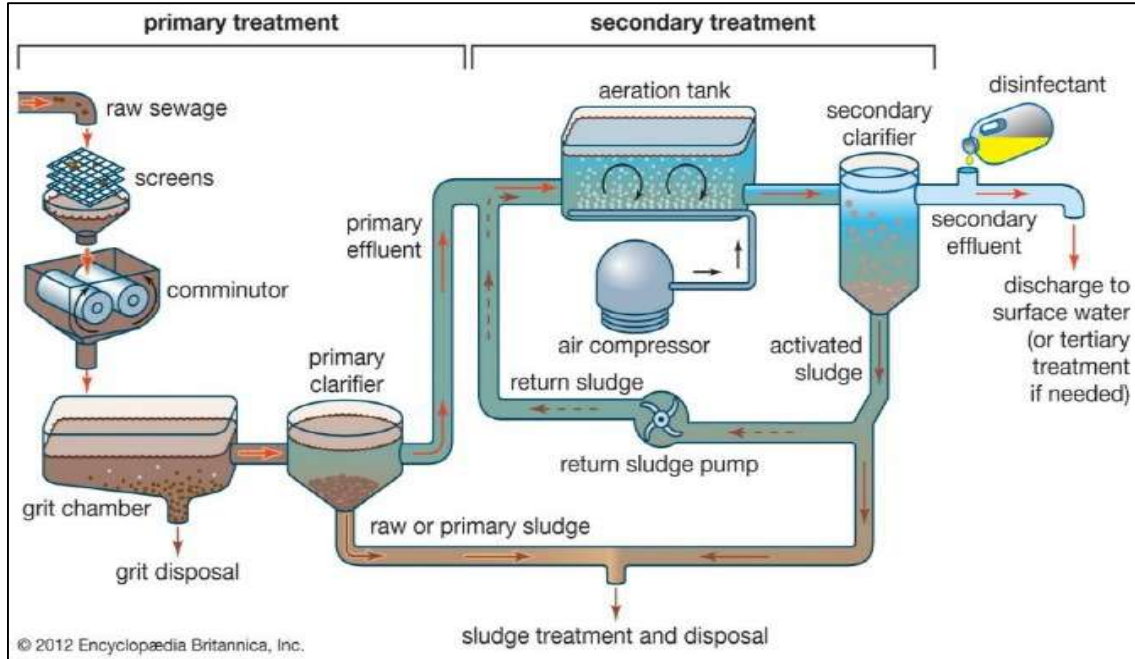


Fig 2: The steps of primary sewage treatment

5.1 Bar Screening

The influent sewage passes through a strip screen to remove all large objects such as, can, chafing, sticks, and plastic bags as shown in Table 1 [44]. This is most commonly used with a mechanically automated strip screen in modern plants serving large populations, while in smaller or less modern plants, a manual screen may be used [45].

Table 1: Types of the treatment process

No	Type of treatment	Type of treatment unit	Name of the unit	Type of impurities removed
1	Physical treatment	Physical	Screen	Large suspended and floating matter
		Physical	Grit chamber	Grit
		Physical	Clarifiers	Silt, sand and other heavier matter
2	Chemical treatment	Chemical	Chemical reactors	Dissolved chemicals
3	Biological treatment	Biological	Trickling filters Activated sludge plant Rotating Biological contactors Digesters	Dissolved organic chemical

5.2 Secondary Treatment

This method removes the soluble organic matter that escapes from primary treatment [46]. It also removes more suspended solids and suspended biological materials. Likewise, it may also require a separation process to remove the microorganisms from the treated water before it is discharge [47]. Secondary sewage treatment, which is mostly biological, is designed to remove most of this organic matter and reduce the biochemical oxygen demand as shown in Figure 3. In this process, the wastewater undergoes vigorous aeration to encourage the growth of aerobic bacteria and other microorganisms that oxidize the dissolved organic matter into carbon dioxide and water [48]. Two common secondary treatments are active sludge systems and drip filters as displayed in Figure 3.

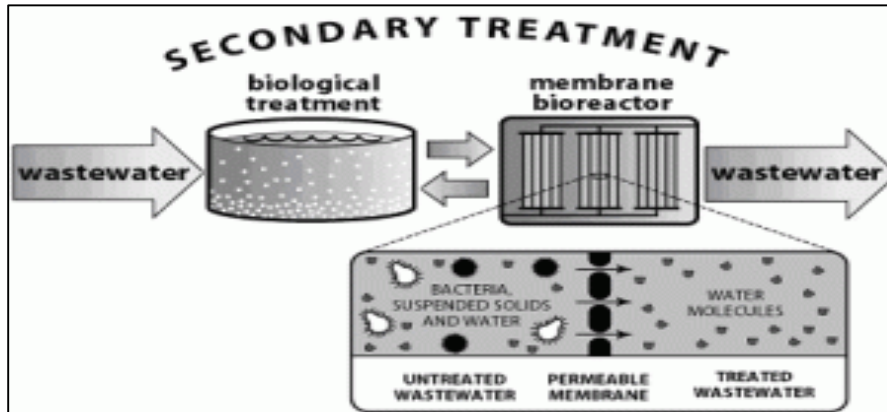


Fig 3: Secondary wastewater treatment

5.3 Tertiary Sewage Treatment

The objective of this operation is to provide a final treatment stage to raise the effluent quality prior it is discharged to the receiving environmental such as: sea, river, lake, ground. More than one tertiary treatment process may be used at any treatment plan as exhibited in Figure 4 [49].

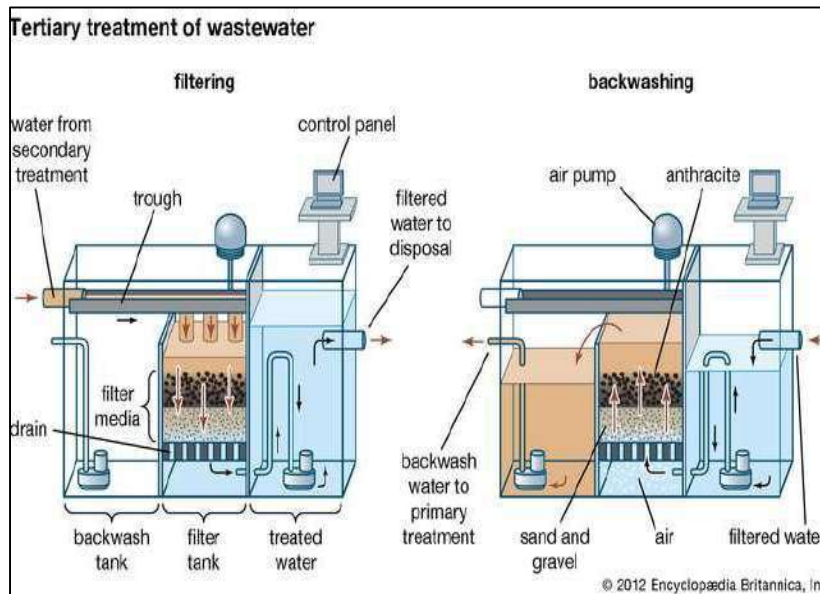


Fig 4: Tertiary Process of wastewater Treatment

6. Conclusion

Organic and inorganic substances released into the environmental as a result of household, agricultural and industrial aquatic activities lead to organic and inorganic pollution. Regular primary and secondary treatment of this wastewaters has been introduced in an increasing number of places, in order to get rid of easily sedimentary matter and oxidize the organic matter available in wastewater. Pollution is caused by different organic and inorganic substances into the environmental. Furthermore, pollution sources include household, agricultural and industrial waters. Traditional techniques such as chemical precipitation, carbon adsorption, ion exchange, evaporations and membrane operate have been found to be effective in treatment of waste and wastewater. From the literature, it is showed that the new ways of wastewater treatment are due to microalgae and they are prone to be efficient in decreasing toxic components. It is noted that the traditional techniques are not efficient in decreasing toxic, heavy metals, nitrogen, phosphorous.

References

- [1] M. O. Awaleh and Y. D. Soubaneh, "Waste water treatment in chemical industries: the concept and current technologies," *Hydrology: Current Research*, vol. 5, p. 1, 2014.
- [2] G. Crini and E. Lichtfouse, "Advantages and disadvantages of techniques used for wastewater treatment," *Environmental Chemistry Letters*, vol. 17, pp. 145-155, 2019
- [3] M. Elgallal, L. Fletcher, and B. Evans, "Assessment of potential risks associated with chemicals in wastewater used for irrigation in arid and semiarid zones: A review," *Agricultural Water Management*, vol. 177, pp. 419-431, 2016
- [4] H. Shon, S. Vigneswaran, and S. Snyder, "Effluent organic matter (EfOM) in wastewater: constituents, effects, and treatment," *Critical reviews in environmental science and technology*, vol. 36, pp. 327-374, 2006.
- [5] C. Siebe and E. Cifuentes, "Environmental impact of wastewater irrigation in central Mexico: an overview," *International Journal of Environmental Health Research*, vol. 5, pp. 161-173, 1995.
- [6] M. Abou-Seeda, H. El-Aila, and A. Shehata, "Waste water treatment for irrigation purposes. 2.-sequential extraction of heavy metals in irrigated soil after one year," *Mansoura University Journal of Agricultural Sciences (Egypt)*, 1997.
- [7] L. M. Fry, J. R. Mihelcic, and D. W. Watkins, "Water and nonwater-related challenges of achieving global sanitation coverage," *Environmental Science & Technology*, vol. 42, pp. 4298-4304, 2008.
- [8] T. Kaosol, "Sustainable solutions for municipal solid waste management in Thailand," *World Academy of Science, Engineering and Technology*, vol. 60, pp. 665-70, 2009.
- [9] P. Rajasulochana and V. Preethy, "Comparison on efficiency of various techniques in treatment of waste and sewage water-A comprehensive review," *Resource-Efficient Technologies*, vol. 2, pp. 175-184, 2016.
- [10] X. Ye, X. Guo, X. Cui, X. Zhang, H. Zhang, M. Wang, et al., "Occurrence and removal of endocrine-disrupting chemicals in wastewater treatment plants in the Three Gorges Reservoir area, Chongqing, China," *Journal of Environmental Monitoring*, vol. 14, pp. 2204-2211, 2012.
- [11] M. S. Alshammari, "Assessment of sewage water treatment using grinded bauxite rock as a robust and low-cost adsorption," *Journal of Chemistry*, vol. 2020, 2020.
- [12] M. A. El-Khateeb, W. M. Emam, W. A. Darweesh, and E. El-Sayed, "Integration of UASB and down flow hanging non-woven fabric (DHNW) reactors for the treatment of sewage water," *Desalin. Water Treat.*, vol. 164, pp. 48-55, 2019.
- [13] J. S. Chauhan and S. Kumar, "Wastewater ferti-irrigation: an eco-technology for sustainable agriculture," *Sustainable Water Resources Management*, vol. 6, pp. 1-11, 2020.
- [14] L. Guardabassi, D. M. L. F. Wong, and A. Dalsgaard, "The effects of tertiary wastewater treatment on the prevalence of antimicrobial resistant bacteria," *Water Research*, vol. 36, pp. 1955-1964, 2002.

- [15] Y. Wang, K. Fenner, and D. E. Helbling, "Clustering micropollutants based on initial biotransformations for improved prediction of micropollutant removal during conventional activated sludge treatment," *Environmental Science: Water Research & Technology*, vol. 6, pp. 554-565, 2020.
- [16] F. Marshall, J. Holdenn, C. Ghose, B. Chigala, V. Kapungwe, M. Agrawal, et al., "Contamination of Irrigation Water and Food Safety for Urban and Periurban Poor: Appropriate Measures for Monitoring and Control from Field Research in India and Zambia. Inception Report DFID Enkar R8160 SPRU, University of Sussex," ed, 2007.
- [17] I. M. Shalaby, A. D. Altalhy, and H. A. Mosallam, "Preliminary field study of a model plant for sewage water treatment using gravel bed hydroponics method," *World Appl Sci J*, vol. 4, pp. 238-43, 2008.
- [18] W. S. A. Alawsy, L. A. S. Alabadi, and H. M. Khaeim, "Effect of sewage water irrigation on growth performance, biomass and nutrient accumulation in maize and barley," *International Journal of agricultural and statistical sciences*, vol. 14, pp. 519-524, 2018.
- [19] K. Paliwal, K. Karunaichamy, and M. Ananthavalli, "Effect of sewage water irrigation on growth performance, biomass and nutrient accumulation in *Hardwickia binata* under nursery conditions," *Bioresource Technology*, vol. 66, pp. 105-111, 1998.
- [20] L. A. S. Alabadi, W. S. A. Alawsy, H. M. Khaeim, and A. H. AL-Hadithy, "Utilization of treated wastewater in irrigation and growth of *Jatropha* plant to protect the environment from pollution and combating desertification," *Plant Archives*, vol. 18, pp. 2429-2434, 2018.
- [21] R. E. Masto, P. K. Chhonkar, D. Singh, and A. K. Patra, "Changes in soil quality indicators under long-term sewage irrigation in a sub-tropical environment," *Environmental Geology*, vol. 56, pp. 1237-1243, 2009.
- [22] A. Feigin, I. Ravina, and J. Shalhevet, *Irrigation with treated sewage effluent: management for environmental protection* vol. 17: Springer Science & Business Media, 2012.
- [23] R. Rattan, S. Datta, P. Chhonkar, K. Suribabu, and A. Singh, "Long-term impact of irrigation with sewage effluents on heavy metal content in soils, crops and groundwater—a case study," *Agriculture, ecosystems & environment*, vol. 109, pp. 310-322, 2005.
- [24] J. Friedel, T. Langer, C. Siebe, and K. Stahr, "Effects of long-term waste water irrigation on soil organic matter, soil microbial biomass and its activities in central Mexico," *Biology and Fertility of Soils*, vol. 31, pp. 414-421, 2000.
- [25] Z. Jing, Y. Qisheng, W. Duo, S. Liming, and H. Pinjing, "On-site Experiment of Stable Leachate Treatment by Soil-vegetation Irrigation in Sub-tropical Southern China," *Environmental Sanitation Engineering*, p. 05, 2012.
- [26] B. Védry, M. Gousailles, M. Affholder, A. Lefaux, and J. Bontoux, "From sewage water treatment to wastewater reuse. One century of Paris sewage farms history," *Water Science and Technology*, vol. 43, pp. 101-107, 2001.
- [27] P. Singh, P. Deshbhratar, and D. Ramteke, "Effects of sewage wastewater irrigation on soil properties, crop yield and environment," *Agricultural water management*, vol. 103, pp. 100-104, 2012.
- [28] A. Gregory, "Strategic direction of water recycling in Sydney," in *Proceeding of the First Symposium Water Recycling*, 2000, pp. 35-41.
- [29] S. Gunatilake, "Methods of removing heavy metals from industrial wastewater," *Methods*, vol. 1, p. 14, 2015.
- [30] G. Dermont, M. Bergeron, G. Mercier, and M. Richer-Lafleche, "Metal-contaminated soils: remediation practices and treatment technologies," *Practice periodical of hazardous, toxic, and radioactive waste management*, vol. 12, pp. 188-209, 2008.
- [31] F. Fu and Q. Wang, "Removal of heavy metal ions from wastewaters: a review," *Journal of environmental management*, vol. 92, pp. 407-418, 2011.
- [32] A. N. Angelakis, T. Asano, A. Bahri, B. E. Jimenez, and G. Tchobanoglous, "Water reuse: from ancient to modern times and the future," *Frontiers in Environmental Science*, vol. 6, p. 26, 2018.
- [33] R. Burkhard, A. Deletic, and A. Craig, "Techniques for water and wastewater management: a review of techniques and their integration in planning," *Urban water*, vol. 2, pp. 197-221, 2000.
- [34] G. M. Masters, *Introduction to environmental science and engineering: Upper Saddle River, NJ: Prentice-Hall*, 1997.
- [35] D. Singh, A. Tiwari, and R. Gupta, "Phytoremediation of lead from wastewater using aquatic plants," *J Agric Technol*, vol. 8, pp. 1-11, 2012.

- [36] S. K. Kansal and A. Kumari, "Potential of *M. oleifera* for the treatment of water and wastewater," *Chemical reviews*, vol. 114, pp. 4993-5010, 2014.
- [37] R. L. Droste and R. L. Gehr, *Theory and practice of water and wastewater treatment*: John Wiley & Sons, 2018.
- [38] S. Naidoo and A. O. Olaniran, "Treated wastewater effluent as a source of microbial pollution of surface water resources," *International journal of environmental research and public health*, vol. 11, pp. 249-270, 2014.
- [39] I. Rawat, R. R. Kumar, T. Mutanda, and F. Bux, "Dual role of microalgae: phycoremediation of domestic wastewater and biomass production for sustainable biofuels production," *Applied energy*, vol. 88, pp. 3411-3424, 2011.
- [40] A. Demirbas, G. Edris, and W. M. Alalayah, "Sludge production from municipal wastewater treatment in sewage treatment plant," *Energy Sources, Part A: Recovery, Utilization, and Environmental Effects*, vol. 39, pp. 999-1006, 2017.
- [41] J. Fu, X.-J. Yang, R.-Q. Chen, Y. Luo, C.-C. Wu, H.-T. Jia, et al., "Distributed treatment of domestic wastewater using an integrated equipment. Part-I. Pilot study on the treatment of domestic wastewater by sequencing batch biofilm reactor," *Energy Education Science and Technology Part A-Energy Science and Research*, vol. 30, pp. 445-458, 2012.
- [42] A. Markin, A. Lepikhin, and S. Ulianov, "Sewage treatment," 2020.
- [43] S. Lasee, J. Mauricio, W. A. Thompson, A. Karnjanapiboonwong, J. Kasumba, S. Subbiah, et al., "Microplastics in a freshwater environment receiving treated wastewater effluent," *Integrated environmental assessment and management*, vol. 13, pp. 528-532, 2017.
- [44] W. H. Carter, *Flushed: how the plumber saved civilization*: Simon and Schuster, 2006.
- [45] J. Ajobo and A. Abioye, "A methodology for proper waste disposal, treatment, and management enhancing sustainable development in the third world," *Pac J Sci Technol*, vol. 15, pp. 318-326, 2014.
- [46] S.-N. Nam and G. Amy, "Differentiation of wastewater effluent organic matter (EfOM) from natural organic matter (NOM) using multiple analytical techniques," *Water Science and Technology*, vol. 57, pp. 1009-1015, 2008.
- [47] I. I. Baharuddin, "Wastewater Treatment Technologies (a review of advantages and drawbacks)," *Teknik Mesin TEKNOLOGI*, vol. 12, 2012.
- [48] E. W. Low and H. A. Chase, "Reducing production of excess biomass during wastewater treatment," *Water research*, vol. 33, pp. 1119-1132, 1999.
- [49] T. Asano, "Water from (waste) water—the dependable water resource (The 2001 Stockholm Water Prize Laureate Lecture)," *Water science and technology*, vol. 45, pp. 23-33, 2002.

Statistical Distribution State Estimation Algorithm to Determine Electric Network State Variables

Rashid El-feres¹

¹Gaser Ben Gashire High institute of Science and Technology

Abstract This work proposes a three phase statistical distribution network state estimation algorithm formulated on weighted least mean squares method (WLMS) to calculate the network voltage magnitude at each node on the network. The state estimation method used in this work is based on the methods used on transmission network. To overcome the lack of real time measurements which normally exist on 11kV distribution network, this work uses historical data acquired from billing system authority to make the state estimator observable.

Key words: DSE distribution state estimation algorithm, Distribution Network Topology.

1. Introduction,

The primary purpose of an electric distribution system is to meet the customer's demands for energy after receiving the bulk electrical energy from transmission or sub- transmission substation. There are basically two major types of distribution substations: primary substation and customer substation. The primary substation serves as a load center and the customer substation interfaces to the low voltage (LV) network. Customer substation is referred to a distribution room normally provided by the customer. The distribution room can accommodate a number of HV switchgear panel and the transformer to enable LV connection to the customer incoming switchboard. Depending on the geographical location, the distribution network can be in the form of overhead lines or underground cables. Cables are commonly used in urban areas and overhead lines are adopted for rural areas. Distribution networks start from distribution substations to the service entrance of the electricity consumers, including distribution substations, primary feeders, distribution transformers, and secondary systems [1-2]. The existing distribution networks can only serve the requirements and standards of past decades and are not able to meet renewed duties and upcoming challenges. Distribution systems and loads will be subject to dramatic changes over the next 20 to 50 years. To name a few of the changes, we can mention customers' expected services, the reliability level of the system, the characteristic of the new loads, marginal costs, and existing numerous DG generators also future distribution system heading toward central controlling and these need load and distributed generation information.

In the modern energy management System (EMS) State estimation (SE) program processes a set of raw measurement data and provides a real-time load flow solution which is the basis of the advanced functions for system security monitoring and control.

Real time control of the distribution system requires an estimate of the system state. In the past most distribution system was not monitored, therefore, there was no need for SE. To achieve real time monitoring on some existing distribution system are considered to be costly and more capital were needed. In order to reduce these customers cost on real-time

monitoring historical consumption data from billing system were used instead. These data are then fed to load flow calculation technique. Under this condition, distribution system load flow program is often used for planning , such as in computing system losses of distribution feeder configuration for system losses reduction, various technique have been proposed to obtain distribution system load flow solution [3-6] . State estimation (SE) program processes a set of raw measurement data and provide real-time load flow solution .The SE was formulated as a equality constrained weighted least squared problem. A distribution system SE that uses a minimum number of remote measurement was presented in [7]. In literature, the expertise and trends related to some of the main aspects of DSE algorithms are analyzed. For example, the authors of [8] review the requirements of state estimation and the differences between state estimation in transmission and distribution systems. Furthermore, in [9], the authors focus on model-based and forecast aided DSSE algorithms, while in [10]. SE is based on the mathematical relations between the system state variable (e.g. bus voltage magnitudes and angles),and the measurement. Various technique have been used to obtain an SE solution, number of studies [11-12] provide surveys on SE algorithms.

. An iterative procedure based on load flow was used to obtain the distribution system SE. These paper introduce distribution state estimation (DSE) to calculate distribution system state..

2. Development of State Estimator Algorithm

The main part of the state estimation technique is the algorithm used to solve weighted least square which derived in the following equation [13]

$$\hat{f} = \frac{\sum_{j=1}^{N_m} w_j \hat{e}_j}{\sum_{j=1}^{N_m} \frac{1}{\sigma_j^2}} = \frac{\sum_{j=1}^{N_m} \frac{\hat{e}_j}{\sigma_j^2}}{\sum_{j=1}^{N_m} \frac{1}{\sigma_j^2}} = \frac{\sum_{j=1}^{N_m} \frac{(z_j - f_j(x))^2}{\sigma_j^2}}{\sum_{j=1}^{N_m} \frac{1}{\sigma_j^2}} \quad (1)$$

Where z is the $(m \times 1)$ measurement vector, $f_j(x)$ is the $(m \times 1)$ vector of nonlinear functions, x is the $(2n \times 1)$ true state vector, N_m is the number of measurement, n is the number of buses and $(1/\sigma_j^2)$ represents measurement reciprocal variance.

This equation is to find the best network state variable. The function used in state estimator is nonlinear. Therefore, an iterative method is introduced; the Newton iterative method is used to find state variable value to minimize the least square error. In this research an state estimator algorithm was developed in C language.

Once the network topology and all the different measurement are introduced, the state estimator algorithm will automatically start finding solution. Fig.1 shows flow chart of that algorithm. At the start, from the topology the algorithm will find the network admittance to be used to calculate power flow equations [13] shown below.

$$\vec{S}_{ij} = (V_i^2 G_{ij} - V_i V_j G_{ij} \cos(\theta_i - \theta_j) - j V_i V_j G_{ij} \sin(\theta_i - \theta_j)) - j V_i^2 B_{ij} + j V_i V_j \cos(\theta_i - \theta_j) - V_i V_j \sin(\theta_i - \theta_j) \quad (2)$$

The equations of represent active and reactive power are that used in the algorithm to form the Jacobean matrix. Also, the Jacobean can include the voltage measurements derivative. The algorithm also builds the [R] matrix which represents the measurement weighting matrix. After all parts of equation 1 were formed, with the initial value the algorithm will start finding solution.

In order to start the iterative process and initial value for each of the state variables is required. 1 p.u voltages is selected and 0.000001 rad for the angle. Using the initial value of [x], [H] and [a] are calculated. Then the value of [Δx] is obtained using equation 3.

Adding this value to [x], the state variables are updated:

$$[x] = [x] + [\Delta x] \quad (3)$$

The next iteration is started beginning with [x] the new initial value of the state variables. If Δx is small enough, the algorithm will stop, and if not it will go for another loop until it converge. Sometime this kind of algorithm will never give solution or it can't converge due to that the gain matrix is singular which it's determinant is zero.

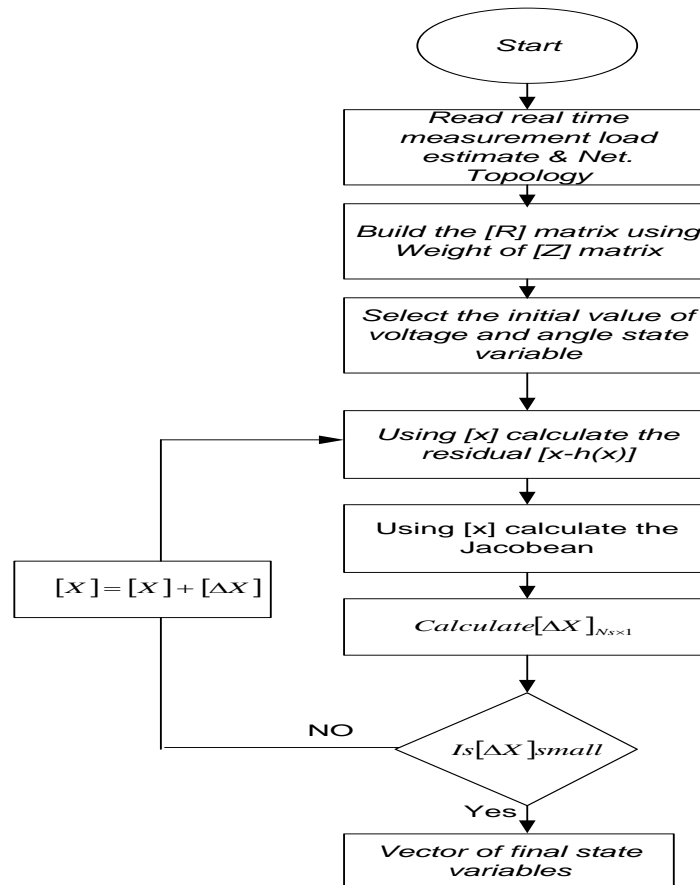


Fig. 1: Flow chart of state estimator algorithm

1.1 State Estimator Requirements

The state estimator required a number of information in order to estimate the system variables or give an output. Figure 3 shows all the possible input information in blocks and the possible output of the state estimator. For more details the state estimator has been divided into an input and output block as follows;

1.1.1 State Estimator Input

The state estimator needs input information in order to give output results. The input information as shown in fig. 2 includes measurements, weighting of these measurement and topology of the network used. The measurements divided into real time measurements, pseudo measurements and virtual measurements.

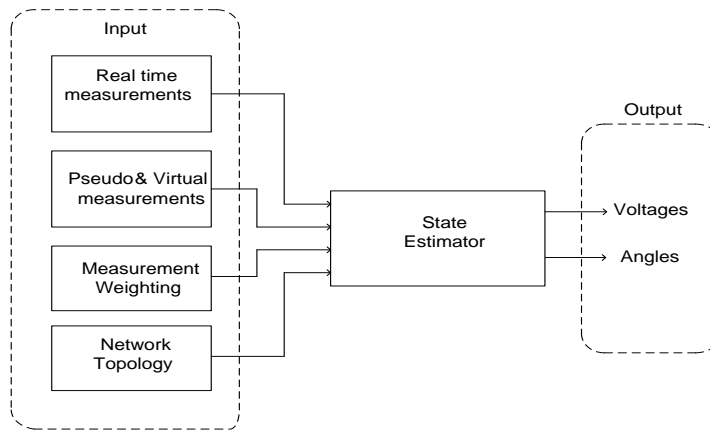


Fig. 2: State estimator blocks

I) Real Time Measurement

The real time measurements are very essential to the state estimator in order to predict system solution similar that of load flow solution. The real time measurements can be voltage magnitude, power flow or current measurement. These measurements are very important to state estimator algorithm. Usually, these measurements are expected to be accurate or having less error. In distribution network because of expenditure control to make the system competitive using for example voltage meter with high accuracy [15] its price increases dramatically. It is found that maximum accuracy of voltage measurement at reasonable price is around $\pm 0.5\%$. The accuracy of an 11 kV voltage measurement should be between ± 1 and $\pm 2\%$. In these research to study the influence of distributed generator measuring the active and reactive power were highly needed to achieve good state estimator results so they given high accuracy same as that of real time. Acquiring the DG power is a little bit more difficult to obtain due to location of DGs in distribution system, so remote terminal unit connected through communication is needed. The general practice assumed the accuracy of the DGs power meters should be around $\pm 3\%$.

II) Pseudo Measurements

The pseudo measurements are historic data used to replace the shortage of real time measurements which are required by state estimator. The pseudo measurement can be extracted, for example, through monthly billing data, monthly peak loading, the transformer's peak load analysis and existing diversified load curves. Because this data has big probability of lack of accuracy so it is given low degree of accuracy than the real time measurements.

III) Virtual Measurements

Some of network buses have no load connected to them, therefore the value of active and reactive power (P,Q) consumption in those buses is zero. These virtual measurements act like perfect measurement and very valuable for the distribution state estimator. It assumed extremely perfect. As the weighting in the state estimator used the reciprocal variance and if the error is introduced zero that will give numerical problem to the state estimator, it will collapse. So, it assumed the variance is very small but not zero.

IV) Weighting of Measurements

In this research state estimator all the measurements, pseudo measurements and virtual measurements are assumed to follow normal distribution. Due to the limited availability of real-time data, load demand estimates are used as pseudo measurements. This in conjunction with the weighted-least squares formulation implies that load demands are normally distributed. The normal or Gaussian distribution function is determined by the mean of the data and the standard deviation of the data. If the data has small standard deviation it is more accurate. Fig.3 shows the function of normal distribution function where 99.73% of the curve area was shadowed. The 99.73% is representing that the data has high level of confidence which means that the deviation between the boundary of the interval and the mean value is three times the standard deviation. From the normal distribution function and the standard deviation measurement accuracy can be found using equation 2 as follow:

If the accuracy of a measurement is for example $\pm 4\%$, it can be assumed that the 99.73% of the time the measurement will be inside those given accuracy limits. This assumption allows writing the standard deviation of the distribution using the following equation:

$$3 \cdot \sigma = mean \cdot \frac{accuracy}{100}$$

Exponential

$$\sigma = mean \frac{accuracy}{300} \quad (4)$$

Where σ is the standard deviation and the mean of the measurement or the estimated load of the pseudo-measurement.

For the given example of a measurement of $\pm 4\%$ accuracy and if the measured magnitude is 0.95 p.u. the standard deviation will be:

$$\sigma = 0.95 \cdot \frac{4}{300} = 0.01266 p.u$$

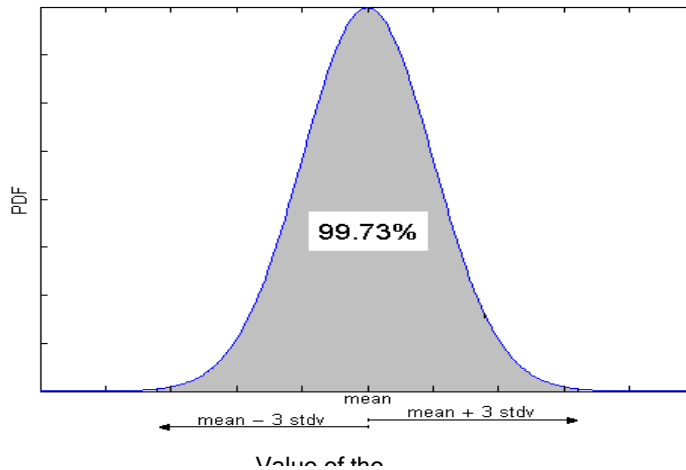


Fig.3: Function of normal distribution [13]

IIV) Network Topology

It is important to define the network for the state estimator in order to calculate line flow and the power consumption at each busbar. The network topology can be represented in the state estimator by line impedance, number of buses and number of branches and the sending end and the receiving end of the branches. Also, the load connected to each busbar.

1.1.2 State Estimation Jacobean

In power system each node has its related differential equation need to be determined to build the system Jacobean [13-16]. The Jacobean is the important part in solving load flow and state estimation problem. It is the matrix forming all differential equation of measurement functions such as active and reactive power measurements of all nodes in relation of state variables which normally means both bus voltage and angles. In order to estimate both voltage and angle magnitudes, the angle at one of the N buses of the system should be taken as a reference for all other angles, which leaves $N - 1$ angles and N magnitudes to be calculated by the following equation.

$$x^{(k+1)} - x^{(k)} = (H_x^T R^{-1} H_x)^{-1} H_x^T R^{-1} \begin{bmatrix} z_1 - h_1(x_1^{(k)}, x_2^{(k)}, \dots, x_{N_s}^{(k)}) \\ z_2 - h_2(x_1^{(k)}, x_2^{(k)}, \dots, x_{N_s}^{(k)}) \\ \vdots \\ z_m - h_{N_m}(x_1^{(k)}, x_2^{(k)}, \dots, x_{N_s}^{(k)}) \end{bmatrix}$$

It is unlike the square Jacobean of Newton Raphson in load flow, it is always has $(2N - 1)$ columns and a larger number N_m of rows. Each row of H_x corresponds uniquely to one of the measured quantities indicated in the network. The general form of H_x matrix is:

$$\begin{bmatrix} \frac{\partial f_1(x)}{\partial x_1} & \frac{\partial f_1(x)}{\partial x_2} & \frac{\partial f_1(x)}{\partial x_3} & \frac{\partial f_1(x)}{\partial x_s} \\ \frac{\partial f_2(x)}{\partial x_1} & \frac{\partial f_2(x)}{\partial x_2} & \frac{\partial f_2(x)}{\partial x_3} & \frac{\partial f_2(x)}{\partial x_s} \\ \frac{\partial f_m(x)}{\partial x_1} & \frac{\partial f_m(x)}{\partial x_2} & \frac{\partial f_m(x)}{\partial x_3} & \frac{\partial f_m(x)}{\partial x_s} \end{bmatrix}_{N_m \times N_s}$$

the Jacobean matrix is called information matrix and each element in the matrix $H(x)$ can be expressed through mathematical derivation by taking the differential of the equation for each measurement with respect to state variables, bus voltage angle δ and magnitude V . The matrix $H(x)$ is arranged so that each row represents the derivative of the active power with respect to a particular busbar voltage and angle. First column of that row is representing derivative of active power in relation of voltage and second column is representing active power derivative in relation with angle and so on for all busbars. The same was repeated in second row where the derivative of reactive power with respect to voltage and angle is taking place. This continues to all busbars where each busbar should have two rows in the Jacobean.

If the voltage measurement is introduced in the state estimation the last rows will include the derivative value of the voltage at that busbar, see the C program in appendix (A).

The transpose of $H(x)$ is $H^T(x)$ and is equal to:

$$H^T = \begin{bmatrix} \frac{\partial f_1(x)}{\partial x_1} & \frac{\partial f_2(x)}{\partial x_1} & \frac{\partial f_3(x)}{\partial x_1} & \frac{\partial f_m(x)}{\partial x_1} \\ \frac{\partial f_1(x)}{\partial x_2} & \frac{\partial f_2(x)}{\partial x_2} & \frac{\partial f_3(x)}{\partial x_2} & \frac{\partial f_m(x)}{\partial x_2} \\ \frac{\partial f_1(x)}{\partial x_s} & \frac{\partial f_2(x)}{\partial x_s} & \frac{\partial f_3(x)}{\partial x_s} & \frac{\partial f_m(x)}{\partial x_s} \end{bmatrix}_{N_m \times N_s}$$

1.1.3 DSE Validation and Sensitivity Studies on Part of Morton Park

The validation and sensitivity studies were carried out on part of Morton park network shown in fig.5 This network is an 11 kV network with 60 buses distributed into six feeders. Appendix A and B presents line, bus parameters and load consumption. This network has 120 power measurements; same data accuracy which was used in previous case of generic network. The real voltage measurements were connected at slack bus and bus number 47 where the DG is connected.

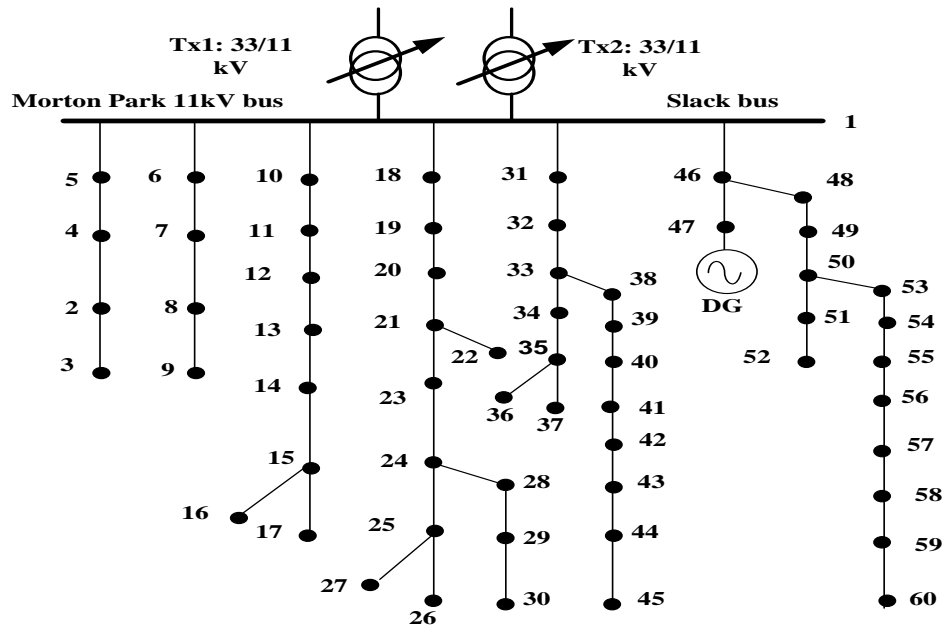


Fig.5: Single line diagram of A 60 nodes of Morton Park network [17]

Fig.6 shows the result of the voltage calculated by the developed C code to each node of the part of Morton Park network

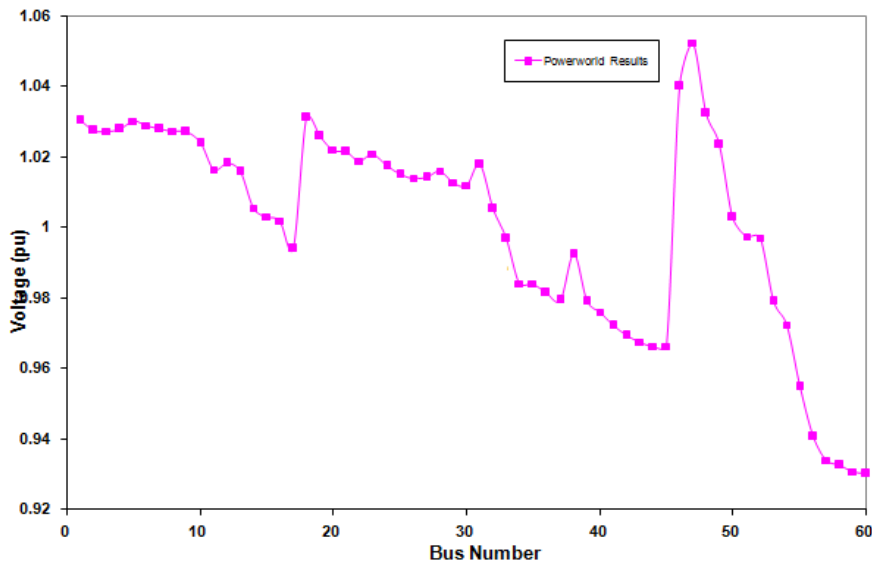


Fig.6: Part of Morton Park node voltage

- DSE Validation study on Part of Morton Park

The result of the state estimation using the developed C code shows similar result to Powerworld load flow package. The state estimation code converges to a result close to the load flow result which was carried out by the Powerworld simulation package. Fig. 7 and fig. 8 show the state estimation results against the Power world result with and without Distributed generator.

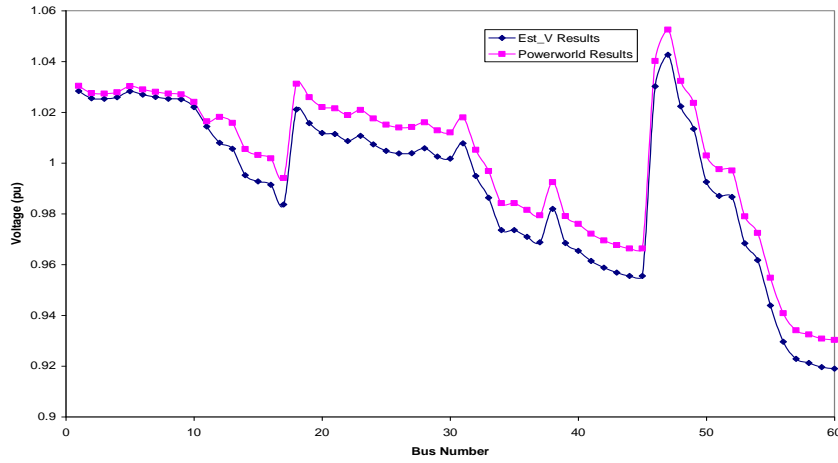


Fig.7: Estimated bus voltage Powerworld results without DG

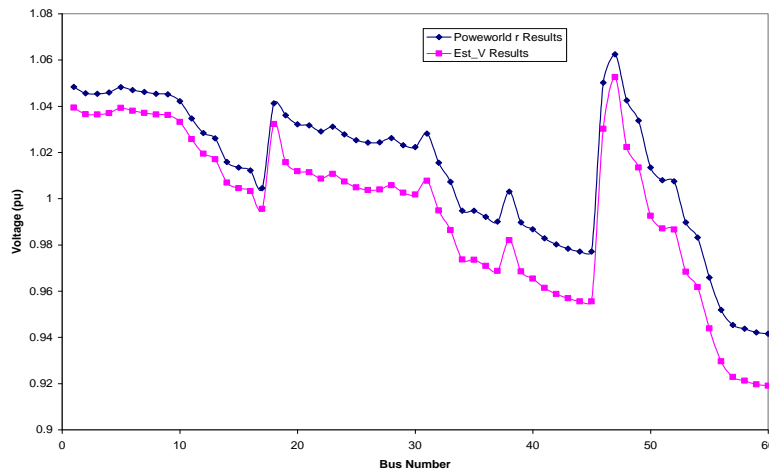


Fig.8: Estimated bus voltage Powerworld results with DG

- Morton Park Network Current and Power Flow Estimation

The developed algorithm also can be used to calculate the Estimated flow of both active and reactive power and flow of current at all branches of the network as shown the following figures respectively.

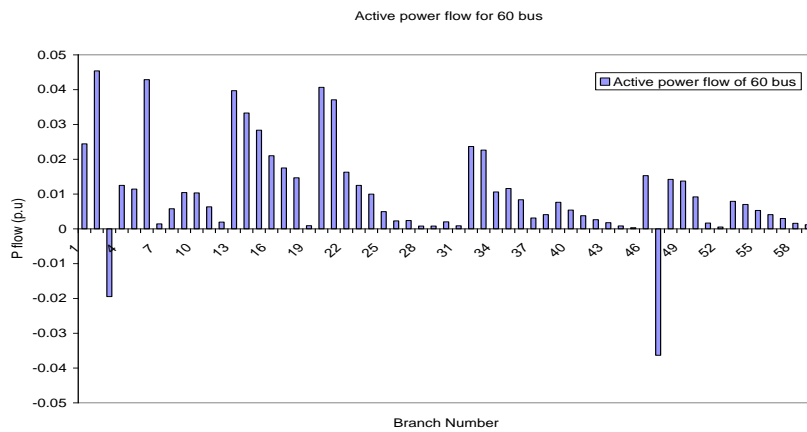


Fig.9: Estimated active power flow of 60 bus network

Fig.9 shows active power of Morton branches. This figure shows that most of power flow has positive direction accept the branch influenced by DG they have negative direction and this indicates power injection from DG side.

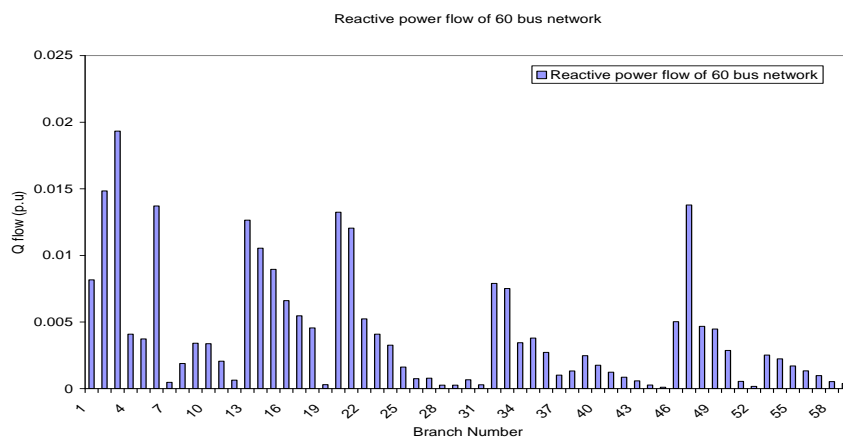


Fig.10: Reactive power flow of 60 bus network

Fig.10 show that directions of reactive power are all positive which means all load and generation are consuming reactive power.

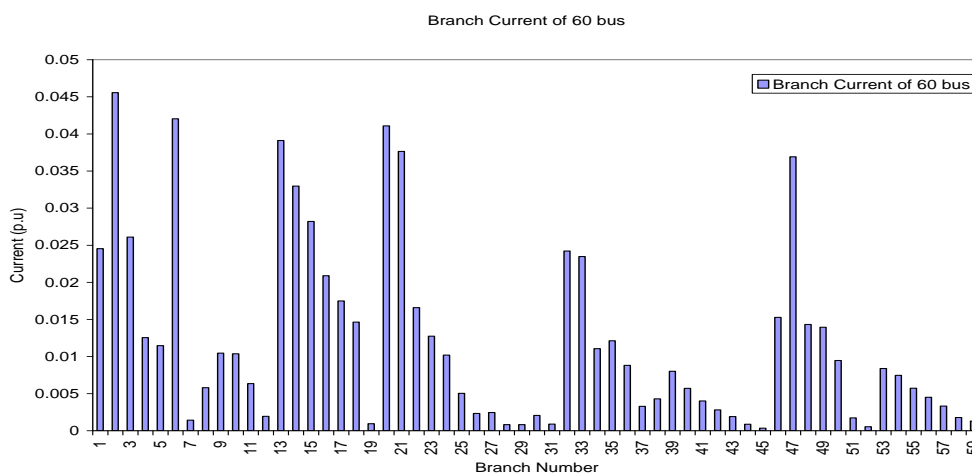


Fig.11 Estimated branch current of 60 bus network

Fig.11 shows the magnitude of branch current of the Morton Park network with one DG connected at bus 47.

1.3 DSE sensitivity study on Morton Park Network

The results presented in this section investigated several parameters affecting the voltage estimation. These parameters are;

- 1-Number of voltage measurements
- 2-Accuracy of the load estimate

- Influence of number of voltage measurements on DSE

In this study all the pseudo measurements of 60 were given the accuracy of $\pm 25\%$ and virtual measurements were given very high accuracy of $\pm 1 \times 10^{-11}$ and the voltage real time measurements were given accuracy of $\pm 1\%$. In this study the number of real time measurements will increased and all other measurements will stay with fixed accuracy. The state estimation results presented in fig.12 show that bus voltage’s uncertainty has increased as the number of real time measurements increasing.

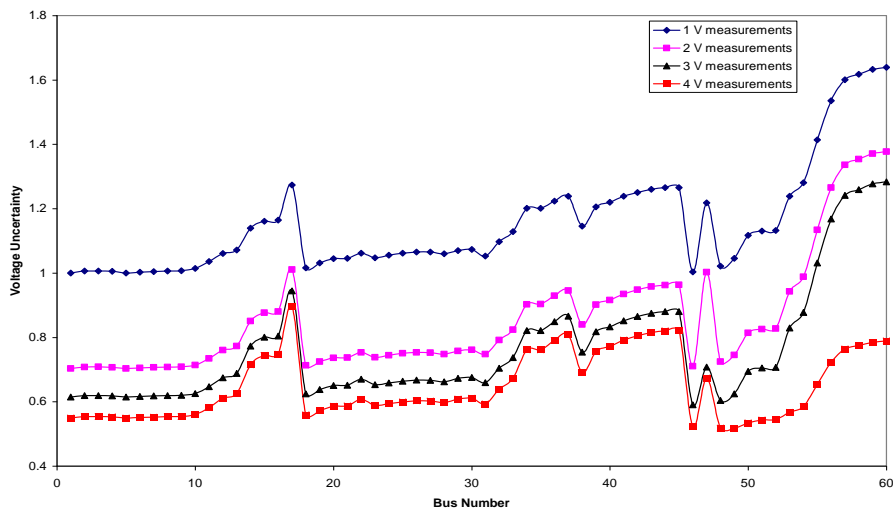


Fig.12: Influence of number real measurement on uncertainty

- Accuracy of the Pseudo Measurements

In this study busbar voltage uncertainty has been checked when all pseudo measurements were given different accuracy ($\pm 25\%$, $\pm 50\%$, $\pm 75\%$, $\pm 100\%$, $\pm 125\%$, $\pm 150\%$, $\pm 175\%$, $\pm 200\%$). The state estimation results presented in fig.13 show that busbar voltage uncertainty has decreased when pseudo measurements accuracy has decreased.

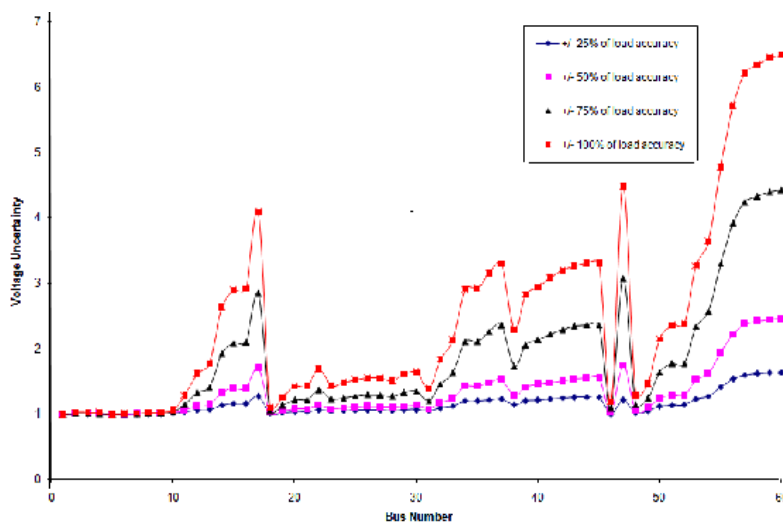


Fig.13: Influence of load accuracy on voltage uncertainty

4 Conclusions

This work presented a three-phase algorithm to determine electric network variables for a distribution system which based on DSE technique. It uses active and reactive power acquired from billing system which used as pseudo measurement to obtain an estimation of real-time system states. Results for the proposed distribution system SE is discussed and there validation was compared and almost show full agreement. The study has carried out the influence of changing the accuracy by giving some high accuracy to some location to reassemble real-time measurement. Also the developed algorithm can calculate line current and a flow of power through all branches of the network which provide away for monitoring and protection. The result gained from the algorithm will facilitate heading toward complete automation and monitoring to any distribution network without causing any change to its infra structure.

References

- [1] "Factors Affecting Electricity Prices – Energy Explained, Your Guide To Understanding Energy – Energy Information Administration". www.eia.gov.
- [2] Retrieved 3 May 2018.
- [3] Prehoda, Emily; Pearce, Joshua; Schelly, Chelsea (2019). "Policies to Overcome Barriers for Renewable Energy Distributed Generation: A Case Study of Utility Structure and Regulatory Regimes in Michigan". *Energies*. 12 (4): 674. doi:10.3390/en12040674.
- [4] C. N. Lu, J. H. Teng, W. H. E. Liu, "Distribution on Power System State Estimation," Vol. 10, No. 1, February 1995.
- [5] F.F. Wu. "Power System State Estimation: A Survey Electrical Power & Energy System, " Vol. 12 No. 2, April 1990.
- [6] M. B. Do Coutto Fiho, A. M. Leite da Silva, and D. M. Falco, " Bibliography on power system state estimation (1968-1989), " IEEE Trans. On Power Systems, Vol. 5, No. 3 Aug. 1990.
- [7] A. Bose, and K. Clements, "Real-Time Modeling of Power Networks," IEEE Proceedings, pp. 1607-1622, Dec. 1987.
- [8] K. L. Geisler, "Ampere Magnitude line measurements for Power System State Estimation," IEEE Trans. on Power Apparatus and Systems, Vol. PAS-103, No, 8, Aug.1984.
- [9] Sarada Devi, M.S.N.G.; Yesuratnam, G. Comparison of State Estimation Process on Transmission and Distribution Systems. In *Advances in Decision Sciences, Image Processing, Security and Computer Vision*; Satapathy, S.C., Raju, K.S., Shyamala, K., Krishna, D.R., Favorskaya, M.N., Eds.; Learning and Analytics in Intelligent Systems; Springer International Publishing: Cham, Switzerland, 2020; Volume 4, pp. 414–423. ISBN 978-3-030-24317-3
- [10] Ahmad, F.; Rasool, A.; Ozsoy, E.; Sekar, R.; Sabanovic, A.; Elita, S. M. Distribution system state estimation-A step towards smart grid. *Renew. Sustain. Energy Rev.* 2018, 81, 2659–2671
- [11] Radhoush, S.; Bahramipناه, M.; Nehrir, H.; Shahooei, Z. A Review on State Estimation Techniques in Active Distribution Networks: Existing Practices and Their Challenges. *Sustainability* 2022, 14, 2520.
- [12] D. I. H. Sun, S. Abe, R. R. Shoultz, M. S. Chen, "Calculation of Energy Losses in Systems," IEEE Trans. on Power Apparatus and Systems, Vol. PAS, 90, No. 4, pp. 1347-1368, July/Aug. 1980.
- [13] I. Roytelman, and S. M. Shahidehpour, "State Estimation for Electric Power Distribution System in Quasi Real-Time Conditions," IEEE paper 93 WM 090-1 PWRD.
- [14] J. J. Grainger, and W. D. Stevenson, "Power System Analysis", Book, International Editions 1994, McGraw-Hill, Inc., ISBN 0-07-113338-0.
- [15] I. Cobelieo, "State Estimation in Distribution Network with DG" Mphil Thesis, Department of Electrical Engineering and Electronics, University of Manchester Institute of Science and Technology, 2003.
- [16] Li, "State Estimation for Power Distribution System and Measurements Impacts" IEEE Transactions on Power Systems, Vol. 11, No. 2, May 1996.
- [17] I. J. Nagrath, and D. P. Kothari, "Modern Power System Analysis" Book, Second Edition, Tata McGraw Hill, 1993, ISBN 0-07-451799-6.
- [18] H. Li, "Load Flow Studies of Morton Park and Pirelli Network" Report for Econnect 967 Project, UMIST, 27 October 2004.

Appendix A

Morton Park Lines and Buses Parameters

Branch No.	Branch		L. Resistance (pu)	L. Inductance (pu)	L. Cap. (pu)
	From	To			
1	1	31	0.7782	0.2684	0
2	1	18	0.141	0.0724	0
3	1	46	0.1435	0.0476	0
4	1	6	0.1007	0.0439	0
5	1	5	0.0085	0.0035	0
6	1	10	0.1349	0.0627	0
7	2	3	0.1209	0.0278	0
8	4	2	0.0616	0.0268	0
9	5	4	0.2016	0.0992	0
10	6	7	0.0767	0.045	0
11	7	8	0.1048	0.0612	0
12	8	9	0.108	0.0222	0
13	10	11	0.1763	0.0784	0
14	11	12	0.1811	0.0628	0
15	12	13	0.0785	0.0272	0
16	13	14	0.47	0.1285	0
17	14	15	0.132	0.0328	0
18	15	17	0.6037	0.1282	0
19	15	16	1.4219	0.1161	0
20	18	19	0.1185	0.0486	0
21	19	20	0.0902	0.0496	0
22	20	22	0.1695	0.0958	0
23	20	21	0.0314	0.0268	0
24	21	23	0.0595	0.0137	0
25	23	24	0.6292	0.2022	0
26	24	28	0.6229	0.2135	0
27	24	25	0.9646	0.3309	0
28	25	27	1.0514	0.3605	0
29	25	26	1.2303	0.4219	0
30	28	29	1.4529	0.4935	0
31	29	30	0.8663	0.2921	0
32	31	32	0.4676	0.2446	0

Rashid El-feres

33	32	33	0.2669	0.3231	0
34	33	38	0.3605	0.1484	0
35	33	34	0.9755	0.3346	0
36	34	35	0.0035	0.0014	0
37	35	37	1.4758	0.1272	0
38	35	36	0.6213	0.0621	0
39	38	39	1.6864	0.1678	0
40	39	40	0.5393	0.0454	0
41	40	41	0.9985	0.0873	0
42	41	42	0.9483	0.0794	0
43	42	43	0.9978	0.0834	0
44	43	44	1.3631	0.5068	0
45	44	45	0.0934	0.032	0
46	46	48	0.4783	0.1618	0
47	46	47	0.737	1.0936	0
48	48	49	0.5125	0.3818	0
49	49	50	1.2433	0.9109	0
50	50	53	2.563	0.211	0
51	50	51	3.092	0.6508	0
52	51	52	0.8221	0.2819	0
53	53	54	0.7919	0.0665	0
54	54	55	2.3917	0.1964	0
55	55	56	2.4871	0.2063	0
56	56	57	1.5092	0.1241	0
57	57	58	0.4802	0.0392	0
58	58	59	0.9473	0.0774	0
59	59	60	0.4144	0.1347	0

Appendix B

Morton Park Load Consumption and Generation

Bus No.	Load Active Power (MW)	Load Reactive Power (kVar)
1	-11.12016	-4.88432
2	0.43478	0.14291
3	0.14165	0.04656
4	0.46433	0.15262
5	0.09953	0.03271
6	0.21832	0.07176
7	0.40043	0.13162
8	0.43801	0.14397
9	0.19214	0.06315
10	0.28978	0.09525
11	0.60676	0.19943
12	0.46628	0.15326
13	0.7155	0.23517
14	0.3294	0.10827
15	0.18533	0.06091
16	0.0895	0.02942
17	1.40804	0.4628
18	0.44352	0.14578
19	0.33995	0.11174
20	0.82021	0.26959
21	0.25133	0.08261
22	1.6385	0.53855
23	0.50512	0.16602
24	0.02751	0.00904
25	0.07904	0.02598
26	0.07942	0.0261
27	0.07891	0.02594
28	0.02571	0.00845
29	0.11386	0.03742
30	0.08571	0.02817
31	0.02955	0.00971
32	0.07283	0.02394
33	0.02847	0.00936

Rashid El-feres

34	0.31349	0.10304
35	0.11706	0.03848
36	0.40573	0.13336
37	0.30954	0.10174
38	0.29158	0.09584
39	0.21561	0.07087
40	0.15984	0.05254
41	0.11306	0.03716
42	0.08422	0.02768
43	0.09478	0.03115
44	0.04968	0.01633
45	0.03135	0.0103
46	0.15097	0.04962
47	-3.47	1.34
48	0.09423	0.03097
49	0.03641	0.01197
50	0.26742	0.0879
51	0.11449	0.03763
52	0.05039	0.01656
53	0.10096	0.03318
54	0.08687	0.02855
55	0.15872	0.05217
56	0.11064	0.03637
57	0.10723	0.03525
58	0.13834	0.04547
59	0.04198	0.0138
60	0.11615	0.03818

The phenomenon of corona and its effect on the transient wave in the transmission line

Ali Abead Dh , Abdulate.A.M.Elganai
Department of Electrical and Electronics Engineering, Bani waleed University

Abstract: Corona effect has been considered as a source of substantial loss due to High Voltage AC Transmission lines. This paper presents a comprehensive account of development of a mathematical model for the Corona Effect which is designed based on the Peek's equation. The scope of this work is determining the corona power losses dependent on conductor's diameters. The simulation is completed using the corona model for 220 kV overhead transmission lines which were developed by Matlab/toolbox (release 2010). The corona effects analysed in high voltage transmission lines, and factors of decreasing the corona losses have been identified. Factors such as increasing the diameter of conductors those lead to increase the critical disruptive voltage. The paper describes the analytical approach, computational tools and simulations models.

Keywords: (Power Losses, Transmission Line, Electric Field, Corona Models, Critical Disruptive Voltage)

Introduction

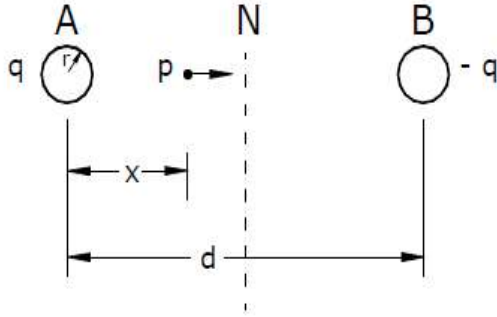
In transmission lines, corona effect causes power loss, audible noise, electromagnetic interference, purple glow, ozone production, etc. Hence to minimize this negative effects, conductor surface condition, size, distance to ground and other conductors have to be considered when planning and construction of overhead power lines . In transmission of electricity ac voltages are used to transmit electric power because of their efficiency against dc voltage. The basic difference between ac and dc coronas in the periodic change in direction of the applied field under ac, and its effect on the residual space charge left over from the discharge during preceding half-cycles. In a ac corona tracheal pulses, negative glow and positive glow and streamer coronas can be observed. This study investigates the effect of ac corona on different type and size of conductors. In order to obtain an ideal corona cage is built. Tests are performed on aluminium, copper and steel conductors. For each bare conductor, the corona inception voltage, extinction voltage and currents at this voltage levels are reported. Moreover, corona power loss is calculated by using common experimental formulas. This work also provides a discussion of corona and induced current effects associated with operation of the proposed high-voltage transmission lines. These effects include audible noise, radio, television, computer monitor interference, gaseous effluents, fuel ignition, and interference with cardiac pacemakers. Since these effects are common to all transmission lines, they have also been investigated generally application. These effects have been assumed to be negligible or non- existent. Due to that, they don't have significant influence on the outcomes and mitigation measures are not required.

I. Corona in transmission line

The phenomenon of corona plays an important role in the design of an overhead transmission line. Therefore, it's profitable to consider the following terms much used in the analysis of corona effects.

II. Critical disruptive voltage:

If one-phase transmission line as shown in Fig(1). Let r assume that a represents the radius of each conductor and d is distance between the conductors such that $d \gg r$. In this single-phase transmission line, let consider q is the charge per unit length on one of the conductors and hence $-q$ on the other. If the operating voltage is U , the potential of conductor A with respect to neutral plane N will be $U/2$ and that of conductor B will be $-U/2$.



Fig(1) 1-phase transmission line

The electric field intensity at P due to the both line charge will be represented as follows:

$$E_x = \left(\frac{q}{2\pi\epsilon_0 x} \right) - \left(\frac{-q}{2\pi\epsilon_0(d-x)} \right) \quad \text{v/m} \quad (1)$$

$$E_x = \frac{q}{2\pi\epsilon_0} \left(\frac{1}{x} + \frac{1}{d-x} \right) \quad (2)$$

The potential different between the conductors can be writing by the following formula :

$$U = - \int_{d-r}^r E_x = \frac{q}{\pi\epsilon_0} \ln \frac{d-r}{r} \quad (3)$$

Since r is very small as compared to d, $d-r = d$. Substituting for q from the above equation

$$q = \frac{\pi\epsilon_0 U}{\ln \frac{d}{r}} \quad (4)$$

$$E_x = \frac{U' d}{x(d-x) \ln \frac{d}{r}} \quad (5)$$

Where U' is the line to neutral voltage of the system.

Critical disruptive voltage can be simply defined as the voltage at which complete disruption of dielectric occurs. This voltage corresponds to the gradient at the surface equal to the breakdown strength of air. This dielectric strength is denoted by g_0 and is equal to 30kV / cm peak at NPT i.e., 25C° and 760 mm OF Hg. At any other temperature and pressure

$$g'_0 = g_0 \delta \quad (6)$$

Where δ is the air density correction factor and is as following:

$$\delta = \frac{3.92 * b}{273 + t} \quad (7)$$

Therefore, the critical disruptive voltage is given by:

$$U_o = r g'_0 \delta \ln \frac{d}{r} \quad (8)$$

For high voltage transmission line the ACSR conductors are used. The cross-section of such conductors a series of arcs of circles each of much smaller diameter then the conductor as a whole. The potential gradient for such conductor will be greater than for the equivalent smooth conductor. The irregularities on the surface are increased further because of the deposition of dust and dirt on its surface and the breakdown voltage is further reduced. Average value for the ration of breakdown voltage for such conductor between a smooth conductor lines and 0.85, and is denoted by m_o . The final expression for the critical disruptive voltage after taking into account the surface of the conductor is given by:

$$U_o = r g_0 \delta m_o \ln \frac{d}{r} \quad [KV] \quad (9)$$

$m_o = 1$ for polished conductor (smooth conductor).
 $= 0.98 \rightarrow 0.92$ for dirty conductor.
 $= 0.87 \rightarrow 0.80$ for stranded conductor.

III. Corona loss

In high voltage transmission line when the applied voltage exceeds a critical disruptive value, the thin layer of air around the transmission line ionizes. This ions result in space charges which move round the conductor. To remain the charges in the motion required the energy derived from the supply system. In order to maintain the flow of energy over the conductor it is necessary to supply this additional loss from the supply system. This additional power is referred to as corona loss. Peek's has been previously studied the effect of various parameters on the corona loss and he deduced an empirical relation:

$$P = 241 * 10^{-5} * \frac{(f+25)}{\delta} * \sqrt{\frac{r}{d}} * (U_p - U_o)^2 \text{ kw/ km} \quad (10)$$

Where

P = corona power loss.
 f = supply frequency .
 δ = air density factors .
 U_p = Phase- neutral voltage.
 U_o = disruptive voltage (r. m .s) per phase.
 r = radius of the conductor (cm).
 d = spacing (or equivalent spacing) between conductor (cm).

In overhead transmission line the following factors affect corona los:

- (i) electrical factors.
- (ii) atmospheric factors and.
- (iii) factors connected with the conductors.

i. Electrical factors:

Referring to the equation (9) it can be notified that the corona loss is a function of frequency. Thus higher values for both or the frequencies of supply and the losses due to corona. This means that dc. corona loss is less as compared with a.c. corona loss. This is because during the corona phenomenon of a.c. the value or always produces third harmonics and hence frequency is not exactly 50 Hz but it also contains a third harmonic component.

ii. Atmospheric Factors:

Atmospheric factors consist in air density and weather condition. Air density affects the generation of corona sources as demonstrated by Peek empirical equation (9). From this equation the losses are a function of air density correction factor δ . The lower value of δ causes higher loss, because it appears directly in the denominator of the equation and indirectly in the value of critical disruptive voltage [2,3,11].

$$U_o = 21.2 * m_o * \delta * \ln \frac{d}{r} \quad (kv) \quad (11)$$

For the lower value of δ , losses will be higher, because the lower value of δ will have the lower value of U_o and hence higher value of $(U - U_o)^2$, where U is the operating voltage in kV. During the bad weather conditions such as rain, snow and hailstorm will diminish the critical disruptive voltage and hence increase the corona loss. These is due to the fact that rain droplets on the transmission line conductors can be viewed as sharp edges which enhances the electric field and therefore reduces the corona disruptive voltage and hence increase the corona power loss. Corona generation increases whenever moisture accumulates on the conductor. Conductor current, if it heats the conductor, will be discouraged the formation of water drops during fog and during high humidity. However, it has little effect during heavy rain and snow. Corona loss observations in the operating lines during the hoarfrost

have shown that the highest corona losses occur when hoarfrost accumulates on a cold conductor, during the night time hours, when load currents are not sufficient to warm the conductors enough to melt the hoarfrost [1,3]. Wind speed has been found to have a very small effect on corona generation unless the wind is blowing particles onto conductors.

iii. Factor connected with conductors:

This factor can be divided into three categories:

- 1- Conductor surface conditions.
- 2- Conductor diameter.
- 3- Number of conductors.

The conductors are exposed to atmospheric conditions; the surface would have dirt.

Deposited on it which will lower the disruptive voltage and increase corona loss. Audible noise is primarily a foul-weather phenomenon therefore conductor-surface conditions are only important inasmuch as they influence water drop formation. From the equation (9) for corona loss, it can be observed that the conductor size appears in two places, it's worth mentioning that the other parts of equation (9) are assumed to be constant, so:

$$P = K \sqrt{\frac{r}{d}} (U_p - U_o)^2 \quad \frac{kw}{km} \quad (12)$$

Equation (12) shows that the first losses are proportional to the square root of the diameter of the conductor, if the diameter of conductor is large, then the loss will also be large. Secondly, since U_o is approximately directly proportional to the diameter of the conductor, hence the large size of the conductor leads to the critical disruptive voltage has to be large and hence the difference between the operate and critical disruptive voltage will be small. Number of conductors is an input into the calculation of the electric field at the surface of conductors. For operating voltage 200 kV and above it, is found that one conductor per phase gives large corona loss and hence large radio interference (RI) level which interferes with the communication lines which are normally run parallel with the power lines. Most research has shown that the RI does not increase with the number of conductors for a fixed conductor diameter[3,4].

The higher the corona losses in the power transmission lines with one conductor is solved with by using two or more than two conductors per phase or as they are known as bundling of conductors. By bundling the conductors the self geometric mean distance (GMD) of the conductors is increased thereby; the critical disruptive voltage is increased and hence corona loss is reduced [1,7,9].

To reducing corona loss can be used following methods:

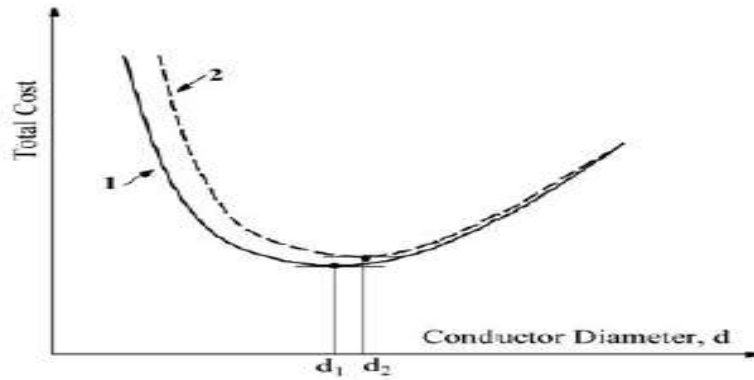
- large diameter of conductors.
- hollows conductors.
- bundled conductors.

With the aim to reduce the corona power losses, have been made experiments and research how affects have the larger diameter and bundled conductors.

If conductor radius is larger, surface field intensity is less and hence corona losses are lower. For the same current carrying capacity, an ACSR conductor has larger radius, therefore the transmission lines with ACSR conductors have lower corona loss. Also, for bundled conductors lines effective radius is larger and hence corona loss is less.

Corona losses do not generally play an important role in the overall design of transmission lines. With most computer programs that evaluate only the cost of resistive losses in overhead transmission lines. But, there are conditions where corona losses may influence the economic choice of conductors, and compact lines may be one of those conditions. The cost of transmission line conductors, usually expressed in terms of an annualized cost, is made up of the annualized cost of capital investment and the annual cost of energy losses incurred during the operation of the line. The capital cost is almost directly proportional to the conductor cross-section, or to d^2 , where d is the conductor diameter. In the absence of corona on conductors, the energy losses consist mainly of the resistive or I^2R losses, where I is the load current flowing through the line, and R is resistance of the conductor. Insulator leakage

losses are generally negligible compared to the resistive losses. The economic choice of conductors, for a given transmission voltage and load current, involves minimizing the total annualized cost of conductors over the expected life of the line. Since the capital losses decreases with d , there is an optimum value of d for which the total cost attains a minimum [6,7,8]. In Figure(2), curve 1 shows the variation of the total cost as a function of conductor diameter d . Minimum total cost is obtained for an optimum conductor diameter d_1 . For conductor sizes either lower or higher than d_1 , the total cost will be higher. The increase in total cost may become important for lower load currents and/or higher energy costs [5,10,11].



Fig(2) Economic choice of conductors

In the presence of corona on conductors, the mean annual corona losses should be added to the resistive losses to determine the annualized the energy losses. As in the case of resistive losses, corona losses decrease as d increases. This is illustrated by curve 2 of Figure 2, which differs from curve 1 at lower values of d and merges asymptotically with curve 1 for the increased value of d . The minimum total cost of curve 2 occurs at a slightly larger diameter d_2 . With the increasing cost of energy, studies carried out in several countries have shown that it is important to take into account the cost of corona losses in the economic choice of conductors particularly for lightly loaded or compact transmission lines in the range of 220–400 kV, lines in traversing regions of high altitude or of extreme pollution, and also for normally loaded lines at voltages above 750 kV [3,5,11].

A. Modeling Of Corona Effect

Since the project is studying the Corona effects in AC transmission lines, the most reliable mathematical equation to simulate the losses is the famous Peek's equation. Peek studied the corona effects and all factors that contribute to all noticeable changes along the transmission lines. An extended empirical peek's equation is presented to compare all variables [7,10]

$$p = 241 * 10^{-5} \frac{(f + 25)}{\delta} \sqrt{\frac{r}{d}} (U_p - U_0)^2 \text{ kw/km.}$$

P is the Corona power loss in kw/km , f is the system frequency, δ is the air density factor, r is the radius of the conductor in cm, d is the distance of two parallel conductors, U_p is the applied voltage (line to neutral) in KV and U_0 is the disruptive voltage of the Corona[2,9,10].

B. Matlab Simulink Model

To study all calculations and all factors manipulation, Matlab tool Simulink is used. Simulink is an easy tool to monitor the output change with respect to each element adjustment. A scope will be put on the output to plot it clearly with all changes.

The sub blocks involved in the design are represented in Fig.3.The sub block has realization of all the factors on which the corona effect depends upon through Peeks equation.

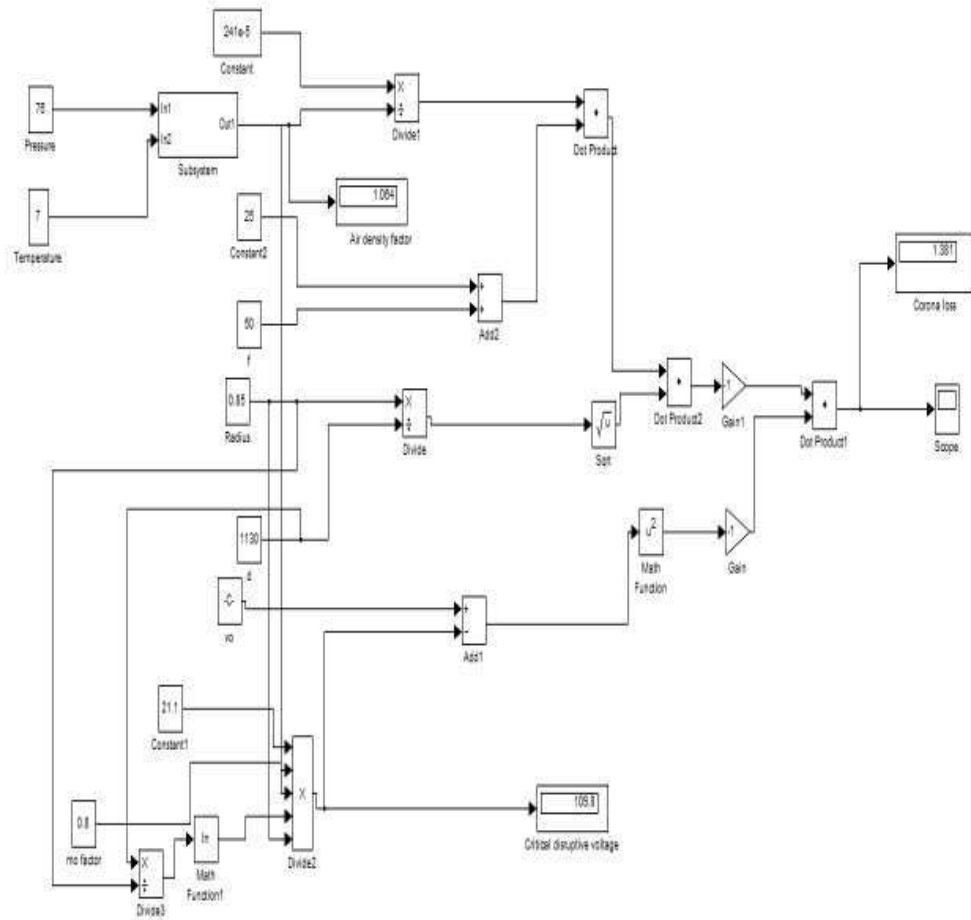


Fig (3):Computational Schematic of Corona Model

$$\delta = \frac{3.92 \cdot b}{273 + T(^{\circ}\text{C})}$$

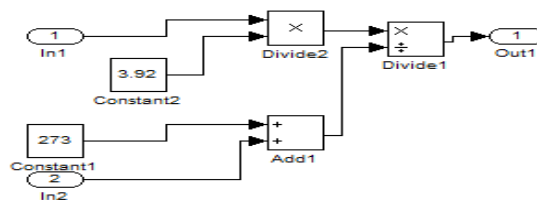


Fig (4): subsystem the air density correction factor

C. Radius Of Conductor Effect On Corona

Could be hallow cable or steel core cable which is relative to radius Conductor Radius is considered to be the most valuable factor in evaluating Corona and also the key point in commercially and economically designing the transmission system. Beside the material of the cable and type, a bigger radius leads to bigger surface area and less field intensity. As a result, Designers tend to be very careful in choosing the size of the cable (sometimes the type because it).

Table(1) corona and disruptive voltage value when Radius of Conductor changes

R (cm)	Critical disruptive voltage kv/ph	Corona loss (kw/km/Ø)
0.76	116.5	0.5256
0.77	117.8	0.4042
0.78	119.2	0.2983
0.79	120.5	0.2081
0.80	121.8	0.1337
0.81	123.1	0.07576
0.82	124.4	0.03372
0.83	125.7	0.008469
0.84	127.00	1.059e-9

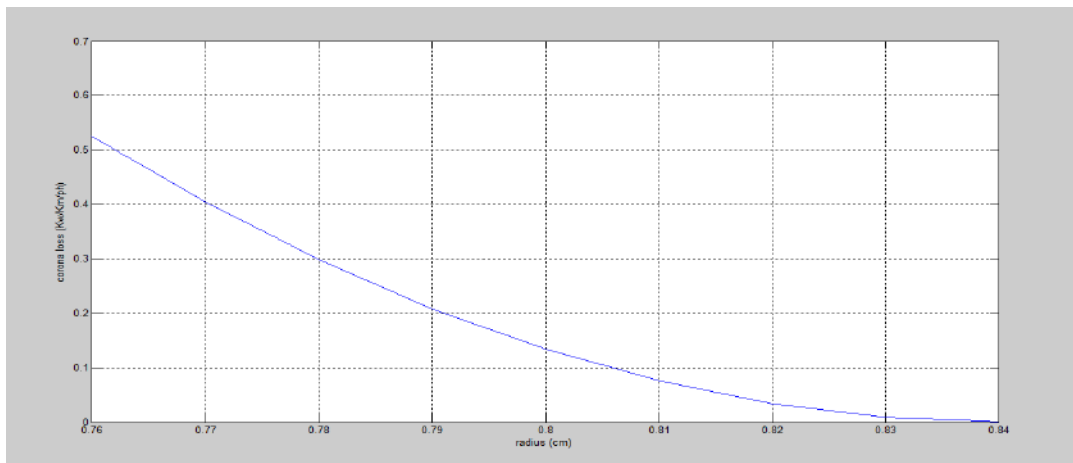


Fig (5): Corona Losses at 220 KV.conductor radius

D. Conductor Distance

Another important factor would be the distance of the parallel conductors as they tend to affect each other through electrostatic energy or electromagnetic energy. As a result, more energy will be given to surface electrons that will knockout more air ions and produce more loss. We took the case of 220kv system with 0.84 cm radius cable and increase the distance gradually and the result is shown in figure 6. And as expected, the corona losses decrease as the distance increases and almost disappear when the distance reaches 10.90 meter. Changing the distance between conductors is done through the transmission lines poles, because their structures define the distances among all lines.

Table(2) corona and disruptive voltage value when Radius of Conductor changes

D (m)	Critical disruptive voltage (kv)	Corona loss (kw/km/Ø)
10.4	126.2	0.003561
10.5	126.4	0.002247
10.6	126.5	0.001247
10.7	126.7	0.000547
10.8	1.26.9	0.0001352
10.9	127	1.059e-9
11	127.2	0.0001301

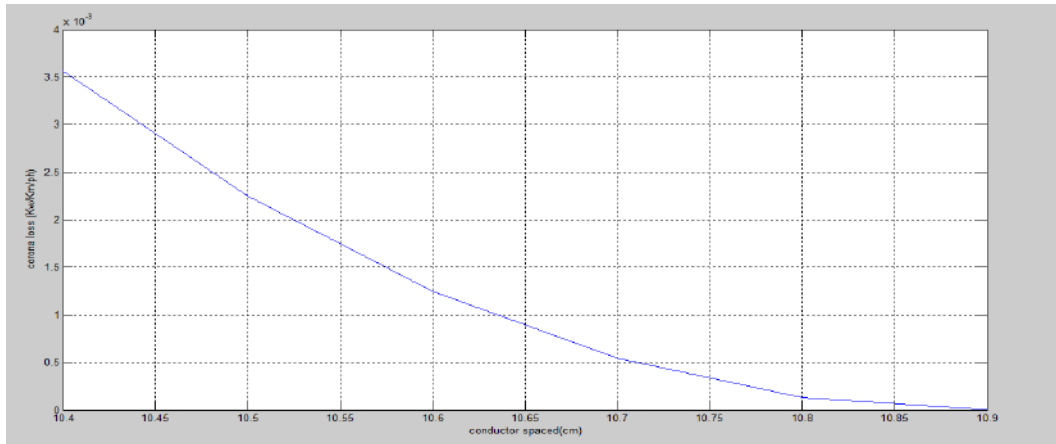


Fig (6): Corona Losses at 220 KV Line vs. distance between conductors

E. Irregularity Factor: is a factor that loses its properties over time in the beginning dose note significantly affect the loss power but when a surface reaches the roughness state most of the transferred power is lost in the loss of the corona.

Table(3) Corona and disruptive voltage value when Irregularity factor changes

Mo	Critical disruptive voltage kv/ph	Power loss kw/km
1	127.00	1.059e-009
0.98	124.5	0.0324
0.96	121.9	0.1296
0.94	119.4	0.2915
0.92	116.9	0.5183
0.90	114.3	0.8098
0.88	111.8	1.166
0.86	109.2	1.587
0.84	106.7	2.073
0.82	104.2	2.624

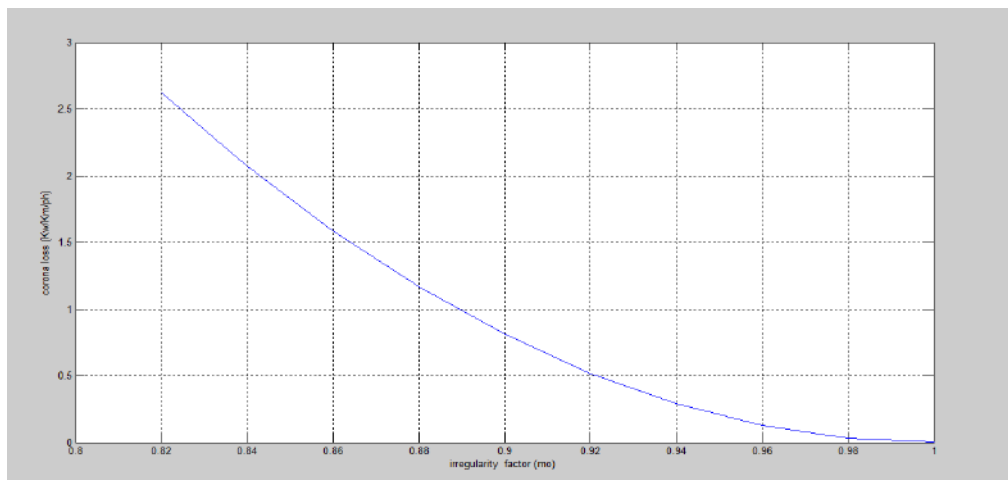


Fig (7): Corona Losses at 220 KV Line vs. Irregularity factor conductor

F. Temperature

Temperature factor plays a small role in corona loss and also it is something that practically cannot be changed. However the figure (8) shown below will examine the influence of changing temperature range, 4 to 48C° degrees Celsius.

Due to the weather effect in corona loss, in fair weather the factor will be considered 1 that will lead to normal disruptive voltage value. On the other hand, since humidity, rain and snow weather affects the corona power loss directly which could lower U_0 to as low as 80%. This is natural factor and unpredictable, so for designers worst condition with bad weather is considered.

Table(4) corona value when temperature changes

Temperature (C°)	Critical disruptive voltage (kv)	Corona loss (kw/km/Ø)
48	117.9	0.4478
45	119	0.3418
42	120.2	0.2493
39	121.3	0.1707
36	122.5	0.1064
33	123.7	0.06585
30	124.9	0.02243
28	125.8	0.00813
25	127.00	1.059e-9
22	128.3	0.008284
19	129.6	0.03349
16	131	0.07614
13	132.3	0.1368
10	133.7	0.216
7	135.2	0.3144
4	136.6	0.4326

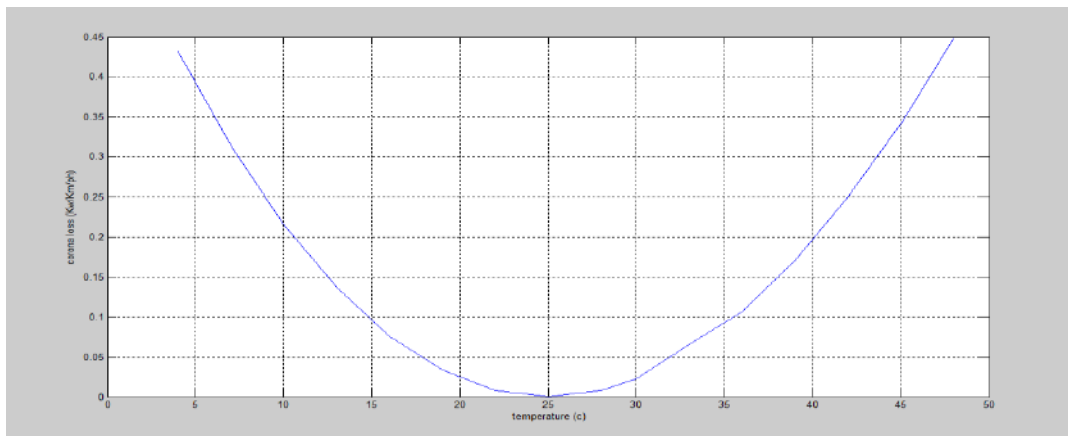


Fig (8): Corona Losses at 230 KV vs. Temperature

G. Types Of Conductors

Transport line 220kv extends in Libya from the middle of several areas where temperatures vary from region to region, in the following tables the best designs for the 220kv transmission line contain the lowest corona losses according to temperature change from 44C° to 7C°, these designed in terms of diameter of the conductor and the distance between the conductor can match the specifications of the transmission line previously established in Libya , if we did not get exact parameters for this line, but these designs were carefully selected. So we can know value the corona loss and that by the temperatures and diameter of the conductor and the distance any blasé in Libya.

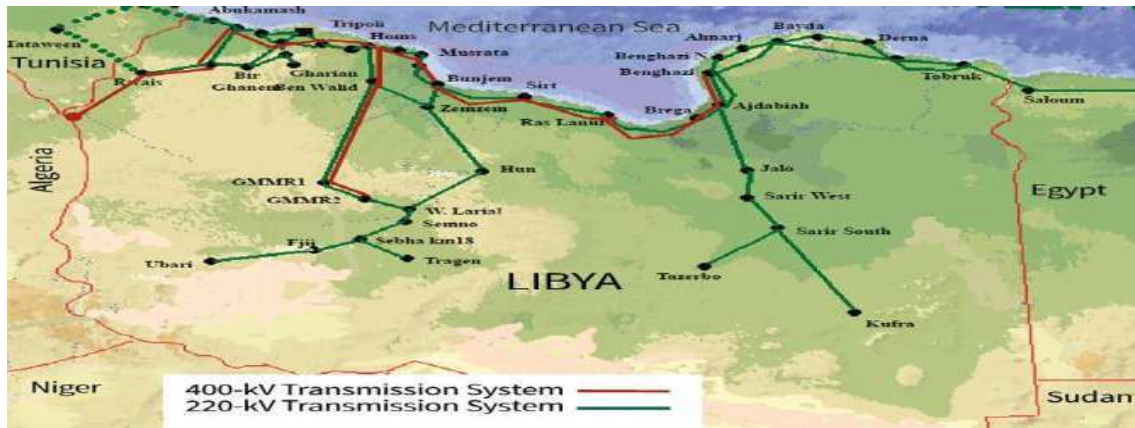


Fig (9): distribution of transmission lines 220kv and 400kv in Libya

Conclusion

Various factors affecting corona loss play a vital role in the prevention of corona. Among those factors some are natural and some are equip mental factors in which we cannot fully control the natural causes but we can take certain measures. All model results were in line with theory expectations with regards to each factor effect on corona loss. Peek's equation based model has proven to be affect to all variables studied in this work and the reliability is high when inputting reasonable values for all.

In the temperate atmosphere (25 C° and 760mmhg), the best measurements in line with the design of the 220 kv transmission line are (D=1090cm and R=0.84cm). when the transmission line is detected in high-temperature areas, the distance between the conductor must be increased as showing in types of conductors. Corona power can be acceptable to a certain level but yet it should always be considered while designing the transmission system beside resistive power loss calculations.

Moreover, economical study has to be on estimating the optimal parameters for all the system to utilize best reliable delivered power with least cost as this is the deal goal from engineering perspective. Full awareness of corona effects should be passed on to all industries dealing with power energy transmission. Yet, the corona phenomenon brings a great usage to some applications and further researches and studies should focus on this field.

References

- [1] Philip Koshy panicker - "Ionization of air by corona discharge" The University of texas at Arlington August 2003.
- [2] Muhammad Ahmed Dawood¹, Dr. Ghous Buksh Narejo² "Modeling of Corona Effect in AC Transmission Systems" ISSN 2229-5518.
- [3] Dr jp holtzausen¹ , Dr wl vosloo² - "High voltage engineering practice and theory" - ISBN: 978 - 0 - 620 - 3767 - 7.
- [4] Isuf Krasniqi¹ , Vjollca Komoni² - "Corona Losses Dependence from the Conductor Diameter" , ISBN: 978-1-61804-041-1.
- [5] D. Das - "Electric Power System" ISBN (13): 978-81-224-2515-4.
- [6] Prof. Dr. ahdab Elmorshedy "High voltage engineering" .
- [7] F.W. Peek, "Dielectric Phenomena in High Voltage Engineering" , McGraw-Hill, 1929.
- [8] N.H. Malik, A. Al.Qureshi, M.I. Qureshi, "Electrical Insulation in Power Systems" , 1st ed., Marcel Dekker, New York, 1998.
- [9] Abdulate.A.M.ELGANAI "The Corona Effect on High Voltage Transmission Lines" . IJSETR International Journal of Scientific Engineering and Technology Research, ISSN 2319-8885 Volume.08, Jan-Dec-2019, Pages: 29-31.
- [10] Abdulate.A.M.ELGANAI "Corona Losses Reliance from the Conductor Diameter Developed in Matlab/Simulink". IJSETR International Journal of Scientific Engineering and Technology Research, ISSN 2319-8885, Volume No.07, Issue No.12, December-2018, Pages: 1989-1993
- [11] M. Khalifa, High-Voltage "Engineering, Theory and Practice" , Marcel Dekker, Inc., New. York, 1990.

Radiological assessment of cancer risk and Human Health Risk in Bani Waleed city, Libya

Mahfoud Aghanaya,
oil and gas department , Engineering College/Bani Waleed University, Libya

Abstract: Under specific circumstances, the natural radioactive ^{226}Ra , ^{232}Th , and ^{40}K materials can reach dangerous radiological levels. As a result, research on the levels of natural radioactivity in soil is required to estimate the dose to the population, analyze the health risks, and establish a baseline for potential future changes brought on by human activity.

Hyper-pure germanium (HPGe) gamma ray spectrometry was utilized to examine three sites in Bani Waleed, Libya, in order to determine the radiological health risks, excess lifetime cancer risks, and Effective Dose to Different Body Organs (D_{organ}) associated with the use of the soil. Nine samples were collected from each of the three sites (Tagrafeet, Sakia, and City Center) at a depth of ten cm, measured and use an HPGe detector, and the results were compared to the global permissible value. The excess lifetime cancer total, both indoor and outdoor average values were lower than the world permissible value, and the results of all different body organs were below the accepted international limits of 1.0 mSv^{-1} , indicating that the radiation levels in the study area are safe and do not pose a health risk to the local population. The results of this research could serve as significant radiometric baseline data for upcoming epidemiological investigation and prosecution and environmental monitoring programs.

Keywords: Bani Waleed, Tagrafeet, Sakia, City Centre, HPGe.

1.0 Introduction

Background radiation that comes from both natural and man-made sources is exposed to humans. Commonly, natural radioactive elements of both terrestrial and cosmic origin account for 85% of a person's annual total radiation dose [1], [2]. According. A person has a higher risk of developing cancer the more radiation they receive. There is no level below which we can say an exposure does not pose a risk to life, and the cancer may not manifest itself for many years (typically 10 to 40 years) after the radiation dose is received [3].

Because these substances emit radiation as a result of the breakdown of natural radionuclides and contribute to the total absorbed dose through ingestion, inhalation, and external irradiation, the study of the radioactive components in soil is a key component in understanding the behavior of radioactivity in the ecosystem [4] The researchers, who have led the surveys across the world are therefore very interested in measurements of natural radioactivity in soils and radiation doses. [5],[6].

There have been many surveys to determine the background levels of radionuclides in soils which have been turned out to calculate the absorbed dose in air [7].

This paper presents the indoor and outdoor the annual effective dose equivalent rate (AEDE) and the excess lifetime cancer risk (ELCR) and Effective Dose to Different Body Organs (D_{organ}) for the occupationally exposed and non-occupationally exposed living within Bani Waleed City.

2.0 Supplementary Materials And Methods

2.1 Research area

City of Bani Waleed located at 170 kilometres south of Tripoli, at 14 00 50" E and 31 45 43" N, and about 837 feet above sea level as shown in Fig 1. The city has a population of about 100,000. The structural geology of the area mainly sedimentary rocks with minor metamorphic and igneous rocks distributed at the surface. It is famous by olive trees, which extends along the valley. The city is characterized by a semidesert climate, where the temperature in summer reaches 45 degrees Celsius and drops to about 15 degrees Celsius in winter. The city of Bani Waleed was subjected to two wars in 2011 and 2012, which caused complete destruction to some places, including the three sites as shown in Fig. (1a, 1b and 1c) that are investigated in this study.

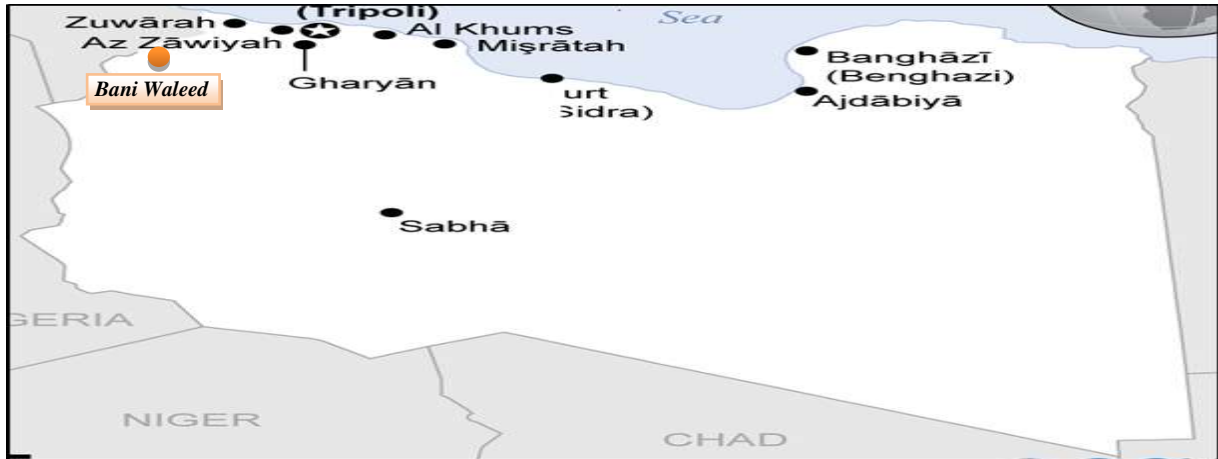


Fig. 1: Bani Waleed Location



Fig. 1a: Tagrafeet location



Fig. 1b: City Centre location.



Fig. 1c: Sakia Camp.

2.2 Sample Collection and Preparation

Nine samples were taken from the three different sites, and the soil samples were determined by using a portable Global Positioning System (GPS). The samples were taken 10 cm below the surface, placed in coded polythene bags, and sent to the Environmental Studies radiation laboratory at Alexandria University's Institute of Graduate Studies and Research (IGSR), where a high gamma spectrometry (HPG) detector was employed to evaluate the radionuclide activity concentration. The samples were air dried then, weighed using an electronic balance, and thereafter drained in a 110 °C oven. The samples were reduced to a fine powder and sieved through a mesh with just a 2 mm pore size. The ^{226}Ra and ^{232}Th short-lived daughter radionuclides were then properly sealed and stored for a month to achieve secular equilibrium with their long-lived parent radionuclides.

2.3 Gamma-ray spectra measurements.

The γ -ray spectra of the soil samples were evaluated using a high purity vertical HPGe detector (p-type with a relative efficiency of 25% and peak to Compton ratio of 54:1). The detector's energy resolution (FWHM) for the 1332 keV ^{60}Co γ -ray line source was 1.9 keV. The Genie-2000 analysis software, version 3.0, was used with the detector in conjunction with the Canberra data acquisition system to perform peak area determination, background subtraction, as well as γ -ray energy and radionuclide identification. A lead cylinder measuring 10 cm in thickness that was internally lined with a copper cylinder measuring 2 mm in thickness served as a shield for the HPGe detector. For counting during an accumulation time of 14400s, the Sample containers were placed one at a time on top of the detector (just below the shield). For back scattering and background radiation, all measurements were

adjusted. Based on the energy of its γ -ray line, which is 1460.8 keV, the activity of ^{40}K has been calculated. The specific activity of ^{232}Th has been calculated using γ -ray lines of energies 338.4 keV and the 911.2 from ^{228}Ac , the 727.3 keV from ^{212}Bi , and the 583.2 keV from ^{208}Tl decay products. The activities of the decay products ^{214}Pb and ^{214}Bi were taken to represent ^{226}Ra using the γ -ray lines of energies 295.2 keV and 351.9 keV from ^{214}P [8]. The γ -ray spectra of the samples were measured at The Environmental studies. Department, Institute of Graduate studies and Research, Alexandria University, Egypt.

3.0 Calculations of activities, hazard indices and dose parameters

The activity concentrations of ^{226}Ra for ^{238}U , ^{232}Th , and ^{40}K radionuclides were represented in the calculations in this section by the symbols A_{Ra} , A_{Th} , and A_{K} , respectively.

3.1. activity concentration (A) in (Bq kg⁻¹)

For the radionuclides ^{226}Ra , ^{343}Th , and ^{40}K , the activity concentration A_i of any taken γ -ray line to represent this parameter has been calculated using the relation [9].

$$A_i(\text{Bq kg}^{-1}) = \frac{C_i}{\epsilon(E) \times t \times m} \quad (1)$$

Where C_i is the net peak area of the γ -ray line at energy E after subtracting the background, $\epsilon(E)$ is the detector efficiency of such a γ -ray line, t is the measurement time in seconds, and m is the sample mass in kg. For ^{226}Ra , ^{232}Th , and ^{40}K , the globally recognized criteria of A are 35, 30, and 400 Bqkg⁻¹, respectively.

3.2 Annual effective dose equivalent (AEDE)

With an outdoor occupancy factor of 0.2 and an indoor occupancy factor of 0.8, the conversion factor (0.7 SvGy⁻¹) from absorbed dose rate in air in nGyh⁻¹ to effective dose rate in mSvyr⁻¹ is used to estimate the AEDE. The following equation was used to determine the AEDE (Indoor and Outdoor) . [2].

$$AEDA(\text{indoor})(\text{mSv}^{-1}) = D_{\text{air}}(\text{nGy h}^{-1}) \times 8766\text{h} \times 0.8 \times 0.7\text{Gy}^{-1} \times 10^{-6} \quad (2)$$

$$AEDA(\text{outdoor})(\text{mSv}^{-1}) = D_{\text{air}}(\text{nGy h}^{-1}) \times 8766\text{h} \times 0.2 \times 0.7\text{Gy}^{-1} \times 10^{-6} \quad (3)$$

These metrics assess the likelihood of both stochastic and deterministic effects in irradiated people. The annual effective dose equivalent should not exceed 0.48 mSvyr⁻¹, and the total annual effective dose equivalent (indoors and outdoors) should not exceed 1 mSvyr⁻¹ [2].

3.3 Excess Lifetime Cancer Risk (ELCR):

As a result, the in-situ measurement processing can determine the corresponding annual equivalent dose, taking into account both the exposure level and the risk of developing cancer in the future. [10], [11], [12]. used the mathematical relationship represented by the following equation to calculate the ELCR rate in mSvy⁻¹.

$$ELCR = (AEDE \times DL \times RF) \quad (4)$$

Where RF is the risk factor (Sv), or the likelihood of dying from cancer per Sievert, and DL is the average life expectancy (70 years) for the general population, the [13]. Used RF = 0.05 for stochastic effects.

Therefore, we use the equations (5, 6) below to evaluate the Indoor and Outdoor ELCR.

$$ELCR_{OUTDOOR} = (E_{OUT} \times DL \times RF) \quad (5)$$

$$ELCR_{INDOOR} = (E_{IN} \times DL \times RF) \quad (6)$$

3.4 Effective Dose to Different Body Organs (D_{organ}).

The effective dose to the organ (D_{organ}) is a measure of the amount of radiation absorbed by the various organs and tissues of the body.

Equation (7) is used to calculate the (D_{organ}) of the body due to inhalation [10].

$$D_{organ}(mSvy^{-1}) = AEDE_M \times F \quad (7)$$

F is the conversion factor of organ dose from air dose, and $AEDE_M$ is the mean annual effective dose equivalent (indoor and outdoor). The F values for the lungs, ovaries, bone marrow, testes, kidney, liver, and entire body, according to [14]. are 0.64, 0.58, 0.69, 0.82, 0.62, 0.46, and 0.68.

4.0 Result and Discussion:

The sampling points shown in the table (1)) below were utilized to determine the activity concentrations of the three naturally occurring radionuclides ^{226}Ra , ^{232}Th , and ^{40}K in the soil throughout the study area. The activity concentration values of ^{226}Ra varied from 22.01 ± 0.085 to 86.53 ± 0.155 Bqkg⁻¹, with an overall mean value of 50.46 ± 0.118 Bqkg⁻¹ exceeding the permissible world value of 35 Bqkg⁻¹ while the activity concentration values of ^{232}Th ranged from 11.46 ± 0.056 to 61.84 ± 0.131 Bqkg⁻¹ and the mean average value is 31.72. The ^{40}K ranged between 381 ± 0.325 and 707.4 Bqkg⁻¹, with an overall average value of 477.92 ± 0.364 Bqkg⁻¹. Samples from B2 in City Centre had the highest average concentration of ^{40}K , while B3 in City Centre had the lowest value.

The annual effective dose equivalent (AEDE) were calculated for the three sites in Bani Waleed City and found that the values ranges from 0.028, 0.112 and 0.140 mSvy⁻¹ to 0.118, 0.474 and 0.592 mSvy⁻¹ for $AEDE_{out}$, $AEDE_{in}$ and $AEDE_T$ respectively. The mean values are 0.077, 0.310 and 0.387 mSvy⁻¹ respectively, All the average values are lower than that of the world average of (1.0 mSvy⁻¹).

Tables (2)), shows the ELCR for the three zones, a comparison with the global average as shown in Fig.2. The outdoor ELCR ranges from 0.10×10^{-3} to 0.41×10^{-3} , with a mean of 0.0725×10^{-3} , which is below the global average of 0.29×10^{-3} [11]. According to a summary of the ELCR (Table (2)), the indoor ELCR ranges from 0.30×10^{-3} to 1.66×10^{-3} with a mean value of 0.27×10^{-3} as shown in Fig.3. These low excess lifetime cancer risk levels imply that there is a low likelihood that residents will develop cancer.. The total excess life cancer risk (ELCR_T) was also calculated using equation (4) and the results were displayed in Table (2)) and Fig.4. The ELCR_T ranged from 0.49×10^{-3} to 0.207×10^{-3} with a mean

value of 1.35×10^{-3} , exceeding the global average of 0.29×10^{-3} . With an average range of 0.95×10^{-3} , the safe range for ELCR is between 0.70×10^{-3} and 1.33×10^{-3} . [15], [16].

Table 1. The Radioactivity Concentrations of ^{226}Ra , ^{228}AC and ^{40}K (BqKg^{-1}) in the Soil Samples from three Locations in the City of Bani Waleed

Sites	Sample No.	^{226}Ra	^{228}AC	^{40}K
Tagrafeet	A1	34.32 ± 0.097	29.23 ± 0.090	570.3 ± 0.398
	A2	40.39 ± 0.105	21.63 ± 0.077	511.4 ± 0.376
	A3	62.49 ± 0.131	37.90 ± 0.102	408.2 ± 0.336
City Center	B1	30.46 ± 0.091	11.46 ± 0.056	51.99 ± 0.120
	B2	59.16 ± 0.128	61.84 ± 0.131	707.4 ± 0.443
	B3	45.51 ± 0.112	19.95 ± 0.074	381.2 ± 0.325
Sakia	C1	69.3 ± 0.138	29.54 ± 0.090	480.9 ± 0.365
	C2	26.01 ± 0.085	40.84 ± 0.106	640.7 ± 0.421
	C3	86.53 ± 0.155	33.11 ± 0.095	549.2 ± 0.390
Min		26.01 ± 0.085	11.46 ± 0.056	381.2 ± 0.325
Max		86.53 ± 0.155	61.84 ± 0.131	707.4 ± 0.443
Mean Value		50.46 ± 0.118	31.72 ± 0.093	477.92 ± 0.364
World average value		35	30	400

Table 2. The absorbed dose rate (D_R), the outdoor (AEDE_{out}) and indoor (AEDE_{in}) annual effective dose equivalent, the total effective dose equivalent (AEDE_T), the total excess life cancer risk (ELCR), indoor (ELCR_{in}) and outdoor (ELCR_{out}) for the soil samples collected from Bani Waleed city -Libya.

Sites	Sample ID	DR (nGy h^{-1})	AEDE_{out} (mSv y^{-1})	AEDE_{in} (mSv y^{-1})	AEDE_T (mSv y^{-1})	ELCR_{in} (mSv yr^{-1})	ELCR_{out} (mSv yr^{-1})	ELCR (mSv yr^{-1})
Tagrafeet	A1	58.53	0.072	0.287	0.359	0.00100	0.00025	0.00126
	A2	53.56	0.066	0.263	0.329	0.00092	0.00023	0.00115
	A3	69.33	0.085	0.340	0.425	0.00119	0.00030	0.00149
City Center	B1	22.83	0.028	0.112	0.140	0.00039	0.00010	0.00049
	B2	96.62	0.118	0.474	0.592	0.00166	0.00041	0.00207
	B3	49.03	0.060	0.241	0.301	0.00084	0.00021	0.00105
Sakia	C1	69.83	0.086	0.343	0.429	0.00120	0.00030	0.00150
	C2	65.69	0.081	0.322	0.403	0.00113	0.00028	0.00141
	C3	82.48	0.101	0.405	0.506	0.00142	0.00035	0.00177
Min		22.83	0.028	0.112	0.140	0.00039	0.00010	0.00049
Max		96.62	0.118	0.474	0.592	0.00166	0.00041	0.00207
Mean value		63.09	0.077	0.310	0.387	0.00027	0.0000725	0.00135
World av. value		60	0.07	0.50	1.0			$0.29 \times$

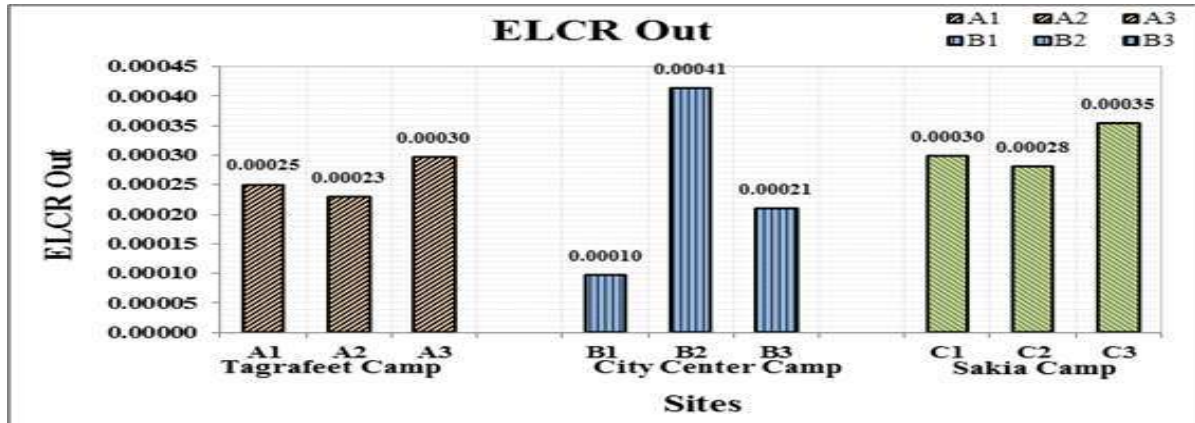


Fig. 2: Excess Lifetime Cancer Risk Outdoor (ELCR_{out}) in the Study Area.

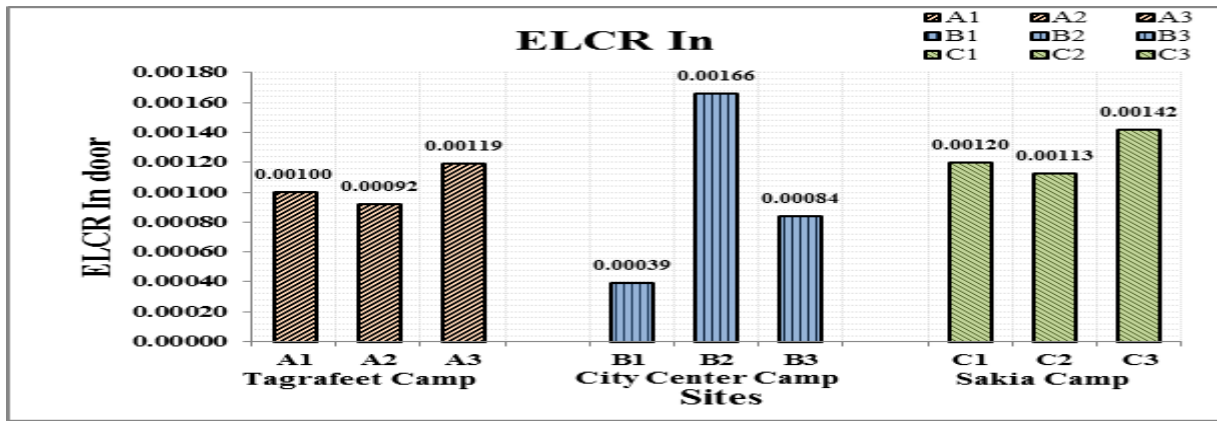


Fig. 3: Excess Lifetime Cancer Risk Indoor (ELCR_{in}) in the Study Area.

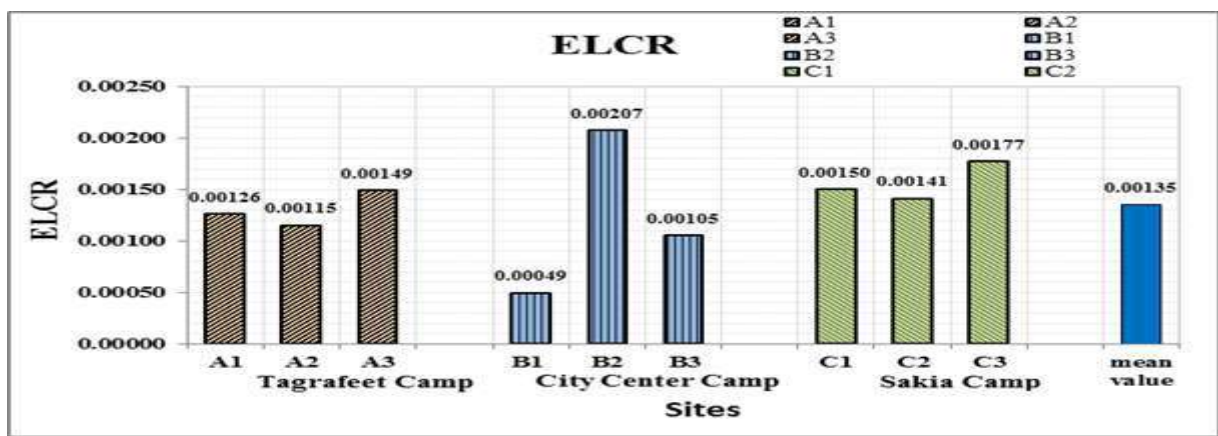


Fig. 4: Total Excess Lifetime Cancer Risk (ELCR_T) in the Study Area.

Table (3) show the estimated D_{organ} values for radiation exposure and inhalation in the lungs, ovaries, bone marrow, testes, kidney, liver, and entire body in the selected area. Fig.5 shows the variation of D_{organ} to the different organs. These results are all below the tolerable international limits of 1.0 mSv⁻¹,

indicating that the radiation levels in the study area do not pose a health risk. [10], [17], [18]. The results show that the whole body have the highest sensitivity to radiation (0.46) while the liver have the lowest sensitivity to radiation, respectively (0.141).

Table 2. Mean Annual Effective Dose Equivalent ($AEDE_m$) and Effective Dose rate (D_{organ}) to different body organs and tissues in the study area.

Sites	$AEDE_m$ ($mSv \cdot yr^{-1}$)	Lungs	Ovaries	Bone marrow	Testes	Kidney	Liver	Whole Body
Tagrafeet Camp	0.371	0.237	0.215	0.256	0.304	0.230	0.170	0.252
City Center Camp	0.344	0.220	0.200	0.238	0.282	0.213	0.158	0.234
Sakia Camp	0.445	0.285	0.258	0.307	0.365	0.276	0.205	0.303
Mean value	0.387	0.196	0.178	0.212	0.252	0.190	0.141	0.46
World Mean value	1.0	0.64	0.58	0.69	0.82	0.62	0.46	0.68

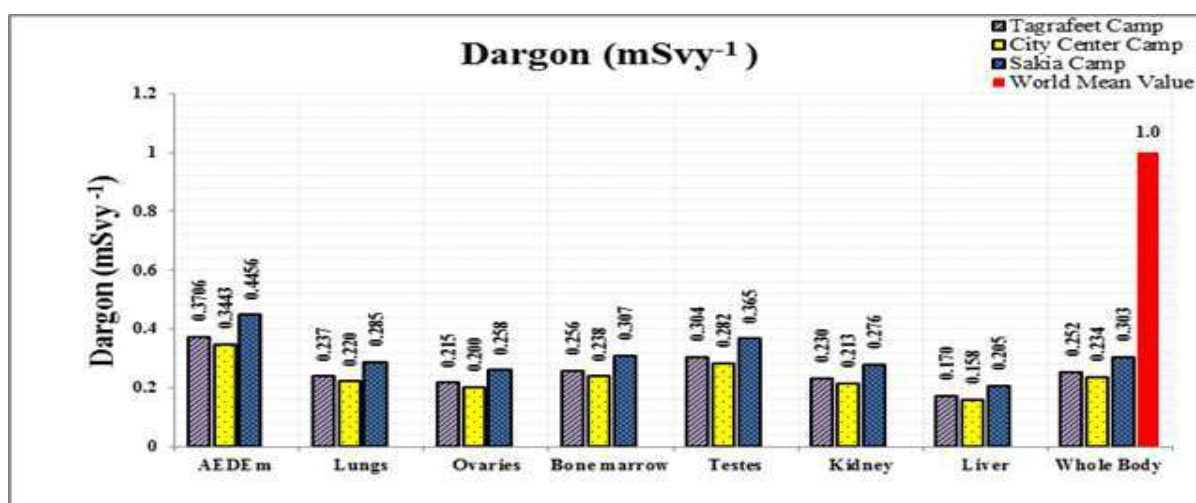


Fig. 5: Effective Dose Rate (D_{organ}) to Different Body Organs and Tissues in the Study Area.

5.0 Conclusion sand recommendation

Nine soil samples from three sites in Bani Waleed have been analyzed using hyper-pure germanium (HPGe) γ -ray spectrometry. The values of activity concentration of ^{226}Ra , ^{232}Th and ^{40}K were excess of the permissible Global value 35, 30 and 400 $mSv \cdot yr^{-1}$ respectively, and The $AEDE_T$, (outdoor and indoor) equivalent dose rate results were all below the 1.0 $mSv \cdot yr^{-1}$. The values of the total excess Life Cancer Risk $ELCR_T$, (outdoor and indoor) for the three zones were comparison with the global average and are below the world permissible value.

The D_{organ} values for radiation exposure and inhalation in the lungs, ovaries, bone marrow, testes, kidney, liver, and entire body in the selected area are all below the tolerable international limits of 1.0 mSv .

Which further indicates that the radiation levels of the studied area do not pose immediate health effect on residents of the city.

Abbreviations	
HPGe	Highper-Pure Germanium
²²⁶ Ra	Radium 226
²³² Th	Thorium 232
⁴⁰ K	Potassium 40
FWHM	Full width high measurement
Γ-Ray	Gamma Ray
mSvGy ⁻¹	Mill Sievert Gray per year
nGyh ⁻¹	Nano gray per hour
DR	Dose Rate
AEDE _T	Total Annul effective dose Equivalent
AEDE _{in}	Annul effective dose Equivalent indoor
AEDE _{Out}	Annul effective dose Equivalent outdoor.
AEDE _M	Mean Annul effective dose Equivalent
ELCR _T	Total Excess Life Cancer Risk.
ELCR _{IN}	Excess Life Cancer Risk indoor.
ELCR _{OUT}	Excess Life Cancer Risk outdoor

6.0 References

- [1] Belivermis, M; Kilic, N; Cotuk, Y; Topcuoglu, S., (2010).The effects of physicochemical properties on gamma emitting natural radionuclide levels in the soil profile of Istanbul, *Environ Monit Assess.*163 (1-4): pp 15-26.
- [2] UNSCEAR (2000). United Nation Scientific Committee on the Effects of Atomic Radiation.Sources and effect of Ionizing radiation. Report to the general assembly with scientific annexes. United Nations; New York.
- [3] Awwiri GO; Enyinma P; Aghalagba EO. (2010). Occupational Radiation Levels in Solid Mineral Producing Areas of Abia, State. *Nigeria Scientia Africana*, Vol. 9 (No. 1), pp 93-97.
- [4] Steinhausler, F. (1992). The natural radiation environment: future perspective. *Radiation Protection Dosimetry*, 45,19-23.
- [5] Karahan, G. and Bayulken, A. Assessment of gamma dose rates around Istanbul (Turkey).*J.Environ. Radio act.*47, 213-211 (2000).
- [6] Deger lier, M .,Karahan, G.and Ozger., (2008). (Radioactivity concentrations and dose assessment for soil samples, around Adana, Turkey. *J. Environ. Radio act.* 99, (6),1018-1025.
- [7] Kannan, V., Rajan, M .P, Ly enga A. and Ramesh, R., (2002).Distribution of natural and anthropogenic radionuclides in soil and beaches and Samples of Kalp akkam (India). *App l.Rodiat. Isot.*57,109-119.
- [8] Debertain, K., & Helmer, R.G., (1988). Spectrometry with semiconductor detectors. North-Holland Amsterdam.
- [9] Amrani, D., & Tahtat, M. (2001). Natural radioactivity in Algerian building materials. *Applied Radiation and Isotopes*, 54, 687-689.
- [10] Darwish DAE; Abul-Nasr KTM; El-Khayatt AM (2015) The assessment of natural radioactivity and its associated radiological hazards and dose parameters in granite samples from South Sinai, Egypt. *Journal of Radiation Research and Applied Sciences* 8, 17- 25.
- [11] Qureshi AA; Tariq S; Din KU; Manzoor S; Calligaris C; Waheed A (2014) Evaluation of Excessive lifetime cancer risk due to natural radioactivity in the rivers sediments of Northern Pakistan. *Journal of Radiation Research and Applied Sciences*, 7 (4): 438-447.
- [12] Ravisankar,R.,Sivakumar,S.,Chandrasekaran ,A.,Prince Prakash Jebakumar, J., Vijayalakshmi,I., Vijayagopal, P., et al. (2014). Spatial distribution of gamma radioactivity levels and radiological hazard in dicesin the east coast sediment of Tamilnadu, India with statistical approach. *Radiation Physics Chemistry*, 103, 8-98.
- [13] ICRP 106. (2008). Radiation dose to patients from radio-pharmaceuticals. Addendum 3 to ICRP Publication 53. ICRP Publication -106. *Ann. ICRP* 38, pp.1-2.
- [14] International Commission on Radiological Protection (ICRP), International Commission on Radiological Protection Age-dependent Doses to Members of the Public from Intake of Radionuclides. Part 5, Compilation of Ingestion and Inhalation Coefficients ICRP Publication 72, Pergamon Press, Oxford, 1996.
- [15] Ramasamy,V.Suresh,Meenakhisundaram,v. and Gajendran, v.,(2009). Evaluation of natural radionuclide content in river sediments and excess lifetime cancer risk due to gamma Radioactivity. *Research journal of environmental and earth sciences*, vol. 1, no. (1), pp. 6-10.
- [16] Taskin, H., Karavus, M., Topuzoglu, P., AY, A., Hindiroglu, S. and Karahan, G. (2009), Radionuclides concentrations in the soil and lifetime cancer risk due to gamma's radioactivity in kirklareli, Turkey. *Journal of environmental radioactivity*, vol. 100, no. 1,pp.49. Doi:10.1016/j.jenvrad.2008.10.012.
- [17] Agbalagba OE (2017). Assessment of excess lifetime cancer risk from gamma radiation levels in Effurun and Warri city of Delta state, Nigeria. *Journal of Taibah University for Science* 11(3): PP.367-380.
- [18] Ugbede FO; Benson ID., (2018). Assessment of outdoor radiation levels and radiological health hazards in Emene Industrial Layout of Enugu State, Nigeria. *Int. J. Phys. Sci Vol.* 13 (20), pp. 265-272.

Study and simulation of electrical transformer protection using (differential protection)

Abdalfettah Aljedk

Electrical and Electronics Engineering, Faculty of Engineering / Bani waleed University, Libya

Abstract: The continuity of electric energy and its availability provision at an appropriate price is a measure of the country's progress, and the electric power system, which consists of generation units and networks for the transmission and distribution of electric power, requires enormous efforts and large and diverse equipment in order to deliver the electric current to the consumer in a correct and continuous manner. The electrical power system, including its components, such as generators, transformers, overhead transmission lines, and cables for transmitting and distributing electrical power, is exposed to some malfunctions that may cause the system to stop working due to a malfunction or damage to one of the elements of this system and consequently a power outage if the necessary preventive measures are not taken, and accordingly This paper presents a study on the differential protection of electrical transformers This is due to the importance of transformers in raising and lowering the voltage in the electrical power system and transferring power over very long distances from its generation sites to its utilization sites. where has been made Conducting of a simulation through the work of transformers and the causes that lead to malfunctions in these transformers, to arrive at the appropriate protection method for these transformers based on the study of the problems that caused these malfunctions.

Keywords: (power system, transmission lines, differential protection)

Introduction:

The electrical transformer is considered the most widespread and common element of the electrical network in its forms, sizes and functions. The electrical network contains dozens of generators, but it contains tens of thousands of transformers. Of course, only cables and overhead lines compete with it in this wide spread within the electrical power system, but the diversity in shapes, sizes and functions Electrical transformers are considered the most important among the elements of electrical power systems, and the electrical transformer is a very important part in the electrical circuit, and without it, the following vital purposes would not have been achieved:

- Transferring electrical power in huge quantities over very long distances from the sites of its generation to the areas of utilization on high electrical voltages.[1]
- Distributing electrical power over areas to benefit from it with appropriate efforts for the purposes of using it in homes and factories, and aligning any electrical device regardless of the effort it works with.[2]

Therefore, in this paper focused on how to protect electrical transformers using differential protection devices, as they are among the most important devices used in the electrical network, due to their sensitivity, reliability, selectivity and speed.

And Due to the problems that electrical transformers are exposed to as a result of lightning strikes, trees, birds and others, which leads to malfunctions on the transformers or an increase in currents and transient voltages, and electrical transformers are considered among the most important elements in the electrical network, so protecting these transformers is one of the basics of Electric power to ensure the continuity of the transmission of electric power without permanent interruption that affects consumers directly.

In this paper, a differential protection was designed on the electrical transformer and this protection was tested by placing faults inside the area in which the transformer is located (the area to be

protected) and outside the area, and since we noticed that this protection works when the fault is in the area to be protected and does not work if the fault is outside it.

differential protection:

The use of surge relays does not meet all the necessary protective conditions in the electrical power system.[3-10]

We have noticed that the separation time always increases towards the source regardless of the gradient method used, and this in turn may pose a danger to the generation stations as well as to the transfer stations in addition to the direct impact on the balance of the network Therefore the method of unit protection or differential protection is used to protect Generators, transformers, engines and bus bar.[4]

- fault type and their effects:

In order to design a suitable protection system for voltage transformers, it is necessary to be aware of most of the errors that the transformer is exposed to.[6-8]

1. An external short (ground) on the ends of the high voltage coil cables.
2. An external short (between two sides) on the ends of the cables connecting the high voltage coils.
3. An internal short (ground) on one of the high voltage coils.
4. An internal short (between two faces) in the direction of high voltage.
5. A short circuit between the windings of the high voltage coil.
6. An external fault (ground) on the ends of one of the cables connecting the low voltage coils.
- 7- An external short (between two sides) on the ends of the cables for connecting the low voltage coils.
8. An internal short (ground) on one of the low voltage windings.
9. An internal short (between two sides) of the low voltage coils.
10. A short circuit between the windings of the low voltage coil.
11. Ground floor near the generator.
12. A palace between two faces.

Classification of faults:

Malfunctions are often classified as:

according to the number of phases affected by the fault The may be:

- single line to ground.
- Double lines to ground.
- Three lines.
- Two lines touching together Phase to Phase.
- Three lines to ground.[5]

THE RESULTS AND DISCUSSIONS:

Protection of electrical transformers using differential protection:-

The following figure shows how to protect electrical transformers using differential protection.

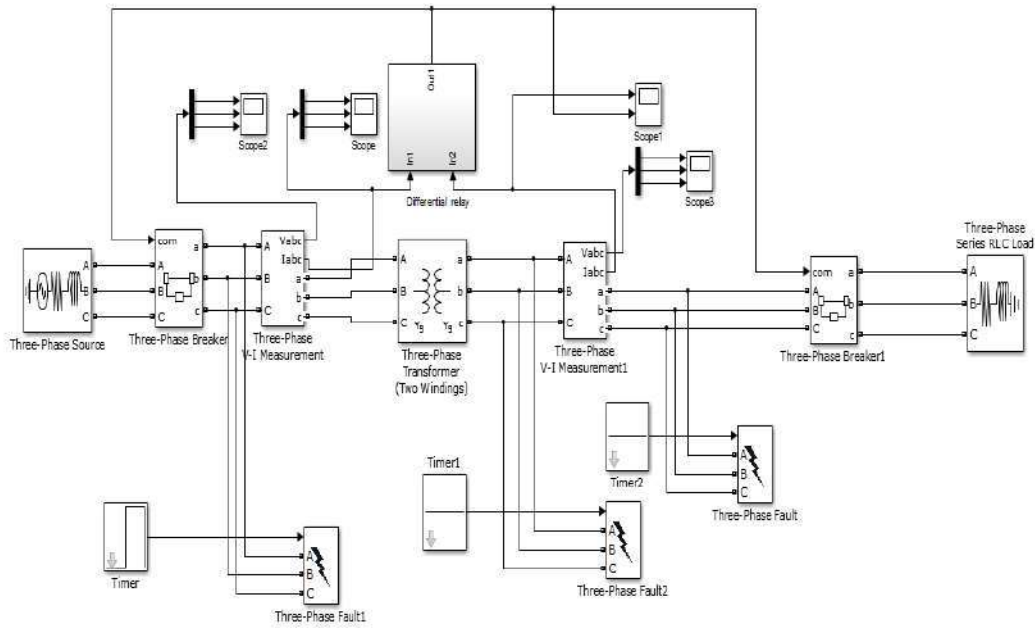


Fig (1) How to protect electrical transformers using differential protection

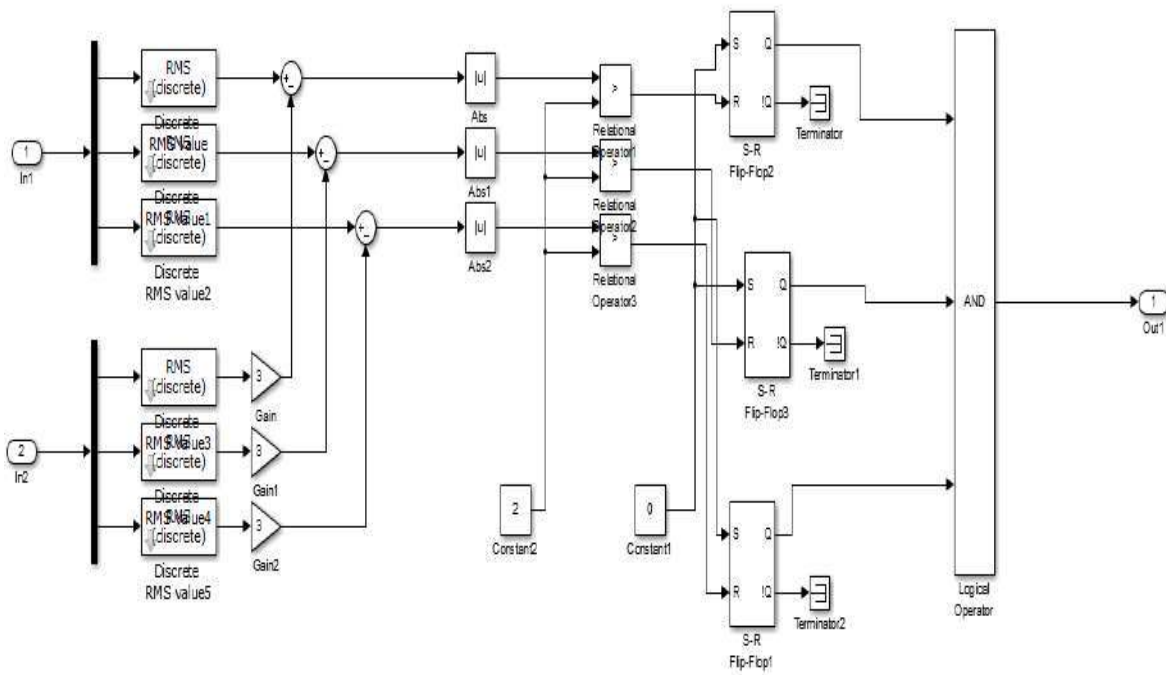


Fig (2) Internal logic Circuit

case1: In the case of no failure on the transmission line:

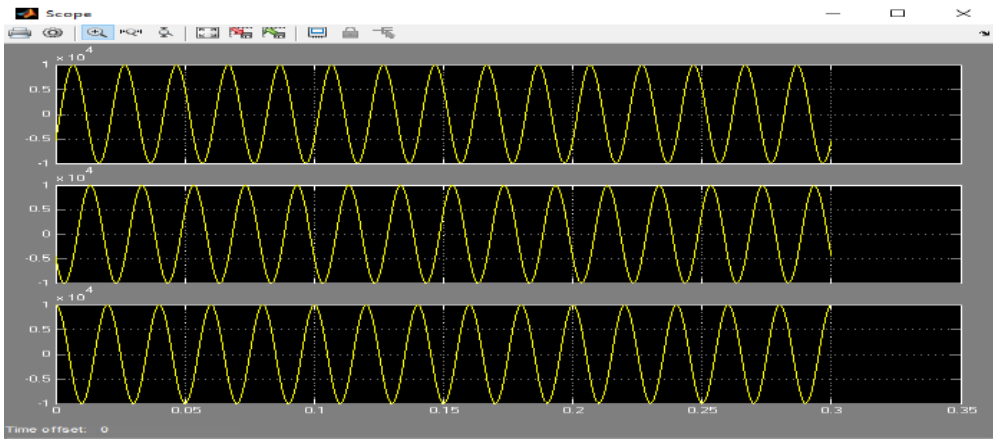


Fig (3) Stabilization of currents in the system (before the transformer).

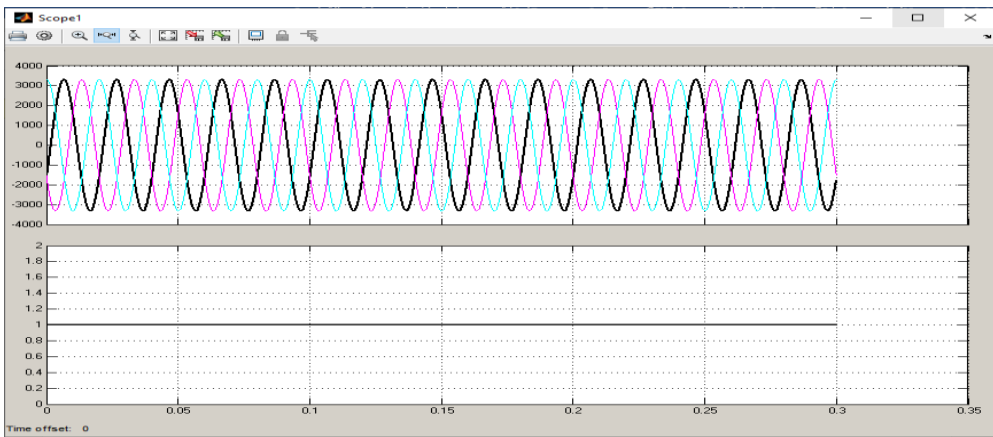


Fig (4): The currents are stable in the system (after the transformer) and the relay is not working

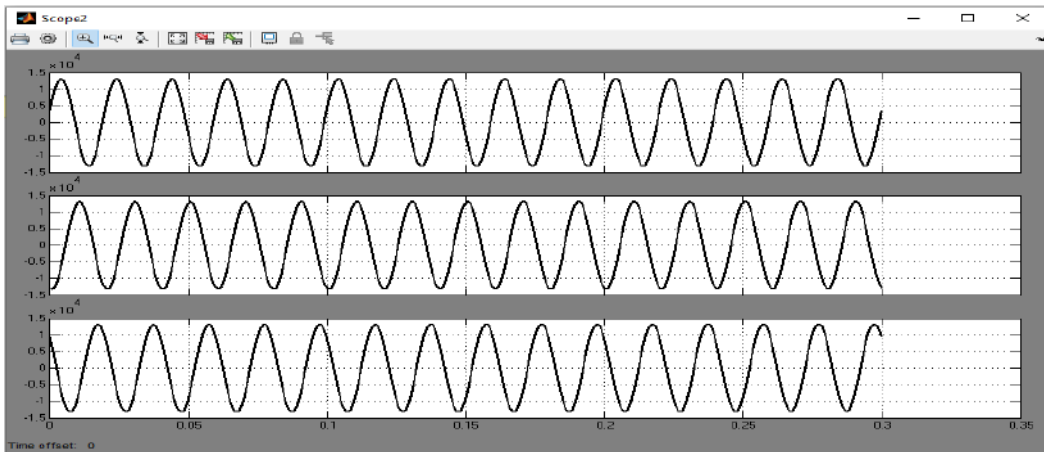


Fig (5) Stabilization of voltages in the system (before the transformer)

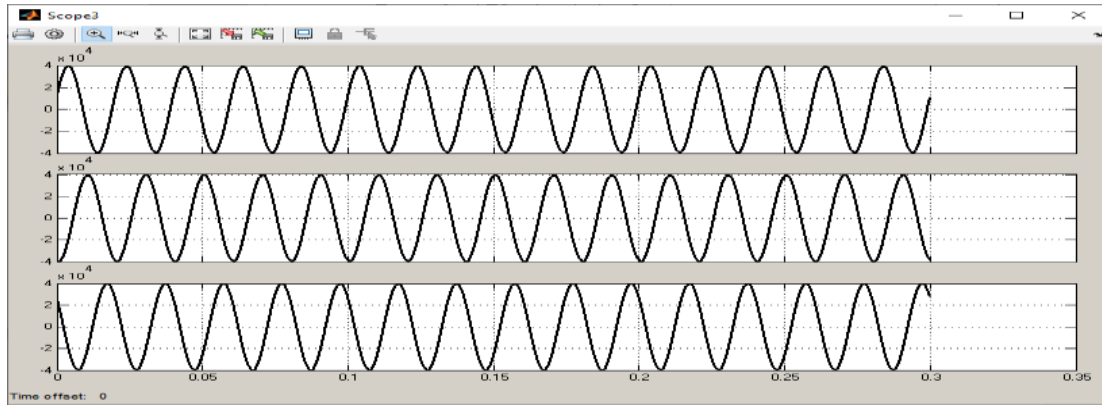


Fig (6) Stabilization of voltages in the system (after the transformer).

case2: In the case of a failure on the transmission line:

When a malfunction occurs on the transmission line, the places where the malfunction occurs can be as follows: -

1- The beginning of the transmission line and outside the protected area.

-2 Inside the protected area, i.e. next to the voltage transformer.

3- The end of the transmission line and outside the protected area.

- If we assume that there are faults in each of the previous cases on the transmission line, let us see what will happen to the currents and voltages before and after the transformer, and what can happen to the relay when the fault is inside or outside the protected area.

- In the case of the fault occurring at the beginning of the transmission line and outside the protected area, knowing that the fault could be one of the following types of faults:

- Single line to ground (S-L-G).

- Line To Line (L-L).

- Double Line To Ground (D-L-G).

- Three Line To Ground (T-L-G).[9]

it's worth mentioning that There are other types of malfunctions, but the aforementioned are the mostly need types in comparison with other types.

case3: In the case of a fault type (S-L-G) at the beginning of the transmission line and outside the protected area.

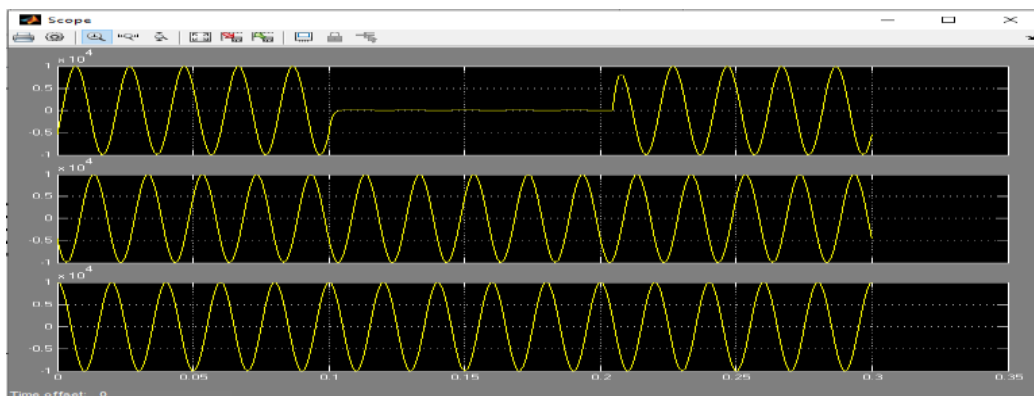


Fig (7) Waves of currents (before the transformer) and the type of fault (S-L-G).

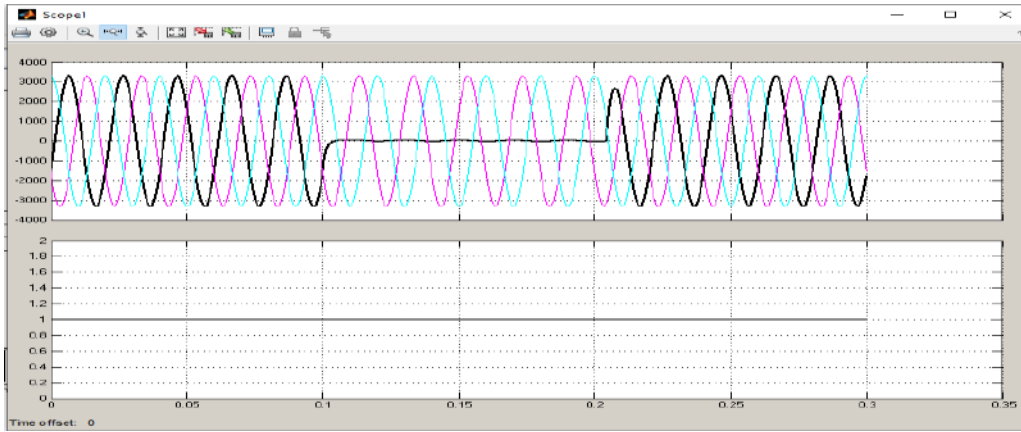


Fig (8) Waves of currents (after the transformer), the signal of the relay (not working) and the type of fault (S-L-G).

case4: In the case of a fault type (L-L) at the beginning of the transmission line and outside the protected area.

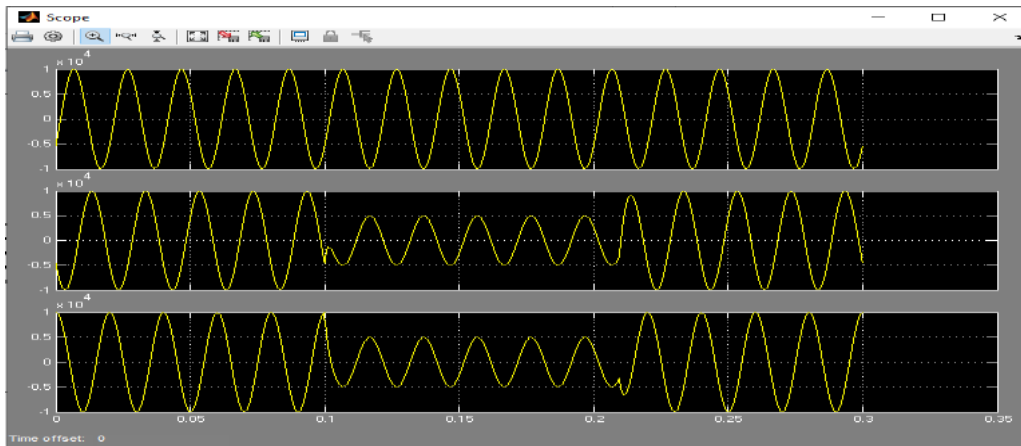


Fig (9) Waves of currents (before the transformer) and the type of fault (L-L).

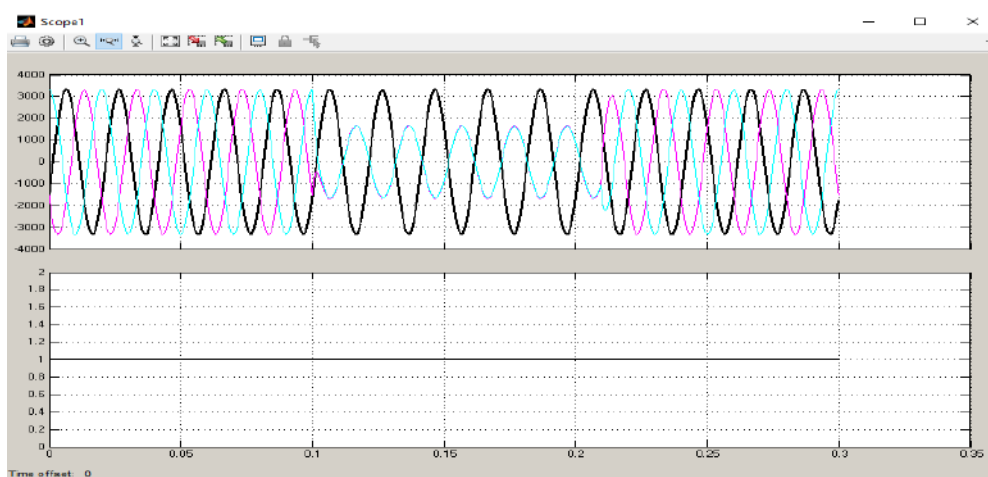


Fig (10) Waves of currents (after the transformer), the signal of the relay (not working) and the type of fault (L-L).

case5: In the case of a fault type (D-L-G) at the beginning of the transmission line and outside the protected area.

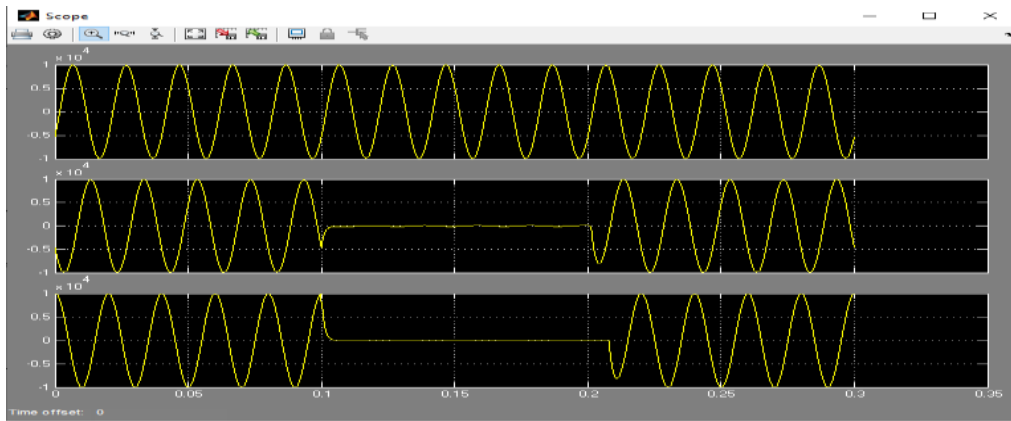


Fig (11) Waves currents (before transformer) and fault type (D-L-G)

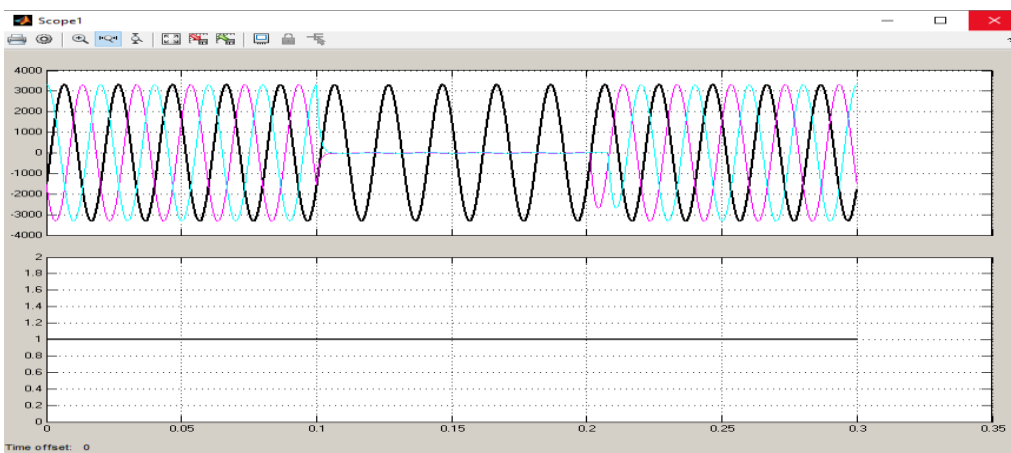


Fig (12) Waves of currents (after the transformer), relay signal and fault type (D-L-G).

Case6: In the case of a fault type (T-L-G) at the beginning of the transmission line and outside the protected area.

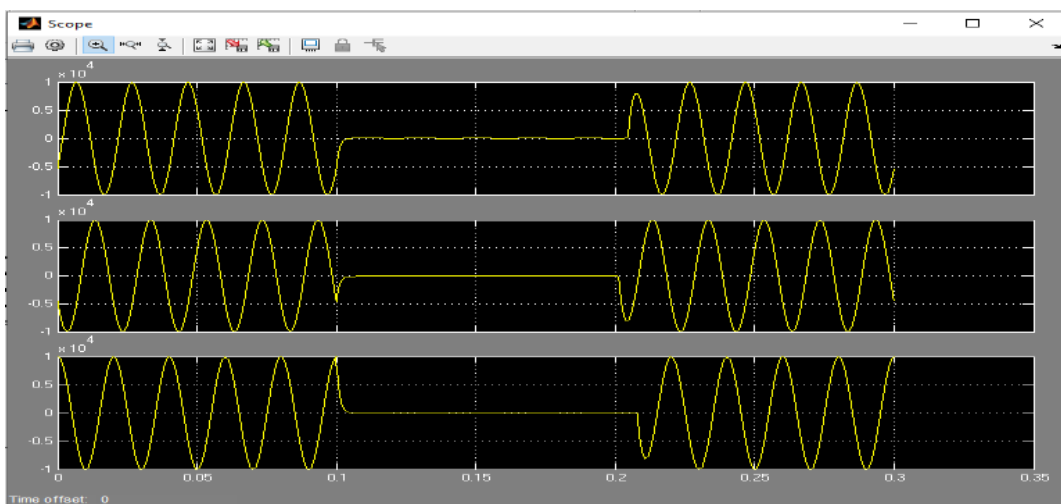


Fig (13) current waves (before transformer) and fault type (T-L-G).

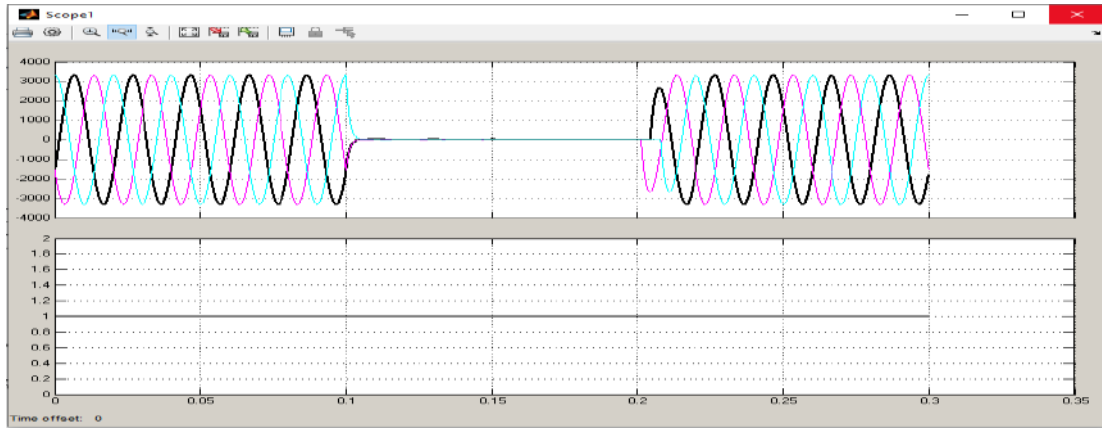


Fig (14) current waves (after the transformer), the signal of the relay (not working) and the type of fault (T-L-G).

case7: If the fault occurs inside the protected area.

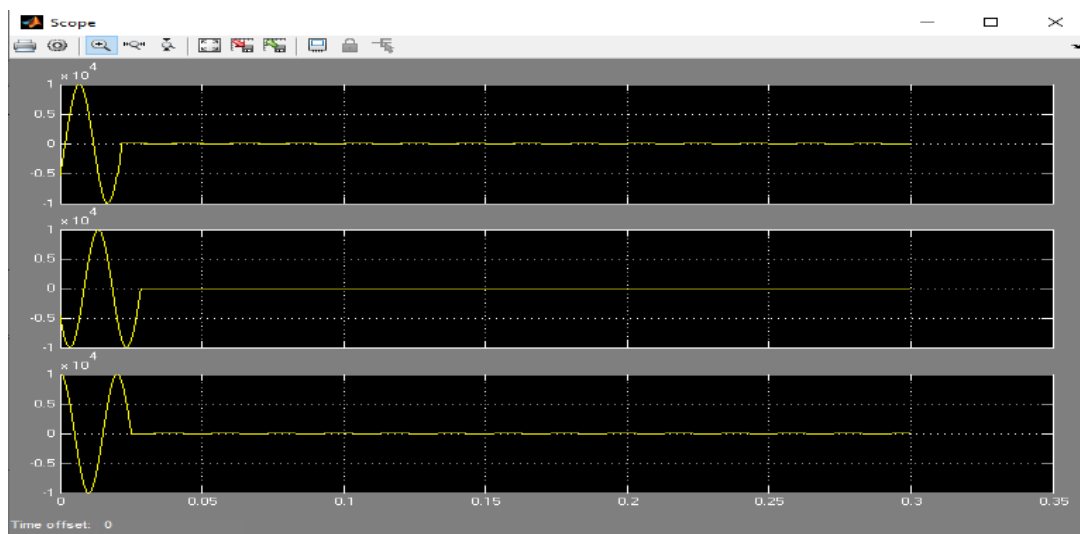


Fig (15) The occurrence of a disconnection on the system due to a malfunction.

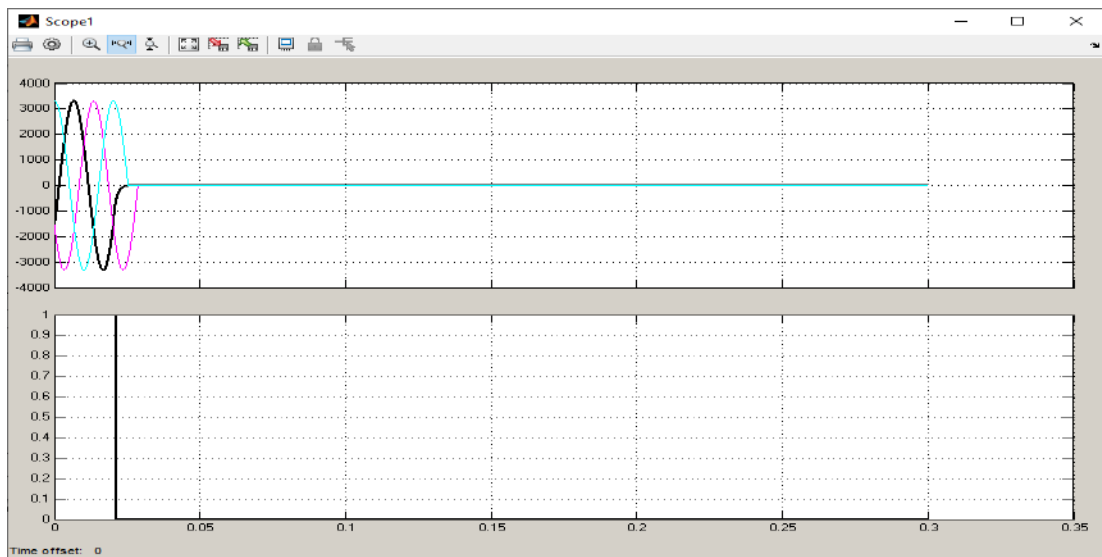


Fig (16) The occurrence of a disconnection on the system due to the work of the relay.

- Likewise, if the fault type was changed at (FauLt-2) to other types

A- Line to Line.

B- Double Line to Ground.

C- Three Line to Ground.[7]

we will notice that the relay responds to all types of faults.

Case8: In the case of a fault occurring at the end of the transmission line and outside the protected area.

A- Assuming the fault type is (S-L-G):

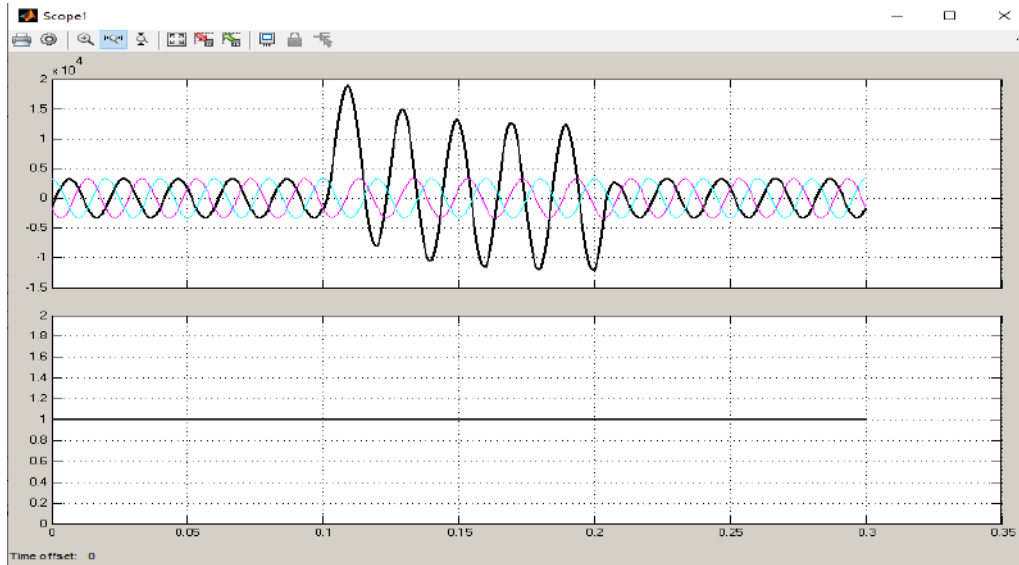


Fig (17) The current waves (after the transformer), the signal of the relay (not working) and the type of fault (S-L-G)

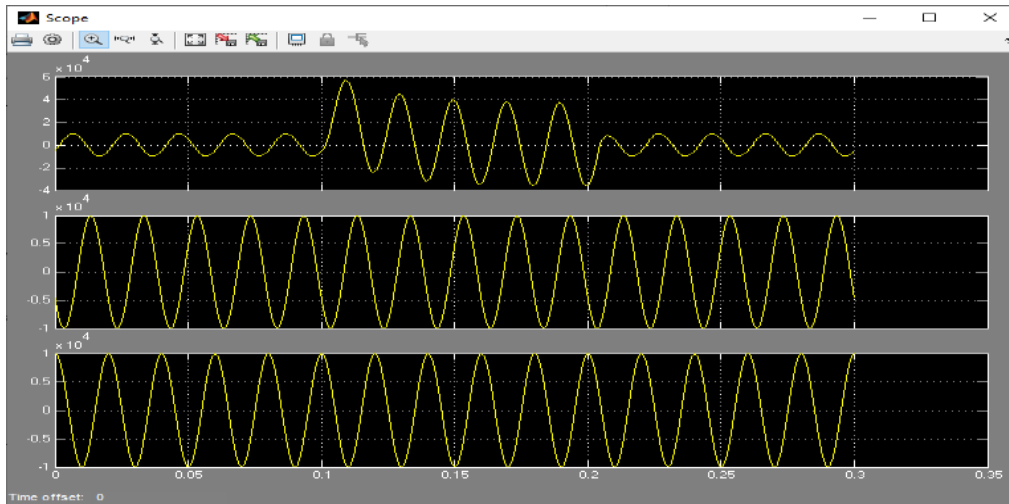


Fig (18) current waves (before the transformer) and the type of fault (S-L-G).

B- In the case of a fault type (L-L):

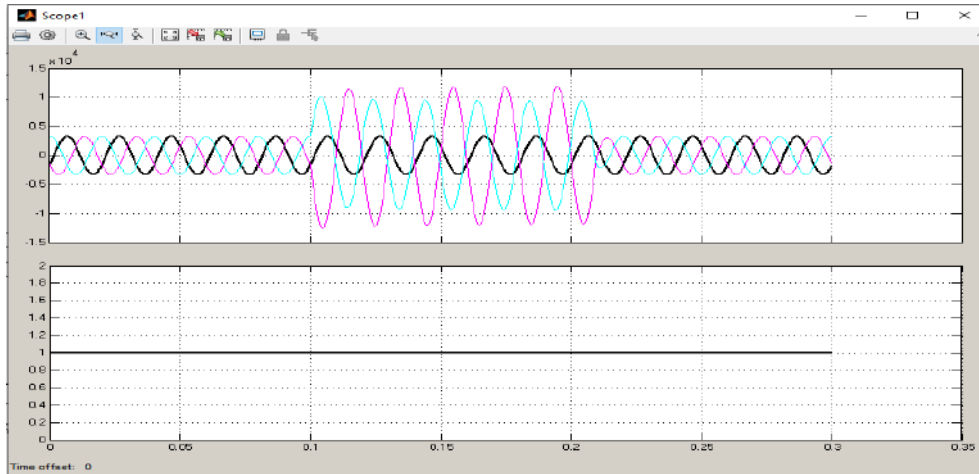


Fig (19) Waves of currents (after the transformer), the signal of the relay (not working) and the type of fault (L-L).

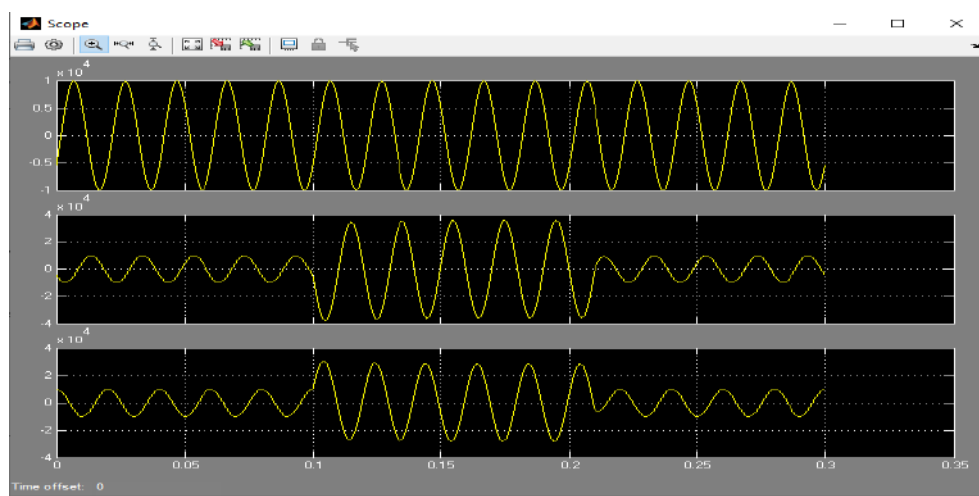


Fig (20) current waves (before transformer) and fault type (L-L).

C - Assuming the occurrence of the fault type (D-L-G):

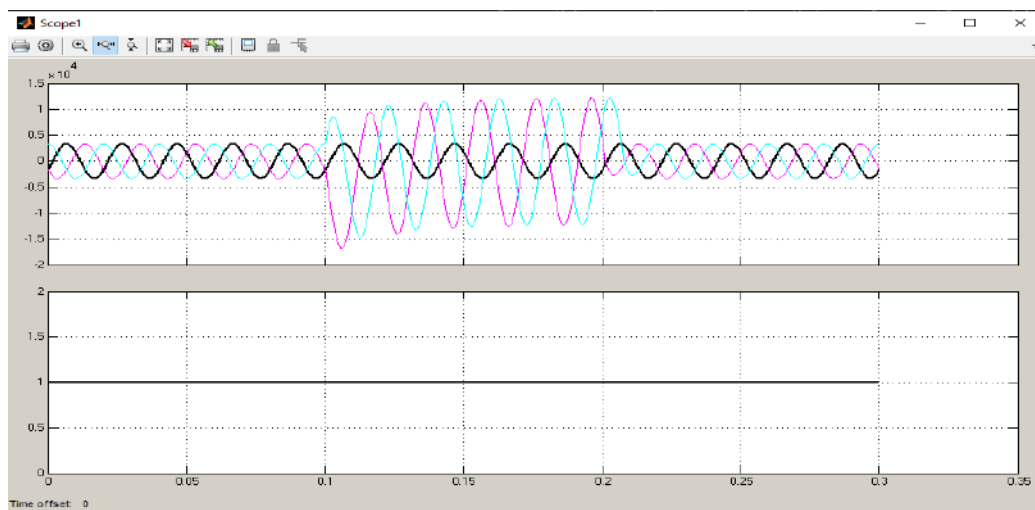


Fig (21) Waves of currents (after the transformer) and the signal of the relay (not working) and the type of fault (D-L-G).

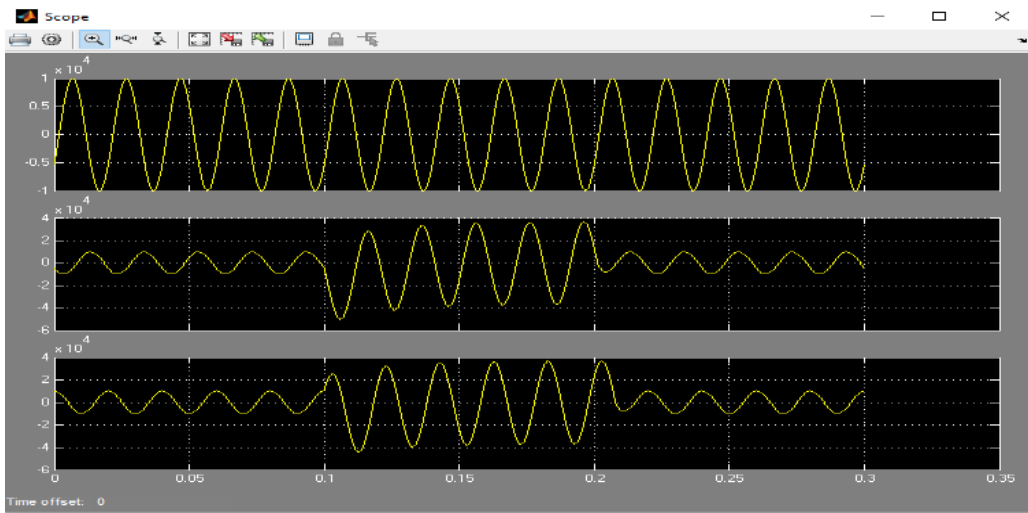


Fig (22) Waves of currents (before the transformer) and the type of fault (D-L-G).

D- In the case of a fault type (T-L-G):

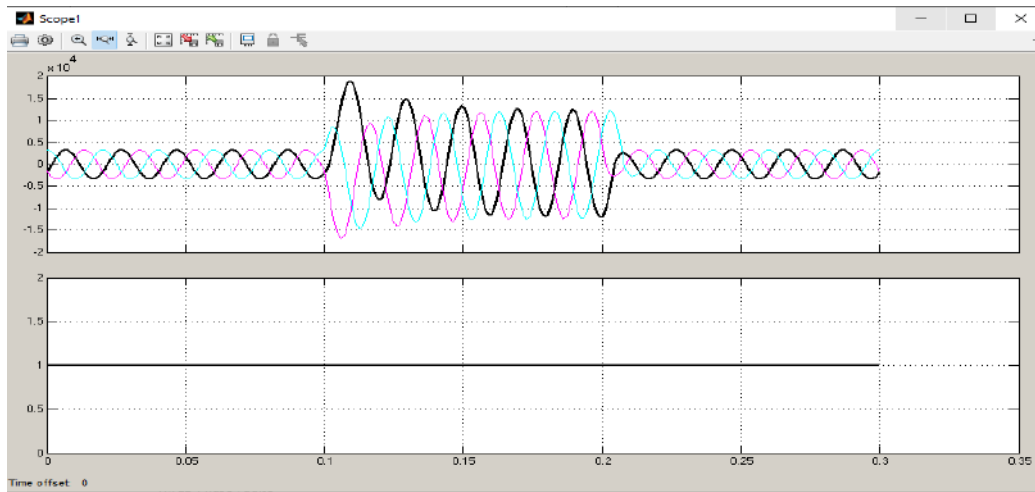


Fig (23) oscillation of the current waves (after the transformer) and the relay does not work and the fault type is (T-L-G).

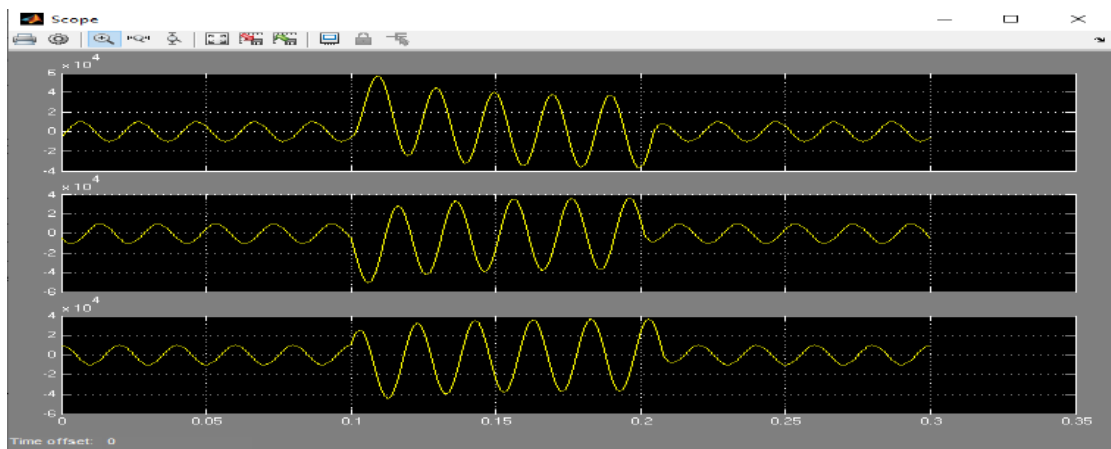


Fig (24) Oscillation of current waves (before the transformer) and the type of fault (T-L-G).

Conclusion:

A Matlab simulation of an electric transformer was presented in this work as shown in the results. This simulation has been tested for many cases and for all cases it gave satisfactory results. Through the study, it became clear that the protection of electrical transformers within an integrated system is of importance, which affects the safety of these transformers and the efficiency of their work in the long run, so that they are not affected by the malfunctions of neighboring devices within the system.

And through practical application, it was found that to reach the goal of protecting transformers, moreover, the structure of the system to implement the transformer protection design without changing the basic course of the system, where attention must be paid to the design plan of the protection system to match the capacity of the internal system.

References:

- [1] M. A. Rahman and B. Jeyasurya, "A state-of-the-art review of transformer protection algorithms", IEEE Trans. Power Delivery, vol. 3, pp. 534–544, Apr. 1988.
- [2] P. M. Anderson, "Power System Protection", Piscataway, NJ: IEEE Press, 1999.
- [3] C. D. Hayward, "Harmonic-Current Restrained Relays for Transformer Differential Protection", AIEE trans., vol. 60, pp 276, 1941.
- [4] M. S. Sachdev, T. S. Sidhu, H. C. Wood, "A Digital Relaying Algorithm for Detecting Transformer Winding Faults", IEEE Transactions on Power Delivery, vol. 4, No. 3. July 1989.
- [5] K. Yabe, "Power Differential Method for Discrimination between Fault and Magnetizing Inrush Current in Transformers", IEEE Transactions on Power Delivery, Vol. 12, No. 3, July 1997.
- [6] A.R. Van C. Warrington, "Protective Relays Their Theory and Practice", vol. 1, Chapman Hall Press, 3rd edition, 1985.
- [7] M. A. Rahman, Y.V.V.S. Murthy and Ivi Hermanto, "Digital Protective Relay for Power Transformers", U.S. Patent No. 5,172,329, December 1992.
- [8] P.K. Dash and M.A. Rahman, "A New Algorithm for Digital Protection of Power Transformer", Canadian Electrical Association Transactions, Vol. 26, Part 4, 1987, pp. 1-8, (87-SP-169), 1987.
- [9] A. Gangopadhyay, M.A. Rahman, B. Jeyasurya, "Simulation of Magnetizing Inrush Currents in Single Phase Transformers", International Journal of Energy Systems, Vol. 7, No. 1, 1987, pp. 34-38.
- [10] M.A. Rahman and A. Gangopadhyay, "Digital Simulation of Magnetizing Inrushes Currents in Three-Phase Transformers", IEEE Transactions on Power Delivery, Vol. PWRD-1, No. 4, October 1986, pp. 235-242. (Over 100 citations)

Planning preventive maintenance of textile machines in the woolen industries complex in Bani Walid

Salem Milad Abdel Hamid Embaya^a, Omar Ahmed Mohamed Addbeeb^b,
Walid Emhammed Ghaith^c, Meshaal Suliman Almukhtar^d

^{a c d} department of mechanical engineering, Higher Institute of Engineering Technologies,
Bani Walid, Libya

^b department of mechanical engineering, Bani Walid University, Bani Walid, Libya

Abstract Maintenance planning is one of the topics worthy of attention and study due to its importance and its connection to the production processes of the factory, given that the means of production are exposed to machines and equipment in the factory to a number of problems that reduce their production and efficiency and losses as a result of stopping work in production lines and frequent breakdowns that occur in the factory due to delay in preventive maintenance procedures or poor operation and negligence, so it has become necessary that these problems that hinder the production process in the factory. Maintenance work, in its modern scientific concept, relies on planning methods to ensure that these activities are implemented to the fullest, at the lowest cost, and in the shortest possible time. The problem of this research revolves around how the embarrassing path style is used to reduce the time required for maintenance and maintenance work (Textile machines) to improve the production process. Through studying the research, it is possible to reach the weaknesses of planning maintenance work in the factory and from them in particular by applying scientific methods in planning and scheduling maintenance work and benefiting from them and suggesting the best method, as well as the best method for planning maintenance work in the factory will be proposed, with the aim of reducing the time necessary For maintenance that includes lower costs.

Keywords: (critical path style, maintenance planning, maintenance workshops, preventive maintenance)

Introduction

Industrial institutions have invested in the construction of factories and production units in recent years, implemented the development strategies formulated by these institutions, and completed the procurement and installation phase of these factory equipment and started construction. It will continue to operate throughout the planned production period. We clarify that the time factor for maintaining this equipment is very important to avoid all kinds of serious losses due to the interruption of production line work, because this matter requires scientific planning methods, especially operations research methods to achieve the shortest possible time for plant equipment maintenance, and as already mentioned from the front, it is necessary to accompany the modern planning of the modern factory, the method of scientific development and complexity, so the method (critical path) is adopted. This method requires less maintenance time. From this perspective, it is necessary for the remaining agencies to deal with these constraints and variables in the maintenance process in order to achieve their goals and effectively use the resources and opportunities available to them without breaking cost and time permitting. The process of planning and maintaining a project involves the following three factors: time (time), financial resources (cost), and human resources (workers), so the supervisor (decision-making) must combine these three combinations to ensure the

success of maintenance at the lowest possible cost. Network planning method (Bert, critical path), an advanced scientific method for planning and organizing projects in the form of a network, reflecting the temporal and logical sequence of implementing project operations and activities and their interdependencies. It is also an effective organizational tool to control the progress of work and carry out work according to planned procedures, identification of procedures and scheduling of resources

1. Experimental Procedure

Maintenance work with its scientific and modern concept depends on planning methods to ensure full implementation at the lowest cost and time. And based on the data obtained from the factory, using the critical path method is the most appropriate way to plan the maintenance work of the factory according to the type and size of the errors that the machines face the factory. In order to plan the biannual preventive maintenance, the most important machines (fabric), were selected. One of the main lines of the mill (Spinning and Fabrics Department), consisting of (16), has been selected. A machine has been chosen as a model for scheduling semi-annual preventive maintenance [where the machine is maintained twice a year by taking the machine out of service for a period of 3 days (8 hours per day)]. Its purpose is to prepare a maintenance plan based on the manufacturer's specifications and the scope of the maintenance needs of the machine, on the basis of data received from the production department of the factory, and on the basis of the nature and extent of the failures to which the production machine is subjected, in order to provide the shortest possible completion of repair work time and to achieve accurate scheduling, he uses the critical path method as one of the scientific methods for planning maintenance work for the machine under study. For the purpose of applying the critical path style, the basic works (activities) for the maintenance of the machine must be determined in study with the logical sequence of it and the conditions for precedence, which can be clarified in the table (1), which shows the regular time for each activity, which depends on the basis of practical viewing.

Table1: The regular time for each activity that can be adopted to plan the maintenance process

Half yearly Activity		Quarterly Activity		Monthly Activity		Weekly Activity		Daily Activity	
Activity implementation time (MIN)	Activity Symbol	Activity implementation time (MIN)	Activity Symbol	Activity implementation time (MIN)	Activity Symbol	Activity implementation time (MIN)	Activity Symbol	Activity implementation time (MIN)	Activity Symbol
45	O	30	K	30	H	30	D	5	A
30	P	30	L	20	I	30	E	15	B
30	Q	15	M	30	J	20	F	15	C
30	R	60	N			20	G		
30	S								
45	T								
180	U								
120	V								

For the purpose of implementing the critical path style, basic activities must be represented with a network that shows the sequence of these activities, which can be adopted to plan maintenance work as shown in the figure (1).

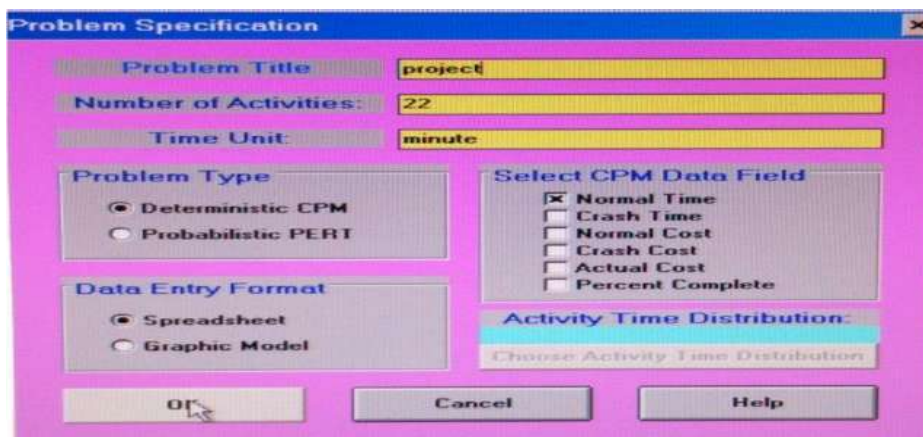


Fig. 1: Win QSP Program

1.1 Solve the problem using the program (WIN QSB)

Based on the study of the problem and to reach accurate results in calculating the times for the activities and determining the critical path and its time, the program (WIN QSB) was used, which contains a package of ready-made programs, one of which is a program for network diagrams (CPM- PERT), which was used in planning maintenance operations. After opening the program window and entering the data of the basic works (activities) for maintaining the machine under study shown in (Table 2), which shows the activities code, previous activities and the usual time. The time calculations for the activities were obtained as shown in Table (3), and the critical path and its time were determined as shown in Table (4).

Table2: symbols of activities, previous activities, and the usual time

Activity number	Activity name	Immediate predecessor (list number/name, separated by ',')	Normal time
1	A		5
2	B	A	15
3	C	A	15
4	D	B,C	30
5	E	D	30
6	F	D	20
7	G	E,F	20
8	H	G	30
9	I	G	20
10	J	H,I	30
11	K	J	30
12	L	J	30
13	M	K,L	15
14	N	K,L	60
15	O	M,N	45
16	P	M,N	30
17	Q	O,P	30
18	R	O,P	30
19	S	Q,R	30
20	T	Q,R	45
21	U	S,T	180
22	V	U	120

Table3: Calculating times for activities

2012-02-10 04:39:05	Activity name	On Critical Path	Activity Time	Earliest start	Earliest finish	Latest start	Latest finish	Slack (LS-ES)
1	A	5	5	0	5	0	5	0
2	B	15	15	5	20	5	20	0
3	C	15	15	5	20	5	20	0
4	D	30	30	20	50	20	50	0
5	E	30	30	50	80	50	80	0
6	F	20	20	50	70	60	80	10
7	G	20	20	80	100	80	100	0
8	H	30	30	100	130	100	130	0
9	I	20	20	100	120	110	130	10
10	J	30	30	130	160	130	160	0
11	K	30	30	160	190	160	190	0
12	L	30	30	160	190	160	190	0
13	M	15	15	190	205	235	250	45
14	N	60	60	190	250	190	250	0
15	O	45	45	250	295	250	295	0
16	P	30	30	250	280	265	295	15
17	Q	30	30	295	325	295	325	0
18	R	30	30	295	325	295	325	0
19	S	30	30	325	355	340	370	15
20	T	45	45	325	370	325	370	0
21	U	180	180	370	550	370	550	0
22	V	120	120	550	670	550	670	0
	project completion	Time	-	670	minutes			
	number of	Critical Paths	-	8				

Table3: Determine the critical path and its time

2012-04-10	CP1	CP2	CP3	CP4	CP5	CP6	CP7	CP8
1	A	A	A	A	A	A	A	A
2	B	B	B	B	C	C	C	C
3	D	D	D	D	D	D	D	D
4	E	E	E	E	E	E	E	E
5	G	G	G	G	G	G	G	G
6	H	H	H	H	H	H	H	H
7	J	J	J	J	J	J	J	J
8	K	K	L	L	K	K	L	L
9	N	N	N	N	N	N	N	N
10	O	O	O	O	O	O	O	O
11	Q	R	Q	R	Q	R	Q	R
12	T	T	T	T	T	T	T	T
13	U	U	U	U	U	U	U	U
14	V	V	V	V	V	V	V	V
Completion Time	670	670	670	670	670	670	670	670

Conclusion

We review the most important conclusions reached by this study, depending on the theoretical side and the applied side:

1. Through the study and practical application of the critical path method for planning maintenance work in the factory, it was found that it is possible to reduce the time taken to perform maintenance work on the machine from (24 hours - 11.17 hours) and thus increase production in the factory.

2. The study provided a scientific example of the effectiveness of the critical path method as one of the scientific methods for planning maintenance work in the factory.
3. Despite the good results obtained through the application of the critical path method for planning maintenance work in the factory, it remains very sensitive to the accuracy of the information and data provided by the factory.
4. Non-application of scientific methods in planning maintenance in the factory has led to an increase in the time spent on preventive maintenance, and thus an increase in costs.
5. The study that was carried out reinforced the hypothesis, which was adopted in the methodology of the study, which states that (there is a weakness in the efficiency of planning maintenance work in the factory, including through the application of scientific methods in planning and scheduling maintenance work, making use of it, and suggesting the best method)

References

- [1] Dr. Rami Hikmat Fouad Al-Hadithi and others, Programmed Maintenance Management, 1st edition, Jordan, Wael Publishing House, 2004 p.: 17.
- [2] Dr. Sonia Muhammad al-Bakri, Total Quality Management, Alexandria, University House for Publishing and Distribution, 2003-2004, p.: 187.
- [3] Dr. Abd al-Karim Mohsen, Dr. Sabah Majeed al-Najjar, "Production and Operations Department," p: 533.
- [4] Dr. Samer Mazhar Qantuji, "Rationalization of Maintenance Operations by Quantitative Methods," p.:49.
- [5] Dr. Farid Al-Najjar, "Experimental Production in Industries and Services", Alexandria, University House, 2007, p.: 470.
- [6] Francis, F.Ogust,A.le, , management delamaintenance,Paris,France, AFNOR,edition GESTON, 1987,P54
- [7] Lonnet, P. optimization dune politique de maintenance,. Paris, France, Fondement edition Technique et documentation, 1993, P:32,

**Cracks in the walls around the windows and doors openings
(CASE STUDY)**

Dr. naji amhimmid salih

Civil Engineering Department-Faculty of Engineering – Bain- Walid University

Abstract: In this study the problem of cracks appearing in walls especially around door openings and windows was addressed Which takes approximately a slope at an angle (45*) and the door and window openings are the weakest part of the wall we also sometimes notice the appearance of horizontal cracks above the windows lintels which are caused by the impact Thermal the appearance of cracks in buildings leads to distortion of the general appearance of the walls whether from the inside or outside it also leads to the leakage of rain water through it and the emergence of this problem is due to many some of the reasons are related to the method of implementation and some are related to the type of bricks used in construction work the other is due to the seasonal change in temperature and humidity in addition to the misuse of opening operations and the lock for doors and windows and therefore the dimensions of the windows compared to the dimensions of the wall it was also discussed the steps that can be taken to avoid the appearance of cracks some of which are related to in proper materials and structural issues-foundation and soil movement and the method of implementation for walls windowsills and doors.

Keywords: cracks, walls, building, horizontal cracks.

Introduction

Cracks around doors and windows in construction are one of the common aesthetic defects when refer to aesthetic is because in most cases these cracks are not caused by major structural damage cracks are the presence of faults or breakage of building materials mainly caused by uneven internal stress or stress concentration [1] it is necessary to ensure the safety durability and serviceability of the buildings [4-6].

Crack can be classified as either structural cracks or non-structural cracks depending on the way of internal stress failure of the building material. Structural defects consist of complete or incomplete separation within a single element or between continuous element of construction or a line along which a material is broken into parts [2-5]. Non –structural cracks develop due to the inducement of initial stresses in building materials and their depth is less only a few mm they exist on the surface only [3]. The cracks around the doors and windows openings are attributed to various effects ranging from humidity and temperature fluctuations poor construction in proper materials and structural issues –foundation and soil movement. To evaluate this problem required to visit one of the houses as case study.

Problem statement:

Due to the prevalence of cracks around the opening s of doors and windows in many new and old buildings implementation for importance the topic requires us to prepare a study to find out the reasons of this problem in the study targeted residential building in the city of Bani Walid it has been implemented for more than thirty years and it has helped me.

The owner of this building that he suffers from the problem of cracks the openings of doors and windows which it appeared in the building shortly after the completion of the finishing work for the building and despite an operation maintenance of the building and its attempt to hide these cracks but they reappeared without knowing the reasons for this problem and accordingly I made a field visit

Cracks in the walls around the windows and doors openings (CASE STUDY)

as case study to the building concerned with the study and it was written down notes and information that can help us to determine the reasons that lead to the emergence of this problem which is next:

- 1- The building has been implemented since 1993
- 2- The building was executed without re-structuring plans.
- 3- There's no soil investigation tests.
- 4- The building was executed without engineering supervision.
- 5- The wall was built from hollow cement blocks.
- 6- The dimensions of the window openings (1×1.2 meters) and the dimensions of the doors (1.0×2.10 meters)
- 7- Most of the width dimensions of the walls with window openings (4.50 meters)
- 8- The building was maintained after twenty years of its implementation.
- 9- The building has inclined cracks approximately at an angle (45) above the door and window openings it is wider at the corner of the door and window and becomes smaller when it moves up as shown in the figures (1,2,3,4). And cracks down the openings windows and horizontal cracks above the lintel of the window openings as shown in the figures (1,2,3,4)
- 10- There's diagonal cracks in the outer and inner walls.
- 11- The building still in good condition structurally (there's no cracks in the main structural elements) .



Fig. 1: shows cracks at the bottom of the window



Fig. 2: shows the cracks at the top of the window



Fig. 3: shows the cracks at the top of the window



Fig. 4: shows cracks at the bottom of the window



Fig. 5: shows the method of supporting the walls with an iron grid of diameter (\varnothing 10mm)

Causes of cracks around the doors and windows openings:

- 1- The lintel is implemented structurally incorrectly as the lintel based on small distances it may not exceed 20 cm
- 2- The subsidence of the foundations leads to the appearance of such cracks
- 3- Poor implementation as sometimes construction operations are not carried out in accordance with the technical requirements in addition sometimes twice the cement mortar.
- 4- Poor quality of bricks used in construction work as they are not made in most brick factories all types of testing are required to determine the quality of the product.
- 5- The dimensions of the window openings compared to the dimensions of the wall sometimes the window openings are large compared to the dimensions of the wall which leads to the weakness of the wall.
- 6- The seasonal change in temperature and humidity has a significant impact on the walls as this results in stress leads to the appearance of cracks in the walls.

Cracks in the walls around the windows and doors openings (CASE STUDY)

- 7- Doors and windows are elements that produce constant movement and impacts when opening and closing in many occasions slamming doors that cause a lot of vibrations these vibrations or shocks create tensions in the plaster or surface coatings.
- 8- This type of cracks caused by differential settlements in the ground is something that cannot be avoided after construction is done.

Recommendations:

- 1- Recommended to execute reinforce concert frame around the doors and windows openings to resist appearance cracks at the angles.
- 2- The walls must be constructed by using good quality of blocks according the specifications.
- 3- The walls must be placed steel mesh each three layers of blocks according the picture (5) to be resist the temperature change and humidity and shear force.
- 4- Lintel must be supported of each side of windows or door opening at least 40 cm to support the weakest part of the door and window.
- 5- Recommended to cast the lintels in situ and the thickness of lintels maximum of (20 cm – 1/8 width of opening).
- 6- Must be used skills labors for masonry work.
- 7- Must be done the steel or plastic mesh in the area around the cracks during the plaster work.

References

- [1] M M Goyal “Handbook of Building Construction Vol II” Second Reprint, 2013.
- [2] Sushil Kumar “Building Construction 20th Edition” Standard Publishes Distributors Del (January 1, 2010).
- [3] Dr. V. K. Raina “Concrete For Construction Facts And Practice” Second Edition: Facts and Practice Vol.1 Hardcover – 16 September 2009.
- [4] EFNARC, Specification and Guide Lines for Self Compacting Concrete,2002, UK
- [5] A. M Neville, Properties of concrete. Fourth edition, Pearson Education Ltd., 1995
- [6] M. Shariat, H. Eskandari-Naddaf, M. Tayyebinia, and M. Sadeghian, “Sensitivity analysis of reinforced concrete deep beam by STM and FEM (Part III),” Materials Today Proceedings, 2018.